Understanding Nucleophilic Attack Chemistry in Main Group Compounds with Density Functional Theory

by

Ruchi Dixit
10CC16A26013

A thesis submitted to the
Academy of Scientific & Innovative Research
for the award of the degree of
DOCTOR OF PHILOSOPHY
in

SCIENCE

Under the supervision of
Dr. Kumar Vanka

National Chemical Laboratory, Pune

Academy of Scientific and Innovative Research
AcSIR Headquarters, CSIR-HRDC campus
Sector 19, Kamla Nehru Nagar,
Ghaziabad, U.P. – 201002, India

January - 2022

Certificate

This is to certify that the work incorporated in this Ph.D. thesis entitled, "*Understanding Nucleophilic Attack Chemistry in Main Group Compounds with Density Functional Theory*", submitted by *Ruchi Dixit* to the Academy of Scientific and Innovative Research (AcSIR), in partial fulfillment of the requirements for the award of the Degree of *Doctor of Philosophy in Science*, embodies original research work carried-out by the student. We, further certify that this work has not been submitted to any other University or Institution in part or full for the award of any degree or diploma. Research material(s) obtained from other source(s) and used in this research work has/have been duly acknowledged in the thesis. Image(s), illustration(s), figure(s), table(s) etc., used in the thesis from other source(s), have also been duly cited and acknowledged.

(Signature of Student)

Ruchi Dixit

Date: 03.01.2022

(Signature of Supervisor)

Dr Kumar Vanka

Date: 03.01.2022

STATEMENTS OF ACADEMIC INTEGRITY

I, Ruchi Dixit, a Ph.D. student of the Academy of Scientific and Innovative Research (AcSIR) with Registration No. 10CC16A26013 hereby undertake that, the thesis entitled "Understanding Nucleophilic Attack Chemistry in Main Group Compounds with Density Functional Theory" has been prepared by me and that the document reports original work carried out by me and is free of any plagiarism in compliance with the UGC Regulations on "*Promotion of Academic Integrity and Prevention of Plagiarism in Higher Educational Institutions (2018)*" and the CSIR Guidelines for "*Ethics in Research and in Governance (2020)*".

Signature of the Student

Date: 03.01.2022

Place: Pune

It is hereby certified that the work done by the student, under my/our supervision, is plagiarism-free in accordance with the UGC Regulations on "*Promotion of Academic Integrity and Prevention of Plagiarism in Higher Educational Institutions (2018)*" and the CSIR Guidelines for "*Ethics in Research and in Governance (2020)*".

Signature of the Supervisor

Name: Dr Kumar Vanka

Date: 03.01.2022

Place: Pune

Dedicated to my parents

Acknowledgement

It is not always the goal, but the path we take, the people we meet and the things we learn which makes the journey exhilarating. My doctoral research journey was one such learning path in my life, which, has finally come to an end. The path has been long, winding, often challenging and ultimately satisfying. It was composed of mixed emotions, and I luckily met a multitude of supportive beings, without whom it would be impossible to traverse my graduate life and reach the destination.

First, I would like to express my gratefulness to my research supervisor, ***Dr. Kumar Vanka****, for his constant guidance and support. Without him, it would have been impossible to reach this point. Furthermore, I am also grateful for the academic freedom he has given me, which motivated me to grow as an independent researcher. Also, his teaching, writing, and communication skills have been inspirational to me throughout my Ph.D.*

I would also thank my Doctoral Advisory Committee members, ***Dr. Sayan Bagchi, Dr. Nayana Vaval****, and DAC chairperson* ***Dr. Ashok Giri*** *for their insightful suggestions and feedback. I am also grateful to* ***Dr. Ashish Lele****, director, CSIR-NCL, and* ***Dr. Ashwini Nangia****, former director of CSIR-NCL. Moreover, I take the opportunity to thank the present and former heads of the Physical and Materials Chemistry Division for their support and providing all facilities during my Ph.D.*

I want to extend my gratitude to all teachers who had taught me during my Ph.D. course work at CSIR-NCL: ***Dr. Kumar Vanka, Dr. Suman Chakrabarty, Dr. Sayan Bagchi, Dr. Nithyanandhan, Dr. Kavita Joshi, Dr. Rajesh Gonnade*** *and* ***Dr. T.G. Ajithkumar****, as well as other scientists in NCL. Let me extend my warm thanks to my research collaborators,* ***Dr. Francine Agbossou-Niedercorn, Dr****.* ***Christophe Michon****,* ***Dr. Ravindar Kontham****,* ***Dr. C. V. Ramana, Dr. Avinash Kumbhar****,* ***Dr. R.G. Bhat, Dr. Sakya S. Sen*** *and his doctoral students* ***Dr. Milan*** *and* ***Dr. Sandeep****. Moreover, I owe to thank my University and school teachers for their support and motivation.*

I also acknowledge all the non-academic staff of CSIR-NCL, and AcSIR, for their support and help during my work. Without the funding, this Ph.D. journey would not have been possible; hence I would like to express my gratitude to the ***Council of Scientific & Industrial Research*** *(CSIR) for the fellowship. Moreover, I want to thank the whole scientific community for being a source of inspiration and motivation.*

No words are enough to thank my friends, who have helped and supported me at various stages. I feel myself to be lucky to have dearest friends ***Dr. Ashish*** *and* ***Dr. Vrushali****. I am immensely thankful to them for being there with me during my ups and downs. My entire Ph.D. duration was memorable with* ***Meenakshi, Divya, Shruti, Sharmila, Diksha, Aishwarya, Shubhra, Dr. Amit,*** *and* ***Dr. Sayantan.*** *I thank them for their company and support.*

I also extend my thanks to my past and present lab mates ***Dr. Manoj, Dr. Jugal, Dr. Mrityunjay, Dr. Yuvraj, Dr. Tamal, Subhrashis, Dr. Anagh, Vipin*** *and* ***Dr. Shailja*** *for their help whenever needed during my Ph.D. Also, my special thanks to* ***Soumya, Ravi, Siddharth, Himanshu*** *and* ***Priyam****.*

*I want to thank the most important people in my life, my family. No words are sufficient to describe their love, affection, and support. I am highly indebted to my Mother (****Javitri Dixit****) and Father (****Mukesh Dixit****) for their unconditional love and the sacrifices they have made for me in their lives. Also, I wish to thank my elder sister (****Dr. Swarnita****) for guiding me throughout my life and taking care of all of us siblings, which helped me focus on my research work. Furthermore, I would like to thank my younger brothers and sister (****Abhishek****,* ***Richa*** *and* ***Aditya****) and extended family member* ***Dr. Ashish Yadav*** *and* ***Dr. Badal Durve*** *for always being there for me.* ***Arti Dixit****, you are always in my thoughts and I hope to keep feeling your loving gaze upon me for all time. I consider myself blessed to have such a beautiful family.*

Finally, I express my gratitude to the Almighty for the blessings and for providing special challenges.

-Ruchi Dixit

Table of Contents

List of Figures

List of Tables

Abbreviations

AIMD	*ab initio* Molecular Dynamics
B3LYP	Becke, 3-parameter, Lee-Yang-Parr
COSMO	Conductor-like Screening Model
DFT	Density Functional Theory
GGA	Generalized Gradient Approximation
IRC	Intrinsic Reaction Coordinate
IE	Interaction Energy
KS	Kohn-Sham
LDA	Local Density Approximation
MP2	Second-order Møller–Plesset Perturbation Theory
MARIJ	Multipole Accelerated Resolution of Identity
M06	Minnesota 06
NCI	Non-covalent Interactions
PBE	Perdew, Burke and Ernzerhof
PCM	Polarizable Continuum Model
RI	Resolution of Identity
SCF	Self-consistent Field
TZVP	Triple Zeta Valence plus Polarization
TS	Transition state

TOF	Turn over Frequency
TON	Turn over Number
HBpin	Pinacolborane
TMSCN	Trimethylsilyl cyanide

Physical Constants

Avogadro's Constant	$(N_A) = 6.02214129 \times 10^{23}\ mol^{-1}$
Atomic Mass Unit	$(u) = 1.660538921 \times 10^{-27}\ kg$
Boltzmann's Constant	$(k) = 1.3806488 \times 10^{-23}\ JK^{-1}$
Bohr Radius	$(a_0) = 5.291772109 \times 10^{-11}\ m$
Elementary Charge	$(e) = 1.602176565 \times 10^{-19}\ C$
Gas Constant	$(R) = 8.3144621\ JK^{-1}mol^{-1}$
Mass of Electron	$(m_e) = 9.10938291 \times 10^{-31}\ kg$
Mass of Proton	$(m_p) = 1.672621777 \times 10^{-27}\ kg$
Mass of Neutron	$(m_n) = 1.674927351 \times 10^{-27}\ kg$
Rydberg Constant	$(R) = 1.097373157 \times 10^{5}\ cm^{-1}$
Speed of Light	$(c) = 2.99792458 \times 10^{8}\ ms^{-1}$
Planck's Constant	$(h) = 6.62606957 \times 10^{-34}\ Js$

Chapter 1

A Brief Introduction about Nucleophilic attack Chemistry in Main Group Transformations

Chapter 1

A Brief Introduction about Nucleophilic attack Chemistry in Main Group Transformations

Abstract

The chemistry of main group compounds has grown in the last decade as a viable alternative to the chemistry of less abundant and toxic transition metal complexes. In the past few years, it has been found that compounds derived from main group elements are efficient for the catalysis of a varied class of reactions such as hydroboration, cyanosilylation, polymerization and alkene hydrogenations. Moreover, recent reports demonstrating catalyst-free and solvent-free hydroboration and cyanosilylation reactions have attracted a significant amount of attention from the scientific community. All the processes reported are interesting examples of reactions that occur through nucleophilic attack. Such selective nucleophilic attack chemistry also plays a key role in the working of molecular machines, as is also discussed in this thesis. However, in these research areas, the factors that affect the rate(s) of the reaction, i.e. the reaction mechanism, are not understood completely. The work discussed in the current thesis details computational studies that we have done in order to determine the mechanisms that are at play in these different systems. In this chapter, an overview of nucleophilic attack chemistry in main group chemistry and basic introductions of hydroboration chemistry, cyanosilylation chemistry, and molecular machines have been provided.

1.1 Introduction to nucleophilic attack chemistry

There are a plethora of reactions involved in the making of compounds in synthetic organic or inorganic chemistry, but none are as versatile as the nucleophilic substitution reactions. As the terminology suggests, it is a reaction involving a competition between a contender functional group and another group (or atom) that is attached to the parent compound. The contender, a nucleophile, is a chemical species with an unshared lone pair that it can share with the electrophile to make a covalent bond. In other words, it is a Lewis base. There are two broad classes of nucleophilic reactions: nucleophilic addition reactions and nucleophilic substitution reactions. As the reactions studied in this thesis pertain to addition chemistry, we will discuss basic nucleophilic addition reactions in brief. In a nucleophilic addition reaction, a nucleophile attacks an electrophilic carbon-containing π bond (having a sp^2 or sp hybridized carbon), leading to the formation of two additional σ bonds, as shown in **Figure 1.1** below.

Nucleophilic addition chemistry is of particular importance to carbonyl compounds, because, when there is an attack of a negatively charged nucleophile towards the electrophilic carbon center, there is no leaving group. This leads to electrons in the π bond being pushed towards the oxygen and the carbonyl carbon converting from sp^2 to sp^3 with a tetrahedral alkoxide intermediate state. This alkoxide can then be protonated by an acid to form an alcohol. For instance, with a carbonyl compound as an electrophile, the nucleophile can be water in hydration to a geminal diol[1] (hydrate), an organometallic nucleophile in the Grignard reaction,[2] or ylides in the Wittig reaction.[3]

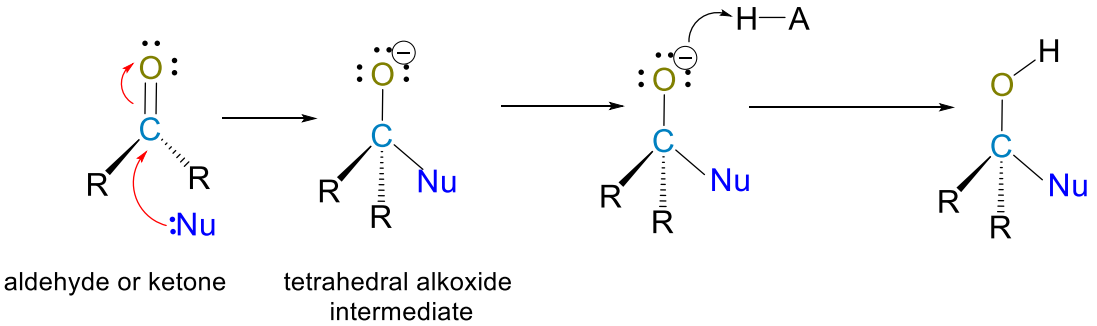

Figure 1.1 The mechanism of the nucleophilic addition reaction.

Other than the addition reaction, the other function that nucleophiles perform is that of a Lewis base: donating a lone pair of electrons, thereby leading to the formation of a bond to a proton (H^+). There are numerous reports where nucleophilic attack chemistry triggers the

reactants in the reaction, without their direct participation, leading to important products formation.

As reported by M. Wasa and coworkers,[4] for direct amination of carbonyl compounds, an atom- and step-economical approach has been found that involves *in situ* nucleophile generation.[5-7] They have used the strategy of a cooperative Lewis acid/Bronsted base catalyst, which leads to both deprotonation of a carbonyl pronucleophile and an enantioselective reaction.[5,8-10]

Recently, nucleophilic attack chemistry has been also explored in an interesting area of research: molecular machines (a detailed description of molecular machines is provided in a later section of this chapter). Base catalyzed chemistry[11-12] has been employed in different reaction mechanisms with the intent of making molecular machines functional and "net-drectional" in nature.

1.2 Main group compounds as an alternative to transition metal complexes

Transition metal catalysts[13] have been the staple of the industry for decades, as they provide excellent regio-[14], stereo-[15], and chemo-[16] selectivity with reduced energy consumption. This is due to the transition metals having multiple oxidation states and their ability to form different complexes for use in both homogeneous[17] and heterogeneous[18] catalysis. But the use of these entities has its own set of drawbacks, ranging from high cost, the low abundance of some key metals, and the ever-present toxicity issues with these elements. This has propelled researchers to look for alternatives to the transition metals, and main group elements[19] have come to the fore riding high on their recent successes with oxidative additions[20], reductive eliminations[21,] and insertions[22] and could prove to be the next big step in environmentally green catalysis. The main group elements consist primarily of s and p block elements such as calcium, magnesium, boron, phosphorus and aluminium, and they have been utilized extensively for homogeneous catalysis in the form of frustrated Lewis pairs[23] (FLPs) or as low valent compounds.[24] As shown by Fontaine and coworkers[25], amine-borane FLPs have been catalyzed the borylation of aromatic heterocycles through C-H activation, driven by H_2 release, as shown in **Figure 1.2** below. Calcium and magnesium, especially, have been shown to perform much efficiently in reactions like polymerization,[26] hydroboration,[27] alkene hydrogenations,[28] imine hydrosilylation[29] or Mannich-type reactions[30].

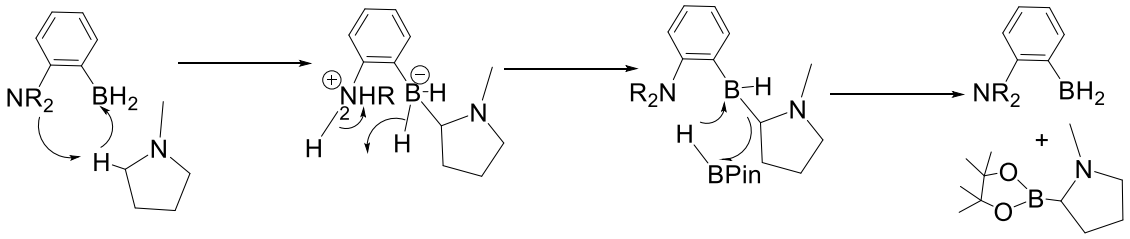

Figure 1.2 The mechanism for borylation catalyzed by FLP, in a report by Fontaine and coworkers.[25]

As catalysis with the aid of main group complexes is fairly new, there is a dearth of mechanistic studies of the processes involved, and of the factors that influence their reaction rates, which makes them a fertile ground for computational investigations.[31] Control of these factors, as well as a thorough understanding of their effect on molecular behavior would provide us with insight that would help improve both the turnover number (TON) and the yield of the reactions. Such mechanistic investigations can be done through computational chemistry, which is a powerful approach for investigating reaction pathways and for predicting product formation. Thus, computational methods could be applied to unravel two important aspects of chemical reactions: the structure and reactivity of systems. This is the main focus of this thesis: to understand the chemistry behind various nucleophilic reactions through computational chemistry. In order to understand the nucleophilic attack chemistry with main group compounds, computational investigations have been carried out with density functional theory (DFT)[32-33] calculations. DFT can handle large chemical systems with high accuracy, due to which it has emerged as a very powerful tool to study the kinetics and thermodynamics of various reactions. The fundamentals of DFT have been discussed in detail in the second chapter of this thesis.

1.2.1 Hydroboration reaction through main group compounds:

The hydroboration reaction[34] was developed by H.C. Brown in 1961, who went on to win the Nobel Prize for his efforts in 1979. This important reaction introduced organoboranes to mainstream chemistry as versatile intermediates. It refers to the addition of a boron-hydrogen (B-H) bond across unsaturated bonds like alkenes, alkynes, carbonyls and nitriles (C=C, C≡C, C=O, C≡N), thereby forming a class of organoboron compounds. It has been utilized extensively in the area of metal-catalyzed hydroboration. These hydroboration reactions are of importance to academia and industry alike, where they are frequently employed in material

synthesis, or for the production of industrial commodities. They are often involved in the synthesis of complex molecules. Classic examples include the oxidative addition of catecholborane (HBcat, 4,4,6-trimethyl-1,3,2-dioxaborinane) to alkenes, which is selective in the presence of the Wilkinson catalyst ($Rh(PPh3)_3Cl$) reported by Kono and Ito.[35] When the reaction is performed in the absence of the metal catalyst, the carbonyl group gets reduced.

However, as discussed above, we need to move away from transition metal complexes and towards main group compounds. Several efforts have emerged in this regard. Calcium compounds of the type LCaR have been widely utilized in hydroboration chemistry. Here, L is the spectator group and R is the reactive species. The chemistry of calcium is very similar to some of the trivalent and redox inactive lanthanides such as Yb^{2+}, given its stable $^{2+}$ oxidation state and its d^0 electronic configuration. The Lewis acidity of Group 2 elements is very similar to that of lanthanides as well. The two principal mechanistic steps in calcium compound chemistry are the σ bond metathesis and the polarized insertion, with the substrate polarity determining the catalytic pathway. The nucleophilicity exhibited by the calcium compounds rivals that of group 1 reagents, which is useful in performing important attack chemistry. Calcium is an important metal to replace the transition metals in catalysis due to its abundance, biocompatibility, its conversion to harmless materials (like $CaCO_3$ and $Ca(OH)_2$), and the promise it has shown in the last decade.

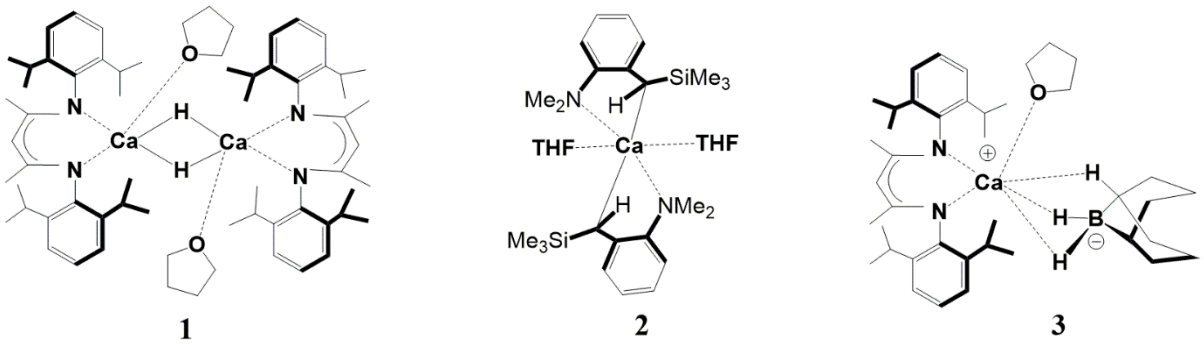

Figure 1.3 Catalysts developed by Harder and Spielmann.[36]

A preliminary study by Harder and Spielmann in 2012 (as shown in **Figure 1.3** above) took three different organocalcium catalysts[36] – **1**. $[DIPPnacnacCaH\cdot(THF)]_2$ (DIPPnacnac = $CH\{(CMe)(2,6\text{-}iPr2C_6H_3N)\}_2$), **2**. $Ca[2\text{-}Me_2N\text{-}\alpha\text{-}Me_3Si\text{-}benzyl)_2\cdot(THF)_2$ and **3**. DIPPnacnacCa(H-BBN)·(THF) (BBN = 9-borabicyclo[3.3.1]nonane) to determine whether the hydroboration of 1,1-diphenylethyelene with catecholborane took place at elevated

temperatures. Although 96% conversion was observed, the reaction product obtained was not the expected $Ph_2CH_2CH_2Bcat$ but $(Ph_2CHCH_2)_3B$. This is due to the decomposition of HBcat to B_2cat_3 and BH_3 in the presence of the organocalcium catalyst, with BH_3 then facilitating the hydroboration reaction. This study, though flawed, opened up the gates for the use of calcium based compounds as catalysts for hydroboration. In 2017, an interesting work was published by Sen and coworkers[37] where they developed an amidinato stabilized monomeric calcium iodide complex $[PhC(NiPr)_2CaI]$ for the hydroboration of carbonyl compounds with HBpin. The reaction was rapid at room temperature with most solvents to form alkoxypinacolboronate esters, but the best conversion was obtained through benzene at 95.0%. High chemoselectivity of this catalyst was also shown when a mixture of benzaldehyde and acetophenone was taken with 1 equivalent of catalyst and the hydroboration of only benzaldehyde was seen, with acetophenone being fully recycled (when 2 equivalents of catalyst were taken, both products were formed). Recently in 2020, another report was published by Steffen and coworkers[38] where they studied the effect of ligands in the calcium catalyzed carbonyl hydroboration. The structure of the organocalcium compound was ^{t}BuAmDIPPCaX, where amidinate ^{t}BuAmDIPP is the spectator ion and X could be (1) I^-, (2) $[B(C_6F_5)_4]^-$, (3) $(Me_3Si)_2N^-$ or (4) H^-. The activities of the complexes governed by the ligand increase along the series $I^- < B(C_6F_5)4^- < (Me_3Si)_2N^- \approx H^-$. The Lewis acidity of the metal plays a major role in the catalyst activities in the first two instances but ligands $X^- = (Me_3Si)_2N^-$ or H^- are superior by far, as is also observed in their magnesium based counterparts.

1.2.1.1 Hydroboration of carbonyl compounds

Hydroboration of carbonyl compounds is an important reaction, as it reduces carbonyls to alcohols with the added benefit of selectivity and reaction yield compared to hydrogenation or other reduction processes. Traditionally, transition metal complexes[39] used in these hydroboration reactions are derived from rhodium, iridium, ruthenium and even some zinc, copper, and gold complexes. In the metal-free hydroboration arena, the Corey-Bakshi-Shibata[40] catalyst has been widely used for the selective asymmetric reduction of ketones. Woodward and coworkers[41] were one of the first to report the use of a main group compound, a chiral Ga-complex ($LiGa(MTB)_2$) (combination of lithium gallium hydride, $LiGaH_4$, and 2-hydroxy-2′-mercapto-1,1′-binaphthyl, (R)-(−)-$MTBH_2$), to catalyze the enantioselective reduction of prochiral ketones. Several reports for the hydroboration of carbonyl compounds using alkaline earth metal-based catalysts have surfaced after magnesium alkyl complexes[42] were successfully used in carbonyl hydroboration. Group 1 compounds are somewhat in their

infancy for their use in this important catalytic reaction, but lithium compounds have proved to be useful as single-component catalysts, as shown through the studies conducted by the groups of Mulvey[43] and Okuda.[44] Many reports with p-block elements, such as P, Al, Ge, Sn, Pb have emerged, where they too have been shown to act as single-site catalysts[45] in carbonyl hydroboration reactions, which has enhanced research interest in such systems.

The hydroboration of amides and ester substrates is an uphill task when compared to the facile hydro-functionalization of other unsaturated compounds, aldehydes, and ketones. Their hydroboration reactions are important in the bulk production of amines and alcohols, as the starting materials are stable and relatively inexpensive.[46] The successive catalytic reduction of amides with HBpin was reported by Sadow and coworkers[47] using a magnesium complex, ToMMgMe. Concurrently, Panda and coworkers[48] reported the same reaction with an aluminium complex, but both of these strategies could only reduce tertiary and secondary amides. In 2020, Mandal and coworkers[49] published a report where they were able to reduce a slew of primary amides with pinacolborane successfully, using a combination of an abnormal NHC and potassium complex as the catalyst. Similar to amides, esters also remain inert in the presence of the mild reducing agent and require relatively harsher reducing agents[50] such as BH_3 and $LiAlH_4$, or metal-catalyzed hydrogenation. These approaches require a significantly higher temperature, with high pressure, and are both costly and pose threats to safety. Thus, the amount of research for the selective hydroboration of ester has remained lackluster, but for a few illuminating reports with magnesium-based catalysts through Herculean efforts of the groups of Sadow,[51] Okuda,[52] Nebennna[53] and Ma.[54]

1.2.2 Cyanosilylation of carbonyl compounds

Similar to hydroboration, the cyanosilylation of carbonyl compounds is an important chemical reaction for the synthesis of diverse compounds such as esters, α-hydroxy acids, acyloins and other biologically active molecules. This reaction proceeds through the addition of the cyano (-CN) and silyl (-$SiMe_3$) groups across the C=O bond, as shown in **Figure 1.4** below, giving rise to a silylated cyanohydrin that could be functionalized to obtain required compounds.

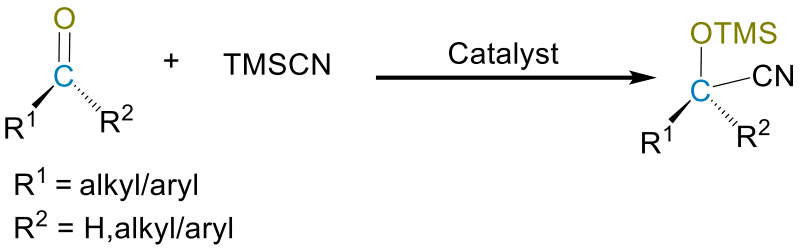

Figure 1.4 The cyanosilylation of carbonyl compounds.

Trimethylsilyl cyanide (TMSCN) is a popular cyanating agent for this process, as it is inherently safer than toxic cyanides like HCN or KCN. For the efficient transfer of the cyanide group from TMSCN[55] to carbonyl in this reaction, many catalysts have been employed, including Lewis acids, Lewis bases, metal halides, metal alkoxides, inorganic salts and iodine. Shibasaki and coworkers[56] introduced a novel Lewis acid-Lewis base bifunctional catalyst for the asymmetric cyanosilylation of aldehydes, whereas the same was achieved by Corey and coworkers[57] using a chiral oxazaborolidinium salt as the catalyst. A few reports exist where heavier main group compounds have been shown to act as single-site catalysts. These include the efforts of Roesky,[58] Zhi,[59] Nagendran[60] and others, but even then, the majority of reactions proceeded only in the case of aldehydes. The field of catalytic cyanosilylation through the use of alkaline earth metals is even more barren, with only two recent independent reports in 2018 – one from Ma and coworkers[61] where they used magnesium(I) complex, $\{(Xylnacnac)Mg\}_2$ (Xyl = 2,6-Me_2-C_6H_3), and the other report from Sen and coworkers[62] using a monomeric calcium complex, $PhC(NiPr)_2CaI$.

1.3 Hydroboration and cyanosilylation in solvent-free and catalyst-free conditions

Recent investigations have revealed that the hydroboration of carbonyl compounds can be achieved quantitatively without the need for any solvent or catalyst and that, interestingly, the addition of the solvent leads only to trace amounts of the product. In 2018, an experimental report by Hreczycho and coworkers[63] was published, where they demonstrated the catalyst-free and solvent-free hydroboration of aldehydes. They noted that the hydroboration of benzaldehyde in the absence of solvent and catalyst afforded the corresponding boronate exclusively in 95% yield. However, they also reported that the addition of toluene in the reaction mixture led to only a trace amount of the product, which is in agreement with the previous observations. Later, another group, Wang and co-workers,[64] have reported the hydroboration of ketones with HBpin, in the absence of solvent and catalyst, taking

acetophenone as the ketone. Similarly, there were three concurrent reports by Panda and coworkers[65], Ma and coworkers[66], and Xue and coworkers[67] on the hydroboration of carboxylic acid in solvent-free and catalyst-free reaction conditions, where they, too, obtained high product yields. Ma and coworkers have also supported their work with DFT based calculations and reported the mechanistic pathway. However, the kinetic barriers reported by them at room temperature are higher than the acceptable range. Lastly, hydroboration of imines has also been reported in the absence of solvent and catalyst by Rit and coworkers.[68]

There have been efforts for solvent-free and catalyst-free reactions other than hydroboration. Leung and coworkers[69] have reported a cyanosilylation reaction in these conditions where they have taken aldehyde as a substrate and TMSCN as a cyanating reagent for the reaction.

These reports have sparked considerable interest in the experimental world resulting in numerous reports emerging within the space of a year, where similar chemistry was reported for a wide variety of substrates under solvent and external catalyst-free conditions. But several unanswered questions need to be addressed for this emerging area:

(1) How does this remarkable chemistry occur, without the need for any external catalyst or solvent? Are there common principles at play in this wide range of reactions?

(2) If so, what are they, and once known, can they be exploited to design new systems where such chemistry can be expanded to external catalyst-free transformations in solution, i.e. closer and more relevant to the experimental conditions in catalysis?

The current work addresses these relevant questions. First, with high-level quantum chemical calculations with density functional theory (DFT) on a wide range of systems, we have shed light on the general mechanism involved in these reactions. We have shown this for two different important functionalization reactions: hydroboration, in Chapter 4, as well as cyanosilylation, in Chapter five of this thesis.

1.4 Molecular Machines

Nature inspires humans, giving birth to artificial objects. The development of ‘molecular machines’ is no exception to this, as it derives its inspiration from the inestimable number of motor proteins carrying out biological work in the live miniscule factory we call the cell.[70] A ‘molecular machine’ is a nanoscale chemical system in which an external stimulus triggers the controlled movement of one molecular or submolecular segment relative to others,

possibly leading to a task being executed by the whole system.[71] Molecular machines are broadly classified into two categories:

1. Molecular Switches – in this type molecular machine, the system is influenced by the change in relative positions of its components as a function of the state of the switch.
2. Molecular Motors – similarly, in motors too, the system is influenced by the change in relative positions of its components, but as a function of the trajectory of its components.

Unlike molecular switches, the work done during the molecular motor's return to its original state is carried forward and not undone. This entails that a molecular motor is capable of performing work progressively, driving the system away from its equilibrium condition. For this property, multitudes of researchers gravitate towards molecular motors but, ironically, these motors are not influenced by the effect of gravity or inertia as the Brownian motion and viscous forces dominate at their operating conditions.[72] Directed motion through these machines is governed by thermal fluctuations in the system and can be influenced by employing ratchet mechanisms, which could be either energy ratchets,[73] or information ratchets.[74]

Several 'molecular walker' mimics were developed by researchers to achieve this net linear directionality[75] based on dynein and kinesin families of the motor proteins that walk on a track. The set of requirements these 'walkers' should fulfill are (a) processivity – the walker should have at least one contact point with the track during its movement, (b) directionality – the movement has to be towards one end of the track, (c) repetitive operation – similar mechanical tasks should be repetitively performed, (d) progressive operation – when the molecular walker returns to its original state at the end of a mechanical cycle, physical work done by it during the cycle should not be undone, (e) autonomous operation – the walker should keep on moving as long as the fuel is present without the need of external intervention.

Leigh and coworkers[76] reported the first synthetic small molecule walker, which had two legs and moved processively over a four-foothold molecular track. This walker was regulated by the change in pH of the system, helped by disulfide and hydrozone exchange reactions with the track. As the directionality for the system was not yet optimal due to the reversibility of disulfide exchange, it was changed to a two-step irreversible redox reaction, culminating in the 43.0% of walkers reaching the end of the track in 1.5 cycles compared to only 19.0% in 3 cycles when disulfide was employed.

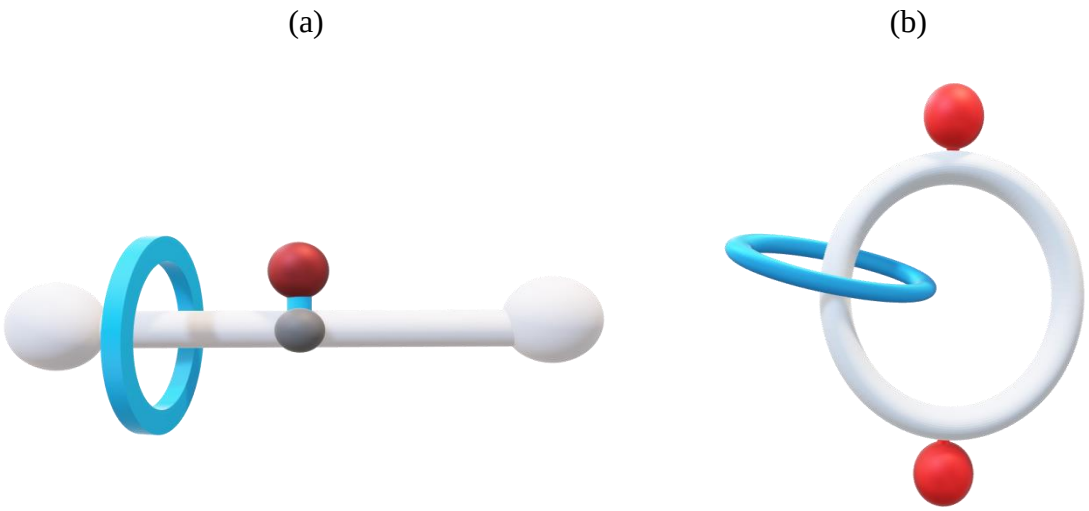

Figure 1.5 (a) A simple rotaxane is made with a ring passing through an axle, in order to prevent the dethreading of the axle, and ring bulky groups are placed at the end. (b) A simple catenane consisting of macrocyclic rings passing through each other. (The number of rings and axle can be more than one in both the rotaxane and the catenane).

Another subclass of molecular motors that comprises of mechanically interlocked molecular components are rotaxanes and catenanes, as shown in **Figure1.5** above. A simple rotaxane has two components: one molecular ring threading a linear molecule functioning as an axle, with two bulky groups at both ends to prevent the ring from leaving the axle. A catenane, on the other hand, has two molecular rings interlocked. Unlike molecular walkers, the motion in rotaxanes and catenanes is inherently processive, and as the freedom of the ring movement is curtailed in two directions, all the energy of the system is utilized for the translational motion. An example of this is shown in **Figure 1.6** below, which was introduced by Leigh and coworkers[76] as the first [2]rotaxane with a ratchet mechanism. The thread here contains two 'stations' –fumaramide and succinamide groups which are partitioned with a relatively bulky silyl ether group. The macrocycle 'ring' can be relocated within the system by attaching and detaching the silyl ether group while simultaneously applying an external stimulus (photoisomerization or thermal isomerization) during the detached phase. A similar approach is utilized by them again in a report where they have tried to achieve net directionality using chemical fuel[77] as an external stimulus for a [2]catenane system, which will be discussed in detail in Chapter 6 of this thesis.

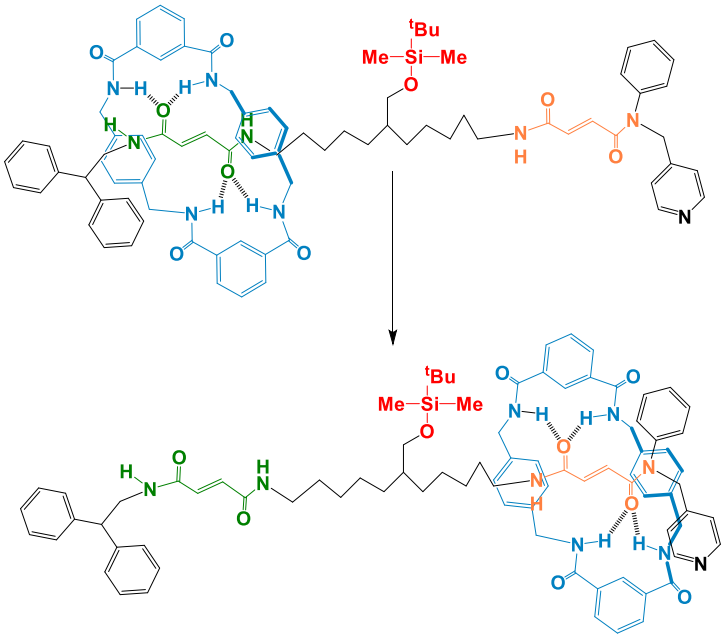

Figure 1.6 The [2] rotaxane designed by Leigh and coworkers[76] operating with a ratchet mechanism.

Among all the systems reported to date, not many computational studies have been done for the fuel-driven molecular motor. Recently Zhao and coworkers[78] have reported a full mechanistic study on a chemically driven simple rotary molecular motor with perfect unidirectionality. But still, there is a need to achieve unidirectionality in larger catenane and rotaxane-based molecular motors.

The current challenge faced in molecular machines is to convert their motion into suitable functions. One of the approaches to overcome the net directional motion being zero is to mount these machines to a surface. Successful implementation of these has been shown where even surface wettability of the terrain was achieved. Other exciting results have been the introduction of nanovehicles (an example being the 'nanoroadster' developed by Tour and coworkers[79]), which can move on the surface when photoinduced, and the movement of a small glass rod (5 x 28 μm) using an alkene based rotary motor.

1.5 Statement of Problem:

Important questions can be asked concerning the chemical systems that have been mentioned in this chapter:

- What is the mechanistic pathway through which calcium compounds act as catalysts for the hydroboration of aldehyde and ketone?
- Does the β-diketiminato ligand with a methyl-pyridine sidearm in the calcium compound have a specific role to play in the catalysis of the hydroboration reaction?
- If the catalysis is done through the β-diketiminato ligand with a methyl-pyridine sidearm of the calcium complex, then what is the role of the calcium metal center?
- Why is a high yield of the hydroboration reaction achieved in the absence of the solvent and an external catalyst? Why does the yield drop when the solvent is introduced into the system?
- Is there any way by which we can achieve a high yield for the hydroboration in the presence of the solvent but in the absence of an external catalyst?
- In order to explain the hydroboration in the absence of the solvent and external catalyst, we have proposed a hypothesis wherein the HBpin acts not only as one of the reactants but also as the "solvent", as well as the "internal" catalyst. As the cyanosilylation reaction is also known to occur with a high yield in solvent-free and catalyst-free conditions, does the same hypothesis also apply for cyanosilylation?
- David Leigh and coworkers, in their work on an interesting molecular system that performs with a net directionality, reveal a sophisticated kinetic model that makes important assumptions about the behavior of different components of the system. Do such assumptions actually all hold true in their system? If not, is there some other mechanism at play, a mechanism that, perhaps, is even more sophisticated than what they have proposed?

In this thesis, we have attempted to answer these questions through computational investigations, followed by experimental corroboration by our collaborators (for certain systems, as detailed in Chapters 3, 4, and 5). Chapter 6, on the other hand, deals with computational findings for an experimentally reported molecular machine system.

1.6 Objectives of this Thesis

A large amount of the chemical reactions take place in the presence of nucleophiles, and nucleophile attack chemistry has been seen to play a distinct part in the chemistry of main group compounds. The reason why the hydroboration and the cyanosilylation reactions yield a high product in solvent-free and external catalyst-free conditions for various substrates reported had not been fully understood. Moreover, the mechanistic details for the molecular motor designed by David Leigh and coworkers, which also depends in part on nucleophilic attack, are not fully understood. In this thesis, we have tried to shed light on these aspects of nucleophilic attack chemistry:

- We have attempted to find the mechanistic pathway for the experimentally observed catalysis with a calcium compound having a β-diketiminato ligand with a methyl-pyridine side arm, employed for the hydroboration of aldehydes and ketones.

- We have tried to deduce why, in solvent and catalyst-free conditions, a high yield of the hydroboration reaction is achieved, and proposed a way to replicate the same in the presence of the solvent, a proposal that has subsequently been proved by experiments by our collaborators.
- We have tried to show how the same hypothesis works for another important reaction - cyanosilylation - in the presence of solvent without any external catalyst.
- We have endeavoured to determine the real function of various components of a molecular machine designed by David Leigh and coworkers and gain insight by studying the actual pathway by which the system operates, insights that can be employed to design better molecular machines in the future.

Hence, in this thesis, we have served to illustrate the vital role of nucleophilic attack chemistry in main group complexes for two very important reactions: hydroboration and cyanosilylation, and also demonstrated its significance in molecular machines.

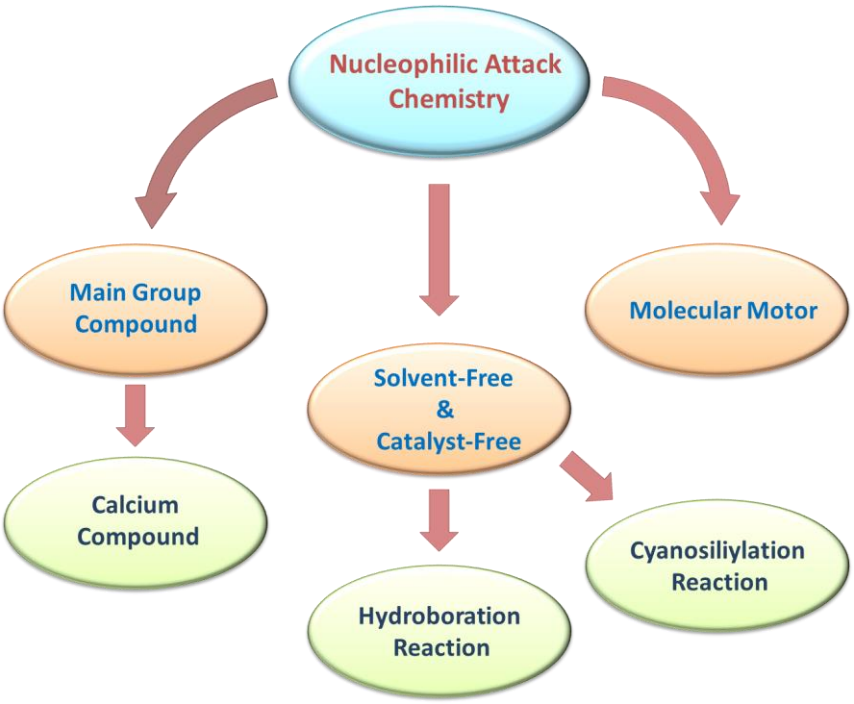

Figure 1.7 Structural representation of the role of the nucleophilic attack chemistry in the main group transformations studied in the current thesis.

1.7 Organization of the Thesis

This thesis is divided into seven chapters.

Chapter-1: A Brief Introduction about Nucleophilic attack Chemistry in Main Group Transformations

In this chapter, a brief introduction to nucleophilic chemistry in main group compounds has been discussed. Mainly, nucleophilic addition reactions are focused upon in this chapter, as in this thesis work, we have computationally investigated the hydroboration reaction (discussed in detail in Chapters 3 and 4) and the cyanosilylation reaction (discussed in detail in Chapter 5), which can be classified under nucleophilic addition reactions. Lastly, we have discussed a molecular machine system, as we have also shown the significance of selective nucleophilic attack chemistry in molecular machines (discussed in detail in Chapter 6).

Chapter-2: Fundamentals Computational Chemistry

This chapter deals with the fundamentals of quantum mechanical methods (QM), density functional theory (DFT), *ab initio* molecular dynamics (AIMD), volume correction methods, turn over frequency (TOF) calculations, and non-covalent interaction (NCI) plots.

Chapter-3: Alkaline Earth Metal Compounds of Methylpyridinato *β* Diketiminate Ligands and Their Catalytic Application in Hydroboration of Aldehydes

In this chapter is discussed a catalytic system: a calcium compound having a *β*-diketiminato ligand with a methyl-pyridine side arm, which is known to act as a catalyst for the hydroboration of a wide range of aldehydes using pinacolborane (HBpin) at room temperature. Employing DFT calculations, we have explained the experimental observations and found that in the presence of this calcium compound, the barrier for the hydroboration of aldehydes and ketones becomes favorable at room temperature and hence the complex can act as a catalyst. Subsequent experimental studies have explored the computational predictions by studying hydroboration with a calcium-based catalyst, and have demonstrated that the yield is indeed enhanced in the presence of the catalyst. The role of the calcium centre in this chemistry is therefore to bind two ligands, each of which is then capable of acting as a catalytic site for the hydroboration. Therefore, the calcium enables the formation of a dual-site catalyst, which would be more efficient than just employing a pyridine moiety as a single-site catalyst in the reaction.

Chapter-4: Substrate, Catalyst, and Solvent: The Triune Nature of Multitasking Reagents in Hydroboration

Recent investigations have revealed that the hydroboration of unsaturated species can be achieved quantitatively without the need for any solvent or catalyst and that, interestingly, the addition of the solvent leads only to trace amounts of the product. This invites questions about the role of the solvent. Does the catalyst act to catalyze the hydroboration reaction or does it function to suppress the deleterious effects of the solvent? Employing DFT calculations, we have tried to explain what happens when the hydroboration reaction occurs in the absence of solvent and why it does not need any external catalyst to give a high yield. We discovered that the HBpin molecule in the absence of solvent acts as an internal catalyst in the hydroboration reaction. Further, we have predicted how the hydroboration activity in solution could be improved by increasing the concentration of HBpin, which then acts as one of the reactants in the reaction. Subsequent experimental studies by collaborators have explored the computational predictions by studying hydroboration with a 5:1 HBpin and benzaldehyde concentration of reactants. They found that the yield was indeed enhanced to almost 100% in the presence of solvent without using any catalyst.

Chapter-5: To Catalyze or Not to Catalyze: That is the Question in Main Group Compound Mediated Cyanosilylation

Another important chemical transformation of relevance to academia and industry is the nucleophilic addition reaction: cyanosilylation. From the insights gained from the case of the hydroboration reaction, we have tested the same hypothesis for the cyanosilylation reaction. We obtained an interesting mechanistic pathway, where the presence of an additional TMSCN molecule was seen to increase the efficiency of the cyanosilylation process, thereby acting, in effect, as a catalyst. This insight was corroborated by experimental studies by collaborators, who obtained a high yield of the cyanosilylated product in solution in the absence of an external catalyst. The current work, therefore, provides insights into how the important chemical transformations represented by cyanosilylation take place in neat TMSCN and uses this knowledge to further the field, by demonstrating how the same can take place in solution without the need for external catalysts.

Chapter-6: Subtle Interplay between the Different Components of a Molecular Machine Gives Rise to Directionality

Another interesting area of research that has captivated the scientific community over many decades is that of molecular machines. A major challenge faced by researchers in the design and development of new molecular machines is to control their directionality. The current work reports a computational study that delves into the mechanism by which net directionality has been achieved in an efficient catenane molecular machine reported by David Leigh and coworkers. Our studies reveal very calibrated interactions between the different components of the machine: the benzylic amide macrocycle (the “ring”) travelling along a larger cyclic ring (“the track”), fumaramide residues (the “glue”), and NEt_3.

Chapter-7: Conclusion and Future Outlook:

In this chapter, ways in which the work detailed in the thesis can be taken forward in the future have been discussed.

1.8 References:

1. E. Burevschi, I. Pena, M. E. Sanz, *J. Phys. Chem. Lett.*, **2021**, *12*, 12419.

2. R. M. Peltzer, J. Gauss, O. Eisenstein, M. Cascella, *J. Am. Chem. Soc*., **2020**, *142*, 2984.

3. D. Reiter, P. Frisch, T. Szilvasi, S. Inoue, *J. Am. Chem. Soc*., **2019**, *141*, 16991.

4. M. Shang, X. Wang, S. M. Koo, J.r. Youn, J. Z. Chan, W. Yao, B. T. Hastings, M. Wasa, *J. Am. Chem. Soc*., **2017**, *139*, 95.

5. (a) T. Vilaivan, W. Bhanthumnavin, *Molecules* **2010**, *15*, 917. (b) A. M. R. Smith, K. K. Hii, *Chem. Rev.* **2011**, *111*, 1637. (c) A. Vallribera, R. M. Sebastian, A. Shafir, *Curr. Org. Chem.* **2011**, *15*, 1539. (d) F. Zhou, F.-M. Liao, J.-S. Yu, J. Zhou, *Synthesis*, **2014**, *46*, 2983.

6. (a) M. Kanai, N. Kato, E. Ichikawa, M. Shibasaki, *Syn. lett.* **2005**, 1491. (b) H. Yamamoto, K. Futatsugi, *Angew. Chem., Int. Ed*. **2005**, *44*, 1924. (c) T. Akiyama, *Chem. Rev.* **2007**, *107*, 5744. (d) M. Terada, *Chem. Commun.* **2008**, 4097. (e) S. Kobayashi, Y. Mori, J. S. Fossey, M. M. Salter, *Chem. Rev.* **2011**, *111*, 2626. (f) B. M. Trost, Bartlett, M. J. Acc. *Chem. Res.* **2015**, *48*, 688. (g) M. Shibasaki, N. Kumagai, In Cooperative Catalysis: Designing Efficient Catalysts for Synthesis; Peters, R., Ed.; Wiley-VCH: New York, **2015**; Chapter 1.

7. (a) Y. Takemoto, *Org. Biomol. Chem.* **2005**, *3*, 4299. (b) M. S. Taylor, E. N. Jacobsen, *Angew. Chem., Int. Ed.* **2006**, *45*, 1520. (c) A. G. Doyle, E. N. Jacobsen, *Chem. Rev.* **2007**, *107*, 5713. (d) S. Mukherjee, J. W. Yang, S. Hoffmann, B. List, *Chem. Rev.* **2007**, *107*, 5471.

8. (a) D. A. Evans, S. G. Nelson, *J. Am. Chem. Soc.*, **1997**, *119*, 6452. (b) M. Marigo, K. Juhl, K. A. Jorgenson, *Angew. Chem., Int. Ed.* **2003**, *42*, 1367. (c) T. Mashiko, K. Hara, D. Tanaka, Y. Fujiwara, N. Kumagai, M. Shibasaki, *J. Am. Chem. Soc.* **2007**, *129*, 11342. (d) T. Mashiko, N. Kumagai, M. Shibasaki, *J. Am. Chem. Soc.* **2009**, *131*, 14990. (e) S. Mouri, Z. Chen, H. Mitsunuma, M. Furutachi, S. Matsunaga, M. Shibasaki, *J. Am. Chem. Soc.* **2010**, *132*, 1255. (f) W. Li, X. Liu, X. Hao, X. Hu, Y. Chu, W. Cao, S. Qin, C. Hu, L. Lin, X. Feng, *J. Am. Chem. Soc.* **2011**, *133*, 15268.

9. (a) S. Saaby, M. Bella, K. A. Jorgensen, *J. Am. Chem. Soc.* **2004**, *126*, 8120. (b) X. Liu, H. Li, L. Deng, *Org. Lett.* **2005**, *7*, 167. (c) X. Xu, T. Yabuta, P. Yuan, Y. Takemoto, *Synlett* **2006**, *137*. (d) Y. Hasegawa, M. Watanabe, I. D. Gridnev, T. Ikariya, *J. Am. Chem. Soc.* **2008**, *130*, 2158. (e) H. Konishi, T. Y. Lam, J. P. Malerich, V. H. Rawal, *Org. Lett.* **2010**, *12*, 2028. (f) M. Terada, K. Amagai, K. Ando, E. Kwon, H. Ube, *Chem. - Eur. J.* **2011**, *17*, 9037. (g) Y.

Hasegawa, I. D. Gridnev, T. Ikariya, *Bull. Chem. Soc. Jpn.* **2012**, *85*, 316. (h) T.Takeda, M. Terada, *J. Am. Chem. Soc.* **2013**, *135*, 15306. (i) C. Xu, L. Zhang, S. Luo, *Angew. Chem., Int. Ed.* **2014**, *53*, 4149. (j) H. M. Nelson, J. S. Patel, H. P. Shunatona, F. D. Toste, *Chem. Sci.* **2015**, *6*, 170. (k) X. Yang, F. D. Toste, *J. Am. Chem. Soc.* **2015**, *137*, 3205.

10. (a) A. Bogevig, K. Juhl, N. Kumaragurubaran, W. Zhuang, K. A. Jorgensen, *Angew. Chem., Int. Ed.* **2002**, *41*, 1790. (b) B. List, *J. Am. Chem. Soc.* **2002**, *124*, 5656. (c) N. Kumaragurubaran, K. Juhl, W. Zhuang, A. Bogevig, K. A. Jorgensen, *J. Am. Chem. Soc.* **2002**, *124*, 6254. (d) N. S. Chowdari, D. B. Ramachary, C. F. Barbas, *Org. Lett.* **2003**, *5*, 1685. (e) Y. Hayashi, S. Aratake, Y. Imai, K. Hibino, Q.-Y. Chen, J. Yamaguchi, T. Uchimaru, *Chem. - Asian J.* **2008**, *3*, 225.

11. L. Zhang, V. Marcos, D. A. Leigh, *PNAS*, **2018**,*115*, 9397.

12. M. Wilson, J. Sola, A. Carlone, S. M. Goldup, N. Labrasseur, D. A. Leigh, *Nature*, **2016**, *534***,** 235.

13. (a) I. Beletskaya, A. Pelter, *Tetrahedron* **1997**, *53*, 4957. (b) N. Miyaura, in Catalytic Heterofunctionalization, ed. A. Togni, H. Grützmacher, Wiley-VCH,Weinhein, 2001, pp. 1–46. (c) C. M. Vogels, S. W. Westcott, *Curr. Org. Chem.* **2005**, *9*, 687–699.

14. (a) D.A. Evans, G.C. Fu, A. H. Hoveyda, *J. Am. Chem. Soc.* **1988**, *110*, 6917. (b) S.A. Westcott, H.P. Blom, T.B. Marder, R.T. Baker, *J. Am. Chem. Soc.* **1992**, *114* 8863. (c) D.A. Evans, G.C. Fu, A.H. Hoveyda, *J. Am. Chem. Soc.* **1992**, *114*, 6671.

15. (a) K. Burgess, M. J. Ohlmeyer, *Tetrahedron Lett.* **1989**, *30*, 395. (b) K. Burgess, J. Cassidy, M.J. Ohlmeyer, *J. Org. Chem.* **1991**, *56*, 1020. (c) K. Burgess, M.J. Ohlmeyer, J. Org. Chem. 1991, 56, 1027.

16. D. Mannig, H. Noth, *Angew. Chem. Int. Ed. Engl.* **1985**, *24*, 878.

17. Obligacion, J.V., Chirik, P.J. *Nat Rev Chem* **2018**, *2***,** 15.

18. Youqi Zhu, Tai Cao, Chuanbao Cao, Jun Luo, Wenxing Chen, Lirong Zheng, Juncai Dong, Jian Zhang, Yunhu Han, Zhi Li, Chen Chen, Qing Peng, Dingsheng Wang, and Yadong Li. *ACS Catalysis* **2018,** *8*, 10004.

19. (a) P. P. Power, *Chem. Rec.* **2011**, *12*, 238. (b) T. Chivers, J. Konu, *Comments Inorg. Chem.* **2009**, *30*, 131. (c) S. Yao, Y. Xiong, M. Driess, *Organometallics* **2011**, *30*, 1748. (d) D. W. Stephan, *Org. Biomol. Chem.* **2008**, *6*, 1535.

20. T. Chu, G. I. Nikonov *Chemical Reviews* **2018,** *118*, 3608.

21. R. Rodriguez, Y. Contie, R. Nougue, A. Baceiredo, N. S. Merceron, J.-M. Sotiropoulos, T. Kato, *Angew. Chem., Int. Ed.* **2016**, *55*, 14355.

22. J. D. Erickson, J. C. Fettinger, P. P. Power, *Inorg. Chem.* **2015**, *54*, 1940.

23. D. W. Stephan, *J. Am. Chem. Soc.* **2015**, *137*, 10018–10032.

24. (a) A. Jana, G. Tavcar, H. W. Roesky, M. John, *Dalton Trans.* **2010**, *39*, 9487. (b) K. Leszczynska, A. Mix, R. J. F. Berger, B. Rummel, B. Neumann, H.-G. Stammler, P. Jutzi, *Angew. Chem. Int. Ed.* **2011**, *50*, 6843.

25. M.-A. Courtemanche, M.-A. Legare, L. Maron, and F.-G. Fontaine *Journal of the American Chemical Society,* **2013,** *135*, 9326.

26. N. Ebadipour , S. Paul , B. Katryniok, F. Dumeignil, *Catalysts* **2021**, *11*, 1247.

27. (a) F. Buch, J. Brettar, S. Harder, *Angew. Chem. Int. Ed.*, **2006**, *45*, 2741. (b) J. Spielmann, F. Buch, S. Harder, Angew. Chem. Int. Ed., **2008**, *47*, 9434. (c) M. R. Crimmin, I. J. Casely, M. S. Hill, *J. Am. Chem. Soc.*, **2005**, *127*, 2042. (d) S. Datta, P. W. Roesky, S. Blechert, *Organometallics*, **2007**, *26*, 4392. (e) S. Datta, M. T. Gamer, P. W. Roesky, *Organometallics*, **2008**, *27*, 1207.

28. (a) F. Buch, S. Harder, Z. Naturforsch. B, **2008**, 63, 169. (b) J. Jenter, R. Köppe, P. W. Roesky, *Organometallics*, **2011**, *30*, 1404. (c) M. Arrowsmith, M. R. Crimmin, A. G. M. Barrett, M. S. Hill, G. Kociok- Köhn, P. A. Procopiou, *Organometallics*, **2011**, *30*, 1493. (d) T. D. Nixon, B. D. Ward, *Chem. Commun*., **2012**, *48*, 11790. (e) B. Liu, T. Roisnel, J.-F. Carpentier, Y. Sarazin, *Chem. Eur. J.*, **2013**, *19*, 2784.

29. (a) C. Glock, F. M. Younis, S. Ziemann, H. Gorls, W. Imhof, S. Krieck, M. Westerhausen, *Organometallics*, **2013**, *32*, 2649. (b) M. R. Crimmin, A. G. M. Barrett, M. S. Hill, P. B. Hitchcock, P. A. Procopiou, *Organometallics*, **2007**, *26*, 2953. (c) B. Liu, J.-F. Carpentier, Y. Sarazin, *Chem. Eur. J.*, **2012**, *18*, 13259. (d) S. Harder, *Chem. Rev.*, **2010**, *110*, 3852. (e) 19. M. S. Hill, D. J. Liptrot, C. Weetman, *Chem. Soc. Rev*., **2016**, *45*, 972.

30. W. Wang, M. Luo, J. Li, S. A. Pullarkat, M. Ma, *Chem. Commun.*, **2018**, *54*, 3042.

31. b) N. Kuriakose, K. Vanka, *Dalton Trans.* **2014**, *43*, 2194; c) Y. Wang, J. Ma, *Journal of Organometallic Chemistry*, **2009**, *694*, 2567.

32. a) M. H. N. Assadi, D. A. H. Hanao *J. Appl. Phys*. **2013**, *113*, 233913; b) M. D.Segall, P. J. D. Lindan, M. J. Probert, C. J. Pickard, P. J. Hasnip, S. J. Clark, M. C. Payne, *J. Phys: Condens. Matter*, **2002**, *14*, 2717; c) J. P. Perdew, K. Schmidt, *AIP Conf. Proc*. **2000**, *577*, 1.

33. a) F. R. Somayeh, H. Soleymanabadi, *J. Mol. Model*. **2014**, *20*, 2439; b) F. R. Somayeh, H. Soleymanabadi, *J Mol Model*, **2013**, *19*, 3733; c) D. Music, R. W. Geyer, J. M. Schneider, *Surface & Coatings Technology*, **2016**, *286*, 178.

34. H.C. Brown, *Tetrahedron*. **1961**, *12*, 117.

35. H. Kono, K. Ito, *Chem. Lett.* **1975**, 1095.

36. S. Harder, J. Spielmann, *Journal of Organometallic Chemistry*, **2012**, *698*, 7.

37. S. Yadav, V. S. V. S. N. Swamy, R. G. Gonnade, S. S. Sen, *ChemistrySelect*, **2016**, *1*, 1066.

38. S. Brand, A. Causero, H. Elsen, J. Pahl, J. Langer, S. Harder, Eur. *J. Inorg. Chem*. **2020**, 1728.

39. (a) G. I. Nikonov, *ACS Catal.* **2017**, *7*, 7257. (b) D. Mukherjee, Okuda, J. *Angew. Chem. Int. Ed.* **2018**, *57*, 1458.

40. (a) E. J. Corey, R. K. Bakshi, S. Shibata, *J. Am. Chem. Soc.* **1987**,*109*, 5551. (b) E. J. Corey, S. Shibata, R. K. Bakshi, *J. Org. Chem.* **1988**,*53*, 2861.

41. A. J. Blake, A. Cunningham A. Ford, S. J. Teat, S. Woodward, *Chem. - Eur. J.* **2000**, *6*, 3586.

42. M. Arrowsmith, T. J. Hadlington, M. S. Hill, G. Kociok-Kohn, *Chem. Commun.* **2012**, *48*, 4567.

43. (a) R. McLellan, A. R. Kennedy, R. E. Mulvey, S. A. Orr, S. D. Robertson, *Chem. - Eur. J.* **2017**, *23*, 16853. (b) V. A. Pollard, S. A. Orr, R. McLellan, A. R. Kennedy, E. Hevia, R. E. Mulvey, *Chem. Commun.* **2018**, *54*, 1233.

44. (a) D. Mukherjee, H. Osseili, T. P. Spaniol, J. Okuda, *J. Am. Chem. Soc.* **2016**, *138*, 10790. (b) H. Osseili, D. Mukherjee, K. Beckerle, T. P. Spaniol, J. Okuda, *Organometallics* **2017**, *36*, 3029. (c) H. Osseili, D. Mukherjee, T. P. Spaniol, Okuda, J. *Chem. - Eur. J.* **2017**, *23*, 14292.

45. (a) T. J. Hadlington, M. Hermann, G. Frenking, C. Jones, *J. Am. Chem. Soc.* **2014**, *136*, 3028. (b) J. Schneider, C. P. Sindlinger, S. M. Freitag, H. Schubert, L. Wesemann, *Angew.*

Chem. Int. Ed., **2017**, *56*, 333. (c) Y. Wu, C. Shan, Y. Sun, P. Chen, J. Ying, J. Zhu L(Leo). Liu, Y. Zhao, *Chem. Commun.* **2016**, *52*, 13799. (d) C.-C. Chong, H. Hirao, R. Kinjo, *Angew. Chem. Int. Ed.*, **2015**, *54*, 190. (e) Z. Yang, M. Zhong, X. Ma, S. De, C. Anusha, P. Parameswaran, H. W. Roesky, *Angew. Chem. Int. Ed.*, **2015**, *54*, 10225. (f) V. K. Jakhar, M. K. Barman, S. Nembenna, *Org. Lett.* **2016**, *18*, 4710. (g) J. R. Lawson, L. C. Wilkins, R. L. Melen, *Chem. - Eur. J.* **2017**, *23*, 10997. (h) C. Weetman, M. D. Anker, M. Arrowsmith, M. S. Hill, G. Kociok-Kohn, D. J. Liptrot, M. F. Mahon, *Chem. Sci.* **2016**, *7*, 628. (i) C. Weetman, M. S. Hill, M. F. Mahon, *Chem. Commun.* **2015**, *51*, 14477

46. (a) A. M. Smith, R. Whyman, *Chem. Rev.* **2014**, *114*, 5477. (b) D. L. Dodds, D. J. Cole-Hamilton, Catalytic Reduction of Amides Avoiding LiAlH4 or B2H6. In Sustainable Catalysis: Challenges and Practices for the Pharmaceutical and Fine Chemical Industries, ed. P. J. Dunn, K. K. Hii, M. J. Krische, M. T. Williams, Wiley, Hoboken, NJ, 2013, pp. 1–36. (c) U. Biermann, W. Friedt, S. Lang, W. Luhs, G. Machmuller, J. O. Metzger, M. R. Klaas, H. J. Schafer, M. P. Schneider, *Angew. Chem. Int. Ed.* **2000**, *39*, 2206. (d) T. L. Lohr, Z. Li, T. Marks, *J. Acc. Chem. Res.* **2016**, *49*, 824. (e) L. Wu, T. Moteki, A. A. Gokhale, D. W. Flaherty, F. D. Toste, *Chem* **2016**, *1*, 32. (f) C. Hu, D. Creaser, S. Siahrostami, H. Groonbeck, H. Ojagh, M. Skoglundh, *Catal. Sci. Technol.* **2014**, *4*, 2427. (g) T. Turek, D. L. Trimm, N. W. Cant, *Catal. Rev.: Sci. Eng*. **1994**, *36*, 645.

47. N. L. Lampland, M. Hovey, D. Mukherjee, A. D. Sadow, *ACS Catal.* **2015**, *5*, 4219.

48. Das, S.; karmakar, H.; Bhattacharjee, J.; Panda, T. K. *Dalton Trans.* **2019**, *48*, 11978–11984.

49. M. Bhunia, S. R. Shaoo, A. Das, J. Ahmed, P. Sreejyothi, S. K. Mandal, *Chem. Sci.* **2020**, *11*, 1848.

50. I. Ojima, M. Nihonyanagi, T. Kogure, M. Kumagai, S. Horiuchi, K. Nakatsugawa, *J. Organomet. Chem.* **1975**, *94*, 449.

51. S. Patnaik, A. D. Sadow, *Angew. Chem. Int. Ed.* **2019**, *58*, 2505.

52. D. Mukherjee, A. Ellern, A. D. Sadow, *Chem. Sci.* **2014**, *5*, 959.

53. Barman, M. K.; Baishya, A.; Nembenna, S. *Dalton Trans.* **2017**, *46*, 4152.

54. X. Cao, W. Wang, K. Lu, W. Yao, F. Xue, M. Ma, *Dalton Trans.* **2020**, *49*, 2776.

55. (a) P. Saravanan, R. V. Anand, V. K. Singh, *Tetrtahedron Lett.* **1998**, *39*, 3823. (b) N. Khan, S. Agrawal, R. I. Kureshy, H. R. Sayed, S. S. Singh, R. V. Jasra, *J. Organomet. Chem.* **2007**, *692*, 4361. (c) B. Karimi, L. MaMan, *Org. Lett.* **2004**, *6*, 4813. (d). M. L. Kantam, P. Sreekanth, P. L. Santhi, *Green. Chem.* **2000**, *2*, 47. (e) K. Iwanami, J. C. Choi, T. Sakakura, H. Yasuda, *Chem Commun.* **2008**, 1002. (f) M. Bandini, P. G. Cozzi, A. Garelli, P. Melchiorre, A. Unami-Ronchi, *Eur. J. Org. Chem.* **2002**, 3243. (g) Y. Suzuki, M. D. Abu Bakar, K. Muramatsu, M. Sato, *Tetrahedron* **2006**, *62*, 4227. (h) S. T. Kadam, S. S. Kim, *Appl. Organometal. Chem.* **2009**, *23*, 119.

56. Y. Hamashima, D. Sawada, M. Kanai, M. Shibasaki, *J. Am. Chem. Soc.* **1999**, *121*, 2641.

57. D. H. Ryu, E. J. Corey, *J. Am. Chem. Soc.* **2004**, *126*, 8106.

58. Z. Yang, M. Zhong, X. Ma, S. De, C. Anusha, P. Parameswaran, H. W. Roesky, *Angew. Chem. Int. Ed.* **2015**, *54*, 10225.

59. Y. Li, J. Wang, Y. Wu, H. Zhu, P. P. Samuel, H. W. Roesky, *Dalton Trans.* **2013**, *42*, 13715.

60. R. K. Sitwatch, S. Nagendran, *Chem. - Eur. J.* **2014**, *20*, 13551.

61. W. Wang, M. Luo, J. Li, S. A. Pullarkat, M. Ma, *Chem. Commun.* **2018**, *54*, 3042.

62. S. Yadav, R. Dixit, K. Vanka, S. S. Sen, *Chem. - Eur. J.* **2018**, *24*, 1269.

63. H. Stachowiak, J. Kazmierczak, K. Kucinski, G. Hreczycho, *Green Chem.* **2018**, *20*, 1738-1742.

64. W. Wang, M. Luo, W. Yao, M. Ma, S. A. Pullarkat, L. Xu, P.H. Leung, *New J. Chem.* **2019**, *43*, 10744-10749.

65. A. Harinath, J. Bhattacharjee, T. K. Panda, *Chem. Commun.* **2019**, *55*, 1386-1389.

66. W. Wang, M. Luo, D. Zhu, W. Yao, L. Xu, M. Ma, *Org. Biomol. Chem.* **2019**, *17*, 3604.

67. X. Xu, D. Yan, Z. Zhu, Z. Kang, Y. Yao, Q. Shen, M. Xue, *ACS Omega* **2019**, *4*, 6775.

68. V. K. Pandey, S. N. R. Donthireddy, A. Rit, *Chem. Asian J.* **2019,** *14*, 3255-3258.

69. W. Wang, M. Luo, W. Yao, M. Ma, S. A. Pullarkat, L. Xu, P.H. Leung, *ACS Sustainable Chem. Eng.* **2019**, *7*, 1718-1722.

70. (a) M. A. Hoyt, A. A. Hyman, M. Baehler, *Proc. Natl. Acad. Sci. U. S. A.*, **1997**, *94*, 12747. (b) H. Lodish, A. Berk, S. L. Zipursky, P. Matsudaira, D. Baltimore, J. Darnell, *Molecular Cell Biology*, *W. H. Freeman, New York*, 4th edn, **2000**. (c) B. Alberts, A. Johnson, J. Lewis, M. Raff, K. Roberts and P. Walter, *Molecular Biology of the Cell, Garland Science, New York, 4th edn,* **2002**

71. M. N. Chatterjee, E. R. Kay, D. A. Leigh, *J. Am. Chem. Soc.*, **2006**, *128*, 4058.

72. R. D. Astumian, *Phys. Chem. Chem. Phys.*, **2007**, *9*, 5067.

73. V. Serreli, C.-F. Lee, E. R. Kay, D. A. Leigh, *Nature*, **2007**, *445*, 523.

74. (a) M. von Delius, D. A. Leigh, *Chem. Soc. Rev.*, **2011**, *40*, 3656.

75. (b) M. von Delius, E. M. Geertsema, D. A. Leigh, *Nat. Chem.*, **2010**, *2*, 96. 42 M. von Delius, E. M. Geertsema, D. A. Leigh, D.-T. D. Tang, *J. Am. Chem. Soc.*, **2010**, *132*, 16134

76. M. N. Chatterjee, E. R. Kay, D. A. Leigh, *J. Am. Chem. Soc.*, **2006**, *128*, 4058.

77. M. R. Wilson, J. Sola, A. Carlone, S. M. Goldup, N. Lebrasseur, D. A. Leigh, *Nature*, **2016**, *534*, 235.

78. Y. Zhang, Z. Chang, H. Zhao, S. Crespi, B. L. Feringa, D. Zhao, *Chem*, **2020**, *6*, 2420.

79. V. Garcıa-Lopez, P. T. Chiang, F. Chen, G. Ruan, A. A. Martı´, A. B. Kolomeisky, G. Wang, J. M. Tour, *Nano Lett.*, **2015**, *15*, 8229.

Chapter 2

Fundamentals of Computational Chemistry

Chapter 2

Fundamentals of Computational Chemistry

Abstract

In this chapter, we have discussed in brief the theoretical background for the various computational techniques such as quantum mechanics (QM), *ab initio* molecular dynamics (AIMD), and density functional theory (DFT) that are applied in this thesis. The full QM and DFT methods have allowed us to compute the minimum energy pathways of systems as a function of energy and electron density. Moreover, DFT has become a powerful tool to study reactivity, structures, transition states, spectra, and other properties of chemical systems with accuracy. After establishing the favorable reaction mechanism (lowest energy), turnover frequency (TOF) calculations, interaction energy calculations, volume correction in the entropy, and NCI plot analyses have been carried out in this thesis work. In this chapter, the theoretical background of these methods has been described in brief.

2.1 Introduction

Computational chemistry is a branch of chemistry that employs computer algorithms to support in solving chemical problems rather than developing new algorithms or theoretical methods. It incorporates methods of theoretical chemistry into computer programs and calculates the structures and properties of complexes, groups of molecules, and solids.

The father of the Hartree-Fock theory, Douglas Hartree was the first scientist who used external "computers" for theoretical calculations of molecules in 1946.[1] Computational methods can be employed today for geometry optimizations of different molecules, for determining the energy of the system, transition state searches, IR, Raman, NMR and circular dichroism spectra analysis, bond and orbitals analysis, the determination of polarizability, electron affinities, population analysis, as well as to study the effect of dispersion interactions. They can also predict the possibility of new chemistry that has not yet been explored by experimental methods and also sometimes find the unknown reasons for the failure of computational methods and thereby help in the modifications required to convert failures to successes. Single-step and multistep reaction pathways can be represented as energy profile diagrams derived from the analysis of potential energy surfaces. Computational chemistry involves the following methods to study various chemical problems:

i) Molecular mechanics: This is based on force fields and does not use a wave function. Hence, molecular mechanics methods cannot be used to study electronic effects. However, these methods are faster than quantum chemical methods.

ii) *Ab initio* quantum chemistry methods: As *ab initio* stands for “from the beginning” or “first principles”, these methods are based on the Schrödinger equation. Major examples of *ab initio* quantum chemistry methods are Hartree Fock, post Hartree Fock, and quantum Monte Carlo methods.

iii) Semi-empirical methods: These methods use the modified Hartree-Fock equation with a simpler Hamiltonian rather than the exact molecular Hamiltonian, and the use of empirical (derived from experimental evidence) information. This method is mainly for larger systems. where the parameterization of the two-electron integrals, reduces the computational cost.

iv) Density functional theory (DFT): This is an alternative method to solve the many-electron problem, and is based on electron density. In DFT, the density of the electron is the basis for determining the energy and other ground state properties of the system, and can be represented with three coordinates. Furthermore, DFT methods can handle large chemical systems with accuracy.

v) *Ab initio* molecular dynamics (AIMD): The AIMD method combines Newton's equations of motion with the Schrödinger equation, with the force being calculated from Newton's equations and the energy being determined from the Schrödinger equation.

In addition to these methods, there are a*b initio* quantum chemical methods such as coupled- cluster $(CC)^2$ and configuration interaction $(CI)^3$, which are computationally expensive. In this thesis, quantum chemical calculations with DFT and *ab initio* molecular dynamics (AIMD) have been performed, as these are the best theoretical methods to study large systems with accuracy.[4] In Section 2.3 and Section 2.5 of this chapter, the fundamentals of DFT and AIMD have respectively been provided. Furthermore, elementary quantum mechanics has been considered in the next section of this chapter to understand the basis of AIMD and DFT. Moreover, the volume correction method, turnover frequency (TOF) calculations with the energetic span model (ESM), and the method of non-covalent interaction (NCI) plot analysis have been discussed briefly in this chapter.

2.2 Elementary Quantum Mechanics

2.2.1 The Schrödinger Equation, Hamiltonian Operator, and the Wave Function

In 1926, the time-dependent non-relativistic Schrödinger equation was proposed by Erwin Rudolf Josef Alexander Schrödinger. Modern quantum mechanics is based upon solving this equation, because it allows us to calculate the wave function at any time. However, the aim of quantum chemical approaches towards any chemical system is to solve the time-independent Schrödinger equation (TISE), as most of the time-dependent interactions are not compellingly significant in chemical problems. The many-body TISE for the chemical system with n number of electrons and m number of nuclei is given by:

$$\hat{H}\Psi(x_1x_2,x_3\ldots\ldots x_n,r_1,r_2\ldots\ldots\ldots r_m) = E\Psi(x_1x_2,x_3\ldots\ldots x_n,r_1,r_2\ldots\ldots\ldots r_m) \qquad (2.11)$$

Where, E(eigen value) represents the total energy of the system, and $\Psi(x_n, r_m)$ (eigen function) is the wavefunction for the system, which is a function of 3m space coordinates of nuclei and 3n space coordinates and n spin coordinates of electrons. x and r variables are used here to represent the electronic co-ordinates and the nuclei, respectively.

Moreover, a wave function is also known as a state function that contains all possible information regarding the system. All the information about the system can be obtained from the wave function by employing a suitable operator on it. The square of $\Psi(x_n, r_m)$ – the

probability density ($|\Psi(x_1, x_2, x_3 \ldots x_n)|^2$), provides the basis for the physical interpretation of the wave function. The wavefunction is a composite of electronic and nuclear wave functions. The probability density can be determined after separating the electronic and nuclear wavefunctions. Equation 2.12 represents the probability of finding the electrons 1, 2,...,n in given volume element dx_1, $dx_{2.....}dx_n$.

$$\int|\Psi(x_1,x_2,x_3 \ldots x_n)|^2 \, dx_1.dx_2 \ldots .dx_n \tag{2.12}$$

$\hat{H}(x_n, r_m)$ is a Hamiltonian operator, which is represented as:

$$\hat{H} = \frac{-\hbar}{2}\sum_{a=1}^{m}\frac{1}{m_a}\nabla_a^2 - \frac{\hbar}{2m_e}\sum_{i=1}^{n}\nabla_i^2 \sum_a \sum_{a>b}\frac{Z_a Z_b e^2}{r_{ab}} - \sum_a \sum_i \frac{Z_a e^2}{r_{ia}} + \sum_j \sum_{i>j}\frac{e^2}{r_{ij}} \tag{2.13}$$

In the above equation (2.13), the first two terms in the Hamiltonian operator represent the kinetic energy of the nuclei and electrons, respectively. The other three terms represent the nuclear-nuclear repulsion, nuclear-electron attraction, and electron-electron repulsion terms respectively; $\hbar = h/2\pi$ and h is the Planck's constant. The indices i and j indicate a total number of n electrons, whereas indices a and b denote a total of the m nuclei of the system. The masses of the nuclei are represented by m_a, and m_e represents the masses of the electrons. Z_a and Z_b represent the charges of nuclei, r_{ab} is the distance between the nuclei a and b, whereas, r_{ia} represents the distance between the i^{th} electron and the a^{th} nuclei and r_{ij} is the distance between the i^{th} and the j^{th} electrons.

2.2.2 The Born-Oppenheimer Approximation

In theoretical calculations, the most common approximation employed is the Börn - Oppenheimer approximation. In order to simplify the Schrödinger equation (S.E.), Börn and Oppenheimer proposed this approximation in 1927, based on the important fact that nuclei move much slower than electrons, because nuclei are much heavier than electrons. Hence, we can presume that all electrons exist in the field of fixed nuclei, *i.e.*, the nuclear kinetic energy is zero, and that the nuclear potential energy is merely a constant. Therefore, the molecular Hamiltonian operator adequately reduces to the electronic Hamiltonian, shown in equation 2.14.

$$\hat{H}_{el} = \frac{-\hbar}{2m_e}\sum_{i=1}^{n}\nabla_i^2 - \sum_a \sum_i \frac{Z_a e^2}{r_{ia}} + \sum_j \sum_{i>j}\frac{e^2}{r_{ij}} \tag{2.14}$$

The Schrödinger equation with the electronic Hamiltonian is further represented as:

$$\hat{H}_{el}\Psi_{el} = E_{el}\Psi_{el} \quad (2.15)$$

Now as the total energy of the system is:

$$E_{tot} = E_{el} + E_n \quad (2.16)$$

Where E_{el} is the electronic energy and E_{nn} is the nuclear-nuclear repulsion, which is given by:

$$E_{nn} = \sum_a \sum_{a>b} \frac{Z_a Z_b e^2}{r_{ab}} \quad (2.17)$$

2.2.3 The Variational Principle

The strategy for illustrating the electronic energy of a real system is complicated and painstaking. To solve the S.E. for any particular system, first we need to construct a Hamiltonian operator corresponding to that system and then find the eigenfunctions and eigenvalues for the Hamiltonian operator. However, there is no actual process to solve the Schrödinger equation precisely for any system. Hence, to sidetrack this laborious process, a trial wave function could be used to get an accurate electronic energy value. The variational principle gives us the opportunity to solve this problem. This principle states that *"the energy calculated using a trial wave function is always an upper bound to the original ground state energy (E_0) of the system of interest."*

$$E(\Psi) = \frac{<\Psi|\hat{H}|\Psi>}{<\Psi|\Psi>} \geq E_0 = \frac{<\Psi_0|\hat{H}|\Psi_0>}{<\Psi_0|\Psi_0>} \quad (2.18)$$

Where, $\frac{<\Psi|\hat{H}|\Psi>}{<\Psi|\Psi>}$ is expectation value of energy (E[Ψ]), and $<\Psi|\hat{H}|\Psi> = \int \Psi^* \hat{H} \Psi d\tau$.

Ψ_0 is the true ground state wave function. The corresponding energy E_0 can be found by the full minimization of the given functional $E(\Psi)$ with respect to all of the allowed n electronic wave functions.

2.3 Density Functional Theory

The quantum mechanical strategies based on the wave function (Ψ) are found to be more costly because the wave function is a 4n variable: 3n for space variables, and n for spin variables for each electron. Also, the multifaceted nature of the wave function increases with the number of electrons in the system. To reduce this intricacy in the calculations of essential properties of any system, it is necessary to consider an alternative for a wave function that could be implemented for estimating the total electronic energy of a multi-electronic system. A

distinctly advantageous method, in comparison to other approaches of wave function based strategies, in terms of efficiency and accuracy, is density functional theory (DFT). DFT allows us to compute any molecule's energy and other properties by using the electron density as a fundamental parameter. Unlike the wave function, the electron density is an experimental observable and a quantifiable quantity and relies on three spatial coordinates. Therefore, electron density-based methods are more economical than wave function-based methods. Moreover, one can employ DFT for computing different types of properties of many different types of systems, including large systems. In the next subsection, the functional and the electron density have been reviewed in brief.

2.3.1 Functional

A function of another function is defined as a functional. The difference between them is that a functional takes a function as an input and provides an output, whereas a function takes a number as an input to give an output. For example, the variational integral $F[\emptyset] = <\emptyset|\hat{H}|\emptyset>/<\emptyset|\emptyset>$ is a functional of the variation function $\emptyset$. Like a function, one can find the derivative of a functional. The differentiation of a functional F[g] is represented as:

$$\partial F[g] = F[(g + \partial x)] - F[g] = \int \frac{\partial F}{\partial g(x)} \partial g(x).\, dx \tag{2.19}$$

Different types of functional such as local-density, generalized gradient, meta-generalized gradient, and hybrid approximations can be used in the DFT method

2.3.1.1 Local-Density approximation (LDA)

LDA is applicable to the homogeneous gas system, where the electron density $\rho(\vec{r})$ varies slowly with the position. In particular, the electron density can be treated locally as a uniform electron gas in this approximation. Thus, at every position in this model, the exchange-correlation factor is the same. LDA is the uncomplicated approximation to discover the exchange-correlation. According to LDA, exchange- correlation can be represented as:

$$E_{XC}^{LDA}[\rho] = \int \rho(\vec{r}) \in_{XC} \left(\rho(\vec{r})\right) dr \tag{2.20}$$

where $\in_{XC}$ is the exchange-correlation energy per particle of a homogeneous electron gas of

electron density ρ. Further, the exchange-correlation energy can be defined as the summation of exchange and correlation terms. $\in_{XC}(\rho) = \in_X(\rho) + \in_C(\rho)$

The LDA approximation is applicable for closed-shell systems, while LSDA (local spin density approximation) is relevant for open-shell system (free radical) calculations.

2.3.1.2 Generalized Gradient Approximation (GGA)

LDA fails when the density changes significantly with distance, as in molecules. In order to solve this issue, one has to consider the gradient of the electron density ($\nabla(\rho)$) and think of the exchange-correlation term in the energy expression. $E_{XC}^{GGA}[\rho]$ can split into the exchange and correlation parts: $E_{XC}^{GGA}[\rho] = E_X^{GGA}[\rho] + E_C^{GGA}[\rho]$

In order to improve DFT calculation, in 1988, Becke introduced B88, Bx88, and Becke88 GGA exchange functionals. The commonly utilized GGA correlation functionals are Perdew (P86 or Pc86), Perdew-Wang (PW91 or PWc91), and Lee-Yang-Parr (LYP functional such as B88LYP or BLYP). Furthermore, we can combine any exchange functional with the correlation functional in DFT calculations. For instance, the BLYP functional represents the combination of the Becke exchange functional and the LYP correlation functional. Currently, both empirical and nonempirical GGA functionals are accessible for use. Perdew-Burke Ernzerhof (PBE), a commonly used GGA functional, does not involve empirical parameters.

2.3.1.3 Meta-Generalized Gradient Functionals

Meta-GGA functionals are an extension of GGA functionals that rely on the second derivatives of the electron density (kinetic-energy density). In the meta-GGA approximation, the exchange-correlation energy can be determined as:

$$E_{XC}^{MGGA}\left[\rho^{\alpha}\rho^{\beta}\right] = \int f\left(\rho^{\alpha}, \rho^{\beta}, \nabla\rho^{\alpha}, \nabla\rho^{\beta}, \nabla^2\rho^{\alpha}, \nabla^2\rho^{\beta}, \tau_{\alpha}, \tau_{\beta}\right)dr \qquad (2.21)$$

where, $\tau_{\alpha}, \tau_{\beta}$ are the non-interacting kinetic energy density terms that can be defined as

$\tau_{\alpha} = \frac{1}{2}\sum_i \left|\nabla\theta_{i\alpha}^{KS}(r)\right|^2$ where, the $\theta_{i\alpha}^{KS}$ are the Kohn-Sham orbitals for the electrons that have α spin.

Although the meta-GGA functionals are more accurate and exact, they are computationally more expensive than the GGA functionals. For example, M06-L is a meta-GGA functional that gives a superior performance as it contains 37 optimized parameters. Another illustration of a meta-GGA functional is TPSS, a nonempirical meta-GGA functional which provides better results in compare to the PBE functional.

2.3.1.4 Hybrid Functionals

Nowadays, the most utilized functionals are hybrid exchange-correlation functionals, which provide precise results. These useful functionals include an exact exchange term from Hartree-Fock theory along with the exchange-correlation energy from other sources such as empirical and *ab initio*. The HF exchange energy, given underneath, is the exact exchange energy for an arrangement of the non-interacting electrons with electron density equal to the real system.

$$E_X^{HF} = \sum_{i=1}^{n}\sum_{i=1}^{n} < \Psi_i^{KS}(1)\Psi_j^{KS}(2)\left|\frac{1}{r_{ij}}\right|\Psi_i^{KS}(2)\Psi_j^{KS}(1) > \qquad (2.22)$$

Axel Becke, in 1993, introduced a hybrid approach for DFT calculations which was later modified by Stevens *et al.*, in 1994. The most popular hybrid DFT functional is B3LYP or Becke3LYP. It is difficult to say which DFT functional is best because the use of the functional depends on the type of framework and the properties are being calculated.

2.3.2 The Electron Density

The electron density is a fundamental aspect of density functional theory. It is characterized as the probability of finding one electron of random spin within a specific volume. The electron density can be shown by the following integral equation.

$$\rho(\vec{r}) = N\int\ldots\int|\Psi\,(\vec{x}1\ldots\ldots\ldots\vec{x}n)|^2\,ds_1\,d\vec{x}_2\ldots..d\vec{x}_n \qquad (2.23)$$

where, $\vec{x} = \vec{r}$.s and $\rho(\vec{r})$ are defined as the probability of finding any of the N electrons in the volume $d\vec{r_1}$, with arbitrary spin. The remaining N-1 electrons will have arbitrary positions and spins in the state denoted by Ψ. Additionally, $\rho(\vec{r})$ (electron density) is a quantum-mechanical observable and can be estimated by experimental techniques such as x-ray diffraction, electron diffraction, and scanning tunneling microscopy. Furthermore, $\rho(\vec{r})$ is a non-negative

function of three spatial coordinates that integrate to the total number of electrons, *i.e.*, $\rho(\vec{r}) \geq 0$ and $\int \rho(\vec{r})d(\vec{r_1}) = N$ where $\rho(\vec{r} \rightarrow \infty) = 0$. In order to quantify and analyze the topology of ρ, the gradient of ρ (first derivative, $\nabla(\rho)$) has to be considered. Since at inflection points the slope vanishes, the characteristic of critical points is calculated by the Hessian of ρ (second derivative, $\nabla^2(\rho)$). Besides, the probability of finding an electrons pair with spins σ_1 and σ_2 simultaneously within two different volume elements $d\vec{r_1}$ and $d\vec{r_2}$, while other N-2 electrons have subjective spins and positions, is known as the pair density, given as:

$$\rho(\vec{x_1}, \vec{x_2}) = N(N-1) \int \dots \int |\psi(\vec{x_1}, \vec{x_2} \dots \dots \vec{x_n})|^2 \, d\vec{x_3} \dots .. d\vec{x_n} \quad (2.24)$$

The pair density is also a positive quantity like electron density. It is vital since it contains data about electron correlation.

2.3.3 The Hohenberg-Kohn Theorems

DFT was first proposed by Walter Kohn in 1964.[5.] He demonstrated two theorems regarding the electron density – the basis of DFT. In other words, these theorems are the basis of Kohn-Sham density functional theory. The subtleties and verification of the two H.K. theorems have been given underneath.

Theorem 1:

'The external potential $\hat{V}_{ext}(\vec{r})$ *is within a trivial additive constant a unique functional of the electron density* $\rho(\vec{r})$. *Since* $\hat{V}_{ext}(\vec{r})$ *fixes H, we see that the full many-particle ground state is a unique functional of* $\rho(\vec{r})$'.

Proof

We can assume two external potentials $\hat{V}_{ext}(\vec{r})$ and $\hat{V}_{ext}(\vec{r})$ (these differ from each other by more than an additive constant), giving the same ground-state electron density $\rho(\vec{r})$. These two different external potentials will definitely relate to two individual electronic Hamiltonian operators $\hat{H}$ and $\widehat{H'}$ respectively, and $\widehat{H}$ and $\widehat{H'}$ will belong to two distinctive ground state wave functions Ψ, and Ψ' respectively. E_0 and E_0' are the ground state energies corresponding to the two wave functions Ψ, and Ψ' respectively.

i) E_0 and E_0' ii) $\hat{H}$ and $\widehat{H'}$ can be expressed as follows:

$$E_0 = \langle \Psi | \hat{H} | \Psi \rangle, \; E'_0 = \langle \Psi' | \widehat{H'} | \Psi' \rangle, \text{ where } E_0 \neq E'_0 \quad (2.25)$$

$\hat{H} = \hat{T} + \hat{V}_{ee} + \hat{V}_{ext}$

$\widehat{H'} = \hat{T}' + \hat{V}'_{ee} + \widehat{V'}_{ext}$

As both the wave functions give rise to the same electron density, hence we can represent them as:

$$\hat{V}_{ext} \Rightarrow \hat{H} \Rightarrow \Psi \Rightarrow \rho(\vec{r}) \Leftarrow \Psi' \Leftarrow \hat{H}' \Leftarrow \hat{V}'_{ext}$$

Now, if we apply the variational principle, where Ψ' is a trial wave function for $\hat{H}'$:

$$E_0 < \langle\Psi_0|\hat{H}|\Psi_0\rangle = \langle\Psi_0|\widehat{H'}|\Psi_0\rangle + \langle\Psi_0|\hat{H} - \widehat{H'}|\Psi_0\rangle \quad (2.26)$$

After putting the value of $\hat{H}$ *and* $\widehat{H'}$,

$$E_0 < E_0' + \langle\Psi_0|\hat{T} + \hat{V}_{ee} + \hat{V}_{ext} - \widehat{T'} - \hat{V}'_{ee} - \widehat{V'}_{ext}|\Psi_0\rangle = E_0 < E_0' + \int \rho(\vec{r})\{\hat{V}_{ext} - \widehat{V'}_{ext}\}dr \quad (2.27)$$

The right-hand side of equation (2.26) can also be written as:

$$E_0 < E_0' - \int \rho(\vec{r})\{\hat{V}_{ext} - \widehat{V'}_{ext}\}dr \quad (2.28)$$

The addition of equations (2.26) and (2.27) leads to the following results:

$E_0 + E_0' < E_0' + E_0$, $0<0$

Therefore, it has been proved that there cannot be two different $\hat{V}_{ext}$ that give the same ground-state electron density.

The ground state energy is a functional of ground-state electron density and can be represented as:

$$E_\upsilon[\rho_0] = T[\rho_0] + V_{ne}[\rho_0] + V_{ee}[\rho_0] \quad (2.29)$$

$$E_\upsilon[\rho_0] = \int \rho(\vec{r})\,\upsilon(\vec{r})d\vec{r} + T[\rho_0] + V_{ee}[\rho_0] \quad (2.30)$$

Where $\rho(\vec{r})\upsilon(\vec{r})d\vec{r}$ is the system-dependent part, and $T[\rho_0] + V_{ee}[\rho_0]$ is the system independent part. The latter is called the Hohenberg-Kohn functional $F_{Hk}[\rho_0]$ (given below).

$$F_{Hk}[\rho_0] = T[\rho_0] + V_{ee}[\rho_0] \quad (2.31)$$

F_{Hk} is the universal functional of electron density, which is independent of the external potential (V_{ext}).

Up to this, we have perceived that the ground state electron density alone is sufficient to calculate all properties of the framework chosen. However, it does not illuminate us on the most proficient method to guarantee that the electron density employed to estimate the properties is the true ground-state electron density for the system. In the second Hohenberg-Kohn theorem, the remedy for this has been provided.

Theorem 2:

"$F_{HK}[\rho_0]$, the functional that delivers the ground state energy of the system, delivers the lowest energy, in the case that the input density is true ground state density, ρ_0."

This theorem can be represented as

$$E_0 \leq E[\acute{\rho}] = T[\acute{\rho}] + E_{ne}[\acute{\rho}] + E_{ee}[\acute{\rho}] \quad (2.32)$$

Proof

We can assume that the guess density that will have its own Hamiltonian $\widehat{H'}$ and wave function Ψ. This wave function can be used as a guess wave function for the Hamiltonian, which is created from the external potential V_{ext}. Hence, we can represent:

$$\langle\Psi_0|\hat{H}|\Psi_0\rangle = \langle\Psi_0|\widehat{H'}|\Psi_0\rangle + \langle\Psi_0|\hat{H} - \widehat{H'}|\Psi_0\rangle$$

$$\langle\Psi|\hat{H}|\Psi\rangle = T[\acute{\rho}] + V_{ee}[\acute{\rho}] + \int \rho(\vec{r})\hat{V}_{ext}\, d\vec{r} = E[\acute{\rho}] \geq E_0[\rho_0] = \langle\Psi_0|\hat{H}|\Psi_0\rangle \quad (2.33)$$

2.3.4 The Kohn-Sham approach

As examined in the past segment, the electron density is a fundamental entity for calculating the ground state properties of any atomic or molecular framework. The Hohenberg-Kohn theorem proposes that the ground state energy of an atomic or molecular framework can be expressed as:

$$E_0 = \min_{\rho\to N}(F_{H.K.}[\rho] + \int \rho(\vec{r})V_{Ne}(\vec{r})\, d\vec{r} \quad (2.34)$$

Where $F_{H.K.}[\rho]$ is a universal functional; it consists of the kinetic energy, the classical Coulomb interaction, as well as the non- classical contribution.

$$F[\rho(\vec{r})] = T[\rho(\vec{r}) + J[\rho(\vec{r})] + E_{ncl}[\rho(\vec{r})] \quad (2.35)$$

Here $J[\rho]$ is known, but the kinetic energy term (which is a significant part of the total energy) $T[\rho(\vec{r})]$ is unknown. In 1965, Kohn and Sham published a paper where the concept of the reference framework of non-interacting electrons was mentioned, and could be used to calculate the kinetic energy exactly. The non-interacting reference framework is built from a set of orbitals in the Hohenberg-Kohn formalism such that the kinetic energy can be obtained with adequate accuracy. Hence,

$$T_s = -\frac{1}{2}\sum_i^N < \Psi_i \,|\nabla_2|\Psi_i > \text{ and } \rho_s(\vec{r}) = \sum_i^N \sum_s |\Psi_i(\vec{r}, s)|^2 = \rho(\vec{r}) \quad (2.36)$$

where T_s is the kinetic energy, and Ψ_i is the wave function of the reference framework. By using this, the kinetic energy term can be calculated. Regardless, if both the frameworks (interacting, as well as non-interacting) have the same electron density, it is noticeable that $T_s \neq T$. However, the major portion of the kinetic energy $T[\rho(\vec{r})]$ is recovered *via* T_s. To correct this blunder, Kohn and Sham introduced the partition of the universal functional, where the exchange-correlation energy $E_{XC}[\rho]$ was added[6]. Therefore, the universal functional can be written as:

$$F[\rho] = T_s[\rho] + J[\rho] + E_{XC}[\rho] \quad (2.37)$$

$$\text{where, } E_{XC}[\rho] = (T[\rho] - T_s[\rho]) + Eee[\rho] - J[\rho]) \quad (2.38)$$

The segments of energy that are unknown or difficult to acquire from other theoretical methods (such as the contribution of electron exchange and electron correlation, the correction for the self-interaction, the residual portion of the kinetic energy (not included in the term T_s)), are associated in this functional ($E_{XC}[\rho]$).

The next question would then be: how can we locate the potential $V_s(\vec{r})$ for the non–interacting reference framework, which is associated with the same density as the interacting framework? In order to address this issue, we will rewrite the energy of the framework as given below:

$$E[\rho] = T_s[\rho] + J[\rho] + E_{EX}[\rho] + E_{Ne}[\rho] \quad (2.39)$$

The further expansion of terms involved in equation (2.38) will lead to

$$E[\rho]=T_s[\rho]+\frac{1}{2}\frac{\iint \rho(\vec{r}_1)\rho(\vec{r}_2)}{r_{12}}d\vec{r_1}\,d\vec{r_2}+E_{EX}[\rho]+\int V_{Ne}\rho(\vec{r})\,d\vec{r} \quad (2.40)$$

$$=-\frac{1}{2}\sum_i^N <\Psi_i|\nabla^2|\Psi_i> +\frac{1}{2}\sum_i^N\sum_j^N\iint |\Psi_i(\vec{r_1})|^2\frac{1}{r_{12}}|\Psi_j(\vec{r_1})|^2 d\vec{r_1}d\vec{r_2}+E_{EX}[\rho]-$$

$$\sum_i^N\int\sum_A^M\frac{Z_A}{r_{1A}}|\Psi_i(\vec{r_1})|^2 d\vec{r_1} \quad (2.41)$$

In equation (2.39), the only unknown term is $E_{EX}[\rho]$. Now, according to the variational principle, minimization of the energy under the constraint $<\Psi_i|\Psi_j>=\delta_{ij}$ leads to the *Kohn-Sham equation*.

$$-\frac{1}{2}\nabla^2+[\int\frac{\rho(r_2)}{r_{12}}dr_2]+V_{XC}(r_1)-\sum_A^M\frac{Z_A}{r_{1A}}])\Psi_i=\varepsilon_i\Psi_i \quad (2.42)$$

where $V_{XC}(\vec{r})$ can be defined as:

$$V_{XC}(\vec{r})=\frac{\partial E_{XC}[\rho(\vec{r})]}{\partial\rho(\vec{r})} \quad (2.43)$$

A new, improved potential $V_{eff}(\vec{r})$ can be calculated from these equations, which will ultimately give self-consistency. Furthermore, the hypothetical mapping in between the kinetic energy and the density can be done by using Ψ_is. Besides, Ψ_is is not equivalent to the real orbitals of the framework. Furthermore, the Kohn-Sham wave function is a solitary determinant approach that fails in the case of multiple determinants. DFT is subsequently employed to find better approximations to these two quantities (V_{XC} *and* E_{XC}) that will provide functionals and permit the computation of the energy of the frameworks.

Figure 2.1 below describes a self-consistent cycle for the K.S. iteration.

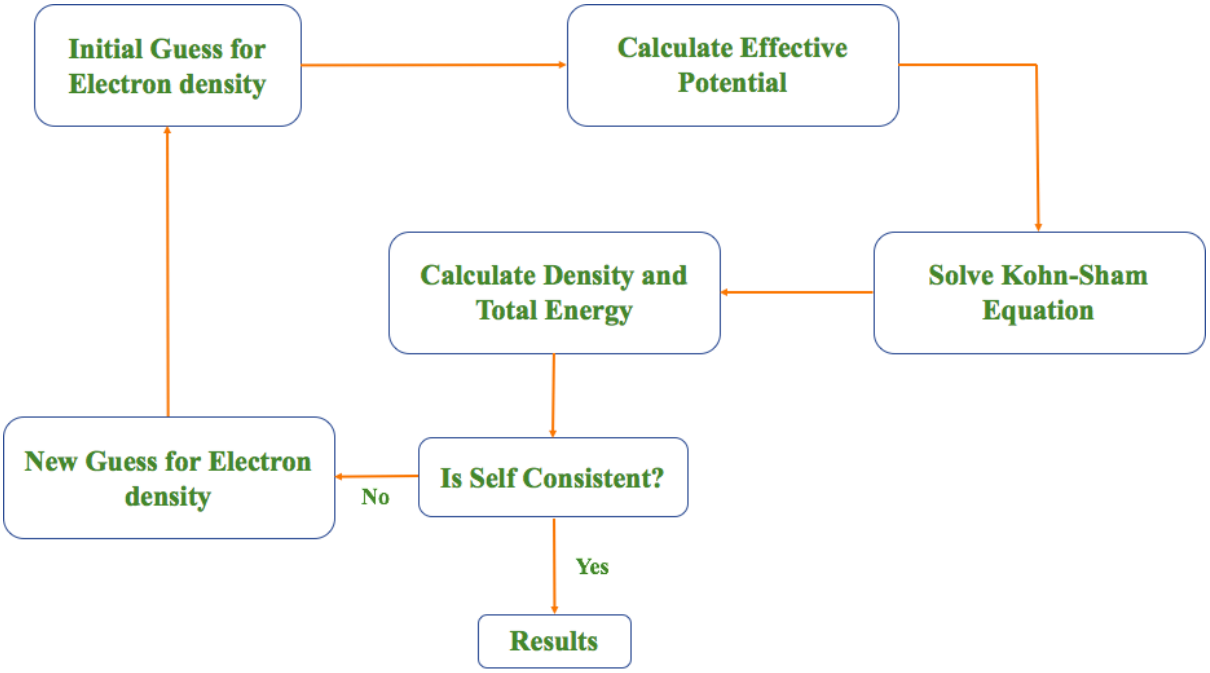

Figure 2.1 The flow chart of the self-consistent cycle for Kohn-Sham iterations for the single step during optimization.

2.3.5 Dispersion Corrections

One of the principal van der Waals interactions between directly non-bonded atoms and molecules are dispersion interactions. Mostly, GGA and hybrid functionals that replace part of the local by nonlocal H.F. exchange cannot describe long-range (dispersion interactions) interactions.[7] As the van der Waals (vdW) interactions play a demanding role in many chemical systems, it is important to implement dispersion effects in the calculations. The effective inclusion of dispersion corrections (DFT-D) by Grimme gives an elaborate explanation for the non-covalent interactions or dispersion interactions.[8-11] The total energy of the chemical system acquired after inclusion of dispersion corrections to the functional can be written as:

$$E_{MF\text{-}D} = E_{MF} + E_{disp} \quad (2.44)$$

where E_{MF} is the mean-field energy calculated by H.F. or DFT, and E_{disp} is the dispersion energy, which does not have physical meaning - it is a model-dependent quantity. This can be represented as:

$$E_{disp} = -S6\sum_{i=1}^{N_{at}-1}\sum_{j=i+1}^{N_{nat}}\frac{C_6^{ij}}{R_6^{ij}}f_{dmp}(R_{ij}) \quad (2.45)$$

where N_{at} is the number of atoms in the system, C_6^{ij} is the dispersion coefficient for the ij atom pair, S6 is a global scaling factor, R_{ij} is the interatomic distance, and f_{dmp} is a damping function, described by:

$$f_{dmp}(R) = \frac{1}{1+e^{-a(\frac{R}{R_0}-1)}} \tag{2.46}$$

Here, R_0 is the sum of atomic van der Waals radii.

2.4 The Volume Corrections Method for Determining the Translational Entropy

To calculate the free energy of any reaction, the calculation of entropy is a fundamental task. It is well known that the total entropy is the sum of translational, vibrational, and electronic components.

$$S_{tot} = S_{trans} + S_{rot} + S_{vib} + S_{el} \tag{2.47}$$

The translational entropy can be calculated by using the Sackur-Tetrode equation,[12] which is given by

$$S_{trans} = R\ln[(\frac{(10)^{-15/2}}{N_A^4[X]})((\frac{2\pi MRTe^{5/3}}{h^2})^{3/2})] \tag{2.48}$$

where [X] is the concentration of the particle, T is the temperature, M is the mass of the particle, NA is the Avogadro number, k is the Boltzmann constant, and h is the Planck constant.

However, in liquid or in the solution phase, the Sackur-Tetrode equation overestimates the translational entropy, as it ignores the molecular volume (V_{mol}). To overcome this problem, Mammen *et al.* introduced the *free volume* correction to the translational entropy that calculates the more accurate translational entropy.[14] In this method, it has been presumed that the volume of molecules in solution is smaller than the total volume.

$$V_{free} = C_{free}\left(\sqrt[3]{\frac{10^{27}}{[X]N_0}} - \sqrt[3]{V_{molec}}\right)^3 \tag{2.49}$$

Where C_{free} is 8 (for cube), and N_0 is the Avogadro's number. After free volume correction to Equation 2.47, the translational entropy is expressed by

$$S_{trans}^{analyte} = R\ln[(\frac{(10)^{-15}/_2 V_{free}^{solvent}}{N_0^4[analyte]})((\frac{2\pi MRTe^{5/3}}{h^2})^{3/2})] = 11.1 + 12.5\ln(T) + 12.5\ln(M) + 8.3\ln V_{free}^{solvent} \quad (2.50)$$

Where, T is the temperature, and $V_{free}^{solvent}$ is the free volume. Therefore, this equation provides the translational entropy in solution.

2.5 *Ab initio* Molecular Dynamics Simulations (AIMD)

Molecular Dynamics is an extensively used form of computer established simulation through which the dynamic evolution of molecules are mapped. By solving the Newton's law of motion, the pathway of the atoms in the molecule is unfolded. The forces acting on each atom or particle of the system under simulation study is determined by the classical mechanical force field. On the other hand, these forces can also be calculated from the laws of quantum mechanics, with methods such as density functional theory (DFT), in order to describe the accurate electronic behavior of these simulated systems. This simulation approach is known as *ab initio* Molecular Dynamics (AIMD). As this is a computationally costly approach therefore, the size of molecules for which AIMD simulations can be done for a substantial period of time is quite small.

DFT based molecular simulations could be done by introducing the method of steepest descent to the laws of Newtonian motion to obtain an authentic idea about the electronic structure of the system. Car and Parrinello (CP) proposed this class of simulation for the first time in 1985. They proposed a classical Lagrangian for a system where the coefficients corresponding to the basic functions are considered as the dynamic variables.

In this thesis work, AIMD simulations have been performed with the TeraChem quantum chemistry and AIMD software packages[13-19] using the B3LYP[20] electronic wave function and the 3-21g Gaussian basis set[21] to calculate the Born–Oppenheimer potential energy surface. Newton's equations of motion were calculated using Langevin dynamics with an equilibrium temperature of 1800 K (also the starting temperature of the dynamics). We have used a very high temperature to increase the average kinetic energy of the reactant molecules and for faster dynamics, which breaks non-covalent interactions without breaking the covalent bonds. The calculations were feasible because of the efficiency of TeraChem, which accelerates the calculation by evaluating the two-electron integrals on the GPU. We have used the ADIIS (augmented direct inversion in the iterative subspace) algorithm[22] available in TeraChem, as an alternative tool for self-consistent field calculation at each AIMD step, in which the default DIIS algorithm[23] failed to converge. Spherical boundary conditions apply to prevent the

molecules from flying away, a phenomenon known as the "evaporation" event. The molecules were restricted to move inside a spherical volume by a boundary potential.

2.6 Turnover Frequency Calculation with the Energetic Span Model (ESM)

In order to find the turn over frequency (TOF), we have calculated the relative efficiency with the AUTOF program[24], using the "Energetic Span Model" (ESM), developed by Shaik and coworkers.[25,26] ESM provides a method to calculate the turnover frequencies (TOFs) based on their computed energy profiles of catalytic cycles. The turnover frequency calculations consider the principal rate-determining transition state, potentially rate-influencing transition states, and the intermediates. The turnover frequency (TOF) is calculated by the following equation:

$$TOF = \frac{K_B T}{h} e^{-\delta E/RT}$$

$$\delta E = T_{TDTS} - I_{TDI} \quad \text{if TDTS appears after TDI}$$

$$\delta E = T_{TDTS} - I_{TDI} + \Delta G_r \quad \text{if TDTS appears before TDI} \qquad (2.51)$$

where K_β is the Boltzmann's constant; T is the temperature in K and δE is the effective activation barrier of the global reaction. TDTS and TDI represent the transition state and the intermediate respectively, that maximize δE. This model has been employed to calculate the TOFs at the respective reaction temperatures. Moreover, the ESM model uses all the kinetic information (rate-determining transition state, potentially rate-influencing transition states, and the intermediates) - not just one transition state or intermediate – in order to determine the efficiency of the catalytic cycle. In this thesis, ESM has been applied to find the efficiency of various catalytic systems under study.

2.7 The Non-Covalent Interactions (NCI) Plot

The NCI plot, developed by Yang *et al.*, is useful for analyzing and capturing non-covalent interactions.[27] The NCI plot is a program that shows the graphical representation of inter and intramolecular non-covalent interactions, based on the electron density and its derivatives. Non-covalent interactions have been recognized as low density and reduced gradient regions.

2.8 References:

1. A. Paul Medwick, *Ann. Hist. Comp.* **1988**, *10*, 105.

2. H. G. Kümmel, *Int. J. Mod. Phys. B*, **2003**, *17*, 5311.

3. C. J. Cramer, Chichester: *John Wiley & Sons, Ltd*. **2002**, 191.

4. a) M. H. N. Assadi, D. A. H. Hanao *J. Appl. Phys*. **2013**, *113*, 233913; b) M. D. Segall, P. J. D. Lindan, M. J. Probert, C. J. Pickard, P. J. Hasnip, S. J. Clark, M. C. Payne, *J. Phys: Condens. Matter*, **2002**, *14*, 2717-2743; c) F. R. Somayeh, H. Soleymanabadi, *J. Mol. Model*. **2014**, *20*, 2439-2445; d) F. R. Somayeh, H. Soleymanabadi, *J Mol Model*, **2013**, *19*, 3733-3740; e) D. Music, R. W. Geyer, J. M. Schneider, *Surface & Coatings Technology*, **2016**, *286*, 178.

5. P. Hohenberg, W. Kohn, *Physical review*, **1964**, *136*, B864.

6. W. Kohn, L. J. Sham, *Phys. Rev.* **1965**, *140*, 1133.

7. a) P. Hobza, J. Sponer, T. J. Reschel, *Comput Chem*. **1995**, *11*, 1315; b) M. Allen, D. J. Tozer, *J Chem Phys.* **2002**, *117*, 11113.

8. J. Hepburn, G. Scoles and R. Penco, *Chem. Phys*. *Lett.* **1975**, *36*, 451.

9. (a) S. Grimme, *J. Comput. Chem.* **2004**, *25*, 1463. (b) S. Grimme, *J. Comput. Chem.*, ***2006***, *27*, 1787.

10. S. Grimme, J. Antony, S. Ehrlich, H. Krieg, *J. Chem. Phys*. **2010**, *132*, 154104.

11. R.W. Gurney, Introduction to statistical mechanics; 1st ed.; McGraw Hill, 1949.

12. M. Mammen, E. I. Shakhnovich, J. M. Deutch, G. M. Whitesides, *J. Org. Chem.***1998**, *63*, 3821.

13. S. Ufimtsev, T. J. Martinez, *J. Chem. Theory Comput.*, **2009,** *5*, 2619.

14. S. Ufimtsev, N. Luehr, T. J. Martinez, J. *Phys. Chem. Lett.*, **2011,** *2*, 1789.

15. C. M. Isborn, N. Luehr, I. S. Ufimtsev, T. J. Martinez, *J. Chem. Theory Comput*., **2011**, *7***,** 1814.

16. A.V. Titov, I. S. Ufimtsev, N. Luehr, T. J. Martinez, *J. Chem. Theory Comput*., **2013**, *9***,** 213.

17. I. S. Ufimtsev T. J. Martinez, *Comput. Sci. Eng*., **2008**, *10*, 26.

18. I. S. Ufimtsev, T. J. Martinez, *J. Chem. Theory Comput*., **2008**, *4*, 222.

19. S. Ufimtsev, T. J. Martinez, *J. Chem. Theory Comput*., **2009**, *5***,** 1004.

20. I. D. Becke, *J. Chem. Phys*., **1993**, *98*, 5648.

21. J. S. Binkley, J. A. Pople, W. J. Hehre, *J. Am. Chem. Soc*., **1980**, *102*, 939.

22. X. Hu, W. Yang, *J. Chem. Phys.*, **2010**, *132*, 054109.

23. P. Pulay, *Chem. Phys. Lett*., **1980**, *73***,** 393.

24. S. Kozuch, J. M. L. Martin, *ACS Catal*. **2011**, *1*, 246.

25. A. Uhe, S. Kozuch, S. Shaik, *Comput. Chem*. **2010**, *32*, 978.

26. S. Kozuch, S. Shaik, *Acc. Chem*. *Res.* **2011**, *44*, 101.

27. a) E. R. Johnson, S. Keinan, P. M. Sanchez, J. C. Garcia, A. J. Cohen, W. Yang, *J. Am. Chem. Soc*. **2010**, *132*, 6498. b) J. C. Garcia, E. R. Johnson, S. Keinan, R. Chaudret, J. P. Piquemal, D. N. Beratan, W. Yang, *J. Chem. Theory Comput*. **2011**, *7*, 625.

Chapter 3

Alkaline Earth Metal Compounds of Methylpyridinato *β*-Diketiminate Ligands and Their Catalytic Application in Hydroboration of Aldehydes and Ketones

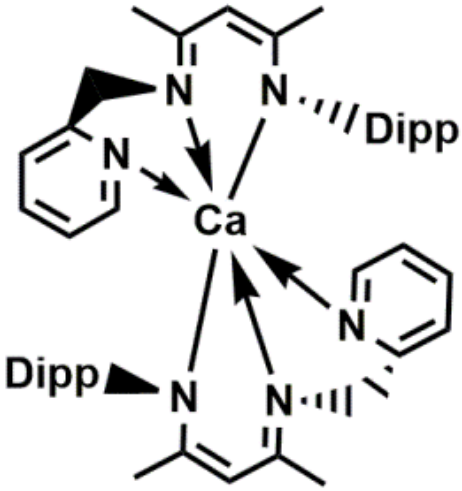

Chapter 3

Alkaline Earth Metal Compounds of Methylpyridinato *β*-Diketiminate Ligands and Their Catalytic Application in Hydroboration of Aldehydes and Ketones

Abstract

Ever increasing demand for green and sustainable chemical processes has set up a drive to replace transition metals. In this regard, the alkaline earth metal complexes have attracted significant attention due to high terrestrial abundance, non-toxicity, and cost-effectiveness. Hence, alkaline earth metals may be a promising alternative to transition and lanthanide metal chemistry. Discussed in this chapter are DFT calculations to investigate the chemistry of a calcium compound that had been experimentally pre-synthesized using a *β*-diketiminato ligand with a methyl-pyridine side arm. We have shown by a mechanistic study that the calcium compound acts as a catalyst for the hydroboration of aldehydes using pinacolborane (HBpin) under ambient reaction conditions.

3.1 Introduction

Alkaline earth metals like beryllium, magnesium, calcium, strontium, barium and radium reside in the 2nd group of the periodic table with a ns^2 valence shell electronic configuration. As the need of the hour is the development of environmentally benign, atom-efficient, and cost-effective reactions, the onus has been on to explore the catalytic potential of these lighter group 2 elements. Calcium, the fourth most abundant elements in the Earth's crust, is indispensable for every living system and it is this biocompatibility that has propelled researchers to explore its chemistry.[1,2]

Activities in organocalcium chemistry has finally started to blossom, after a hundred years of Victor Grignard's breakthrough in organomagnesium chemistry[3]. Various reports have emerged since then, showing calcium complexes acting as catalysts, such as for the hydroamination reactions[4], hydrophosphination reactions[5], hydrosilylation reactions[6], as well as the alkene hydrogenation[7] and carbon-carbon bond formation reactions[8]. A β-diketiminate calcium amide complex [{HC-(C(Me)$_2$N-2,6-iPr$_2$C$_6$H$_3$)$_2$}Ca-{N(SiMe$_3$)$_2$}(THF)] was introduced by Hill and co-workers[9] for the intramolecular hydroamination of α,ω-aminoalkene. Similarly, for the intramolecular hydroamination of non-activated terminal amino alkenes, Roesky and co-workers[10] synthesized aminotroponate and aminotropniminate calcium amide complex [{(iPr)$_2$ATI}Ca{N(SiMe$_3$)$_2$}(THF)$_2$] ((iPr)$_2$ATI = N-isopropyl-2-(isopropylamino) troponiminate) and obtained products under mild reaction conditions. Westerhausen and co-workers[11] took a phenyl substituted alkyne and utilized a homoleptic calcium complex [(thf)$_4$Ca(PPh$_2$)$_2$] as an active catalyst for the alkyne's hydrophosphination. Hydrosilylation of ketones was achieved with the catalytic dimeric calcium hydride complex [(Dippnacnac)CaH·thf]$_2$ {Dippnacnac=CH[(CMe)(2,6-iPr$_2$C$_6$H$_3$N)]$_2$}through the efforts of Harder and co-workers[12]

It should be noted that in all the cases mentioned above, the calcium metal centre was always the site of the catalysis. The possibility of ligand-based catalysis for calcium compounds, or, in general, for other metal-based systems, is not a very explored area of research till date. In 2013, Bergman and co-workers[13] reported a novel method to functionalize vinylic C-H bonds, which takes advantage of the unique ligand-based catalysis of a rare class of metal dinitrosyl complexes, [CpCo(NO)$_2$]. The metal−ligand cooperative catalysis has been further shown for tetranuclear Sr and Ba complexes by Harder and co-workers for intramolecular alkene hydroamination, alkene hydrophosphination, pyridine hydroboration,

pyridine hydrosilylation, and alkene hydrosilylation[14]. Here, instead of the metal centre, the ligand is seen to participate in catalysis. Similarly, for the first time, we are reporting ligand-based catalysis with calcium being the metal centre. In the same vein, although homoleptic alkaline earth metal complexes are usually considered catalytically incompetent, the calcium complex **1** shown in **Figure 3.1** was found to catalyze the hydroboration of aldehydes and ketones with HBpin under mild conditions with high yields.

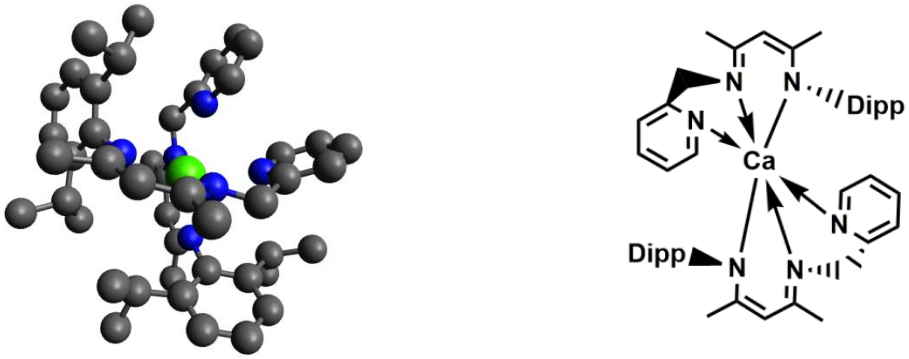

Figure 3.1. The optimized geometry of calcium compound **1**. All hydrogen atoms have been removed for the purpose of clarity.

In alkaline earth metals, the steric saturation of the coordination sphere usually dominates over the electronic effect. Therefore, the exploration of new ligands that can satisfy the coordination requirements is of significant interest. Till now, the alkaline earth metal chemistry has been mainly focused on the use of monoanionic bidentate ligand systems such as amidinate [RC{NR}2]−,[15] guanidinate [RNC(NR$_2$)NR]−,[15] trizenide [(R$_2$N$_3$)]−,[16] β-diketiminate [(R)NC(Me)C(H)C(Me)N(R)]−,[17] diboxmethanide [(4,6-RNCOC$_6$H$_2$) 2CH]−,[18,19] silylated aminopyridinato [(2-R$_3$SiNH- 6-MeC$_5$H$_3$N)]−,[20] etc. The strong binding affinity to the metal center and easily tunable steric and electronic properties of these ligands has been exploited for the stabilization of a plethora of hydrocarbon soluble alkaline earth metal complexes.[21] Roesky's group synthesized a [LCaI(μ-ICaI- μ)ICaL] chain stabilized by two chelating β-diketiminate ligands (L = CH{Et$_2$NCH$_2$CH$_2$N(CMe)}$_2$).[22] The result shows that an additional N→Ae donation can be beneficial to stabilize highly electrophilic alkaline earth metal complexes. This hypothesis was further boosted when Kay and co-workers reported a series of alkaline earth metal complexes of bidentate silylated aminopyridinato ligands as an alternative to amidinate or guanidinate ligands.[20]

The introduction of a methyl-pyridine side arm in the β- diketiminato framework leads to a ligand that is tridentate in its nacnac imino-pyridine state (2,6-iPr_2-C_6H_3NC(Me)CHC-(Me)NH(CH_2py)). The pendant pyridine group on one of the nitrogen centers provides steric support as well as additional electronic stabilization to the metal center. The group of Wolczanski[23] recently employed such a tridentate chelating ligand for preparing a variety of iron and chromium complexes. Chen and co-workers[24] reported β-diketiminato rare-earth metal complexes of composition Ln-(CH_2SiMe_3)$_3$(THF)$_2$ (Ln = Sc and Y) using the same ligand. Despite their ongoing popularity and versatility, there are no examples of group 2 complexes supported by nancnac methylpyridinato ligands in the literature. Herein, we report mechanistic studies of the calcium compound **1**, stabilized by the nancnac methylpyridinato ligand, catalyzing the hydroboration of aldehydes.

3.2 Computational Details

All the DFT calculations were carried out using the Turbomole 7.0 suite of programs.[25] Geometry optimizations were performed using the Perdew, Burke, and Erzenhof density functional(PBE)[26] functional, the electronic configuration of the atoms was described by a triple-ζ basis set augmented by a polarization function (Turbomole basis set TZVP).[27] The resolution of identity (ri)[28] along with the multipole accelerated resolution of identity (marij)[29] approximations were employed for an accurate and efficient treatment of the electronic Coulomb term in the density functional calculations. The real (not model) system has been employed for all the calculations. Care was taken to ensure that the obtained transition state structures possessed only one imaginary frequency corresponding to the correct normal mode, in order to obtain more reliable energy values for the investigated potential energy surface. In addition, intrinsic reaction coordinate (IRC)[30] calculations were done with all the transition states in order to further confirm that they were the correct transition state, yielding the correct reactant and product structures. Solvent effects were introduced by using the COSMO model[31] with the dielectric constant $\varepsilon = 2.27$ employed to model benzene as the solvent. The option "disp" provided in the Turbomole package (DFT-D3) was used for dispersion-corrected DFT calculations for all the calculations with Turbomole.[32] The values reported are ΔG values, with zero-point energy, internal energy, and entropic contributions, with the temperature taken to be 298.15K. The translational entropy term in the calculated structures was corrected through a free volume correction introduced by Mammen *et al.*[33] This volume correction was done to account for the unreasonable enhancement in translational entropy that is generally observed in

computational softwares. Then, in order to find the efficiency of the catalytic cycle in our mechanism, we have calculated the relative efficiency with the AUTOF program by employing the "Energetic Span Model" (ESM), developed by Shaik and coworkers[34-36] on all the free energy profiles discussed in the chapter. The turnover frequency (TOF) calculations take into account the principal rate-determining transition state, potentially rate-influencing transition states as well as intermediates during the catalysis process.

3.3 Results and Discussion

3.3.1 Catalytic Application of calcium compound 1.

The use of transition metal free catalysts for the hydroboration of aldehydes and ketones has been recently explored in depth. Catalysts derived from both s- and p-block elements have been reported with good success. Experimentally, the calcium compound **1** was able to catalyse the hydroboration of a variety of aldehydes and ketones by HBpin under ambient conditions to afford the corresponding alkoxypinacolboronate esters, as shown in **Scheme 3.1** below.

Scheme 3.1. Hydroboration of aldehydes using calcium compound **1**.

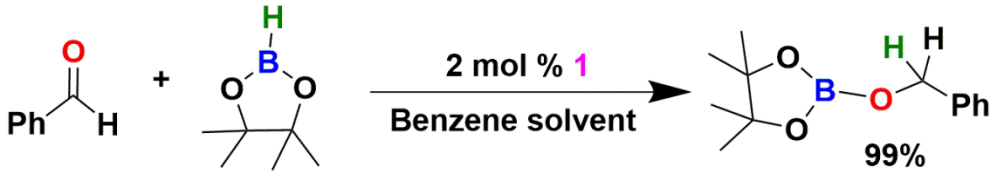

The hydroboration reaction in the absence of catalyst was not observed. As can be seen in **Figure 3.2**, the product is formed after the surmounting of a barrier of 32.8 kcal/mol, which is less feasible under the reaction conditions that had been employed.

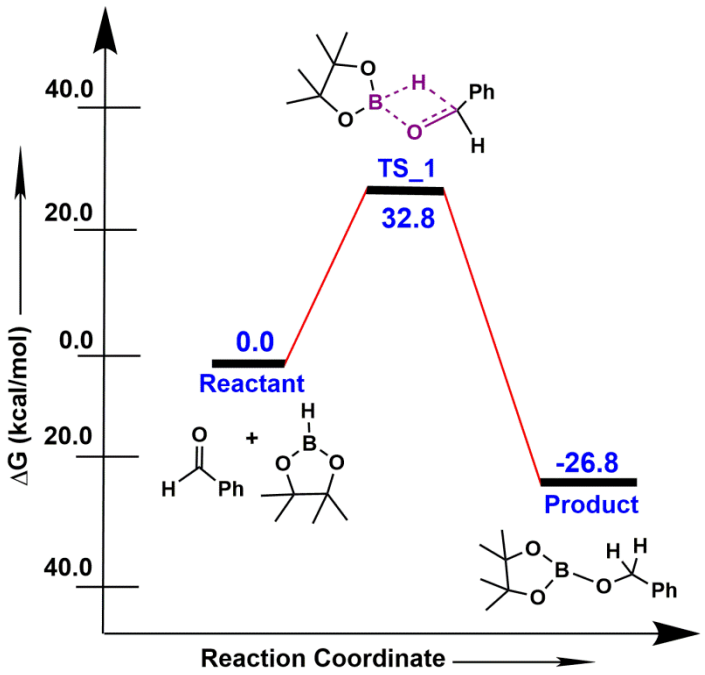

Figure 3.2. The reaction free energy profile diagram for the hydroboration reaction without the calcium compound **1**. The values (in kcal/mol) have been calculated at the PBE/TZVP level of theory.

In order to obtain mechanistic insight, full quantum chemical calculations were done. In the first step of the reaction, the HBpin approaches calcium compound **1** and forms **Int_1** (as shown in Figure **2)** in which the N of one of the pyridine ligands breaks its interaction with the calcium atom and forms a new N−B bond (likely the Lewis acid base adduct, in which N and B contain positive and negative charges respectively) with the B center of HBpin. The thermodynamics (ΔG) for this step is unfavorable by 4.8 kcal/mol. This occurs *via* a "two atoms involved transition state" (**TS_1**) where no bond breaking but only N···B bond formation occurs with a very low free energy (ΔG#) barrier of only 6.4 kcal/mol. In the next step, benzaldehyde approaches the B−H bond of **Int_1**. This is the prelude to the nucleophilic attack by the carbonyl oxygen of benzaldehyde to the adjacent sp2 carbon of pyridine N of **Int_1**, further leading to the neutralization of the charge of N and to the hydride being transferred from the negatively charged center B to the carbonyl carbon of benzaldehyde, which leads to the formation of **Int_2**. This step is favorable by 5.4 kcal/mol. This occurs through a very flexible six membered (C···N···B···H···C···O) transition state (**TS_2**), with a barrier of 29.1 kcal/mol. This is the slowest step of the hydroboration reaction. The ΔG values corresponding to the barriers have been calculated at room temperature.

The values are on the higher side, even after volume corrections for the translational entropy term. This is because the entropy loss during the reaction is overestimated in the calculations, leading to the high values for the barriers. The real values for the barrier heights are, therefore, likely to be much lower. In the transition state corresponding to this step, there is a significant amount of B−H bond activation (1.47 Å distance in the transition state), which allows the hydride transfer from the boron to the carbonyl carbon center, along with the simultaneous occurring of C=O bond cleavage and the formation of another C−O bond. In the last step of the reaction, intramolecular bond forming and bond breaking takes place. The O center of the carbonyl group attacks the B center, along with the formation of the B−O bond and the simultaneous breaking of the N−B and C−O bonds. The last step is very favorable, by 26.6 kcal/mol. This occurs after the surmounting of a four membered transition state (**TS_3**) with a barrier of 15.2 kcal/mol, and also leads to the regeneration of the calcium compound **1**. The fact that the final product is thermodynamically stable, and that the barrier for the slowest step is lower than without the mediation of the catalyst, indicates that the addition of the calcium compound **1** has a salutary effect on the hydroboration reaction.

Calculations with the energetic span model (ESM), developed by Shaik and co-workers, [40] provide insight into the relative efficiency values for the reactions with and without the calcium catalyst, as shown in **Table 3.1**. The TOF values are seen to be quite low, but this is due to the overestimation of the entropy loss in the calculations, leading to the higher values for the barriers, as explained earlier. However, since this overestimation affects the barriers for both the catalyst and non-catalyst cases, what is important to note is that the efficiency of the system is increased by a factor of about 500, which shows the distinct effect of the calcium compound **1** on the efficiency of the hydroboration.

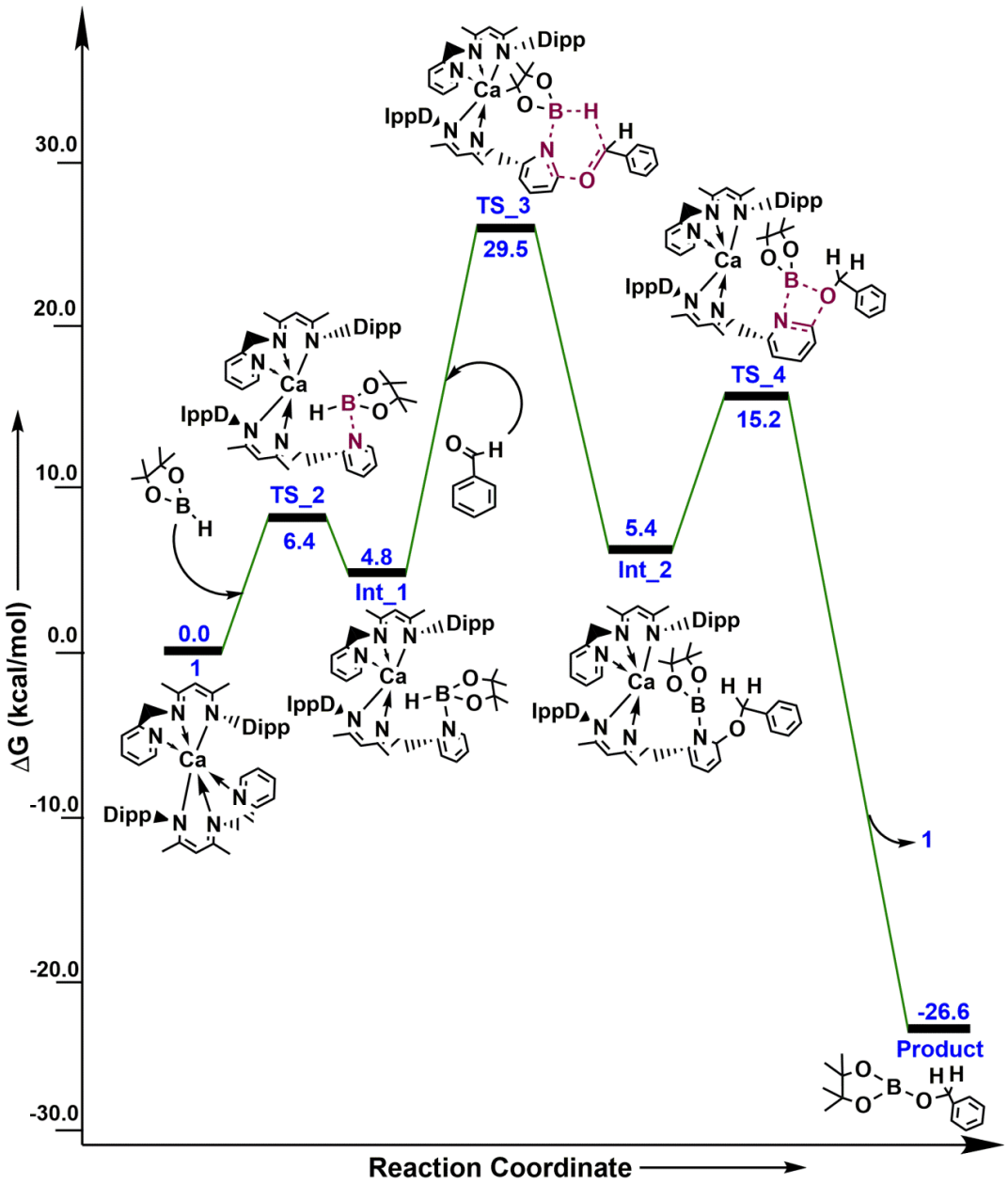

Figure 3.3. The reaction free energy profile diagram for the hydroboration reaction with the calcium compound **1**. The values (in kcal/mol) have been calculated at the PBE/TZVP level of theory.

Table 3.1 The relative efficiency values for the reactions with and without the calcium compound **1**.

Mechanism	Relative Efficiency
With calcium compound **1 (Figure 3.3)**	$2.83*10^{-09}$ / sec
Without calcium compound **1 (Figure 3.2)**	$5.48*10^{-12}$ / sec

3.3.2 Discarded Pathways

We have also investigated the possibility of the calcium center participating in the catalysis process. Several different mechanisms have been studied in this regard. However, these mechanisms have not been seen to be as favorable as the mechanism that is discussed above. We have also investigated the possibility of decoordinating the side arm, i.e., the methylene bridged pyridyl moiety, so as to leave one coordination site free for the aldehyde reactant to approach the calcium center. However, this was found to be significantly unfavourable - by 8.6 kcal/mol (ΔE value). Hence, the calculations suggest that it is the pyridyl moiety without the methylene bridge that is thermodynamically more likely to open its coordination site and provide space for the incoming reagents, in comparison to the methylene bridged pyridyl moiety. The role of the calcium in the chemistry is therefore to bind two ligands, each of which is then capable of acting as a catalytic site for the hydroboration. Therefore, the calcium enables the formation of a dual site catalyst, which would be more efficient than just employing a pyridine moiety as a single site catalyst in the reaction.

3.3.2.1. Discarded Pathway 1

In the mechanism shown below, in the first step of the reaction, HBpin approaches calcium compound **1** and reacts to form **Int_1**, in which the nitrogen of one of the pyridine ligands breaks its interaction with the catalyst and forms a new N-B bond (likely the Lewis acid base adduct in which N and B contain positive and negative charges respectively) with the B centre of HBpin. This step is unfavourable by 4.8 kcal/mol. This occurs through a "two atoms involved transition state" (**N_TS_1**), where no bond breaking but only N... B bond formation occurs with a low barrier of S13 only 6.4 kcal/mol. In the next step, benzaldehyde approaches the B-H bond of **Int_1**. This is followed by nucleophilic attack by the carbonyl oxygen of benzaldehyde to the B centre, with the formation of the B-O bond and the simultaneous transferring of hydride from HBpin to carbonyl carbon of benzaldehyde. This occurs through a four membered transition state (**N_TS_2**) having a barrier of 40.1 kcal/mol, leading to the final hydroboration product along with the regeneration of the catalyst **1**. Since the barrier for the last step is high, this mechanism has been discarded.

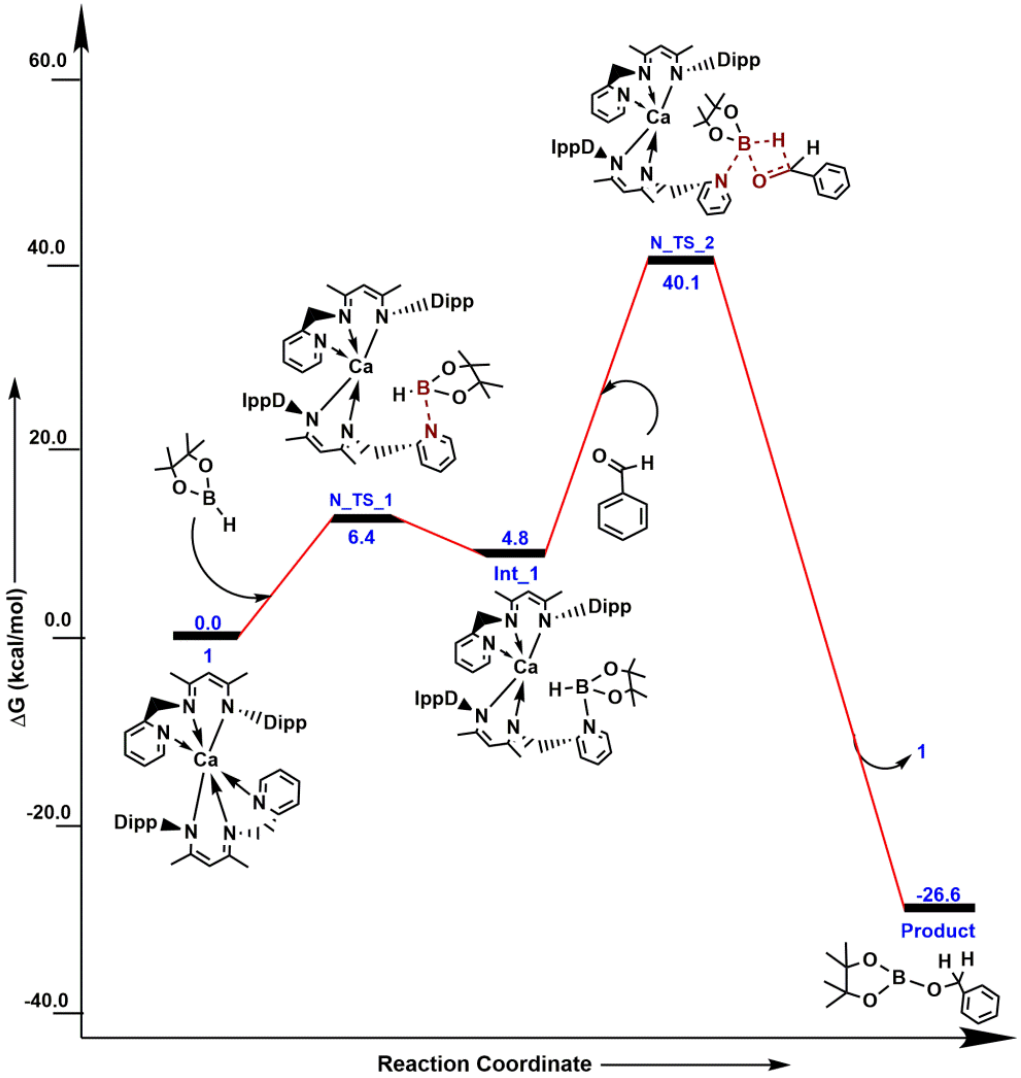

Figure 3.4. An alternative reaction profile for the hydroboration reaction with the calcium compound **1**. The values (in kcal/mol) have been calculated at the PBE/TZVP level of theory.

3.3.2.2. Discarded Pathway 2

In this investigated alternative pathway, the benzaldehyde approaches calcium compound **1** and reacts with it to form **N_Int_1**, in which there is a weak interaction between the calcium of the catalyst and the oxygen of benzaldehyde. This is thermodynamically unfavourable by 3.2 kcal/mol. In the next step, HBpin approaches **N_Int_1**. Nucleophilic attack by the carbonyl O of the benzaldehyde to the B of HBpin occurs subsequently, leading to **N_TS_3** and transferring H from HBpin to the carbonyl carbon of benzaldehyde, which finally leads to the formation of the product. As the barrier for the **N_TS_3** ($\Delta G^{\#}$) is very high: 50.9 kcal/mol, this mechanism has also been discarded.

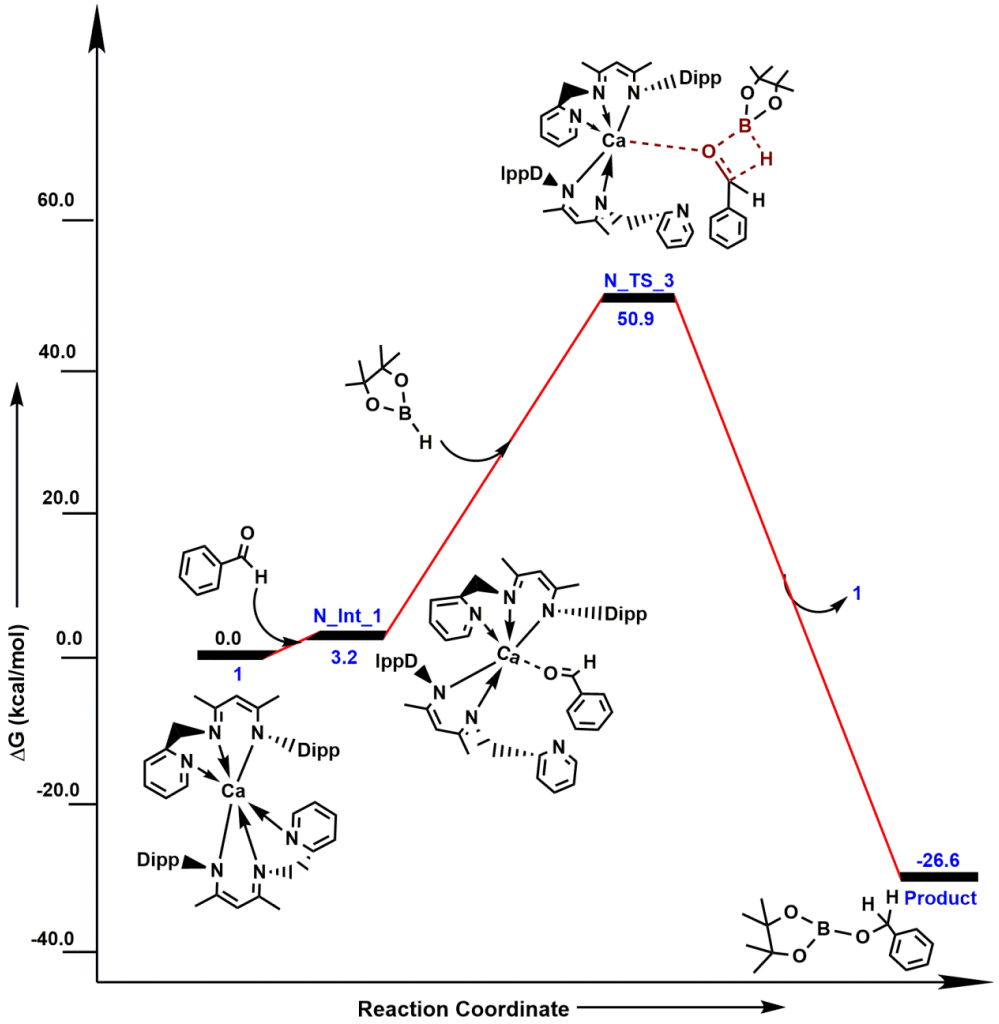

Figure 3.5. Another alternative reaction profile for the hydroboration reaction with the calcium compound **1** in the solvent phase. The values (in kcal/mol) have been calculated at the PBE/TZVP level of theory.

3.3.2.3. Discarded Pathway 3

In this investigated alternative pathway, HBpin approaches the calcium compound **1** and reacts with it to form **Int_1**(ΔE= -3.6 kcal/mol), in which there is a weak interaction between the calcium of the catalyst and the oxygen of HBpin. In the next step, benzaldehyde approaches **Int_1**. This is followed by nucleophilic attack by the carbonyl O of the benzaldehyde to the B of HBpin, leading to **TS** and transferring H from HBpin to the carbonyl carbon of benzaldehyde, which finally leads to the formation of the product. As the barrier for the TS ($\Delta E^{\#}$) is very high: 48.0 kcal/mol, this mechanism has also been discarded.

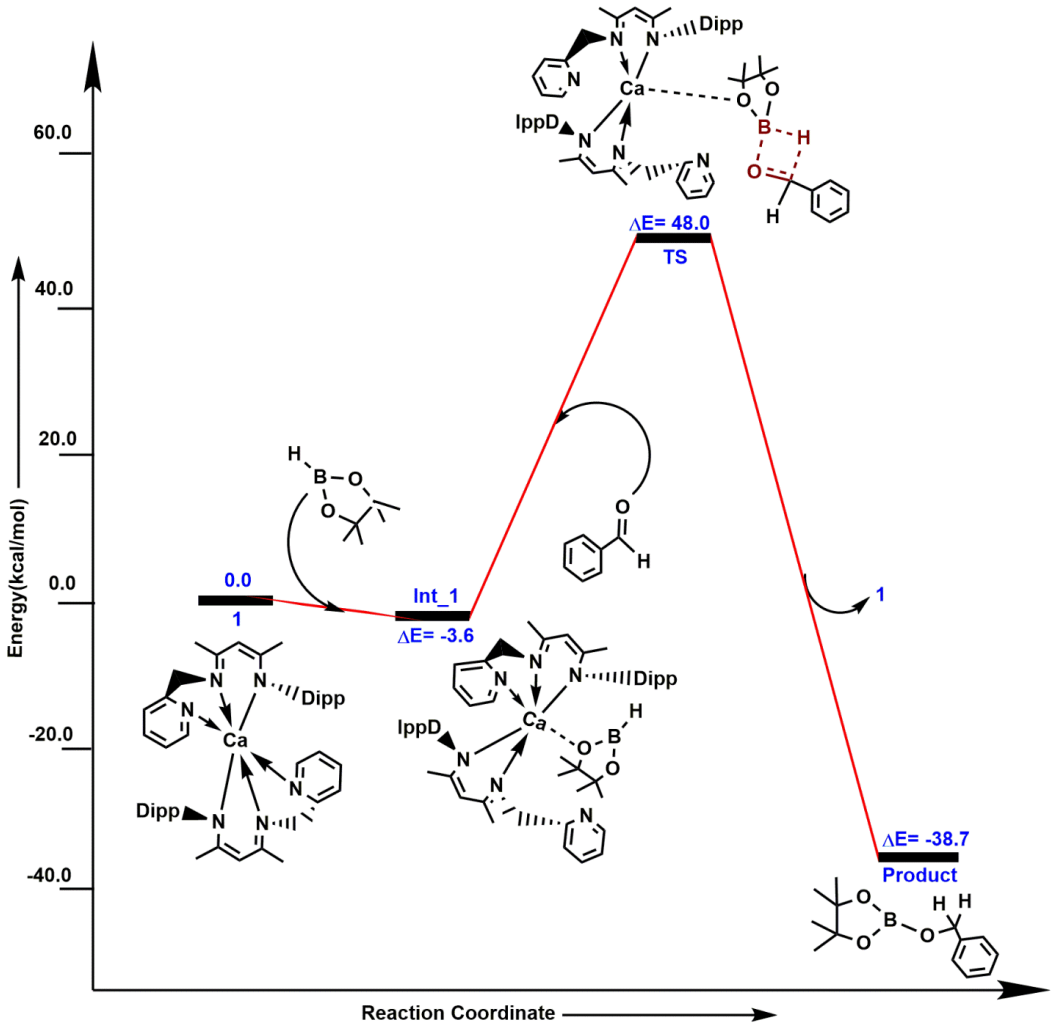

Figure 3.6. Another alternative reaction profile for the hydroboration reaction with the calcium compound **1** in the solvent phase. The values (in kcal/mol) have been calculated at the PBE/TZVP level of theory.

3.3.2.4. Discarded Pathway 4

In this investigated alternative pathway, three molecules of HBpin and one molecule of benzaldehyde approach calcium compound **1** and react with it to give a transition state **TS**. As the barrier for the TS ($\Delta E^{\#}$) is very high: 39.5 kcal/mol, this mechanism has also been discarded.

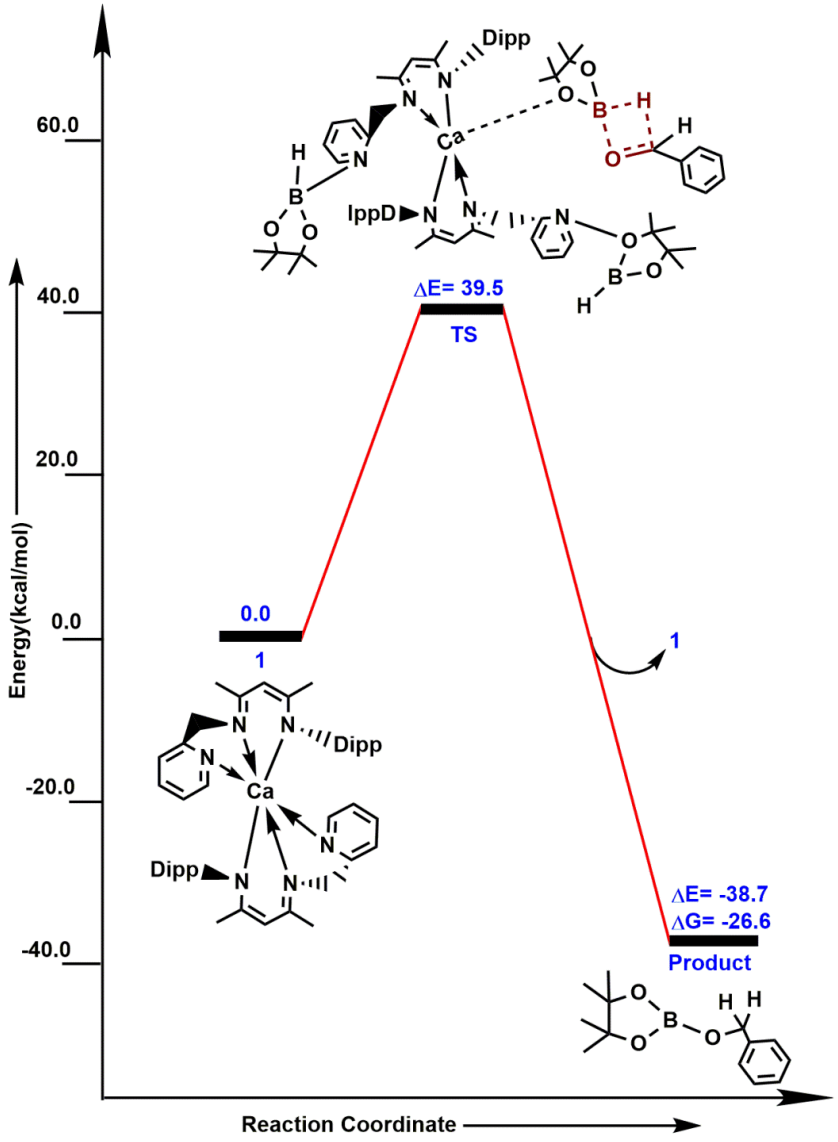

Figure 3.7. Another alternative reaction profile for the hydroboration reaction with the calcium compound **1** in the solvent phase. The values (in kcal/mol) have been calculated at the PBE/TZVP level of theory.

3.4 Conclusion

DFT calculations were done in order to explain the experimentally observed hydroboration of aldehydes by a calcium complex. The calculations revealed that the role of calcium in the chemistry was to bind two ligands, each of which was then capable of acting as a catalytic site for the hydroboration. Therefore, the calcium center enabled the formation of a dual-site catalyst, which would be more efficient than just employing a pyridine moiety as a single-site catalyst in the reaction.

3.5 References

1. (a) S. Harder, *Chem. Rev.* **2010**, *110*, 3852–3876; (b) M. Westerhausen, *Z. Anorg. Allg. Chem.* **2009**, *635*, 13–32.
2. (a) W. D. Buchanan, D. G. Allis, and K. Ruhlandt-Senge, *Chem. Commun.* **2010**, *46*, 4449–4465; (b) A. G. M. Barrett, M. R. Crimmin, M. S. Hill, and P. A. Procopiou, *Proc. R. Soc.* **2010**, *466*, 927–963.
3. V. Grignard, *Ann. Chim.* **1901**, *24*, 433.
4. (a) A. G. M. Barrett, M. R. Crimmin, M. S. Hill, P. B. Hitchcock, G. Kociok-Köhn, and P. A. Procopiou, *Inorg. Chem.* **2008**, *47*, 7366−7376; (b) M. Arrowsmith, M. S. Hill, and G. Kociok-Köhn, *Organometallics* **2009**, *28*, 1730−1738.
5. T. M. A. Al-Shboul, H. Görls, and M. Westerhausen, *Inorg. Chem. Commun.* **2008**, *11*,1419−1421.
6. F. Buch, J. Brettar, and S. Harder, *Angew. Chem. Int. Ed.* **2006**, *45*, 2741−2745.
7. (a) S. Harder, and J. Brettar, *Angew. Chem. Int. Ed.* **2006**, *45*, 3474−3478; (b) P. Jochmann, J. P. Davin, T. P. Spaniol, L. Maron, and J. Okuda, *Angew. Chem. Int. Ed.* **2012**, *51*, 4452−4455; (c)V. Leich, T. P. Spaniol, and J. Okuda, *Angew. Chem. Int. Ed.* **2016**, *55*, 4794−4797; (d) A. Causero, G. Ballmann, J. Pahl, H. Zijlstra, C. Färber, and S. Harder, *Organometallics* **2016**, *35*, 3350−3360; (e) J. Spielmann, F. Buch, and S. Harder, *Angew. Chem. Int. Ed.* **2008**, *47*, 9434−9438.
8. (a) T. Suzuki, N. Yamagiwa, Y. Matsuo, S. Sakamoto, K. Yamaguchi, M. Shibasaki, and R. Noyori, *Tetrahedron Lett.* **2001**, *42*, 4669−4671; (b) G. Kumaraswamy, M. N. V. Sastry, and N. Jena, *Tetrahedron Lett.* **2001**, *42*, 8515−8517; (c) G. Kumaraswamy, N. Jena, M. N. V. Sastry, M. Padmaja, and B. Markondaiah, *Adv. Synth. Catal.*, **2005** *347*, 867−871; (d) T. Tsubogo, Y. Yamashita, and S. Kobayashi, *Angew. Chem. Int. Ed.* **2009**, *48*, 9117−9120; (e) S. Kobayashi, T. Tsubogo, S. Saito, and Y. Yamashita, *Org. Lett.* **2008**, *10*, 807−809; (f) T. Tsubogo, S. Saito, K. Seki, Y. Yamashita, and S. Kobayashi, *J. Am. Chem. Soc.* **2008**, *130*, 13321−13332; (g) S. Kobayashi, and Y. Yamashita, *Acc. Chem. Res.* **2011**, *44*, 58−71; (h) T. Tsubogo, Y. Kano, K. Ikemoto, Y. Yamashita, and S. Kobayashi, *Tetrahedron Asymm.* **2010**, *21*, 1221−1225; (i) T. Poisson, T. Tsubogo, Y. Yamashita, and S. Kobayashi, *J. Org. Chem.* **2010**, *75*, 963−965.
9. M. R. Crimmin, I. J. Casely, and M. S. Hill, *J. Am. Chem. Soc.* **2005**, *127*, 2042−2043.

10. S. Datta, P. W. Roesky, and S. Blechert, *Organometallics* **2007**, *26*, 4392−4394.
11. T. M. A. Al-Shboul, V. K. Pálfi, L. Yu, R. Kretschmer, K. Wimmer, R. Fischer, H. Görls, M. Reiher, and M. Westerhausen, *J. Organomet. Chem.* **2011**, *696*, 216−227.
12. J. Spielmann, and S. Harder, *Eur. J. Inorg. Chem.* **2008**, 1480−1486.
13. C. Zhao, M. R. Crimmin, F. D. Toste, and R. G. Bergman, *Acc. Chem. Res.* **2014**, *47*, 2, 517.
14. B. Freitag, P. Stegner, K. Thum, C. A. Fischer, and S. Harder, *Eur. J. Inorg. Chem.* **2018**, 1938–1944.
15. (a) G. J. Moxey, F. Ortu, L. G. Sidley, H. N. Strandberg, A. J. Blake, W. Lewis, and D. L. Kays, *Dalton Trans.* **2014**, *43*, 4838−4846; (b) R. J. Schwamm, B. M. Day, N. E. Mansfield, W. Knowelden, P. B. Hitchcock, and M. P. Coles, *Dalton Trans.* **2014**, *43*, 14302−14314; (c) B. M. Day, W. Knowelden, and M. P. Coles, *Dalton Trans.* **2012**, *41*, 10930−10933; (d) J. Schwamm, and M. P. Coles, *Organometallics* **2013**, *32*, 5277−5280. (e) S. Yadav, V. S. V. S. N. Swamy, R. G. Gonnade, and S. S. Sen, *Chemistry Select* **2016**, 1, 1066−1071; (f) B. M. Day, N. E. Mansfield, M. P. Coles, and P. B. Hitchcock, *Chem. Commun.* **2011**, *47*, 4995−4997; (g) C. Jones, *Coord. Chem. Rev.* **2010**, *254*, 1273−1289; (h) C. Glock, C. Loh, H. Goerls, S. Krieck, and M. Westerhausen, *Eur. J. Inorg. Chem.* **2013**, *2013*, 3261−3269; (i) M. K. Barman, A. Baishya, and S. Nembenna, *J. Organomet. Chem.* **2015**, *785*, 52−60.
16. (a) S.-O. Hauber, F. Lissner, G. B. Deacon, and M. Niemeyer, *Angew. Chem. Int. Ed.* **2005**, *44*, 5871−5875; (b) A. G. M. Barrett, M. R. Crimmin, M. S. Hill, P. B. Hitchcock, G. Kociok-Köhn, and P. A. Procopiou, *Inorg. Chem.* **2008**, *47*, 7366−7376.
17. (a) S. Nembenna, H. W. Roesky, S. Nagendran, A. Hofmeister, J. Magull, P.-J. Wilbrandt, and M. A. Hahn, *Angew. Chem. Int. Ed.* **2007**, *46*, 2512−2514; (b) A. G. M. Barrett, M. R. Crimmin, M. S. Hill, P. B. Hitchcock, and P. A. Procopiou, *Angew. Chem. Int. Ed.* **2007**, *46*, 6339−6342; (c) C. Ruspic, and S. Harder, *Inorg. Chem.* **2007**, *46*, 10426−10433; (d) M. Westerhausen, M. H. Digeser, C. Gückel, H. Nöth, J. Knizek, and W. Ponikwar, *Organometallics*, **1999**, *18*, 2491− 2496; (e) S. P. Sarish, A. Jana, H. W. Roesky, T. Schulz, M. John, and D. Stalke, *Inorg. Chem.* **2010**, *49*, 3816− 3820; (f) S. P. Sarish, S. Nembenna, S. Nagendran, and H. W. Roesky, *Acc. Chem. Res.* **2011**, *44*, 157−170.
18. (a) I. Koehne, R. Herbst-Irmer, and D. Stalke, *Eur. J. Inorg. Chem.* **2017**, *2017*, 3322−3326; (b) I. Koehne, S. Bachmann, T. Niklas, R. Herbst-Irmer, and D. Stalke, *Chem. Eur. J.* **2017**, *23*, 13141−13149.

19. I. Koehne, N. Graw, T. Teuteberg, R. Herbst-Irmer, and D. Stalke, *Inorg. Chem.* **2017**, *56*, 14968−14978.
20. F. Ortu, G. J. Moxey, A. J. Blake, W. Lewis, and D. L. Kays, *Inorg. Chem.* **2013**, *52*, 12429−12439.
21. S. P. Green, C. Jones, and A. Stasch, *Science* **2007**, *318*, 1754−1757.
22. S. P. Sarish, A. Jana, H. W. Roesky, T. Schulz, D.A. Stalke, *Organometallics* **2010**, *29*, 2901−2903.
23. W. D. Morris, P. T. Wolczanski, J. Sutter, K. Meyer, T. R. Cundari, and E. B. Lobkovsky, *Inorg. Chem.* **2014**, *53*, 7467−7484.
24. X. Xu, Y. Chen, G. Zou, and J. Sun, *Dalton Trans.* **2010**, *39*, 3952−3958.
25. R. Ahlrichs, M. Bar, M. Haser, H. Horn, and C. Kolmel, *Chem. Phy. Lett.* **1989**, *162*, 165.
26. J. P. Perdew, K. Burke, and M. Ernzerhof, *Phys. Rev. Lett*. **1997**, *78*, 1396.
27. S. Ansgar, H. Christian, and A. Reinhart, *J. Chem. Phys.* **1994**, *100*, 5829.
28. K. Eichkorn, O. Treutler, O. H. M. Haser, and R. Ahlrichs, *Chem. Phys. Lett*. **1995**, *240*, 283.
29. M. Sierka, A. Hogekamp, and R. Ahlrichs, *J. Chem. Phys*. **2003**, *118*, 9136.
30. K. Fukui, *Acc. Chem. Res*. **1981**, *14*, 363.
31. A. Klamt, and G. Schuurmann, *Chem. Soc*, *Perkin Trans.***1993**, *2*, 799.
32. (a) J. Hepburn, G. Scoles, and R. Penco, *Chem. Phys*. *Lett.* **1975**, *36*, 451; (b) R. Ahlrichs, R. Penco, and G. Scoles, *Chem. Phys*. **1977**, *19*, 119; c) S. *J.* Grimme, *Comput. Chem.* **2004**, *25*, 1463; d) S. *J.* Grimme, *Comput. Chem.* **2006**, *27*, 1787; e) S. Grimme, J. Antony, S. Ehrlich, and H. J. Krieg, *Chem. Phys*. **2010**, *132*, 154104.
33. M. Mammen, E. I. Shakhnovich, J. M. Deutch, and G. M. Whitesides, *J. Org. Chem*. **1998**, *63*, 3821.
34. S. Kozuch, *WIREsComput. Mol. Sci.* **2012**, *2*, 795.
35. A. Uhe, S. Kozuch, and S. Shaik, *J. Comput. Chem.* **2011**, *32*, 978.
36. S. Kozuch, and S. Shaik, *Acc. Chem. Res.* **2010**, *44*, 101.

Chapter 4

Substrate, Catalyst and Solvent: The Triune Nature of Multitasking Reagents in Hydroboration

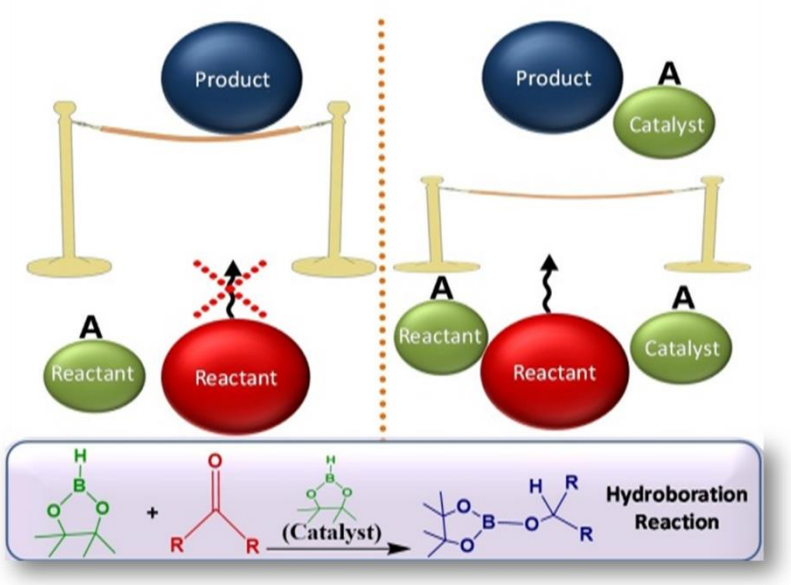

CHAPTER 4

Substrate, Catalyst and Solvent: The Triune Nature of Multitasking Reagents in Hydroboration

Abstract

A truly green chemical process would avoid the use of an external catalyst, while still achieving high efficiency. This has been realized in the very recent past for hydroboration, cyanosilylation, acetalization and the aza-Michael addition, among other reactions. The current, combined computational and experimental study, unlocks the secret to how this highly desirable outcome is accomplished: one of the reactants in the process also acts as the catalyst. Specifically, this is shown for the important hydroboration reaction, with pinacolborane (HBpin) as the hydroborating reagent and benzaldehyde, acetophenone, benzoic acid and *p*-methoxyphenylacetylene as the hydroborated substrates. The mechanistic understanding thus gained has then been further exploited experimentally to bring hydroboration closer to experimental conditions in catalysis. These insights can potentially be expanded to the rapidly growing area of solvent-free and internal catalyst chemistry. It should be noted that my contributions to the work discussed in the chapter pertain to the computational studies done – the experimental aspects (executed by collaborators) are also included in order to provide full context and clarity about the significance of the results obtained.

4.1 Introduction

"The best catalyst is no catalyst"[1] sums up the need for green processes in the current age, and it is gratifying to see increasing application of this dictum to a wider and wider variety of chemical reactions, including hydroboration,[2-5] cyanosilylation,[6,7] acetalization[8] and the aza-Michael addition.[9] However, in order for this to become even more of an important area of development, it is necessary to understand and establish the principles on which this chemistry is founded. The current combined computational and experimental work represents a comprehensive attempt in this direction. To this end, in this chapter, we have focused on a very important chemical processes: hydroboration reaction. Another important related chemical process is the cyanosilylation reaction, which will be discussed in the next chapter.

Hydroboration is one of the most significant chemical reactions employed in academia and industry today, owing to the wide synthetic applicability of functionalized boronates. The hydroborating agent of choice today is pinacolborane, HBpin, as shown in **Figure 1** below. The presence of two B-O bonds allow it to stabilize the positive charge on the boron upon loss of the hydride, thus making hydride transfer with HBpin facile and efficient. It has therefore been employed for a variety of hydroboration reactions,[10] with substrates as varied as alkenes, alkynes, carboxylic acids, aldehydes, ketones, imines, amides, carbodiimides, pyridines, esters and allylic alcohols. What has made HBpin even more attractive is the recent report by Hreczycho and co-workers,[2] where aldehyde hydroboration was demonstrated to occur in neat HBpin, without the need of an external catalyst. This result has led to increased interest in HBpin chemistry, with several reports emerging in the space of a year.[3, 4, 11-12]

What these recent results show is that HBpin is able to efficiently hydroborate different substrates without the need of a solvent or external catalyst, while the same efficiency is not obtained in solution in external catalyst free conditions.[2] It is this unusual and interesting behaviour that has served as the starting point of our investigations. Specifically, we have proposed and validated a hypothesis that explains the behaviour of HBpin, with the aid of density functional theory (DFT), as well as with experimental kinetic studies. What we have found is that neat HBpin, in addition to acting as the "solvent" for the reaction, as well as one of the reactants (as the hydroborating agent), also does the job of a catalyst in facilitating the hydroboration chemistry. Therefore, HBpin can be termed as also acting as an "internal catalyst" during the hydroboration process. Our collaborators have then employed the insights gained to design and execute experiments that show how one can do hydroboration chemistry

in solution with HBpin without loss of yield, thereby bringing this new, external catalyst free hydroboration chemistry closer to the realm of experimental conditions in catalysis.

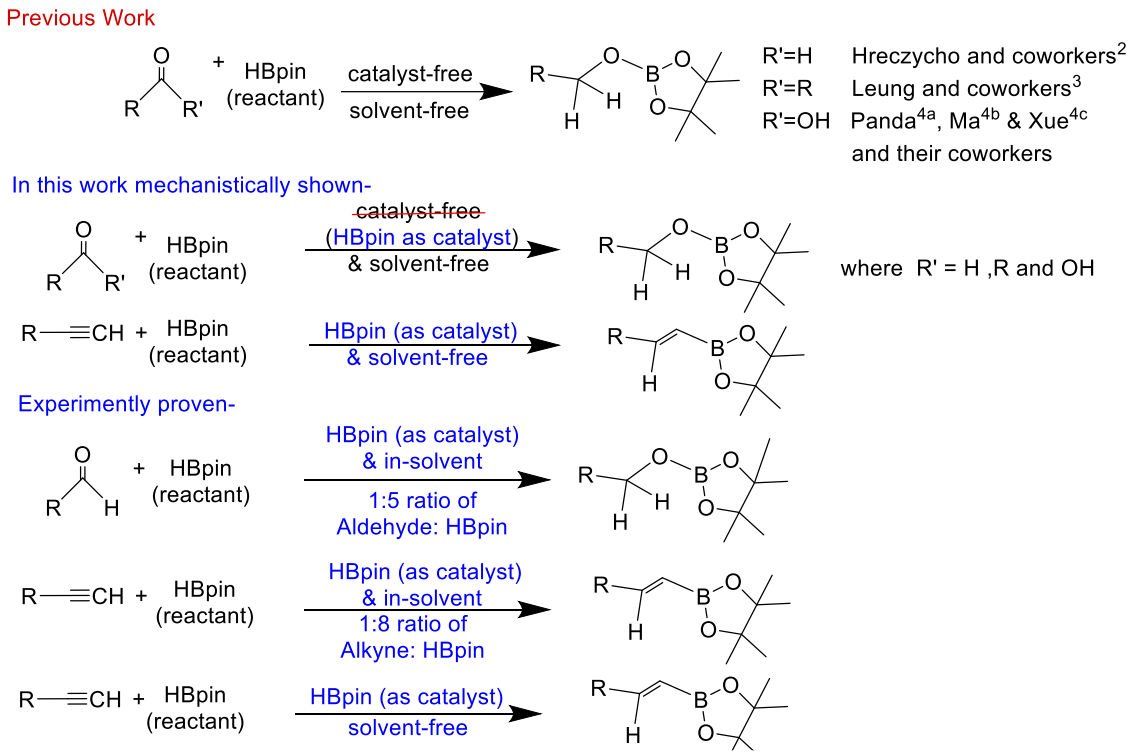

Figure 4.1. Previously reported hydroboration cases in solvent free and catalyst free conditions, as well as new systems designed in the current work with the aid of mechanistic insights through DFT, experimentally proving hetero-functionalisation in solution, not through mediation by an external catalyst, but because one of the reactants acts as the catalyst (an "internal catalyst").

The current work thus furthers different fields of important chemical transformations, by demonstrating how the same can take place efficiently in solution without the need for external catalysts, through this newly discovered "internal catalyst" driven chemical processes.

4.2 Computational Details

All the calculations in this study have been performed with density functional theory (DFT), with the aid of the Turbomole 7.1 suite of programs,[13] using the PBE functional.[14] The TZVP[15] basis set has been employed. The resolution of identity (RI),[16] along with the multipole accelerated resolution of identity (marij)[17] approximations have been employed for an accurate and efficient treatment of the electronic Coulomb term in the DFT calculations. Solvent corrections were incorporated with optimization calculations using the COSMO model, [18] with

benzene (ε = 2.27), HBpin (ε = 2.48), hexane (ε =1.88) and toluene (ε = 2.38) as the solvents. The dielectric constant of HBpin was determined to be 2.48, using the linear relationship between Onsager electric field and the vibrational frequencies.[19] The harmonic frequency calculations were performed for all stationary points to confirm them as local minima or transition state structures. In addition, intrinsic reaction coordinate (IRC)[20] calculations were done with all the transition state structures in order to further confirm that they represented the correct transition states, yielding the correct reactant and product structures for each case. The values reported are ΔG values, with zero-point energy corrections, internal energy and entropic contributions included through frequency calculations on the optimized minima, with the temperature taken to be 25.0 °C for aldehyde hydroboration and carboxylic acid hydroboration and 80.0 °C for ketone hydroboration. These different temperatures were considered keeping in mind the experimental conditions employed in the reporting literature. Lastly, the temperature of 100.0 °C was taken for the hydroboration of alkyne. The translational entropy term in the calculated structures were corrected through a free volume correction introduced by Mammen *et al.*[21] This volume correction is to account for the unreasonable enhancement in translational entropy that is generally observed when employing computational software.

4.2.1 Energetic Span Model (ESM)

To find the turn over frequency (TOF) in the case of the cyanosilylation mechanism, we have calculated the relative efficiency with the AUTOF[22] program, using the "Energetic Span Model" (ESM), developed by Shaik and coworkers.[23,24] The ESM provides a method to calculate the turnover frequencies (TOFs) based on their computed energy profiles of catalytic cycles. The turnover frequency calculations consider the principal rate-determining transition state, potentially rate-influencing transition states, and the intermediates. The turnover frequency (TOF) is calculated by the following equation:

$$\boldsymbol{TOF} = \frac{\boldsymbol{KBT}}{\boldsymbol{h}} \boldsymbol{e^{-\delta E/RT}}$$

$\boldsymbol{\delta E} = \mathbf{T_{TDTS}} - \mathbf{I_{TDI}}$ if TDTS appears after TDI

$\boldsymbol{\delta E} = \mathbf{T_{TDTS}} - \mathbf{I_{TDI}} + \Delta \mathbf{G_r}$ if TDTS appears before TDI

δE is the effective activation barrier of the global reaction. The TDTS and TDI are the transition states, and the intermediate respectively, that maximize δE. This model has been employed to calculate the TOFs at respective reaction temperatures.

4.2.2 *Ab initio* Molecular Dynamics (AIMD)

The AIMD simulations performed with the TeraChem quantum chemistry and AIMD software packages[25-31] using the B3LYP[32] electronic wave function and 3-21g Gaussian basis set[33] to calculate the Born–Oppenheimer potential energy surface The Newton's equations of motion were calculated using Langevin dynamics with an equilibrium temperature of 1800 K (also the starting temperature of the dynamics). We have used very high temperature to increase the average kinetic energy of the reactant molecules and for faster dynamics which breaks all kind of non-covalent interactions without breaking the covalent bonds. The calculations were feasible because of the efficiency of TeraChem, which accelerates the calculation by evaluating the two-electron integrals on the GPU. We have used the ADIIS (augmented direct inversion in the iterative subspace) algorithm[34] available in TeraChem, as an alternative tool for self-consistent field calculation at each AIMD step, in which the default DIIS algorithm[35] failed to converge. Spherical boundary conditions apply to prevent the molecules from flying away which is called "evaporation" event. The molecules were restricted to move inside a spherical volume by a boundary potential.

$$V(r, t) = f(t)\, U(r,k)$$

Where $k = 0.5$ kcal $mol^{-1}Å^{-2}$, $r = 4.5$ Å

We have run AIMD simulations with 3 HBpin molecules atoms (66 atoms) for a total time of ~30 ps with a timestep of 0.5 fs.

4.2.3 Calculation of dielectric constant of HBpin

In the Turbomole software, when the COSMO solvation model is employed, then the dielectric constant is set to the value of the solvent. In COSMO and CPCM solvation models, the only parameter required to describe the solvent is the permittivity epsilon. No other parameter such as a solvent size radius is required: the cavity that is built depends on the solute only. As the dielectric constant of HBpin has not been reported yet, we have estimated the dielectric constant of HBpin using the electric field-IR frequency correlation. The calibration line was constructed using the experimentally obtained carbonyl stretching frequencies of acetone in different polar and non-polar solvents and the estimated electric fields from Onsager electric field theory. The calibration line and the experimental carbonyl frequency of acetone in HBpin allowed the estimation of the Onsager field exerted by HBpin. As the reaction field is a function of the solvent dielectric, the dielectric constant of HBpin was estimated from the Onsager field.

4.3 RESULTS AND DISCUSSION

4.3.1 HBpin Chemistry

As mentioned in the Introduction, HBpin facilitates the hydroboration of a range of different substrates in solvent and external catalyst free conditions, but the same chemistry does not occur in solution in the absence of an external catalyst. So, what explains this unusual behaviour of HBpin? What we propose is that the strength of HBpin – the stabilizing effect of its B-O bonds, as mentioned in the Introduction - is also its weakness. This is because there exists the possibility that the substrate, instead of abstracting the hydride from the boron, can attack one of the two B-O bonds, thereby leading to an unwanted side product. This is shown in **Figure 4.2** below, for the case of the aldehyde substrate studied by Hreczycho and co-workers.[2] If this side reaction is kinetically competitive with the desired hydroboration reaction, then the yield of the desired main product would be reduced.

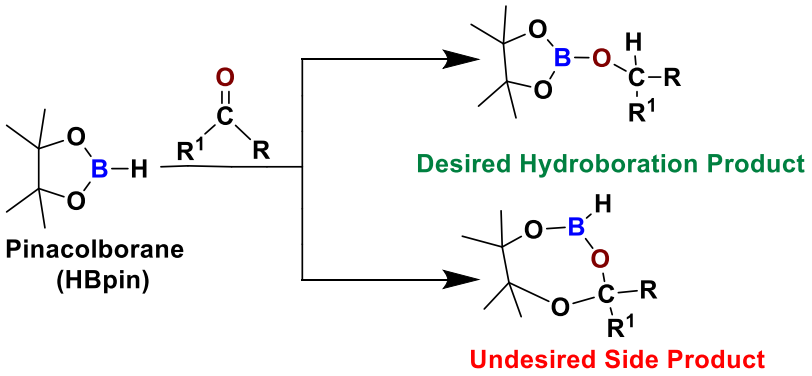

Figure 4.2. Competition between the desired hydroboration reaction, and an undesired side reaction when pinacolborane, HBpin, is employed as the hydroborating agent in solution.

Now, why is the yield restored in the absence of *both* solvent and external catalyst in neat HBpin? We propose that this is due to the ready availability of HBpin molecules in close proximity to each other in neat HBpin. This allows an additional HBpin molecule to act as a hydride relaying catalyst in the hydroboration process, thereby converting the constrained four membered transition state for the hydroboration reaction to a more favourable six membered transition state (see **Figure 4.3** below). It is, of course, true that a similar conversion from a four to a six membered transition state could occur for the undesired side reaction as well, but now, the extra HBpin would act as a reactant rather than as a catalyst, and the reaction would result in a strained, unfavourable six membered heterocycle.

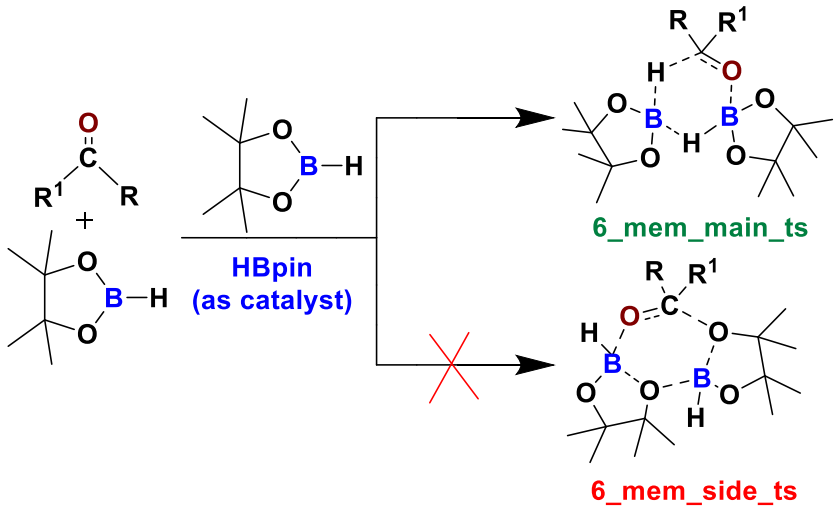

Figure 4.3. An additional HBpin molecule acts as a catalyst and nullifies the competition, increasing the yield of the desired hydroborated product, in liquid HBpin.

As will be shown below, we have proved the validity of this hypothesis with the aid of DFT calculations, taking benzaldehyde, acetophenone, benzoic acid and *p*-methoxyphenylacetylene as substrates, as well as with experimental kinetic studies with *p*-methoxyphenylacetylene as the substrate.

4.3.2 Hydroboration with Aldehyde

The free energy surfaces obtained for the two reactions - the desired hydroboration reaction (in blue) and the undesired side reaction (in red) - are shown together in **Figure 4.4** below. The hydroboration reaction is seen to be thermodynamically favourable by 26.8 kcal/mol, and has a barrier of 32.8 kcal/mol.

While this suggests that the desired reaction itself has a high barrier, another issue is that the first part of the side reaction, indicated with an "A", is kinetically competitive, consisting of two steps having barriers of 32.1 kcal/mol and 32.3 kcal/mol respectively. The heterocyclic intermediate formed from the side reaction, **Int_2**, lies 16.8 kcal/mol above the separated reactants HBpin and benzaldehyde. From this point, there could potentially be a second part to this process, shown as "B" in **Figure 4.4**. This would happen if **Int_2** was to be approached by another benzaldehyde molecule: it could proceed to give the hydroborated product. However, "B" would be unlikely to take place.

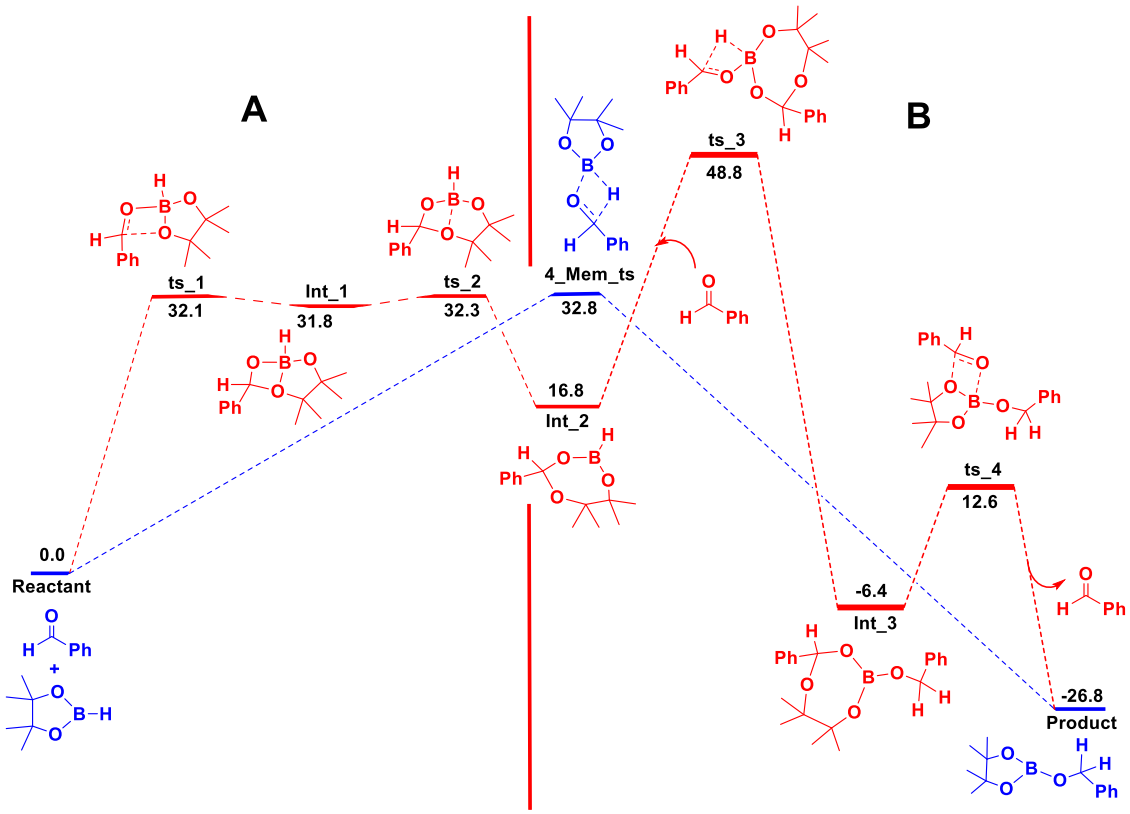

Figure 4.4 The free energy profile of the desired hydroboration reaction and the undesired side reaction for benzaldehyde with HBpin, in benzene solvent. The Gibbs free energy values (in kcal/mol) have been calculated at the PBE/TZVP level of theory.

As **Figure 4.4** reveals, the barrier for the next step, 48.8 kcal/mol, would be too high. The free energy surface for the side reaction therefore indicates that the system can be trapped in "A", moving back and forth between **Int_2** and the starting reactants. While the starting reactants, thus re-formed, would then be able to also pass through the pathway shown in blue to give the desired product, the kinetic competition provided by "A" would act to reduce the yield of the overall reaction.

The same is seen to be true if the reactions were to be considered in neat HBpin. Since the dielectric constants of benzene and HBpin are quite similar (2.27 and 2.48 respectively), the values of the two free energy profiles are also similar (see **Figure 4.5** below). Therefore, regardless of whether the "solvent" was benzene or liquid HBpin, the yield of the final hydroborated product would be reduced by the competing side reaction occurring between the benzaldehyde and HBpin reactants.

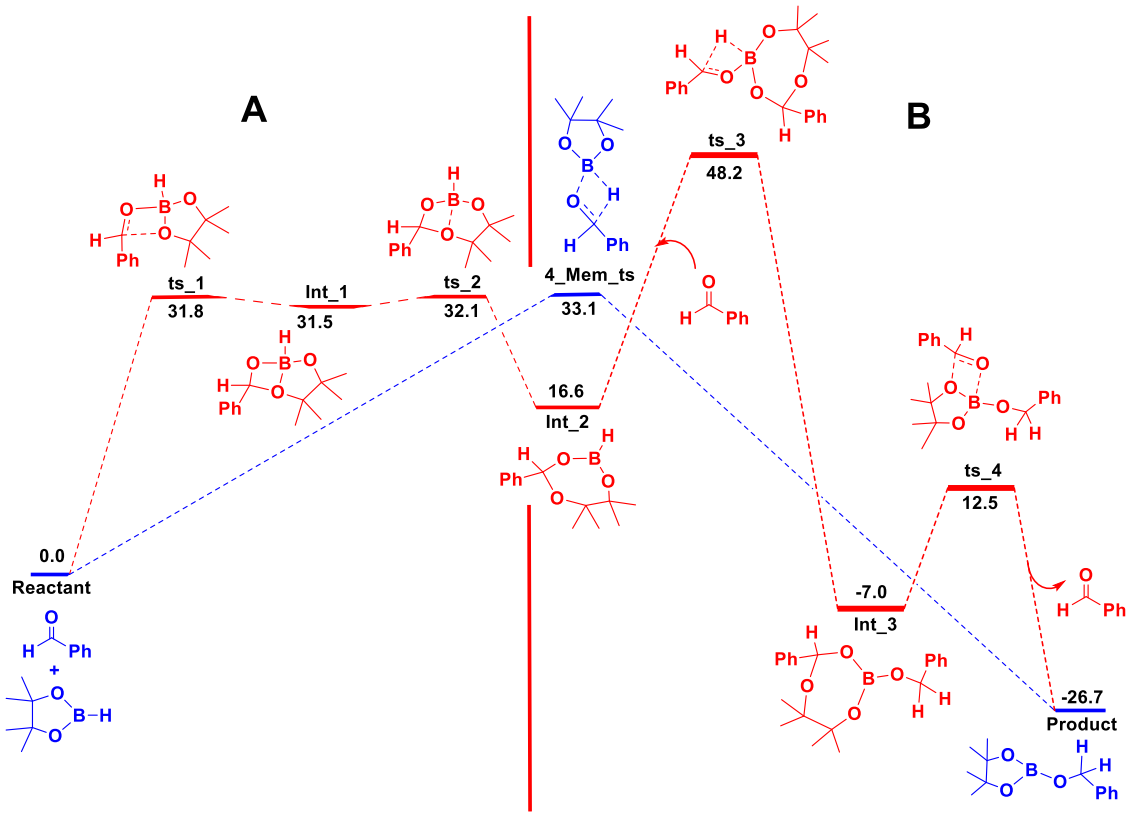

Figure 4.5. The free energy profile of the desired hydroboration reaction and the undesired side reaction for benzaldehyde with HBpin, in liquid HBpin. The Gibbs free energy values (in kcal/mol) have been calculated at the PBE/TZVP level of theory.

However, in liquid HBpin, there exists a second possibility. As mentioned above, an extra HBpin molecule can now act as a hydride relaying catalyst. The result would be the conversion of the four membered transition state to a six membered transition state (see **Figure 4.6** below), and a reduction in barrier from 33.1 kcal/mol to 25.7 kcal/mol. A similar benefit is not received for the side reaction: it is true that the presence of an additional HBpin would create a six membered heterocycle, as had been shown in **Figure 4.3**, but calculations show that such a product would be unfavourable by 21.8 kcal/mol in comparison to the starting reactants. Since this value is close to the barrier for the desired hydroborating reaction, it is clear that the barrier for the formation of this six membered heterocycle side product would be much higher. Thus, the presence of an extra HBpin acting as a catalyst eliminates the competition between the two competing processes, and leads to the preferred formation of the desired hydroborated complex.

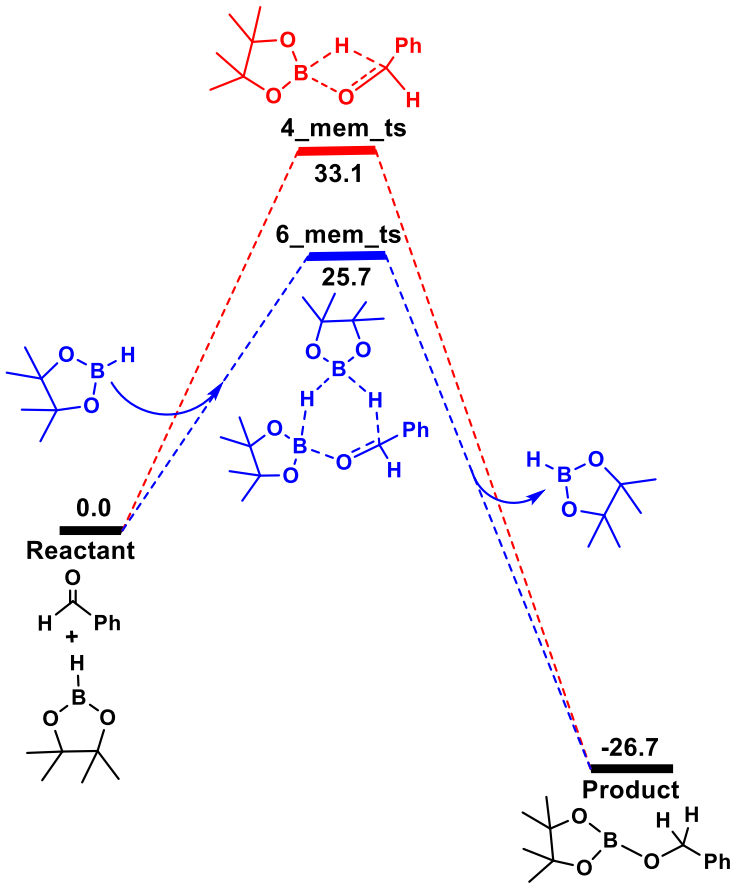

Figure 4.6. The free energy profile for the alternative pathway for benzaldehyde hydroboration in HBpin solvent. The Gibbs free energy values (in kcal/mol) have been calculated at the PBE/TZVP level of theory.

4.3.2.1 Experimental Studies of Hydroboration of Benzaldehyde with HBpin in Solution

What we considered next were the same reactions in solution, in benzene solvent. The results for this are shown in the **Figure 4.7** below. As with the liquid HBpin case, the barriers in benzene solvent become favourable once an additional HBpin molecule is considered, with the barrier found to be 26.5 kcal/mol. The significant drop in barrier height from 32.8 kcal/mol for the four membered transition state to 26.5 kcal/mol for the six membered transition state would be feasible if an extra HBpin molecule could act as a catalyst, i.e., if excess HBpin were to be employed.

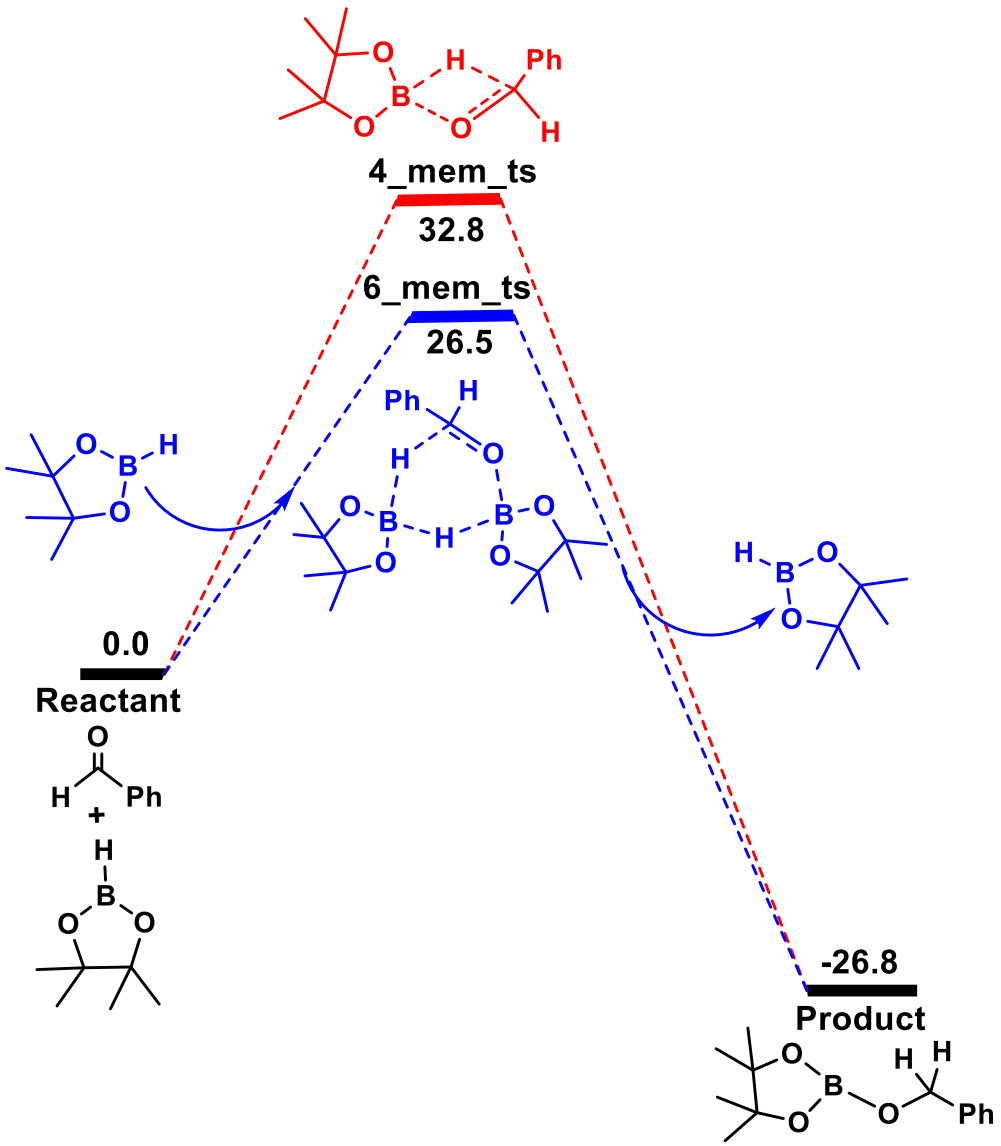

Figure 4.7. Free energy profiles for different competing reactions, now considering an additional HBpin as a hydride relaying catalyst, in benzene solvent. The Gibbs free energy values (in kcal/mol) have been calculated at the PBE/TZVP level of theory.

Under these circumstances, one would not then have to employ an external catalyst. In order to put these insights to the test, our collaborators conducted experiments in benzene solvent, evaluating the possibility of the hydroboration of benzaldehyde with excess HBpin. Several reactions were performed by varying the stoichiometry of benzaldehyde and HBpin in benzene in the absence of an external catalyst. Even after 12.0 h of reaction time, only 20.0% product yield was observed when benzaldehyde and HBpin were treated in a 1:1 ratio. However, gratifyingly, the reaction yield increased from 20.0% to >99.0 % when the concentration of HBpin was increased from 1.0 to 5.0 equivalents.

Furthermore, we note that increasing the concentration of HBpin even further, say, from 1.0 to 8.0 or 10.0 equivalents, i.e., to a significant excess of HBpin, would lead the system from a trimolecular reaction towards a pseudo-bimolecular one. In such a situation, when calculating the ΔG values for the six membered transition state case, one can consider one molecule of benzaldehyde as one reactant, and have two HBpin molecules, in close proximity to one another, as the other reactant species, i.e., the entropic cost of having an additional HBpin molecule in the reaction would be further reduced. Such a situation has been considered in the current work, and the results (see **Figure 4.8** below) show that the barrier is reduced to 22.8 kcal/mol.

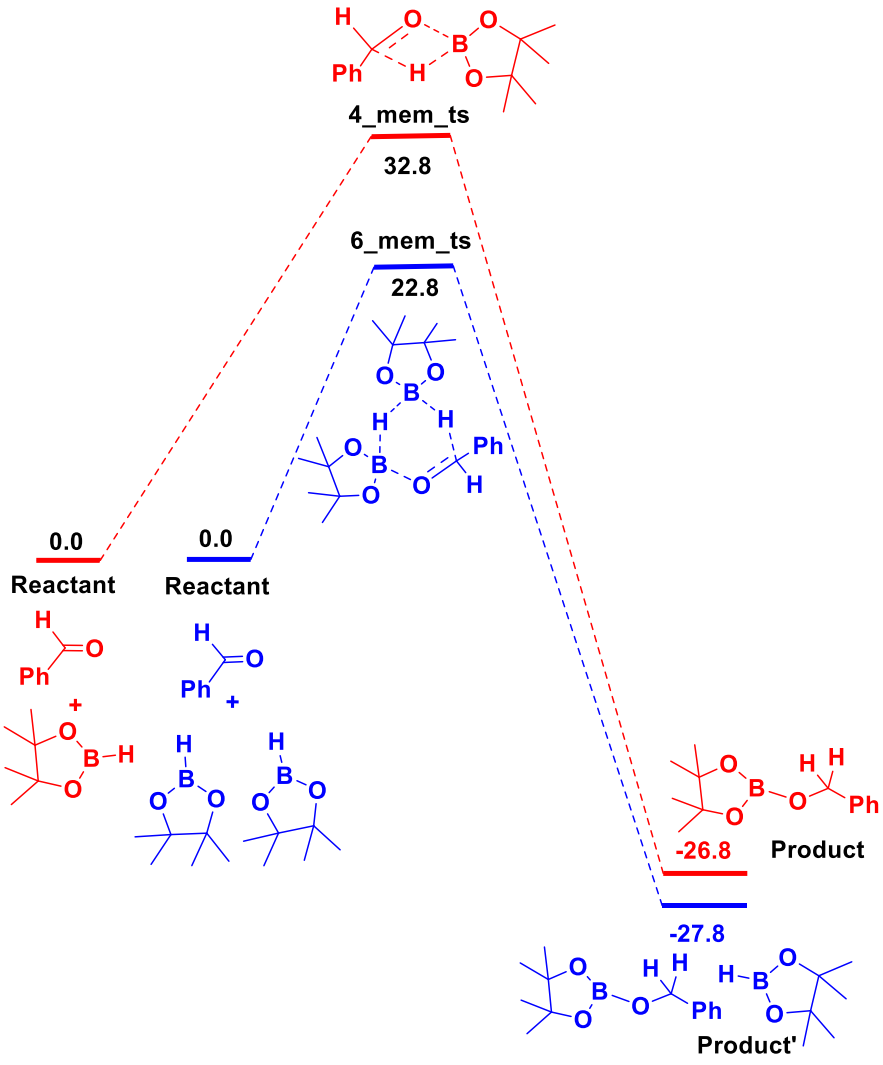

Figure 4.8. Free energy profiles for different competing reactions, now considering an additional HBpin as a hydride relaying catalyst, in significant excess of HBpin in benzene solvent. The Gibbs free energy values (in kcal/mol) have been calculated at the PBE/TZVP level of theory.

Moreover, the efficiency for the hydroboration reaction in solution, calculated using the Energetic Span Model (ESM)[22-24] shown in **Table 4.1** below, indicates that the reaction mechanism involving the six membered transition state in benzene solvent is $4.1*10^4$ times more efficient than the corresponding mechanism involving a four membered transition state (shown in **Figure 4.8**). Now, the mechanism proposed in **Figure 4.8**, considering a significant excess of HBpin, is *$2.5*10^7$ times more efficient*, which shows the value of moving the system towards a pseudo-bimolecular reaction.

Table 4.1. The values for the relative efficiency obtained for benzaldehyde hydroboration reaction in the benzene solvent, for the cases shown in **Figure 4.7** and **Figure 4.8**.

Mechanism	**TOF**
The mechanism in red in **Figure 4.7**	$5.63*10^{-12}$ / sec
The mechanism in blue in **Figure 4.7**	$2.34*10^{-7}$ / sec
The mechanism in blue in **Figure 4.8**	$1.43*10^{-4}$ / sec

What is also important to note here is that the reactions were seen to take place in benzene with >99.0% yield at room temperature. Now, recovering and recycling unused HBpin after the completion of the reaction could be a potential stumbling block to this approach. However, the recovery and recycling of HBpin can be done by fractional distillation, as it has a very low boiling point. In other words, this proposed new approach can be both practical and effective in execution.

4.3.2.2 Possibility of trimer formation in HBpin: *ab initio* molecular dynamics (AIMD) simulations.

The results discussed in manuscript lead to an interesting question: since we have now shown that the B-O bonds in HBpin are susceptible to attack, why cannot HBpin molecules interact among each other in the absence of benzaldehyde (or any other) substrate? In other words, HBpin molecules in close proximity could potentially form heterocyclic species too, through mutual interaction. This is shown in **Figure 4.9** below, where we illustrate the possibility of three HBpin molecules associating to form a trimeric species in liquid HBpin.

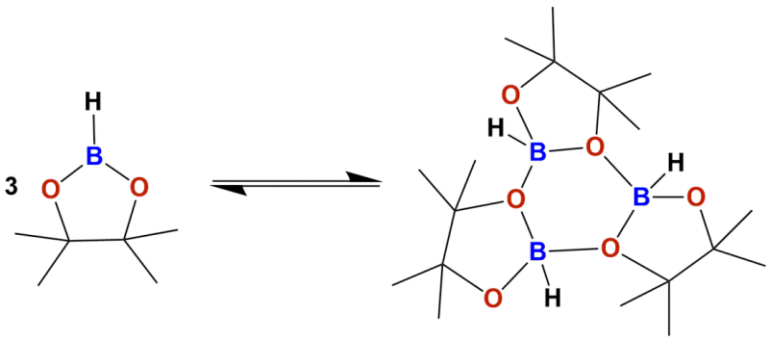

Monomer HBpin **Trimer HBpin**

Figure 4.9. The possibility of monomer-trimer equilibria in liquid HBpin.

We have investigated this possibility with computational studies with DFT. **Figure 4.10** shows the free energy profile for this process. The barrier for the formation of the trimer is quite low: 16.8 kcal/mol, which indicates its feasibility, but the trimer lies 11.4 kcal/mol higher in energy in comparison to the trio of monomers shown in **Figure 4.10** below. This indicates that the equilibrium between HBpin monomers and the trimer would lie significantly towards the side of the monomers. However, the low barrier suggests that such equilibria might still exist in liquid HBpin.

Furthermore, we have also conducted *ab initio* molecular dynamics (AIMD) simulations in order to investigate the possibility of capturing such equilibria. Since B-O bond forming and bond breaking processes are involved, which would require considerably long simulation times, we accelerated the process by conducting AIMD simulations at 1800 K, which allowed us to observe the conversion of three monomers to the trimer and *vice versa* after only 10 ps of simulation. Such an approach has been adopted in AIMD simulations before.[36] Snapshots of the AIMD simulations after different timesteps, indicating the association of the monomers to yield the trimer, and its subsequent dissociation to the monomers again, are shown in **Figure 4.11**. The corresponding dimeric species was not observed in the AIMD simulations, and this is probably due to the disfavouring steric strain that would be present in the four-membered dimer.

However, since the calculations indicate that the equilibrium would lie significantly towards the side of the monomers, the trimer represents a minor species in liquid HBpin. It is conceivable, nevertheless, that benzaldehyde could approach such a trimeric species rather than a monomer in liquid HBpin. In such a case, the only possibility would be the desired hydroboration reaction, as shown in the free energy profile in **Figure 4.10**, because access to

the B-O bonds in HBpin would be cut off in the trimer. As **Figure 4.10** shows, the interaction between benzaldehyde and HBpin would result in the formation of the desired hydroborated product, with the concomitant dissociation of two HBpin molecules from the trimer. The barrier for the process, however, was seen to be high: 41.0 kcal/mol. Overall, the results therefore suggest that species like the HBpin trimer represent interesting, but minor players in hydroboration chemistry.

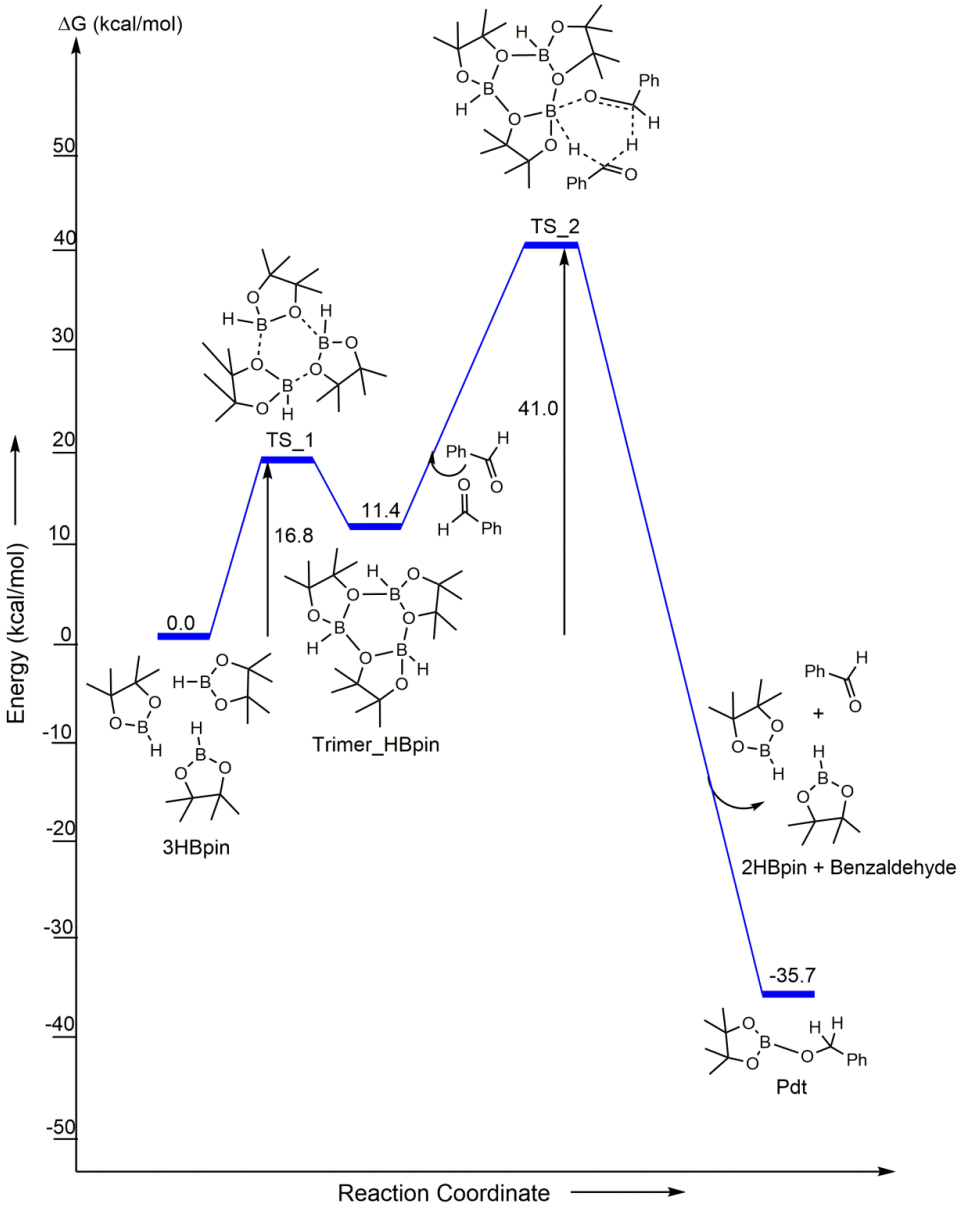

Figure 4.10. The free energy profile for the trimerization equilibrium of the HBpin monomer, and the subsequent hydroboration of the benzaldehyde with the HBpin trimer as the hydroborating agent, in the solvent free system (HBpin considered as solvent). The values (in kcal/mol) have been calculated at the PBE/TZVP level of theory.

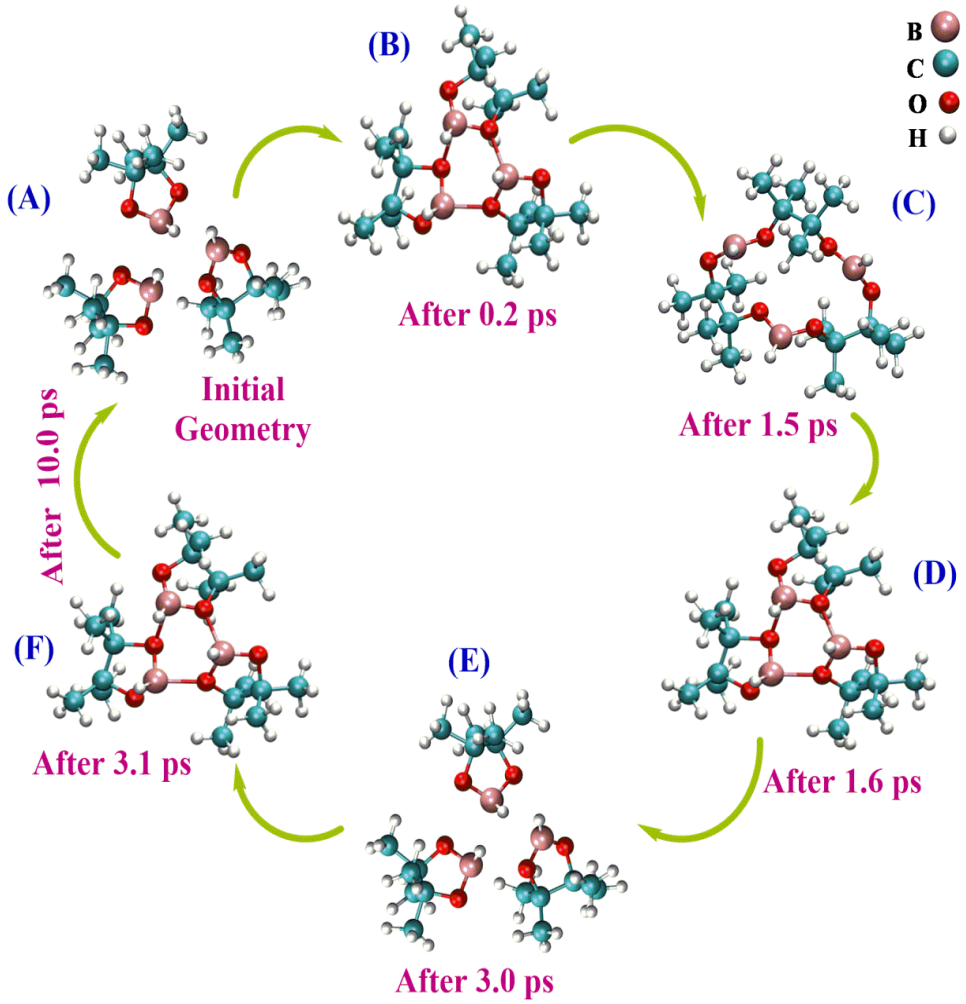

Figure 4.11. Snapshots indicating the state of the chemical system during the progress of *ab initio* molecular dynamics (AIMD) simulations with time. It is seen that three HBpin molecules combine to form a trimer and then break, as the AIMD simulations progress in time.

4.3.3 Hydroboration with Ketones

Leung and co-workers[3] have done the hydroboration of ketone with HBpin, in the absence of solvent and external catalyst, taking acetophenone as the ketone. Like in hydroboration with aldehyde, the possibility of an additional HBpin molecule acting as a catalyst, in this case, would create separation in favorability between the six-membered transition state and the four-membered transition state, favoring the former over the latter (see **Figure 4.12(a)** below). Hence, the calculations indicate that the same factors are in play in the case of ketones, as was observed for the aldehyde case. Likewise, calculations indicate that the additional HBpin molecule acting as a catalyst would also lead to greater efficiency of the hydroboration in solution (specifically the toluene solvent – see **Figure 4.12(b)**).

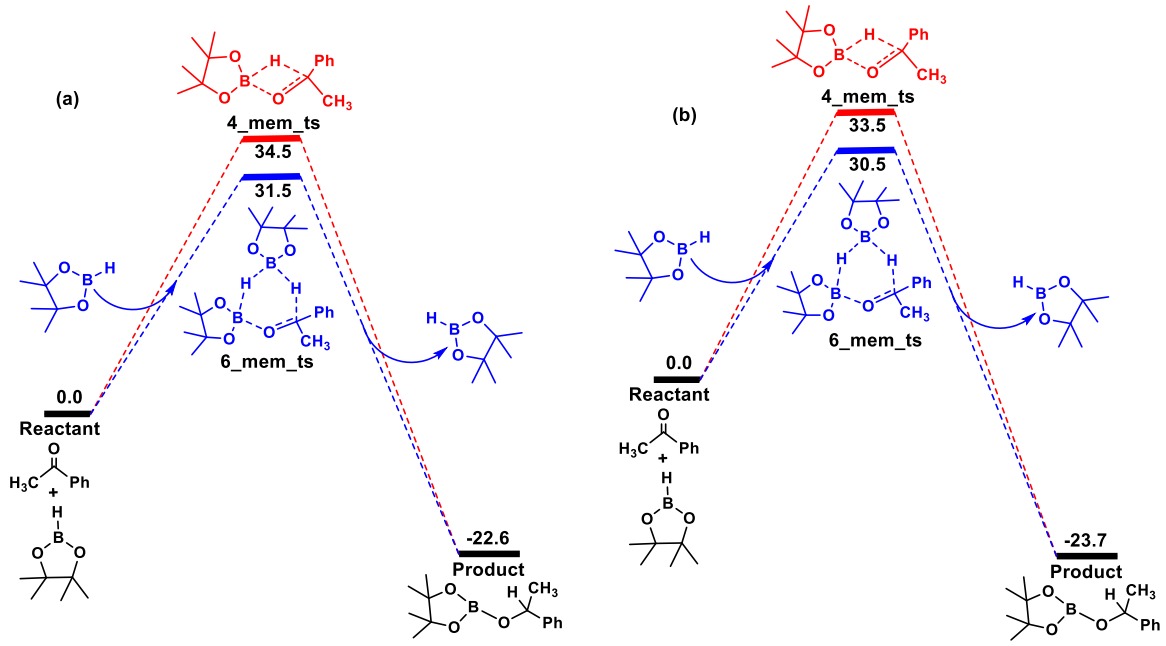

Figure 4.12. Free energy profiles for different competing reactions for the ketone substrate, with and without an additional HBpin as a hydride relaying catalyst, with (a) liquid HBpin as the solvent and (b) toluene as solvent. The Gibbs free energy values (in kcal/mol) have been calculated at the PBE/TZVP level of theory.

Furthermore, the efficiency for the hydroboration reaction in solution calculated using the Energetic Span Model (ESM), has been shown in **Table 4.2**. The results indicate that reaction mechanism involving the six-membered transition state is 71.6 times more efficient than the reaction mechanism involving the four-membered transition state in toluene solvent.

Table 4.2. The values for the relative efficiency obtained for the ketone hydroboration reaction in toluene solvent, for the case shown in **Figure 4.12(b)**.

Mechanism	TOF
in red	$1.37*10^{-8}$ / sec
in blue	$9.82*10^{-7}$ / sec

4.3.4 Hydroboration with Carboxylic acid

Panda, Ma and Xue, and their co-workers[4] were successful in doing the hydroboration of a carboxylic acid with HBpin, in the absence of solvent and external catalyst, taking benzoic acid as the substrate. The hydroboration was achieved in this case at room temperature. The mechanism that they had proposed involves multiple steps and several four-membered

transition states. We have studied the mechanism in the experimentally employed hexane solvent, as well as in liquid HBpin (see **Figure 4.13**, **Figure 4.14**, and **Figure 4.15**). As shown in **Figure 4.13** below, the barriers were seen to be reduced considerably by the inclusion of an additional HBpin molecule as a catalyst. Moreover, as shown in **Table 4.3**, the TOF was calculated using the Energetic Span Model (ESM), which also indicates that hydroboration takes place with high efficiency through the mechanism proposed involving a six-membered transition state with HBpin as the internal catalyst, as shown in **Figure 4.14**: the process is $1.9*10^5$ times more efficient in comparison to the mechanism shown in **Figure 4.13(b)**. Similarly, in hexane solvent (as shown in **Figure 4.15**), the mechanism involving a six-membered transition state with HBpin as the internal catalyst is 17.4 times more efficient than the mechanism shown in **Figure 4.13(a)**.

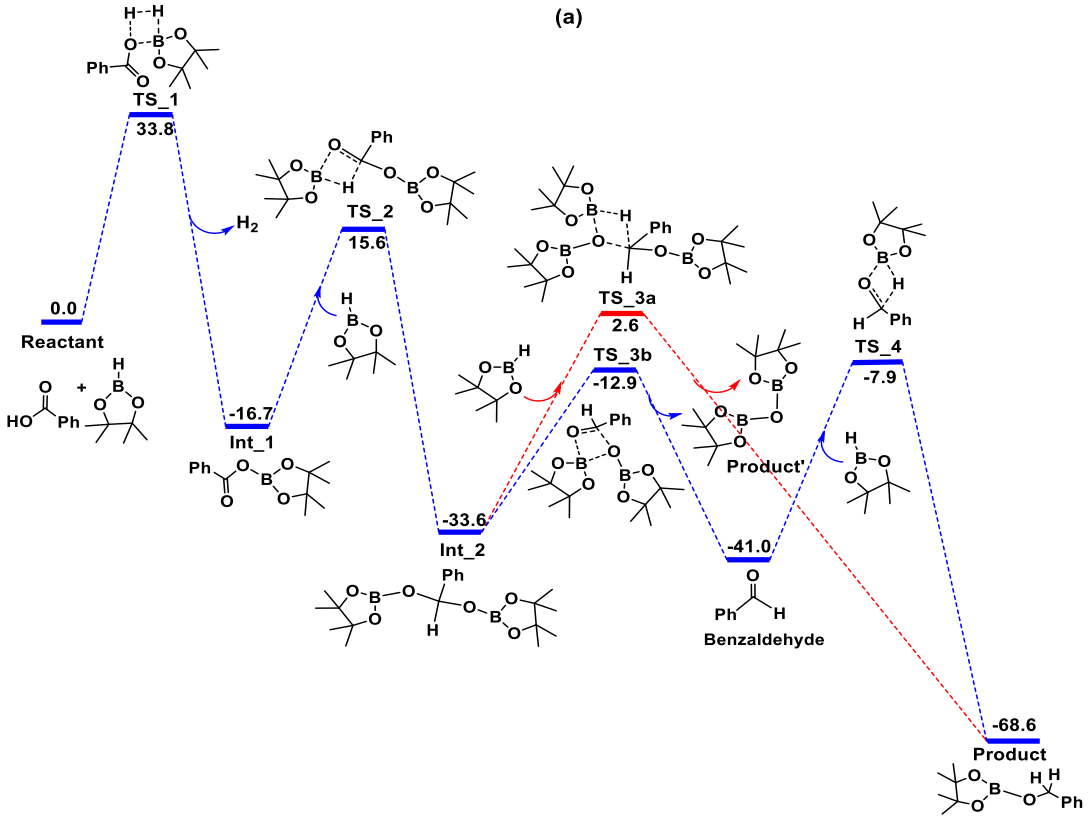

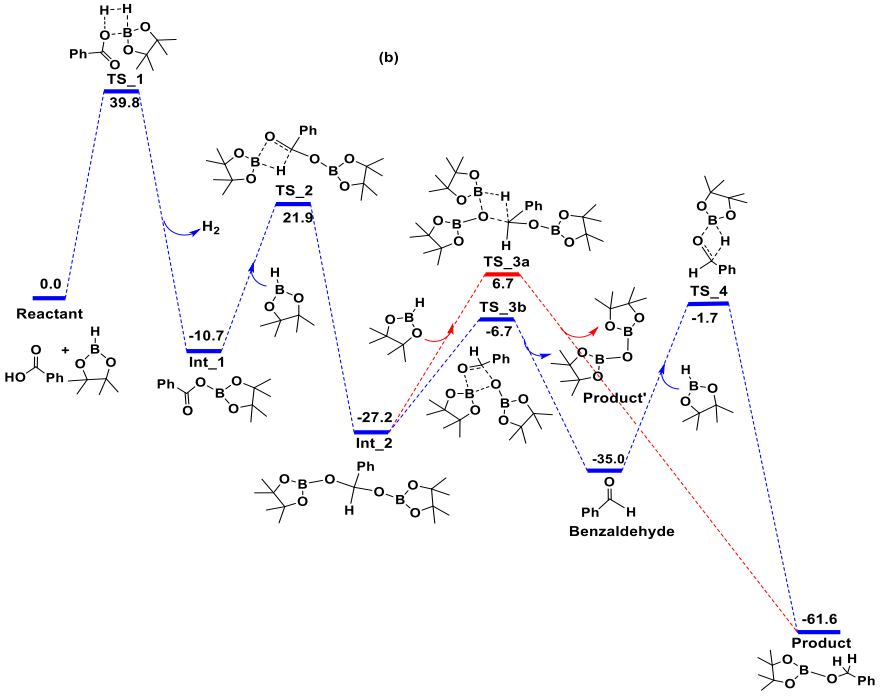

Figure 4.13 The free energy profile of the desired hydroboration reaction for the benzoic acid substrate with HBpin, without the assistance of an additional HBpin molecule, in (a) hexane solvent, and in (b) liquid HBpin. The Gibbs free energy values (in kcal/mol) have been calculated at the PBE/TZVP level of theory.

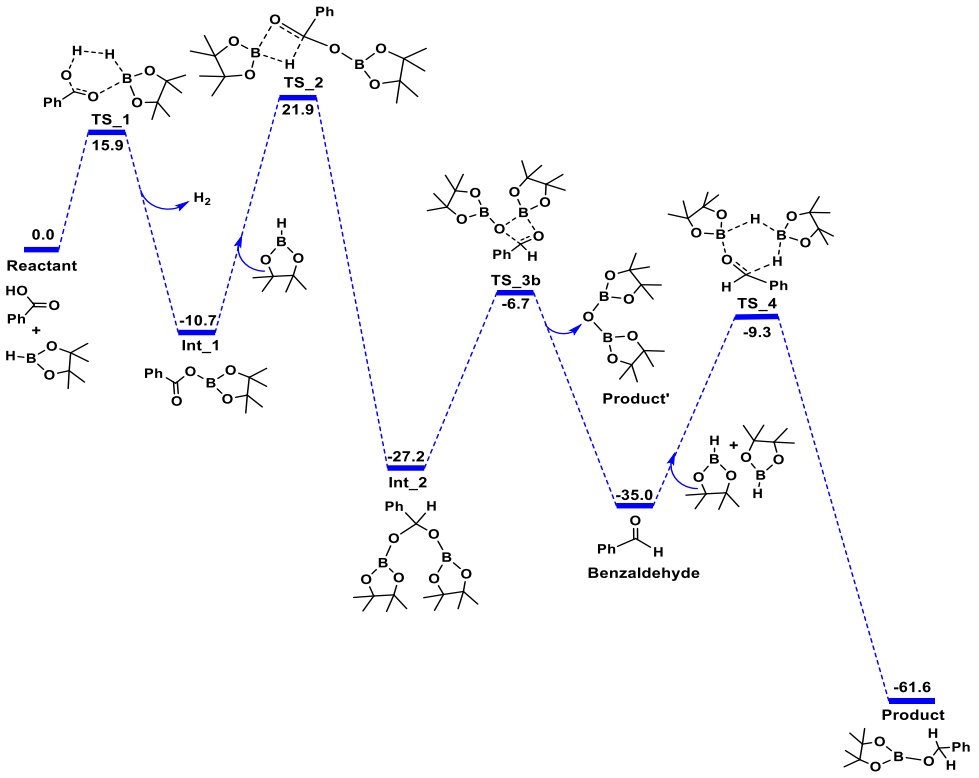

Figure 4.14. The free energy profiles for benzoic acid hydroboration with HBpin, in liquid HBpin, considering an additional HBpin as a catalyst. The Gibbs free energy values (in kcal/mol) have been calculated at the PBE/TZVP level of theory.

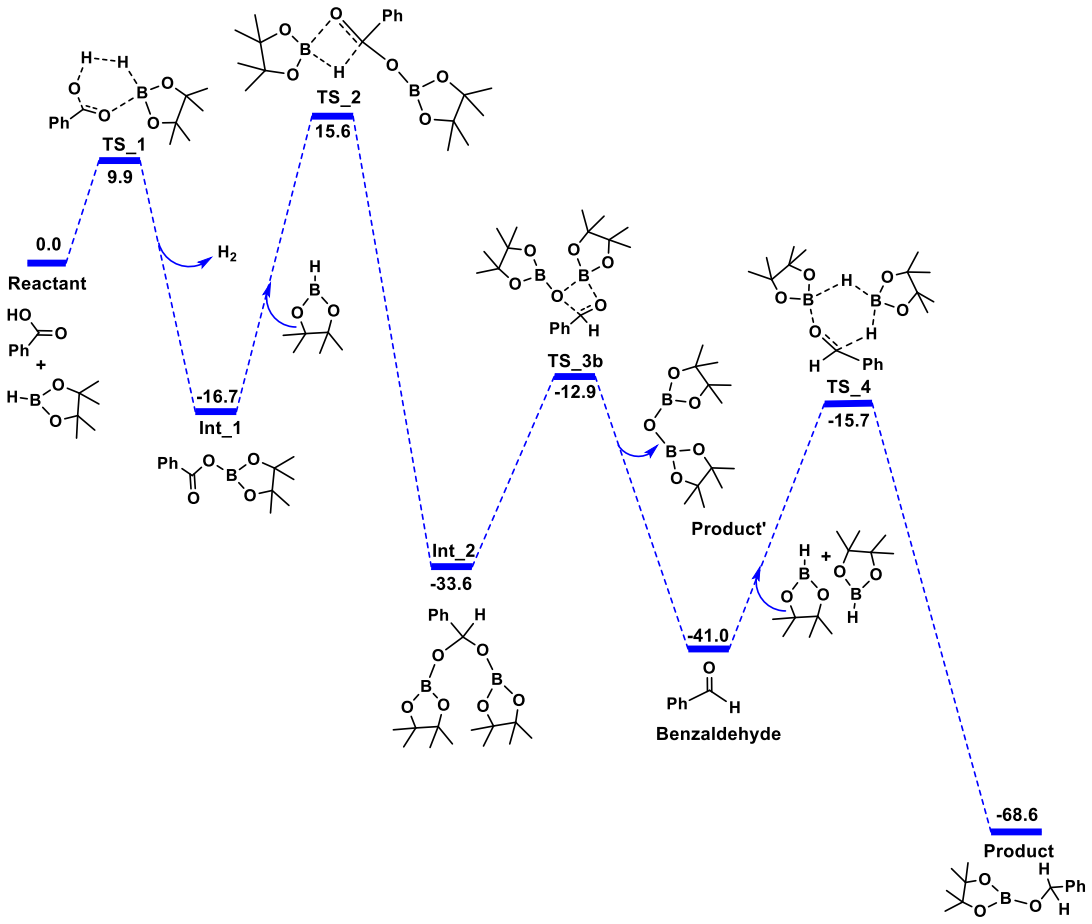

Figure 4.15. The free energy profile of the desired hydroboration reaction for the benzoic acid substrate with HBpin, with the assistance of an additional HBpin molecule, in hexane solvent. The Gibbs free energy values (in kcal/mol) have been calculated at the PBE/TZVP level of theory.

Table 4.3. The values for the relative efficiency obtained for carboxylic acid hydroboration reaction in hexane as well as HBpin solvent, for the cases shown in **Figure 4.13a, 4.13b, 4.14, 4.15.**

Mechanism	TOF
Mechanism in **Figure 4.13a** (in blue)	$7.52*10^{-13}$ / sec
The mechanism in **Figure 4.15**	$1.31*10^{-11}$ / sec
Mechanism in **Figure 4.13b** (in blue)	$4.17*10^{-17}$ / sec
The mechanism in **Figure 4.14**	$7.9*10^{-12}$ / sec

4.3.5 Hydroboration of the Alkyne - *p*-methoxyphenylacetylene with HBpin in Solution

Having validated with experiments the conclusions reached from DFT calculations, we also decided to check whether the insights gained held good for substrates other than aldehyde. To this end, our collaborators proceeded to conduct experimental studies for the external catalyst free hydroboration of the alkyne, *p*-methoxyphenylacetylene, by HBpin in solution. External catalyst aided hydroboration of alkynes has been reported in the literature,[37] but this would represent the first example of the same in solution without the aid of an external catalyst.

Experiments were proceeded with testing the DFT conclusions. When the reaction taking *p*-methoxyphenylacetylene and HBpin in the ratio of 1:1 in solvent free and external catalyst free condition was conducted, a good yield (64.0%) was achieved. On the other hand, in benzene solvent, a good yield (68.0%) was achieved when *p*-methoxyphenylacetylene and HBpin in significant excess were taken in the ratio of 1:8.

DFT calculations show that in solvent free and external catalyst free conditions, the presence of an additional HBpin molecule would act as a hydride relaying catalyst and that would reduce the barrier for the desired hydroboration reaction, as shown in **Figure 4.16** below (**Figure 4.16 (a)**, for a trimolecular reaction and **Figure 4.16 (b)** for the corresponding pseudo-bimolecular case, as discussed above). On the other hand, the hydroboration of *p*-methoxyphenylacetylene in the aromatic solvent benzene was achieved when the ratio of the *p*-methoxyphenylacetylene and HBpin in significant excess was taken as 1:8. This suggests that significant excess of HBpin, i.e., a pseudo-bimolecular reaction, is the preferred route of hydroboration of *p*-methoxyphenylacetylene in benzene solvent. We have therefore considered one molecule of benzaldehyde as one reactant, and have optimized two HBpin molecules in close proximity as the other reactant species. This leads to a reduced barrier of 34.0 kcal/mol (see **Figure 4.17 (a)**). The TOF calculated using the Energetic Span Model (ESM) (see Table 4.4 below) shows that mechanism following this pseudo-bimolecular path is $2.17*10^3$ times favored over the mechanism shown in red which does not involve an extra HBpin molecule. Moreover, even if the reaction goes through the trimolecular path, as shown in **Figure 4.17 (b)** below, the mechanism involving an extra molecule of HBpin would still be favored. This pathway is found to be 2.24 times more efficient (see **Table 4.4**).

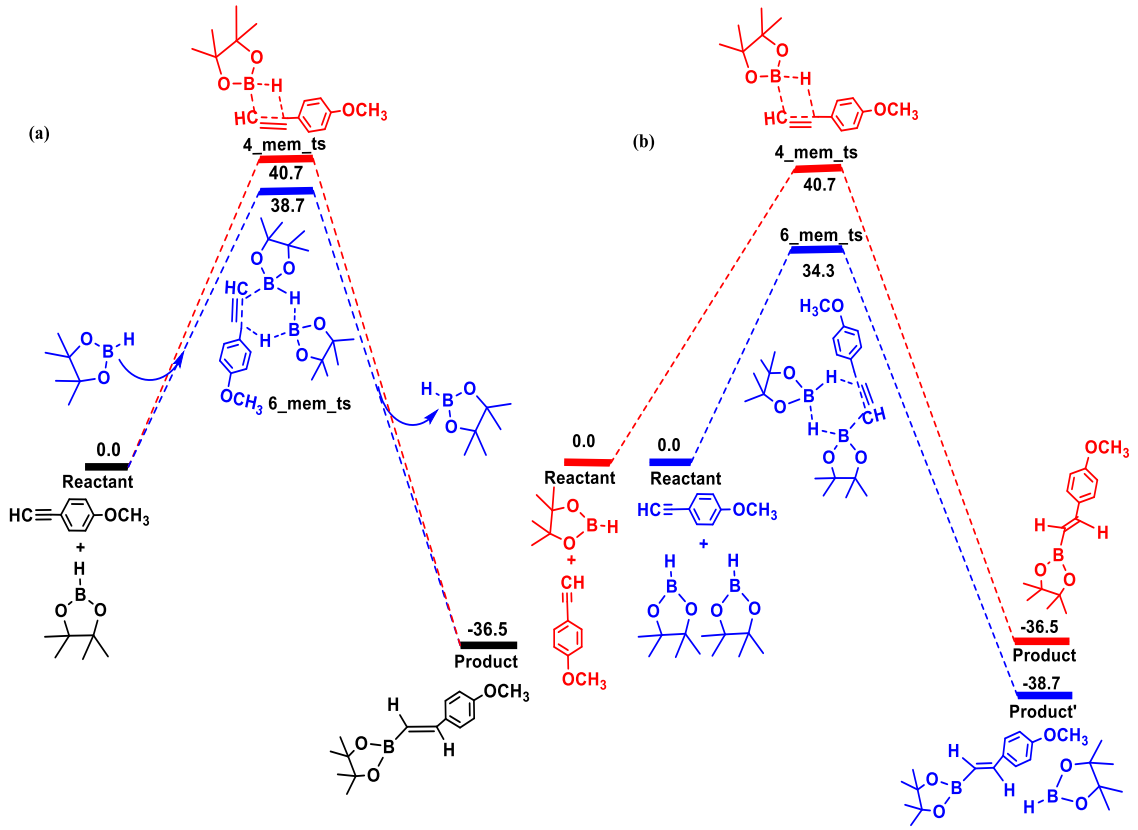

Figure 4.16. The free energy profiles of the desired hydroboration reaction with and without the assistance of an additional HBpin molecule for the *p*-methoxyphenylacetylene substrate in (a) liquid HBpin solvent and (b) significant excess of HBpin in liquid HBpin solvent. The Gibbs free energy values (in kcal/mol) have been calculated at the PBE/TZVP level of theory.

Table 4.4. The values for the relative efficiency obtained for the alkyne hydroboration reaction in benzene solvent, for the cases shown in **Figure 4.17(a)** and **Figure 4.17(b)**.

Mechanism	TOF
The mechanism in red in **Figure 4.17(a)**	$4.36*10^{-11}$ / sec
The mechanism in blue in **Figure 4.17(a)**	$9.79*10^{-11}$ / sec
The mechanism in blue in **Figure 4.17(b)**	$9.5*10^{-8}$ / sec

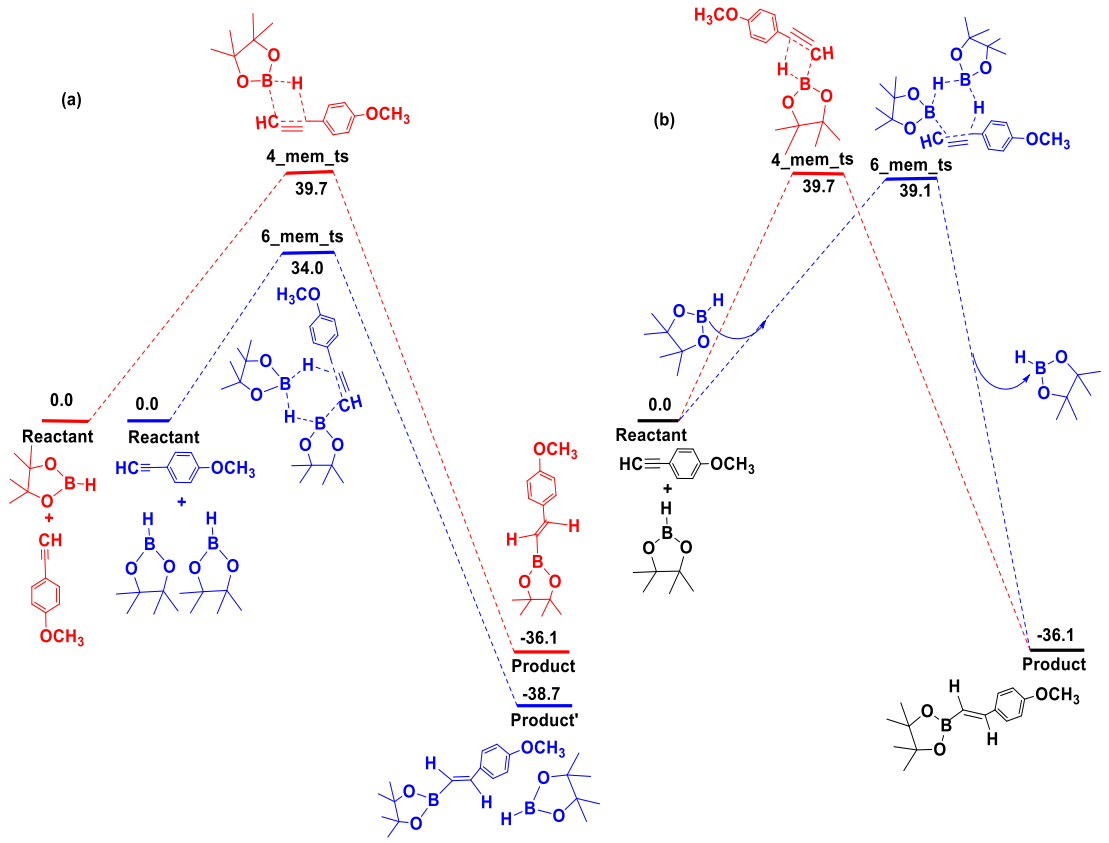

Figure 4.17. The free energy profiles of the desired hydroboration reaction with and without the assistance of an additional HBpin molecule for the *p*-methoxyphenylacetylene substrate in (a) significant excess of HBpin in benzene solvent and (b) in benzene solvent. The Gibbs free energy values (in kcal/mol) have been calculated at the PBE/TZVP level of theory.

4.3.5.1 Procedure for Rate-order determination

Our collaborators have also performed kinetic experiments to further understand the effect of HBpin on the hydroboration reaction. The rate order with respect to the [HBpin] was determined for the hydroborylation of *p*-methoxyphenylacetylene. The order was determined using the initial rate method (see **Figure 4.18** and **Table 4.5** below). The order of the reaction with respect to HBpin was determined to be 1.58. This indicates that for a reaction to proceed, more than one molecule of HBpin is required. This is consistent with our hypothesis (and the attending calculations) that an extra HBpin molecule is participating in the hydroboration reaction.

The rate order of the hydroboration reaction with respect to various components of the reaction was determined using the initial rate method. The data of the concentration (M) of the product vs time (min.) plot was fitted to linear using Origin Pro 8. The slope of the linear fitted

curve represents the reaction rate. The order of the reaction was determined by plotting the log(rate) vs log(conc.) of that particular component.

Table 4.5. Rate of the hydroboration reaction at different initial concentrations of pinacol borane (HBpin).

Experiment	4-OMe phenylacetylene: HBpin	Amount of HBpin (g)	The initial concentration of HBpin (M)	Initial rate [mmol/min] × 10^{-4}
1	1:1	0.032	0.25	0.254
2	1:2	0.064	0.50	0.709
3	1:4	0.128	1.00	2.145
4	1:5	0.160	1.25	3.201

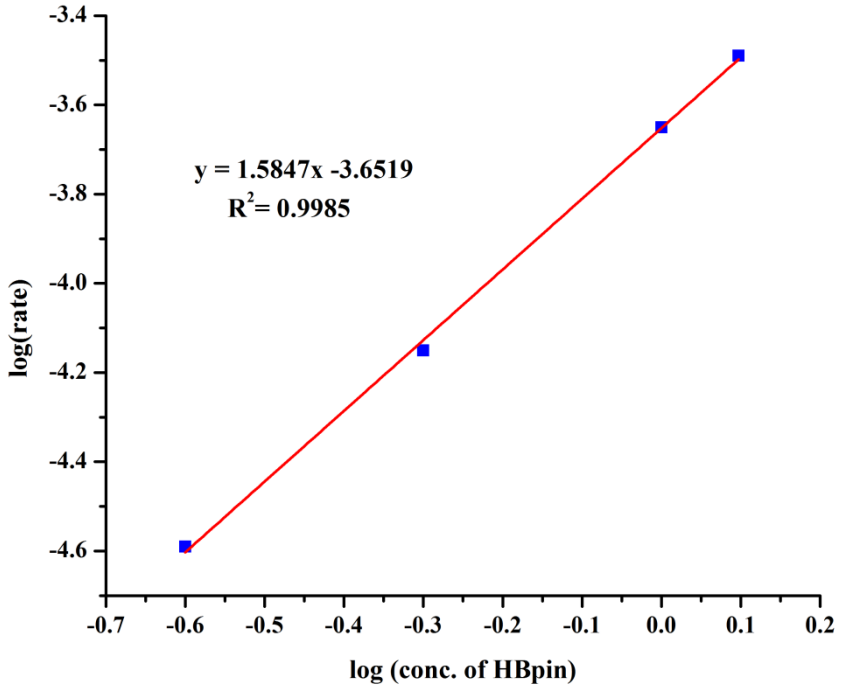

Figure 4.18. log(rate) versus log (conc. of pinacol borane).

4.4 Conclusions

There is an important, environmentally beneficent area of research that has seen impressive growth in recent years. This pertains to the field of solvent and external catalyst free chemistry.[2-9] The current work aims to provide mechanistic understanding into this chemistry. Specifically, we have explored an important functionalization reaction: hydroboration. Investigations with DFT for a range of substrates: benzaldehyde, acetophenone, benzoic acid and *p*-methoxyphenylacetylene for the hydroboration in neat HBpin reveal the favourable intervention of an additional HBpin molecule during the reaction, which makes the chemistry more efficient in the respective cases. In other words, HBpin acts not only as reactant and solvent during the reaction, but also as internal catalyst. Experimental kinetic studies conducted for the hydroboration of *p*-methoxyphenylacetylene with HBpin corroborate these computational findings. These insights have been further tested by experiments by our collaborators, which have validated the computational findings by showing, for the first time, that the use of excess HBpin in solution allowed the hydroboration reactions to take place with good yields without the need of an external catalyst. This has significance because it opens up possibilities of allowing such internal catalyst aided reactions to occur for substrates that dissolve poorly in neat HBpin.

There is also an expanded significance to the obtained results, pertaining to the growing family of reactions taking place in solvent and external catalyst free conditions. These include acetalization,[8] the aza-Michael addition[9] and many more. For instance, in the case of the acetalization of imines, a proton shuttle mechanism has been hypothesized,[8] thereby implying the possibility of the imine in question acting as both reactant and catalyst. One can therefore envisage doing the same chemistry by exploiting the potential of the imine to act as an internal catalyst, by making use of the strategy discussed in the current work. A similar approach could potentially be employed for the aza-Michael addition reaction of cyclohexylamine to diethyl maleate,[9] or the conversion of an aziridine to an oxazolidinone[38] or the synthesis of tetrazoles by choline azide.[39] Furthermore, microkinetic modeling can also be considered in the future in order to get a clearer picture of the internal catalysis process. Hence, the current work is of considerable general significance for internal catalyst aided chemical transformations.

4.5 References

1. R. A. Sheldon, *Chem. Commun*. **2008**, 3352.
2. H. Stachowiak, J. Kazmierczak, K. Kucinski, G. Hreczycho, *Green Chem*. **2018**, *20*, 1738.
3. W. Wang, M. Luo, W. Yao, M. Ma, S. A. Pullarkat, L. Xu, P.H. Leung, *New J. Chem.* **2019**, *43*, 10744.
4. (a) A. Harinath, J. Bhattacharjee, T. K. Panda, *Chem. Commun.* **2019**, *55*, 1386. (b) W. Wang, M. Luo, D. Zhu, W. Yao, L. Xu, M. Ma, *Org. Biomol. Chem.* **2019**, *17*, 3604-3608. (c) X. Xu, D. Yan, Z. Zhu, Z. Kang, Y. Yao, Q. Shen, M. Xue, *ACS Omega,* **2019**, *4*, 6775.
5. V. K. Pandey, S. N. R. Donthireddy A. Rit, *Chem. Asian J.* **2019,** *14*, 3255.
6. W. Wang, M. Luo, W. Yao, M. Ma, S. A. Pullarkat, L. Xu, P.H. Leung, *ACS Sustainable Chem. Eng.* **2019**, *7*, 1718. (b) S. Pahar, G. Kundu, S. S. Sen, *ACS Omega*, **2020**, *5*, 25477.
7. H. Iida, H. Hamana, K. Matsumoto, *Synth. Comm.* **2007**, *37*, 1801.
8. V. J. Lillo, J. Mansilla, J. M. Saa, *Org. Biomol. Chem*. **2018**, *16*, 4527.
9. M. Blaha, O. Trhlikova, J. Podesva, S. Abbrent, M. Steinhart, J. Dybal, M. Duskova-Smrckova, *Tetrahedron* **2018,** *74*, 58.
10. (a) M. L. Shegavi, S. K. Bose, *Catal. Sci. Technol*. **2019**, *9*, 3307. (b) M. K. Bisai, S. Yadav, T. Das, K. Vanka, S. S. Sen, *Chem. Commun*. **2019,** 55, 11711.
11. A. Harinath, J. Bhattacharjee, T. K. Panda, *Adv. Synth. Catal*. **2019**, *361*, 850.
12. W. Liu, Y. Ding, D. Jin, Q. Shen, B. Yan, X. Ma, Z. Yang, *Green Chem*. **2019**, *21*, 3812.
13. TURBOMOLE V7.1 **2016**, a development of University of Karlsruhe and ForschungszentrumKarlsruhe GmbH, 1989-2007, TURBOMOLE GmbH, since **2007**; available from http://www.turbomole.com.
14. J. P. Perdew, K. Burke, M. Ernzerhof, *Phys. Rev. Lett.* **1996**, *77*, 3865.
15. A. Schafer, C. Huber, R. Ahlrichs J. *Chem. Phys.* **1994**, *100*, 5829.
16. k. Eichkorn, O. Treutler, H. Ohm, M. Haser, R. Ahlrichs, *Chem. Phys. Lett*. **1995**, *240*, 283.
17. M. Sierka, A. Hogekamp, R. Ahlrichs, *J. Chem. Phys.* **2003**, *118*, 9136.
18. A. Klamt, G. Schuurmann, *Chem. Soc. Perkin Trans.* **1993**, *2*, 799-805.
19. S. Bagchi, S. D. Fried, S. G. Boxer, *J. Am. Chem. Soc.* **2012**, *134*, 10373.
20. K. Fukui, *Acc. Chem. Res*. **1981**, *14*, 363.
21. M. Mammen, E. I. Shakhnovich, J. M. Deutch, G. M. Whitesides, *J. Org. Chem*. **1998**, *63*, 3821.
22. S. Kozuch, J. M. L. Martin, *ACS Catal*. **2011**, *1*, 246-253.

23. A. Uhe, S. Kozuch, S. Shaik, *Comput. Chem.* **2010,** *32*, 978.

24. S. Kozuch, S. Shaik, *Acc. Chem. Res.* **2011**, 44, 101.

25. S. Ufimtsev, T. J. Martinez, *J. Chem. Theory Comput.*, **2009,** *5*, 2619.

26. S. Ufimtsev, N. Luehr, T. J. Martinez, J. *Phys. Chem. Lett.*, **2011,** *2*, 1789.

27. C. M. Isborn, N. Luehr, I. S. Ufimtsev, T. J. Martinez, *J. Chem. Theory Comput*., **2011**, *7***,** 1814.

28. A.V. Titov, I. S. Ufimtsev, N. Luehr, T. J. Martinez, *J. Chem. Theory Comput*., **2013**, *9***,** 213.

29. I. S. Ufimtsev T. J. Martinez, *Comput. Sci. Eng*., **2008**, *10*, 26.

30. I. S. Ufimtsev, T. J. Martinez, *J. Chem. Theory Comput*., **2008**, *4*, 222.

31. S. Ufimtsev, T. J. Martinez, *J. Chem. Theory Comput*., **2009**, *5***,** 1004.

32. I. D. Becke, *J. Chem. Phys*., **1993**, *98*, 5648.

33. J. S. Binkley, J. A. Pople, W. J. Hehre, *J. Am. Chem. Soc*., **1980**, *102*, 939.

34. X. Hu, W. Yang, *J. Chem. Phys.*, **2010**, *132*, 054109.

35. P. Pulay *Chem. Phys. Lett*., **1980**, *73***,** 393.

36. L.P. Wang, A. Titov, R. McGibbon, F. Liu, V.S. Pande, T.J. Martínez, *Nat Chem.*, **2014**, *6*, 12, 1044.

37. A. Bismuto, M. J. Cowley, S. P. Thomas, *ACS Catal.* **2018**, *8*, 2001.

38. C. Phung, R. M. Ulrich, M. Ibrahim, N.T. G. Tighe, D. L. Lieberman, R. A. Pinhas, *Green Chem.* **2011**, *13*, 3224.

39. J. Azarnia, M. Kobra, A. Mahsa, S. Jalali A. Heydari, *Chemistry Select* **2018**, *3*, 12175.

Chapter 5

To Catalyze or Not to Catalyze: That is the Question in Main Group Compound Mediated Cyanosilylation

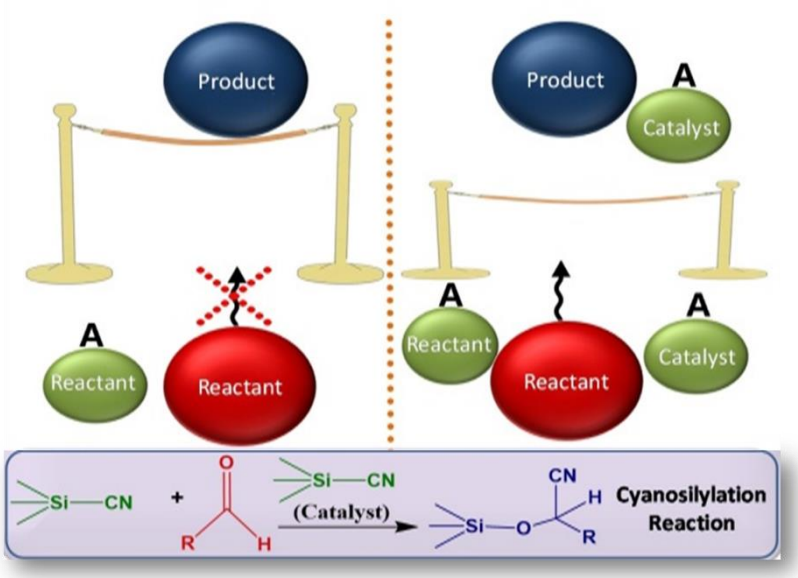

Chapter 5

To Catalyze or Not to Catalyze: That is the Question in Main Group Compound Mediated Cyanosilylation

Abstract

Recent investigations have revealed that the cyanosilylation of unsaturated species can be achieved quantitatively in a solvent-free and external catalyst-free environment, while, interestingly, the addition of the solvent leads only to trace amounts of the product. This invites questions about the role of the solvent. Does the catalyst act to catalyze the reaction or does it function to suppress the deleterious effects of the solvent? Employing DFT calculations, we have tried to explain what happens when the cyanosilylation reaction occurs in a solvent-free environment and why it does not need any catalyst to give a high yield at an elevated temperature. Calculations with trimethylsilyl cyanide (TMSCN) show that neat TMSCN can work as all three: solvent, substrate and catalyst, during the cyanosilylation of benzaldehyde. It has then been demonstrated experimentally how the same reaction can be done in solution in the absence of a catalyst. Our approach thus shows that important new systems (cyanosilylation in this chapter and hydroboration in last chapter) that work in catalyst and solvent free conditions share common mechanistic features, and reveals further through experiments how modifications can be made to such systems to make the reactions occur in solution in catalyst free conditions. These insights can potentially be expanded and applied to the rapidly expanding area of solvent and catalyst free chemistry. It should be noted that my contributions to the work discussed in the chapter pertain to the computational studies done – the experimental aspects (executed by collaborators) are also included in order to provide full context and clarity about the significance of the results obtained.

5.1 Introduction

One of the important chemical transformations, of relevance to academia and industry, is cyanosilylation[1]. This is a powerful C−C bond forming reaction that leads to cyanohydrins, thereby allowing for transformation to a wide variety of compounds useful to the chemical industry. To date, trimethylsilyl cyanide[2] (TMSCN) is the most popular cyanosilylating reagent as shown in **Figure 5.1** below, because it avoids the difficulties that come with the handling of HCN, NaCN or KCN.

Various reagents have been employed as catalysts to effectively transfer the -CN group from the TMSCN to the carbonyl carbon of the target molecule. These include Lewis acids, Lewis bases, metal halides, metal alkoxides, inorganic salts and iodine. The groups of Shibasaki and Corey, independently, have shown that bifunctional catalysts[3] and chiral Lewis acid catalytic systems[4] could be utilized for the asymmetric cyanosilylation of the aldehydes and ketones. Few very interesting reports from the groups of Roesky, Zhi and Nagendran which utilize well-defined neutral heavier main group compounds as single site catalysts[5-13]. Limitations are still present as majority of the examples discussed catalyse only aldehydes[6,8,11].

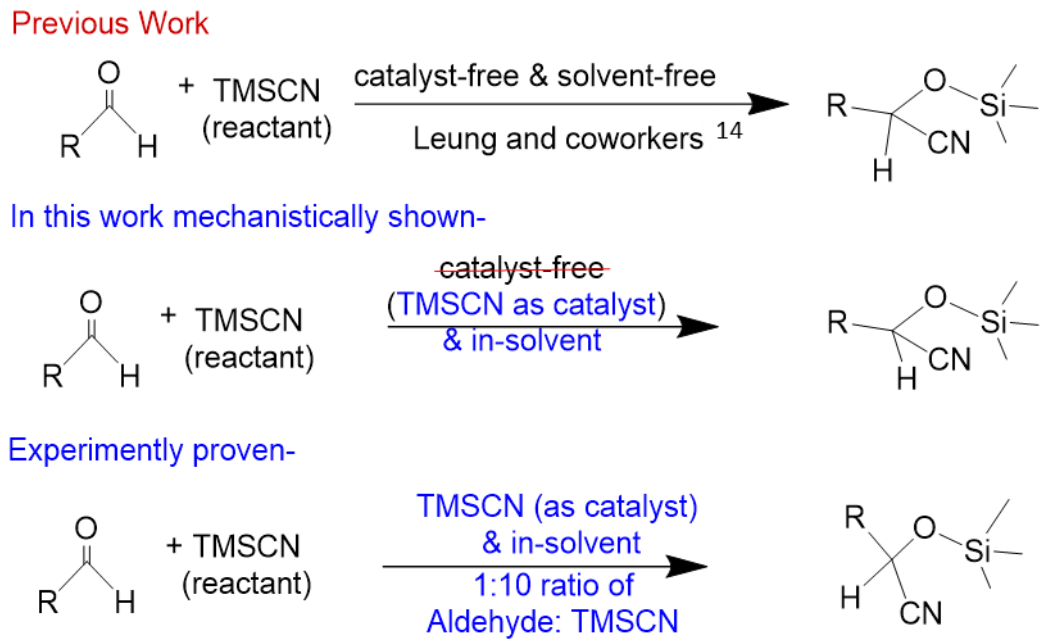

Figure 5.1. The previously reported cyanosilylation case in solvent free and catalyst free conditions, as well as new systems designed in the current work with the aid of mechanistic insights through DFT, experimentally proving hetero-functionalisation in solution, not through mediation by an external catalyst, but because one of the reactants acts as the catalyst (an "internal catalyst").

Various catalysts have been reported as listed above for C=O cyanosilylation with TMSCN but, as with the hydroboration reaction, there are now reports of the cyanosilylation reaction taking place without the need of an external catalyst and solvent[14-15]. This has prompted us to investigate this reaction with DFT calculations followed by experimental corroboration by our collaborators. We have obtained an interesting mechanistic pathway, where the presence of an additional TMSCN molecule was seen to increase the efficiency of the cyanosilylation process, thereby acting, in effect, as a catalyst. Moreover, we have then proceeded to exploit this insight with experimental studies and obtained a high yield of the cyanosilylated product in solution in the absence of an external catalyst. The current work, therefore, provides insights into how the important chemical transformations represented by cyanosilylation take place in neat TMSCN and uses this knowledge to further the field, by demonstrating how the same can take place in solution without the need for external catalysts.

5.2 Computational Methods

All the calculations in this study have been performed with density functional theory (DFT), with the aid of the Turbomole 7.1 suite of programs,[16] using the PBE functional.[17] The TZVP[18] basis set has been employed. The resolution of identity (RI),[19] along with the multipole accelerated resolution of identity (marij)[20] approximations have been employed for an accurate and efficient treatment of the electronic Coulomb term in the DFT calculations. Solvent corrections were incorporated with optimization calculations using the COSMO model, [21] with benzene ($\varepsilon = 2.27$), as the solvent. The harmonic frequency calculations were performed for all stationary points to confirm them as local minima or transition state structures. In addition, intrinsic reaction coordinate (IRC)[22] calculations were done with all the transition state structures in order to further confirm that they represented the correct transition states, yielding the correct reactant and product structures for each case. The values reported are ΔG values, with zero-point energy corrections, internal energy and entropic contributions included through frequency calculations on the optimized minima, with the temperature taken to be 80.0 °C for cyanosilylation of aldehyde. The translational entropy term in the calculated structures were corrected through a free volume correction introduced by Mammen *et al.*[23] This volume correction is to account for the unreasonable enhancement in translational entropy that is generally observed when employing computational software.

5.2.1 Energetic Span Model (ESM)

To find the turn over frequency (TOF) in the case of the cyanosilylation mechanism, we have calculated the relative efficiency with the AUTOF[24] program, using the "Energetic Span Model" (ESM), developed by Shaik and coworkers.[25,26] The ESM provides a method to calculate the turnover frequencies (TOFs) based on their computed energy profiles of catalytic cycles. The turnover frequency calculations consider the principal rate-determining transition state, potentially rate-influencing transition states, and the intermediates. The turnover frequency (TOF) is calculated by the following equation:

$$TOF = \frac{KBT}{h} e^{-\delta E/RT}$$

$\delta E = T_{TDTS} - I_{TDI}$ if TDTS appears after TDI

$\delta E = T_{TDTS} - I_{TDI} + \Delta G_r$ if TDTS appears before TDI

δE is the effective activation barrier of the global reaction. The TDTS and TDI are the transition states, and the intermediate respectively, that maximize δE. This model has been employed to calculate the TOFs at respective reaction temperatures.

5.2.2 NCI-plot

The NCI plot[27] iso-surfaces have been used to characterize noncovalent interactions. They correspond to both favorable and unfavorable interactions, as differentiated by the sign of the second-density Hessian eigenvalue and defined by the isosurface color. The color scheme is a red yellow-green-blue scale with red for ρcut^{+} (repulsive) and blue for ρcut^{-} (attractive).[28] The Turbomole 7.1 suite of programs, using the PBE/TZVP level of the theory have been employed to generate the NCI plots.

5.3 Results and Discussion

5.3.1 Cyanosilylation Chemistry: Cyanosilylation of Aldehydes with TMSCN in Solution

Leung and co-workers[14] reported the successful cyanosilylation of aldehyde with TMSCN in the absence of solvent and catalyst, taking benzaldehyde as the substrate. As for the case of hydroboration, we have considered the possibility that the presence of an additional TMSCN molecule can affect the kinetics of the reaction favorably.

Hence, this was investigated experimentally by our collaborators. When TMSCN was taken in significant excess in benzene solvent, a high yield of 75.0% was achieved in the absence of an external catalyst. [benzaldehyde:TMSCN ratio of 1:10 at 80.0 °C and for 18.0 hours].

As explained in previous cases, here the significant excess concentration of TMSCN in solvent was taken: (1) to make TMSCN act as a catalyst, (2) mimic the solvent free conditions, (3) and to overcome the unfavourable effects of entropy, as the reaction was done in the solvent phase. Due to the significant high concentration of TMSCN in the reaction, it becomes clear that the pseudo-bimolecular pathway (as shown in **Figure 5.2**) would be preferred over the mechanism proposed in **Figure 5.3**.

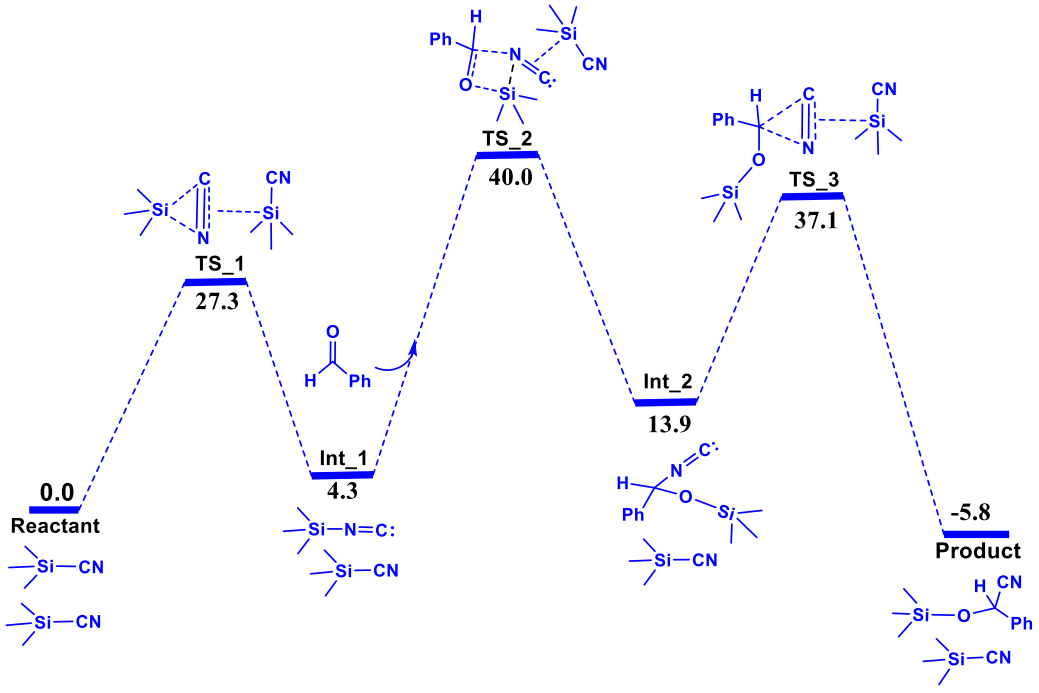

Figure 5.2. The free energy profiles for the benzaldehyde cyanosilylation reaction with TMSCN, in significant excess of TMSCN in benzene solvent, considering an additional TMSCN as a catalyst. The Gibbs free energy values (in kcal/mol) have been calculated at the PBE/TZVP level of theory.

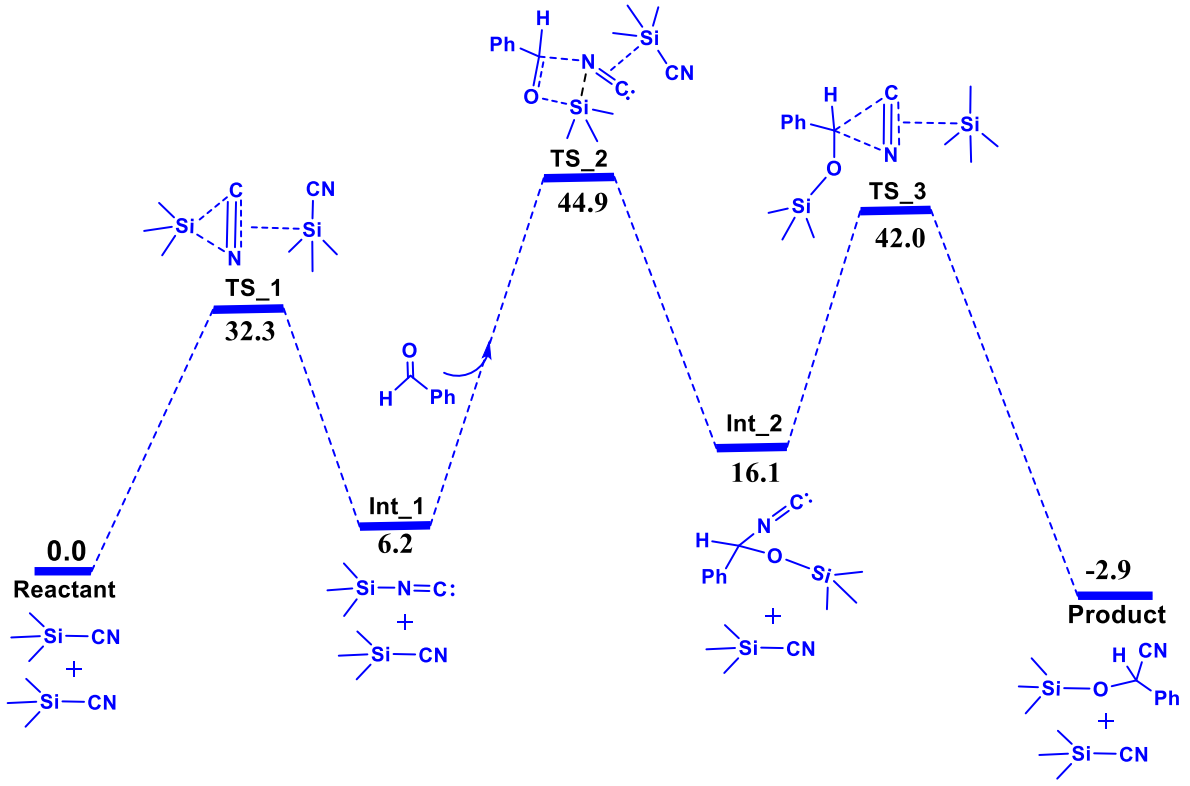

Figure 5.3. The free energy profile of the reaction of benzaldehyde with TMSCN in benzene solution with the assistance of an extra TMSCN molecule. The Gibbs free energy values (in kcal/mol) have been calculated at the PBE/TZVP level of theory.

We have therefore, in the DFT calculations, optimized two TMSCN molecules in close proximity, and have considered the same as the starting species (see **Figure 5.2**). Corey and co-workers had shown that cyanosilylation can proceed through the formation of an isocyanide intermediate.[29-30] Likewise, in our proposed mechanism, the reaction progresses through the formation of TMS-NC (**int_1**) when an additional TMSCN molecule is involved (see **Figure 5.2**). We observed that the barrier for the slowest step (40.0 kcal/mol) of this proposed pathway is 2.5 kcal/mol lower than the pathway involving a 1:1 ratio of TMSCN and benzaldehyde (see **Figure 5.4** below). A barrier of 40.0 kcal/mol is achievable at the elevated temperature of 80 °C.[31-32]

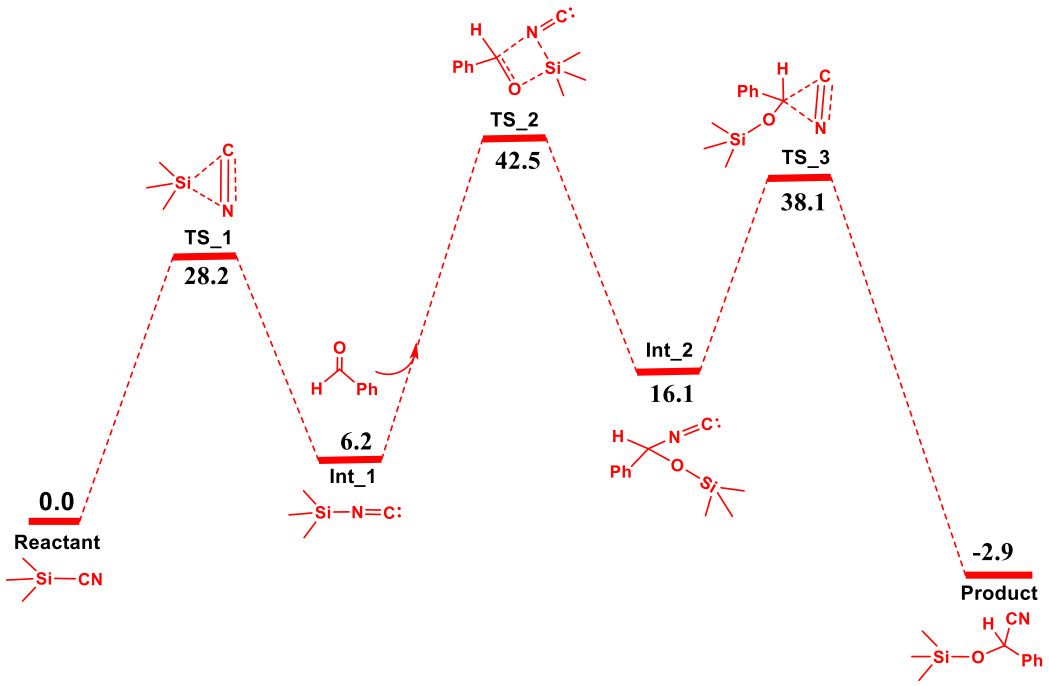

Figure 5.4. The free energy profile of the reaction of benzaldehyde with TMSCN in benzene solution without the assistance of an extra TMSCN molecule. The Gibbs free energy values (in kcal/mol) have been calculated at the PBE/TZVP level of theory.

As **Figure 5.2** illustrates, the other TMSCN molecule does not participate in the mechanism but it still functions to stabilize the transition state by favourable interactions with the NC triple bond: NCI-plots that we have determined reveal the non-covalent interactions between the Si of the other TMSCN and the CN (or NC) group (the green isosurfaces shown in **Figure 5.5** below).

In addition, the ESM calculations (shown in **Table 5.1**) show that the pathway involving an additional TMSCN molecule is 35.3 times more efficient than the pathway for the 1:1 case. The reason for the increased efficiency is that the difference in the energies of the intermediates and the transition states is not significant along the reaction pathway when an additional TMSCN molecule is employed. This, as known from the Sabatier Principle, [33] is a favourable situation.

Table 5.1. The values for the relative efficiency obtained for cyanosilylation in the benzene solvent for the desired reaction as well as with TMSCN acting as the catalyst.

Mechanism	TOF
The mechanism in **Figure 5.4**	$1.04*10^{-17}$ / sec
The mechanism in **Figure 5.3**	$9.94*10^{-16}$ / sec
The mechanism in **Figure 5.2**	$1.28*10^{-12}$ / sec

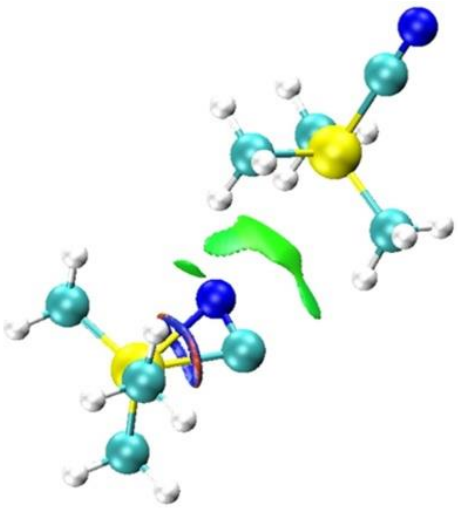	TS_1
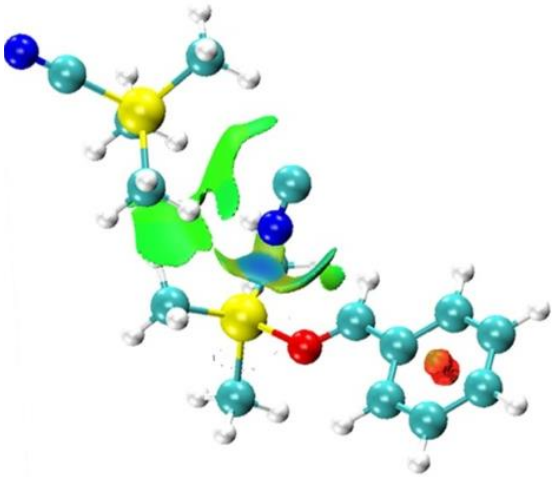	TS_2
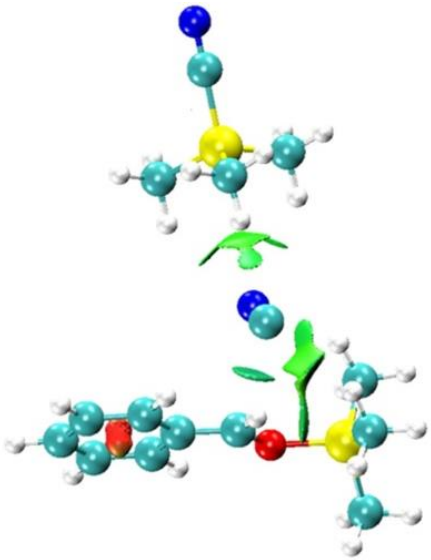	TS_3

Figure 5.5. NCI plots indicating non-covalent interactions (shown in green) between the silicon of an additional TMSCN molecule and the CN or NC group of the reacting TMSCN.

As expected from the DFT studies, a higher ratio of TMSCN to benzaldehyde was required in this case, as well as a higher temperature, but here, too, the experiments have validated the insights gained from the computational studies and provided proof that the cyanosilylation of different substrates with TMSCN could proceed without the aid of external catalysts in solution, through "internal catalyst" chemistry.

Therefore, the calculations and experiments with TMSCN show that internal catalysis chemistry can indeed act as a substitute to external catalysis, provided higher concentrations and slightly elevated temperatures are employed. One question that could be asked is whether a system with higher temperatures and concentrations would be preferable to another with lower temperatures and concentrations but with an external catalyst. We note here that in the latter case:

(1) there is need to synthesis the external catalyst. Sometimes, the synthesis can be tedious and multi-step.

(2) While preparing the catalyst, if one uses noble transition metals, then the entire process becomes expensive. On the other hand, if main group catalysts or first row transition metal-based catalysts are employed, they usually turn out to be air and moisture sensitive. As a result, an appropriate ligand has to be prepared.

(3) Catalyst recycling is a major issue.

(4) Efficiency of the catalyst is lost over multiple uses.

If one employs an internal catalyst, most of the issues raised above are resolved. It is true that the internal catalyst case that we have considered does require elevated temperatures and concentrations, but there are additional benefits:

(1) Obtaining the product becomes much easier and there is no need to remove traces of catalyst after the reaction, something that can cause impurities or degrade the product.

(2) Using internal catalysts could be very effective in large scale processes, something that is very important from an industrial application point of view.

5.4 Conclusions

We have computationally investigated the important question of why the cyanosilylation reaction appears to occur more effectively in a solvent-free environment, but is suppressed in solvent, as well as how the reaction can be made effective again in the solvent phase. The current work, aims to provide mechanistic understanding into this chemistry. Investigations with DFT for benzaldehyde for the cyanosilylation in the solvent reveal the favourable intervention of an additional TMSCN molecule during the reaction, which makes the chemistry more efficient in the respective case. Therefore, TMSCN serves not only as a substrate for the cyanosilylation reactions, but also as the catalyst. These insights have been further tested by experiments by our collaborators, which validated the computational findings by showing, for the first time, that the use of excess TMSCN in solution allowed the cyanosilylation reaction to take place with good yields without the need of a catalyst. This has significance because it opens up possibilities of extending catalyst free reactions to substrates that may dissolve poorly in liquid TMSCN, but could be dissolved along with them in an appropriate solvent, thereby allowing the desired chemistry to take place. The current work therefore represents an important advance in cyanosilylation chemistry and highlights its potential to undertake catalyst free chemistry as multi-tasking agents, both in the liquid form and in solution.

5.5 References

1. (a) R. J. H. Gregory, *Chem. Rev.* **1999**, *99*, 3649. (b) *Tetrahedron* **2004**, *60*, 10371. (c) J. M. Brunel, I. P. Holmes*Angew. Chem. Int. Ed.* **2004**, *43*, 2752. (d) S. C. George, S. S. Kim, *Bull. Korean Chem. Soc.* **2007**, *28*, 1167. (d) M. Kanai, N. Kato, E. Ichikawa, M. Shibasaki, *Synlett* **2005**, 1491.

2. (a) P. Saravanan, R. V. Anand, V. K. Singh, *Tetrtahedron Lett.* **1998**, *39*, 3823. (b) N. Khan, S. Agrawal, R. I. Kureshy, H. R. Sayed, S. S. Singh, R. V. Jasra, *J. Organomet. Chem.* **2007**, *692*, 4361. (c) B. Karimi, MaMan, L. *Org. Lett.* **2004**, *6*, 4813. (d). M. L. Kantam, P. Sreekanth, P. L. Santhi, *Green. Chem.* **2000**, *2*, 47. (e) K. Iwanami, J. C. Choi, T. Sakakura, H. Yasuda, *Chem Commun.* **2008**, 1002. (f) M. Bandini, P. G. Cozzi, A. Garelli, P. Melchiorre, A. Unami-Ronchi, *Eur. J. Org. Chem.* **2002**, 3243. (g) Y. Suzuki, M. D. Abu Bakar, K. Muramatsu, M. Sato, *Tetrahedron* **2006**, *62*, 4227. (h) S. T. Kadam, S. S. Kim, *Appl. Organometal. Chem.* **2009**, *23*, 119.

3. Y. Hamashima, D. Sawada, M. Kanai, M. Shibasaki, *J. Am. Chem. Soc.* **1999**, *121*, 2641.

4. D. H. Ryu, E. J. Corey, *J. Am. Chem. Soc.* **2004**, *126*, 8106.

5. Z. Yang, M. Zhong, X. Ma, S. De, C. Anusha, P. Parameswaran, H. W. Roesky, *Angew. Chem. Int. Ed.* **2015**, *54*, 10225.

6. V. S. V. S. N. Swamy, M. K. Bisai, T. Das, S. S. Sen, *Chem. Commun*. **2017**, *53*, 6910.

7. S.Yadav, R. Dixit, K. Vanka, S. S. Sen, *Chem. - Eur. J.* **2018**, *24*, 1269.

8. Y. Li, J. Wang, Y. Wu, H. Zhu, P. P. Samuel, H. W. Roesky, *Dalton Trans.* **2013**, *42*, 13715.

9. R. K. Sitwatch, S. Nagendran, *Chem. - Eur. J.* **2014**, *20*, 13551.

10. A. L. Liberman-Martin, R. G. Bergman, T. D. Tilley, *J. Am. Chem. Soc.* **2015**, *137*, 5328.

11. Z. Yang, Y. Yi, M. Zhong, S. De, T. Mondal, D. Koley, X. Ma, D. Zhang, H. W. Roesky, *Chem. - Eur. J.* **2016**, *22*, 6932.

12. M. K. Sharma, S. Sinhababu, G. Mukherjee, G. Rajaraman, S. Nagendran, *Dalton Trans.* **2017**, *46*, 7672.

13. W. Wang, M. Luo, J. Li, S. A. Pullarkat, M. Ma, *Chem. Commun.* **2018**, *54*, 3042.

14. W. Wang, M. Luo, W. Yao, M. Ma, S. A. Pullarkat, L. Xu, P.H. Leung, *ACS Sustainable Chem. Eng.* **2019**, *7*, 1718.

15. H. Iida, H. Hamana, K. Matsumoto, *Synth. Comm.* **2007**, *37*, 1801-1805.

16. TURBOMOLE V7.1 **2016**, a development of University of Karlsruhe and ForschungszentrumKarlsruhe GmbH, 1989-2007, TURBOMOLE GmbH, since **2007**; available from http://www.turbomole.com.

17. J. P. Perdew, K. Burke, M. Ernzerhof, *Phys. Rev. Lett.* **1996**, *77*, 3865.

18. A. Schafer, C. Huber, R. Ahlrichs J. *Chem. Phys.* **1994**, *100*, 5829.

19. K. Eichkorn, O. Treutler, H. Ohm, M. Haser, R. Ahlrichs, *Chem. Phys. Lett*. **1995**, *240*, 283.

20. M. Sierka, A. Hogekamp, R. Ahlrichs, *J. Chem. Phys.* **2003**, *118*, 9136.

21. A. Klamt, G. Schuurmann, *Chem. Soc. Perkin Trans.* **1993**, *2*, 799.

22. K. Fukui, *Acc. Chem. Res*. **1981**, *14*, 363.

23. M. Mammen, E. I. Shakhnovich, J. M. Deutch, G. M. Whitesides, *J. Org. Chem*. **1998**, *63*, 3821.

24. S. Kozuch, J. M. L.Martin, *ACS Catal*. **2011**, *1*, 246

25. A. Uhe, S. Kozuch, S. Shaik, *Comput. Chem.* **2010,** *32*, 978.

26. S. Kozuch, S. Shaik, *Acc. Chem. Res.* **2011**, 44, 101.

27. E. R. Johnson, S. Keinan, P. Mori-Sanchez, J. Contreras- Garcia, A. J. Cohen, W. Yang, *J. Am. Chem. Soc.* **2010**, *132*, 6498.

28. J. Contreras-Garcia, E. R. Johnson, S. Keinan, R. Chaudret, J.-P. Piquemal, D. N. Beratan, W. Yang, *J. Chem. Theory Comput.* **2011**, ***7***, 625.

29. H. D. Ryu, J. E. Corey *J. Am. Chem. Soc* **2005,** *127*, 5384.

30. D. H. Ryu, E. Corey, *Ion J. Am. Chem. Soc.* **2004**, *126*, 8106.

31. M. Yamakawa, H. Ito, R.Noyori, *J. Am. Chem. Soc.* **2000**, *122*, 1466.

32. L.P. Wang, A. Titov, R. McGibbon, F. Liu, V.S. Pande, T.J. Martinez, *Nat Chem*. **2014**, ***6***, 1044.

33. A. S. Varela, F. Dionigi, H. Fanchiu, C. Miller, O. L. Trinhammer, J. Rossmeisl, S. Dahl, *J. Chem. Educ*. **2012**, *89*, 1595.

Chapter 6

Subtle Interplay between the Different Components of a Molecular Machine Gives Rise to Directionality

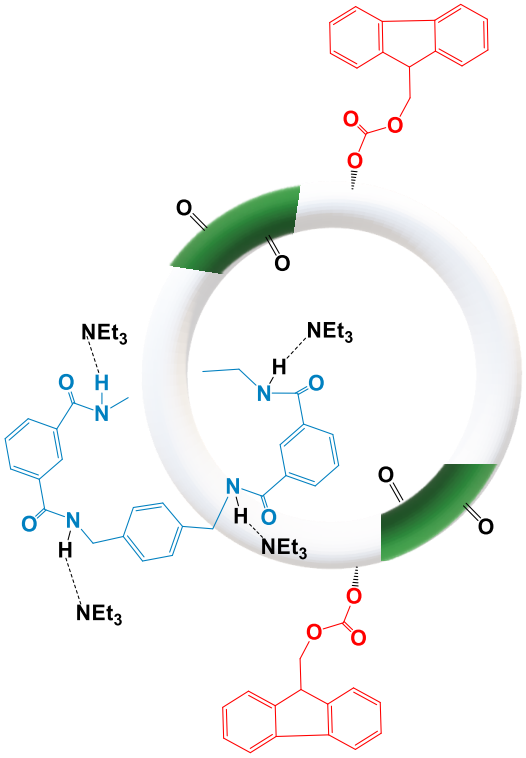

Chapter 6

Subtle Interplay between the Different Components of a Molecular Machine Gives Rise to Directionality

Abstract

An interesting area of research that has inspired a considerable amount of work over many decades is that of molecular machines: molecules synthesized in the laboratory that can move like mechanical engines while displaying efficiency and directionality in their movement. What is discussed in this chapter is a computational study of the workings of an experimentally reported molecular machine based on the concept of rotors. This system, designed by Leigh and co-workers[1], is based on a catenane, consisting of a small macrocycle (the "ring") that is interlocked with a larger, cyclic molecular "track", along which it moves with a net directionality. Such movement is achieved with the help of a molecule that performs the function of a "fuel" for this system, attaching to the track and detaching from it through different mechanisms. The ability of this system to function autonomously is stated by the authors to be based on two factors: (i) the difference in the rates of the reattachment of the fuel to the track, depending on whether the ring is near to or far from the fuel-track interaction, while (ii) the detachment occurs at a rate independent of the location of the ring along the track. The demonstrated directional motion is stated to occur as a result of this design. These results are exciting and represent an advance in the field of autonomous directional molecular machines, but what we contend here is that the actual mechanism by which such a desired result is obtained is quite different. Our DFT studies reveal that factor (ii), as stated in the experimental study, is incorrect: the rate of detachment of the fuel from the track is, in reality, *not* independent of the location of the ring along the track. Why the system still operates like an efficient molecular machine, executing net directional motion, is seen to be due to an accidentally elegant mechanism involving a synchronized series of events, akin to the behaviour of cables, pulleys and levers in a grandfather clock. It is expected that the insights gained from this work will help researchers design more efficient molecular machines in the future.

6.1 Introduction

Molecular machines are ubiquitous in biological systems[2], but developing analogous entities in the laboratory represents a significant challenge. The Holy Grail in such an endeavor would be to create systems that would allow for considerable, if not complete, control over molecular motion and function, leading eventually to the performance of useful work[3]. To this end, a number of synthetic small-molecule machines have been developed, like molecular muscles[4], synthesizers[5], pumps[6], walkers[7], transporters[8], and light[9] and electrically[10] driven rotary motors. However, (1) performing a task and (2) developing directionality have still persisted as major challenges for most of the systems that have been studied and reported. It is in this context that the work of David Leigh and coworkers[1] assumes significance. They have reported a molecular catenane system that displays net directionality with the help of a chemical fuel (Wilson, M. R., et al, *Nature*, **2016,** *534,* 235).

In their work, Leigh and co-workers[1] have described a system in which a small macrocycle (further referred to as a "ring", shown in **Figure 6.1D** in blue) is continuously transported with net directionality around a cyclic "track" (shown below in **Figure 6.1 A and B**), which is powered by irreversible reactions of a chemical fuel, fluorenylmethoxycarbonyl chloride (Fmoc-Cl). They state that the underlining concept behind the design is that the rate of attachment of fuel depends on the position of the ring relative to the track. The rate is faster when the ring is far from reactive site copmpared to when it is close. In their system, the attachment and cleavage of the Fmoc groups (further referred to as "bulk" and shown in red in the **Figures 6.1 B and D**) occur through different processes. They further note that the cleavage reaction occurs at a rate independent of the location of the ring on the track. Till the unreacted fuel remains in the system, the net directional movement of the molecular motor continues. In this process, the ring binds to one or the other of the two fumaramide sites (further referred to as "glue", and shown in green in the **Figures 6.1 B and D**) of the cyclic track. The bulk sterically blocks the passage of the ring and traps it in one compartment or the other (the right or left hand side part of the track divided by the two bulks, as shown in **Figure 6.1**). {It is noted here that, since the catenane molecular machine involves one ring passing through another (the "track"), the portion shown in bold in the figures indicates parts of the smaller ring above the track, and the non-bold section of the ring denotes it passing below the track. This has been done for a better understanding of the figures.} Cleavage of one of the bulk species through a chemical reaction allows the ring to shuttle back-and-forth between the two glue sites. Reattachment of the bulk through another chemical reaction (under the same conditions) locks

in any change of location of the ring (i.e. if the ring has changed the compartment, it is blocked from returning to the original one). The authors indicate that in order to keep the ring moving on the track in a net directional motion, (i) the kinetics for bulk attachment is faster when the ring is far from the reactive site ($k_{far\text{-}attach} > k_{close\text{-}attach}$) due to steric reasons, but (ii) the cleavage reaction occurs at a rate independent of the ring position ($k_{far\text{-}cleave} = k_{close\text{-}cleave}$). The reason, given by Leigh and coworkers[1], for (ii) is that the detachment reaction occurs at a remove of five bonds from the site of attachment and so the influence of the position of the ring on the detachment reaction rate is stated to be minimal.

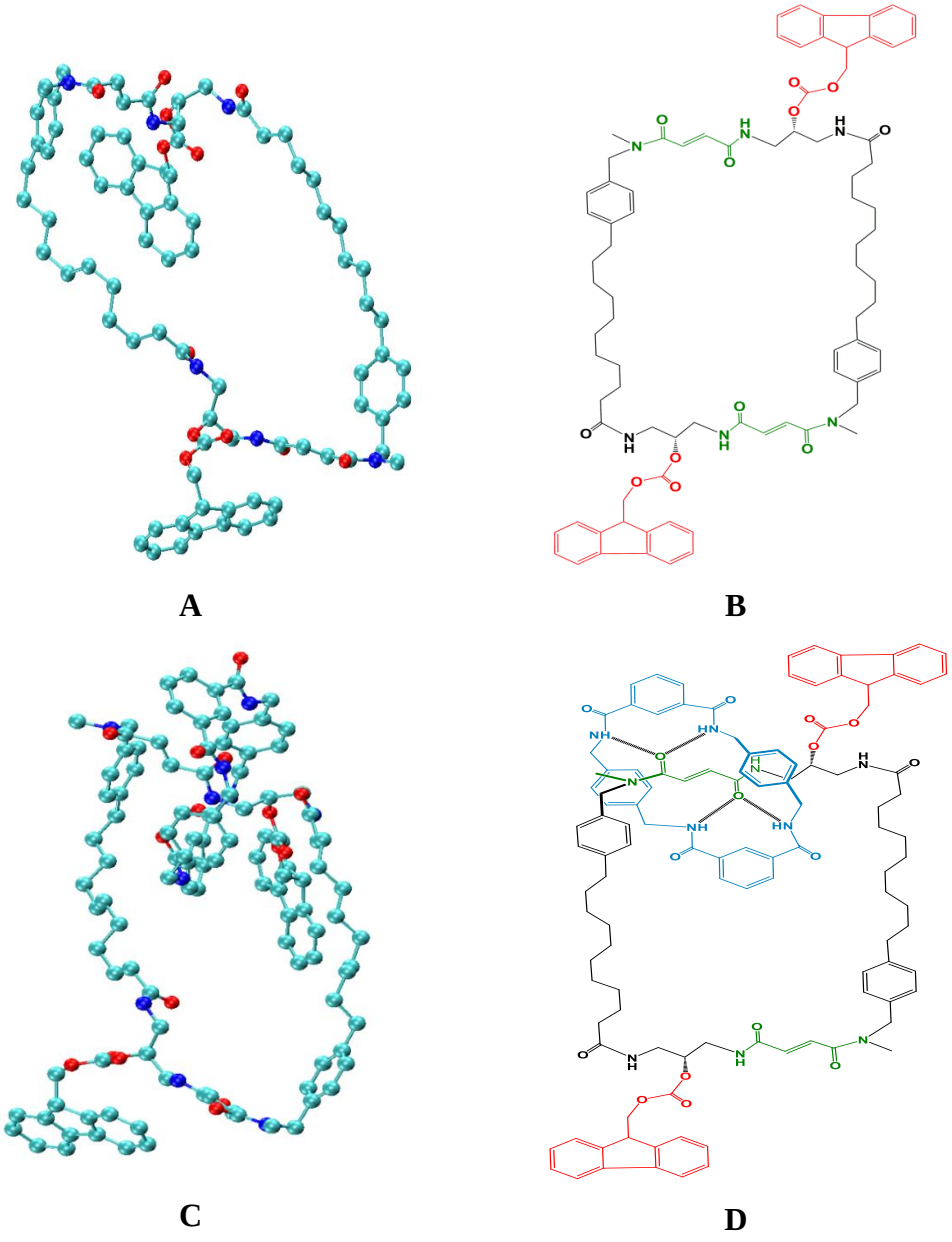

Figure 6.1 The optimized structure of the track (**A** and **B**) without the macrocycle ring and the optimized structure of the catenane (**C** and **D**) have been shown. Hydrogen atoms have been removed for the purpose of clarity.

In effect, Leigh and co-workers[1] describe the design of an elegant molecular machine system that executes a net translational motion with the help of a chemical fuel. However, there are several questions that need to be asked, which in turn might help us to design highly efficient molecular machines with better directionality.

1. Is it really correct that the rates of dissociation of the chemical fuel from the track are the same, irrespective of the position of the ring, as the authors of this work state?
2. What is the role of NEt_3 during the net directional motion of the ring? Is it only limited to extracting the chemical fuel from the track?
3. The design of the molecular machine is primarily based on the idea of a Brownian ratchet mechanism, in which a sequence of events takes place autonomously, and directionality emerges through asymmetry in the kinetic barriers for the different events. What is to be noted in this is that, in the Brownian ratchet mechanism strategy, the primary factor employed in creating asymmetry in the barriers is the sterics of the system. This is true not only for the molecular machine in question but for the design of molecular machines in general. But an important question that needs to be asked is: could not molecular machines be designed by a different approach, where electronic factors such as non-covalent interactions are equally, if not more, important, than the sterics of the system? Could it be that there already exist efficient examples of molecular machines where such factors are already at play, but are not getting the credit that they deserve?

We have attempted to find the answers to these questions with a computational study with density functional theory (DFT). The results obtained point to a system that is seen to function in a considerably more elegant fashion that the authors of the experimental work had described. Indeed, the results indicate that the ring, while moving in a net directional fashion around the track, also does productive work in carrying a "cargo" comprising of one or several NEt_3 molecules as it moves, a cargo that the ring only relinquishes when it attaches itself to the glue near the bulk. The NEt_3, for its part, is seen to be acting as a nucleophilic agent assisting in detaching the bulk from the track with the greatest likelihood when the ring is attached to the glue near the bulk, while minimizing its interaction with the bulk for the rest of the time, . Most importantly, all of this is seen to be moderated by a series of non-covalent interactions between the different components, interactions that create an elegant synchronicity in the behaviour of the molecular machine system. It is expected that such startling insights into the nature and behavior of this molecular machine system will aid researchers in designing more elegant and effective molecular machines in the future.

6.2 Computational Methods

All the transition state search and geometry optimization calculations in this study have been performed with density functional theory (DFT), with the aid of the Turbomole 7.1 suite of programs,[11] using the PBE functional.[12] The TZVP[13] basis set has been employed. The resolution of identity (RI),[14] along with the multipole accelerated resolution of identity (marij)[15] approximations, have been employed for an accurate and efficient treatment of the electronic Coulomb term in the DFT calculations. Solvent corrections were incorporated with optimization calculations using the COSMO model,[16] with dichloromethane ($\varepsilon = 8.93$), as the solvent. The harmonic frequency calculations were performed for all stationary points to confirm them as local minima or transition state structures. In addition, intrinsic reaction coordinate (IRC)[17] calculations were done with all the transition state structures in order to further confirm that they represented the correct transition states, yielding the correct reactant and product structures for each case. The option "disp" provided in the Turbomole package (DFT-D3) was used for dispersion-corrected DFT calculations for all the calculations with Turbomole.[18] The values reported are ΔG values, with zero-point energy corrections, internal energy and entropic contributions included through frequency calculations on the optimized minima, with the temperature taken to be 25.0 °C.

The calculations (i) for the case where the ring is moving away from the bulk in the presence and absence of bulk and (ii) for the case where one to four NEt_3 molecules bind to the ring through hydrogen binding have been performed with the TeraChem 1.9 quantum chemistry software package,[19] using the B3-LYP functional and the 6-31g* basis set.[20] Dispersion effects have been included with the DFT-D3 correction. Solvent effects have been introduced by the conductor-like screening model, COSMO, with ε =8.93 employed to model the solvent dichloromethane. The energy values obtained from both the Turbomole and TeraChem software packages have not been directly compared: we have focused on taking the trends observed for the calculations with the two packages, and noted that they remain the same for both. This has been done for a test system.

6.2.1 NCI-plot

The NCI plot[21] iso-surfaces have been used to characterize noncovalent interactions. They correspond to both favorable and unfavorable interactions, as differentiated by the sign of the second-density Hessian eigenvalue and defined by the isosurface color. The color scheme is a red, yellow, green, blue scale with red for ρcut^{+} (repulsive) and blue for ρcut^{-}

(attractive).[22] The Turbomole 7.1 suite of programs, at the PBE/TZVP level of the theory, have been employed to generate the NCI plots.

6.3 Results and Discussion

6.3.1. Movement of the ring along the track in the presence and absence of the bulk.

One of the principal design factors in the construction of the molecular machine by Leigh and coworkers[1] is the inclusion of the glue at two sites along the cyclic molecular track. The glue region of the track comprises of a fumaramide group having two carbonyl moieties (see **Figure 6.1** above), and lies adjacent to the region in the track where the bulk is present. When the ring, through motion along the track, reaches the glue, the two associates through strong hydrogen bonding interactions. The N-H groups on the ring interact with the oxygens of the two carbonyls (see **Figures 6.1 D**), thereby ensuring that the ring stays tethered to the glue and does not drift away backward (counterclockwise) along the track, in the time required for NEt_3 to interact and extract the bulk. This is the design as envisaged by Leigh and coworkers[1], and the overall success demonstrated experimentally in creating net directional motion of the ring along the track shows that it works.

There is, however, another factor that can promote the sticking of the ring to the track as the glue site: the presence of the bulk. What is noteworthy in both the ring and the bulk moieties is the presence of heteroatoms: nitrogen and oxygen atoms in the ring, and oxygen atoms in the bulk species (see **Figure 6.1**). This can lead to stabilizing non-covalent interactions (NCIs) between the ring and the bulk when they are in close proximity to each other. Such favourable interactions would lead to a further strengthening of the stickiness of the ring. This is made clear in **Figure 6.2** and **Table 6.1** below. As the figure indicates, two situations are considered: (i) the counterclockwise movement of the ring away from the glue when the bulk is present on the track, and (ii) the same movement away from the glue when the bulk is absent, i.e., in a scenario where the bulk has been detached from the track. What is observed is that the energy rises in both these situations, as the ring moves away from the stable glue site, but, importantly, the displacement is more disfavoured when the bulk is present. This shows that the ring is stabilized not only by N-H---O hydrogen bonding interactions between the ring and the glue, but also by NCIs between the ring and the bulk. In other words, both the glue and the bulk serve to “trap” the ring and prevent it from doing the undesirable: reverting back along the track away from the glue site.

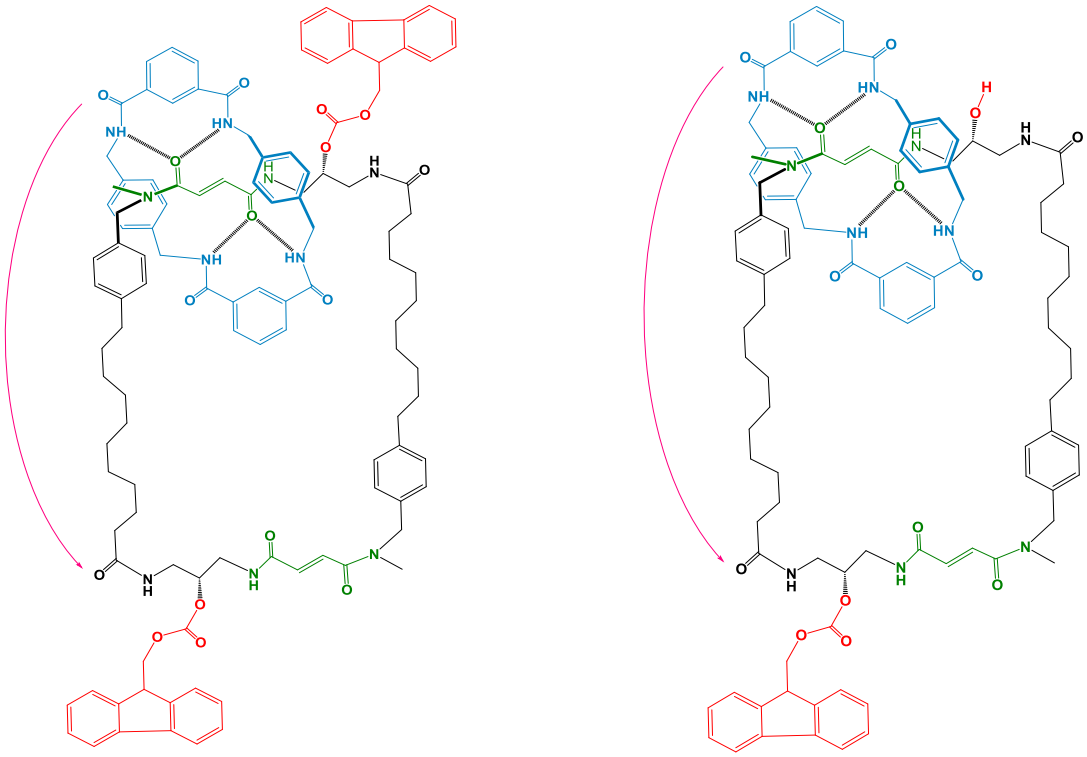

A **B**

Figure 6.2 In **A**, the "ring" moves away in counterclockwise fashion from the "glue" in the presence of the "bulk", and in **B**, the ring moves away from the glue in the same way, in the absence of the bulk. Hydrogen atoms have been removed for the purpose of clarity.

Ring moving away from glue Distance in Å	Energy in kcal/mol with bulk	Energy in kcal/mol no bulk
0.0	0.0	0.0
1.5	0.3	0.7
3.0	0.7	4.5
4.5	22.8	7.5
6.0	19.6	13.3
7.5	33.2	26.2
9.0	20.1	12.5
10.5	22.9	11.8
12	26.6	10.4

Table 6.1 The energy calculated for the system when the ring is moved away from the glue in the presence and absence of the bulk, taking the most stable structure – the ring at the glue site – as the reference energy of 0.0 kcal/mol.

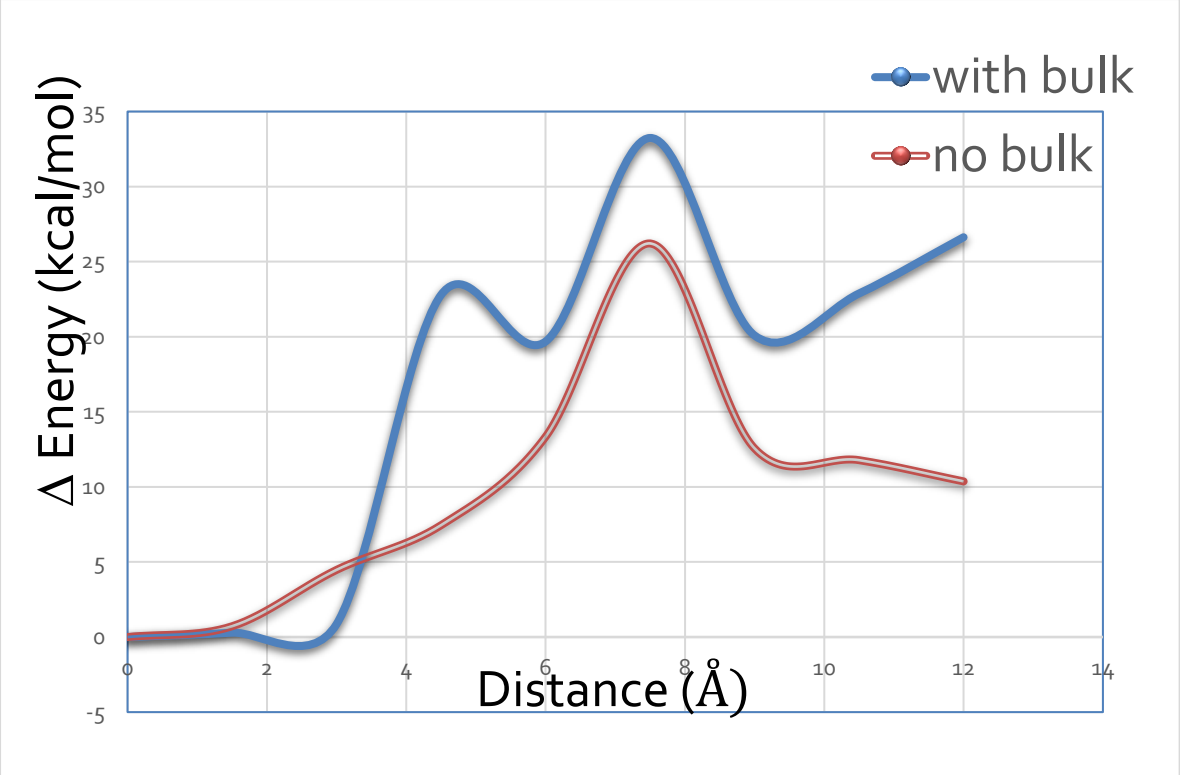

Figure 6.3. The graph above shows the energy calculated for the system when the ring is moved away from the glue in the presence and absence of the bulk.

Nevertheless, this hidden help provided by the bulk in trapping the ring through NCI has an important additional consequence. *This will lead to a difference in the ease of extraction of the proton from the flurenyl methane group of the bulk by the nucleophilic NEt_3, depending on whether the ring is present in the vicinity, or not present.* This is because, in the presence of the ring, the proton extraction by NEt_3 would disrupt some of the ring-bulk NCI interactions in the transition state, while the same would not occur if the ring (and therefore the NCI interactions) were not present near the bulk at all. That this is true is made clear from the NCI plots shown in **Figure 6.4** below, which show reduction in the NCI between the ring and the bulk in the transition states in comparison to the corresponding reactants during nucleophilic NEt_3 attack at the bulk.

Now, what this indicates is that the barrier (the difference in energy between the transition sate and the reactant) would increase for the nucleophilic NEt_3 attack reaction if the ring were present near the bulk, and be lower if the ring were far away from the bulk on the track. In other words, the rates of cleavage of the bulk from the track are not independent of the position of the ring along the track, i.e., the statement, $k_{far\text{-}cleave} \approx k_{close\text{-}cleave}$ made by Leigh and coworkers,[1] is incorrect. The correct statement is: $k_{far\text{-}cleave} > k_{close\text{-}cleave}$.

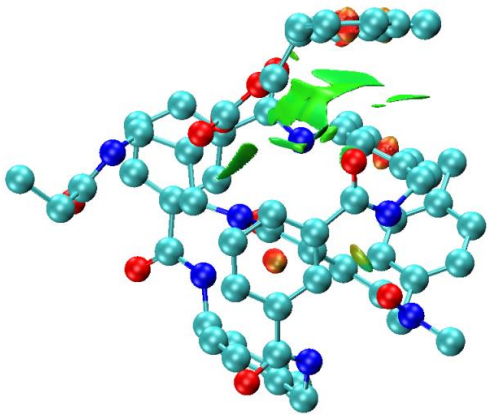 **A**	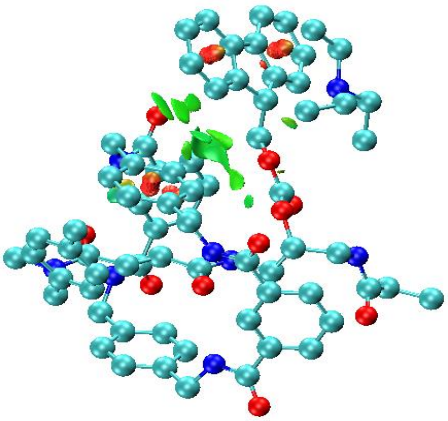 **D**
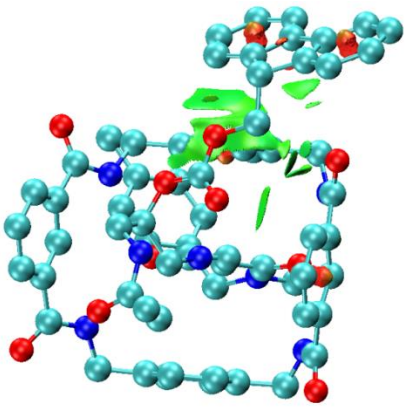 **B**	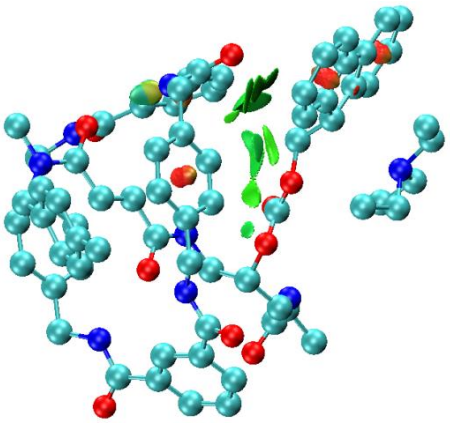 **E**
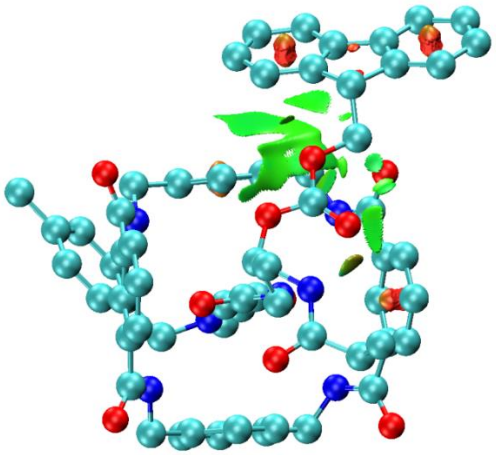 **C**	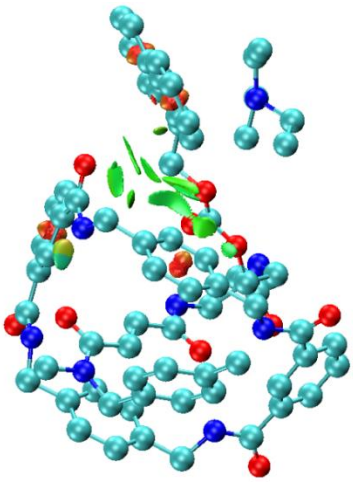 **F**
Optimized structures: ring at the glue in the presence of the bulk	**Transition state structures: ring at the glue in the presence of bulk being attacked by NEt_3**

Figure 6.4 Non-covalent interaction (NCI) plots, with the NCIs shown in green. **1.** Figures A, B and C: the NCIs are shown between the ring and the bulk in optimized structures where the ring is at the glue site along the track in the presence of the bulk. **2.** Figures D, E and F: NCIs are shown between the ring and the bulk, and also between the bulk and NEt_3, in transition state structures where the ring is at the glue site while the bulk is undergoing nucleophilic attack by NEt_3. Hydrogen atoms and rest of the system are not shown for the purpose of clarity.

The fact that this is true is proved further in the next section, where we discuss the determination of the transition states for the cleavage of the bulk from the track in the "far-cleave" and the "close-cleave" cases.

6.3.2. The full mechanistic study for the cleavage of the bulk from the track, when the ring is near and far from the bulk

6.3.2.1. The chopped system

In order to obtain a preliminary understanding of the far and near cleave scenarios, we have first done mechanistic studies with a model system for the molecular machine, having a truncated track, as shown in **Figure 6.5** below.

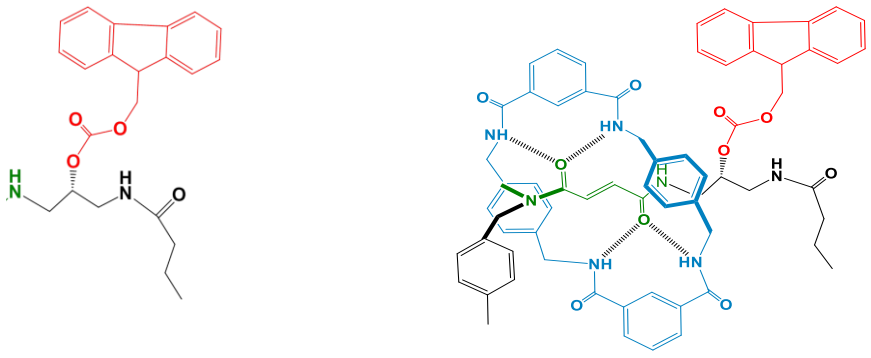

far cleave **close cleave**

Figure 6.5 The optimized geometry of the truncated, model, molecular machine system. The "far cleave" case is the one where the ring is not present at the glue (shown in green), whereas in the "close cleave" case, the ring is present at the glue (shown in green).

The far cleavage mechanism has been studied, as shown in **Figure 6.6.** In the first step, there is a nucleophilic attack of NEt_3 on the bulk and it abstracts the proton from the fluorenyl methine

group, leading to the intermediate **Int_1**. A barrier of 16.7 kcal/mol is involved in this process and the overall process is unfavorable by 11.5 kcal/mol in comparison to the reactants. In the next step, dibenzofulvene is cleaved from **Int_1**, after a barrier of 11.2 kcal/mol is crossed, and this leads to the formation of **Int_2**, which lies 18.3 kcal/mol lower in energy in comparison to the reactants. Finally, in the last step, the NEt_3H^+ formed transfers its proton to oxygen, leading to the formation of a hydroxyl group and the removal of CO_2, which leads to the formation of the final **Product** in the end, favorable by 27.1 kcal/mol. The barrier for the formation of the final **Product** is 5.3 kcal/mol, from **Int_2.**

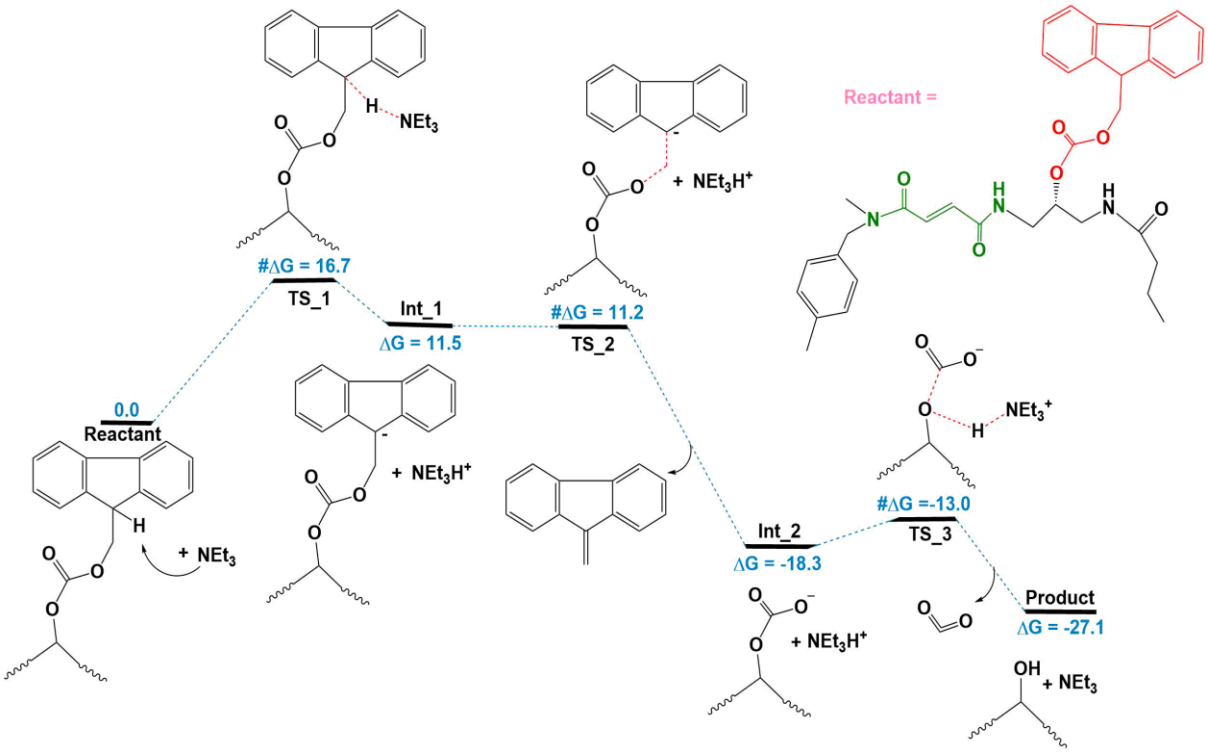

Figure 6.6 The free energy profile (ΔG in kcal/mol) for the cleavage of the bulk from the track when the ring is far from the glue and bulk, which undergoes nucleophilic attack from NEt_3. This pertains to the model molecular machine system.

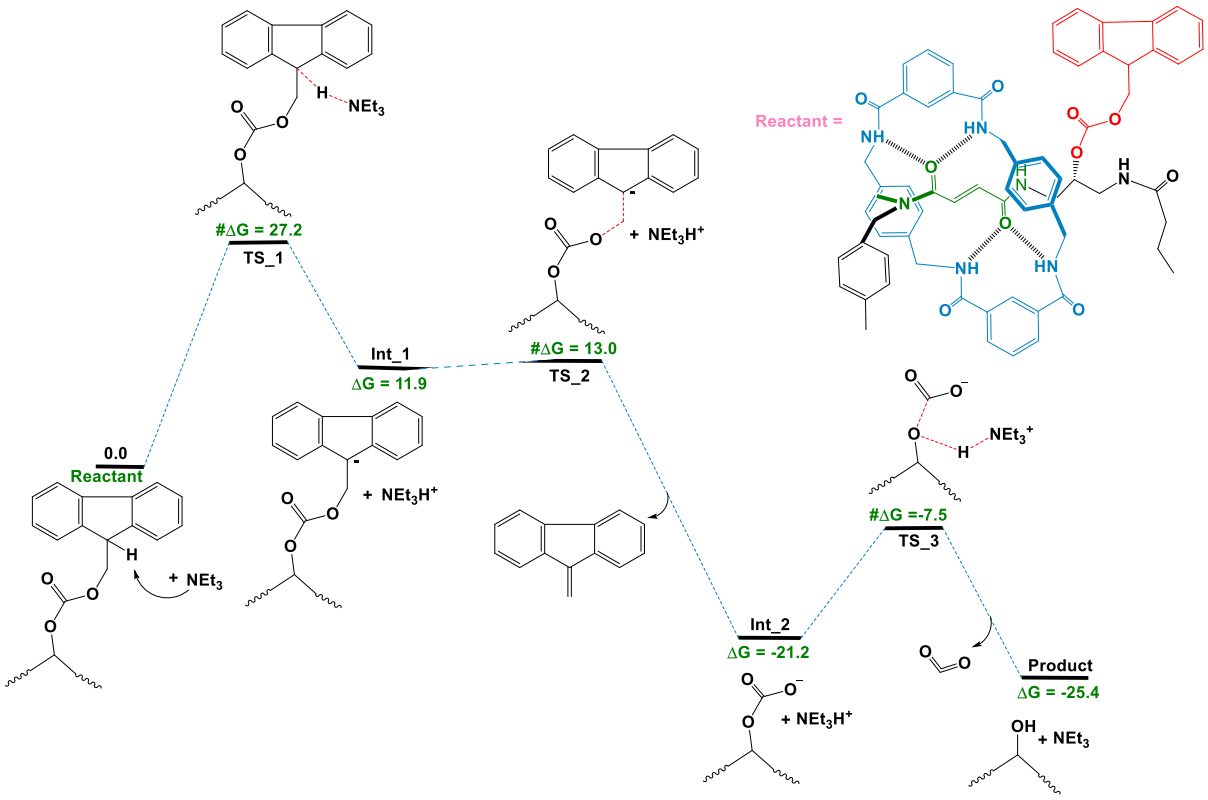

Figure 6.7 The free energy profile (ΔG in kcal/mol) for the cleavage of the bulk from the track when the ring is at the glue and near the bulk, which undergoes nucleophilic attack from NEt_3. This pertains to the model molecular machine system.

The close-cleave mechanism is the same as that for the far-cleave (see **Figure 6.7** above). However, as also illustrated below in **Figure 6.8**, there is a significant difference in the corresponding barriers in the two cases. There is a difference of 10.5 kcal/mol for the first transition state, that is between **C_TS_1** and **F_TS_1**. Similarly, in the case of the second and third transition states, there is a difference of 1.8 kcal/mol and 5.5 kcal/mol respectively. It therefore becomes clear that the rate of the reaction would be higher for the far-cleave case in comparison to the close-cleave. Hence, the chopped system provides a clear idea about the effect of the ring on the cleavage reaction.

It should, however, be noted that the energy difference between **F_Int_1** and **F_TS_2** is very less. This could be because of artifacts introduced by taking a model system. We have therefore further mechanistic studies, considering the real system without any truncation.

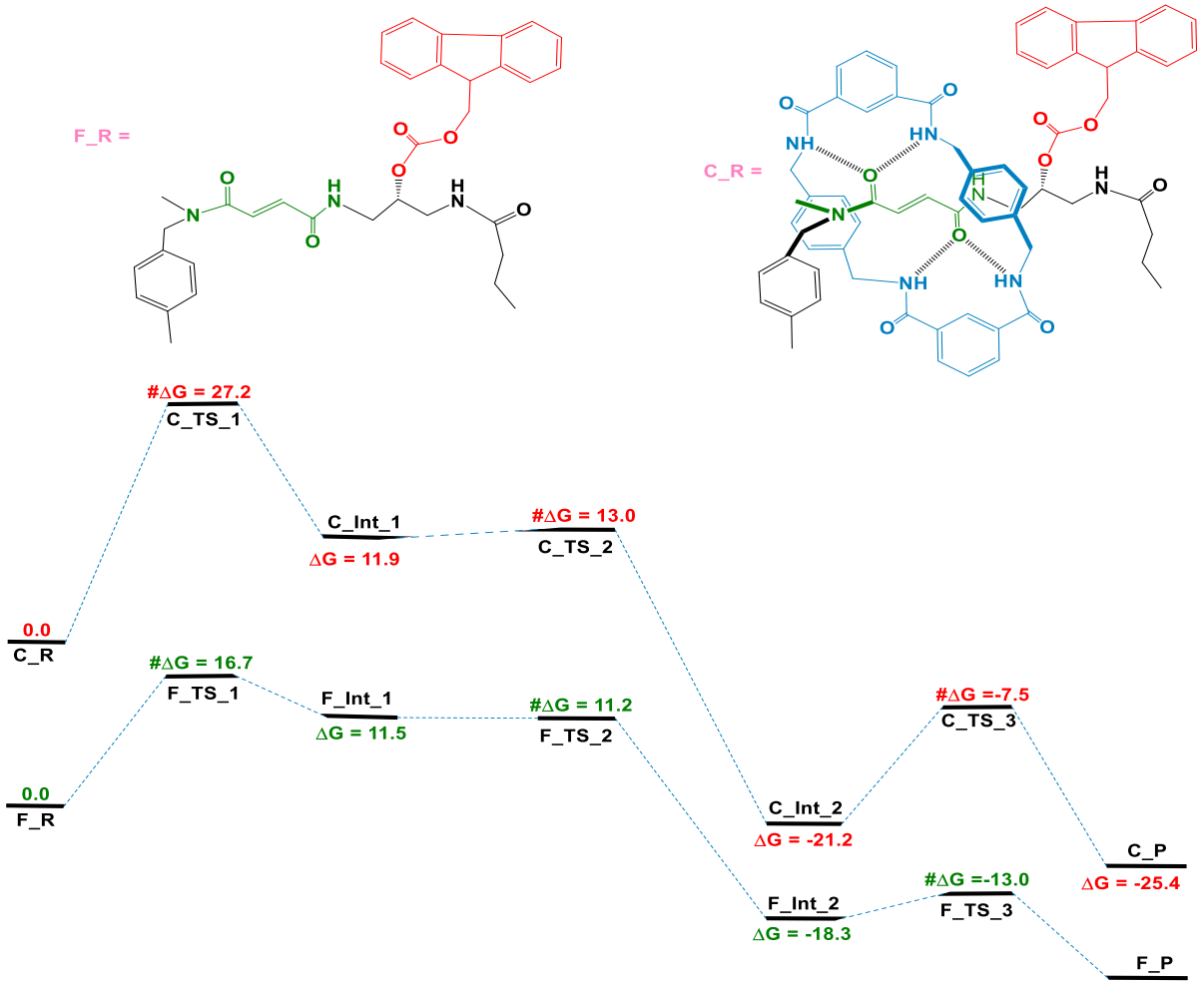

Figure 6.8 A comparison of the free energy profiles (ΔG in kcal/mol) for the cleavage of the bulk from the track when ring is at the glue and near the bulk (in red) and when the ring is far from the glue and the bulk (in green). This pertains to the model molecular machine system.

6.3.3. The full system

In order to prove this hypothesis in a more rigorous manner, we have further taken the real molecular machine system and done mechanistic studies for both the far-cleave and the near-cleave cases. In the first case, as shown in Figure **6.9 A**, the ring is at the glue and the bulk is adjacent to it and is subjected to nucleophilic attack from NEt_3, whereas, in the next case, the ring is situated at the other glue site (shown in green in Figure **6.9 B**), far from the bulk being cleaved. The mechanism for the cleavage of the bulk from the track remains the same irrespective of the position of the ring, as discussed above for the model case. The full mechanistic study and the energy profile for both the cases has been shown in the **Figures 6.10** and **6.11.**

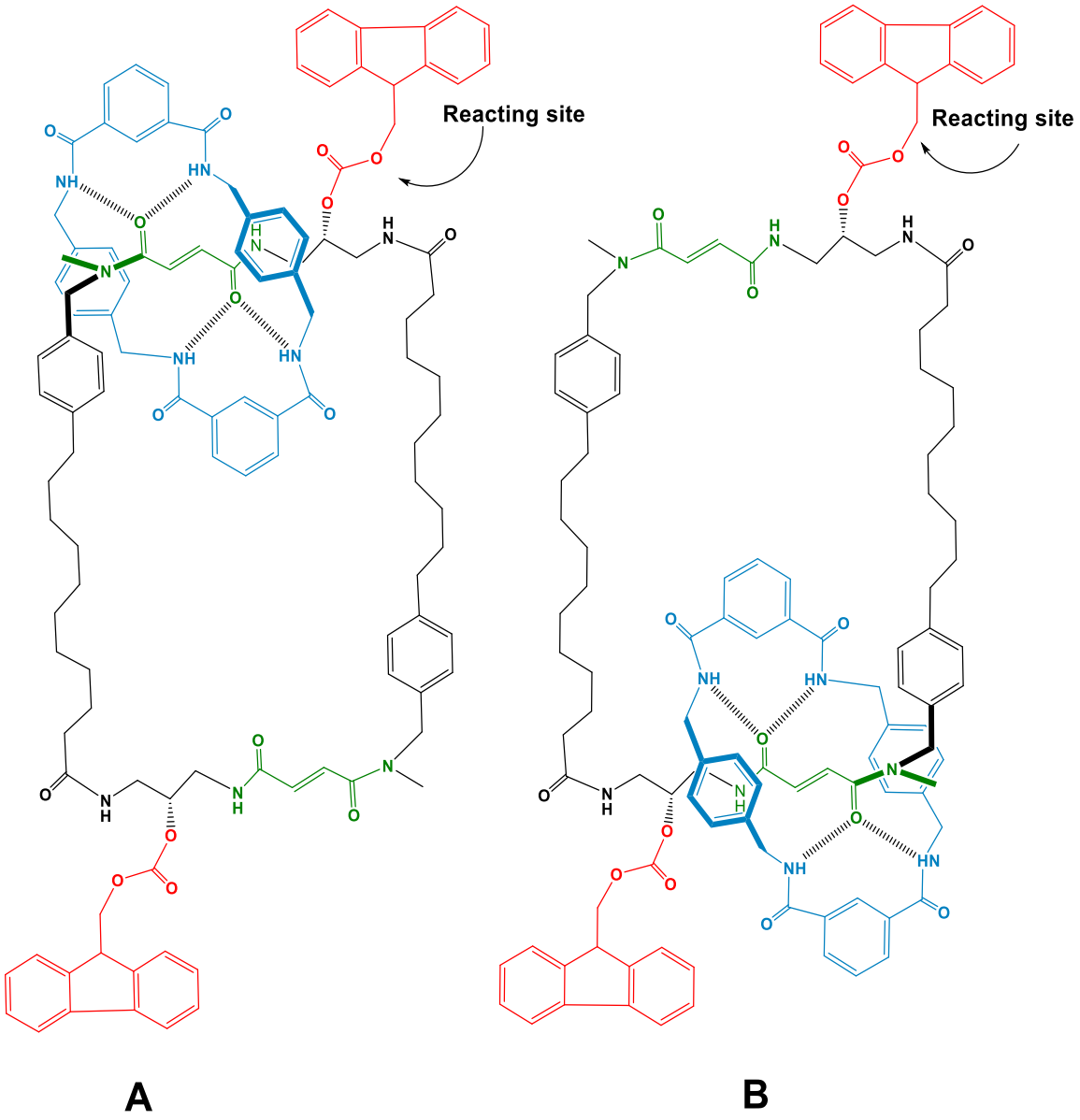

Figure 6.9 The two cases that have been considered for the real molecular machine system. In the close-cleave case (A), the ring is at the glue adjacent to the bulk, and in the far-cleave case (B), the ring is at the glue site distant from the bulk.

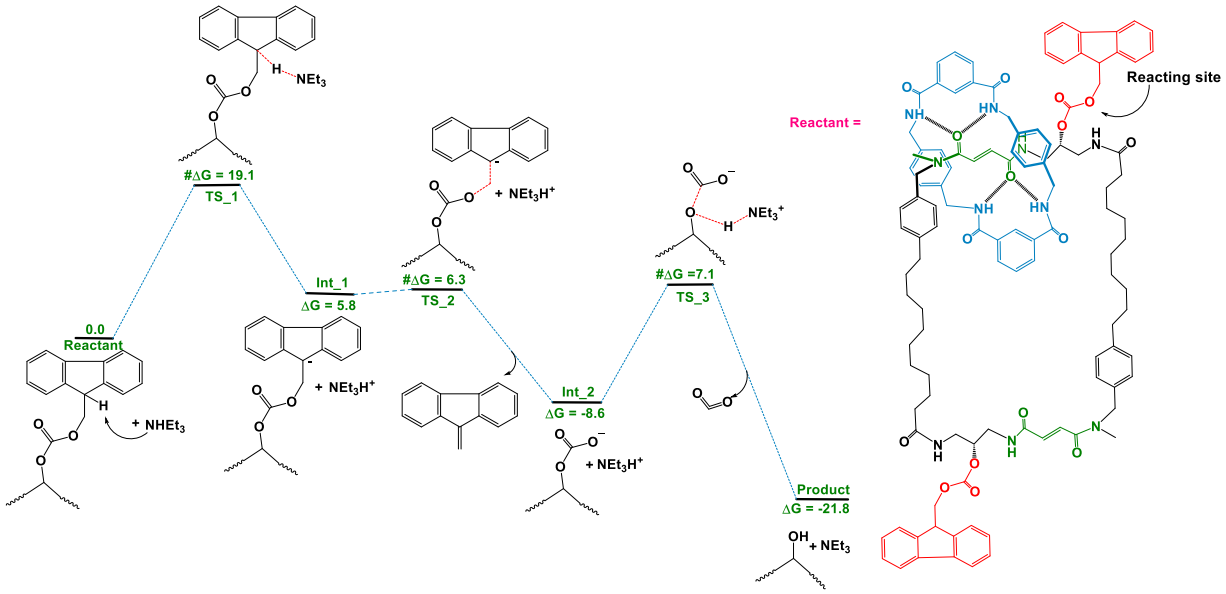

Figure 6.10 The free energy profile (ΔG in kcal/mol) for the cleavage of the bulk from the track, for the close-cleave case. This pertains to the real molecular machine system.

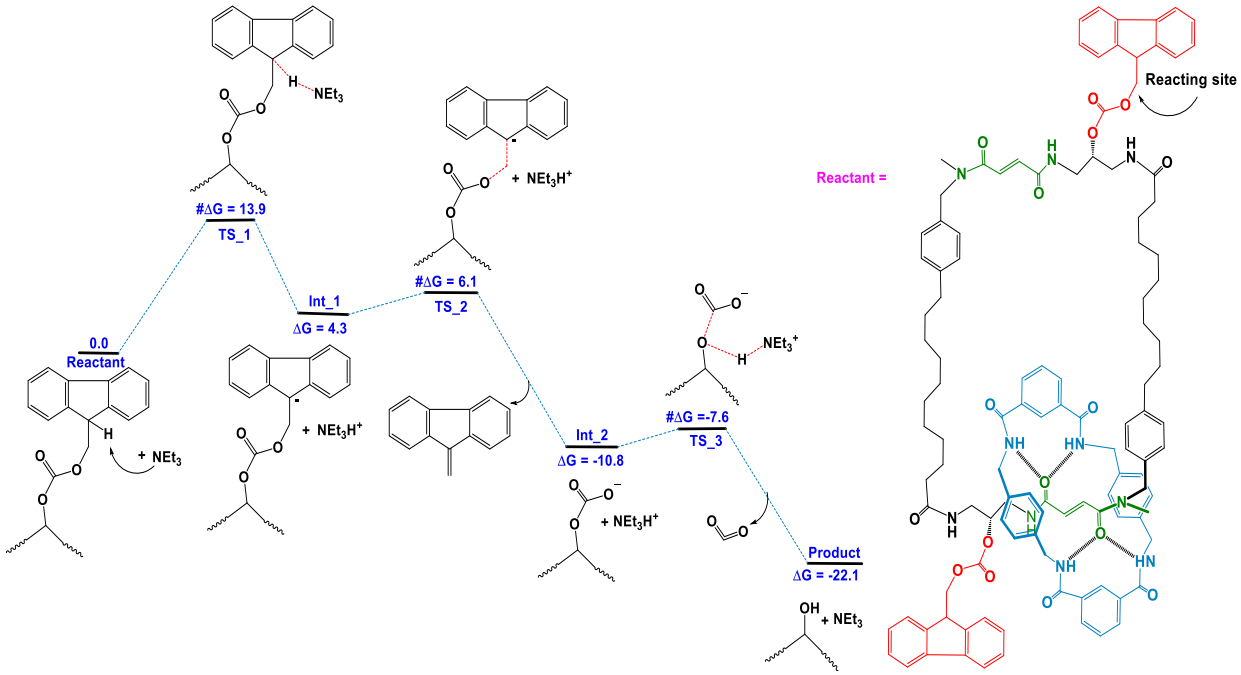

Figure 6.11. The free energy profile (ΔG in kcal/mol) for the cleavage of the bulk from the track, for the far-cleave case. This pertains to the real molecular machine system.

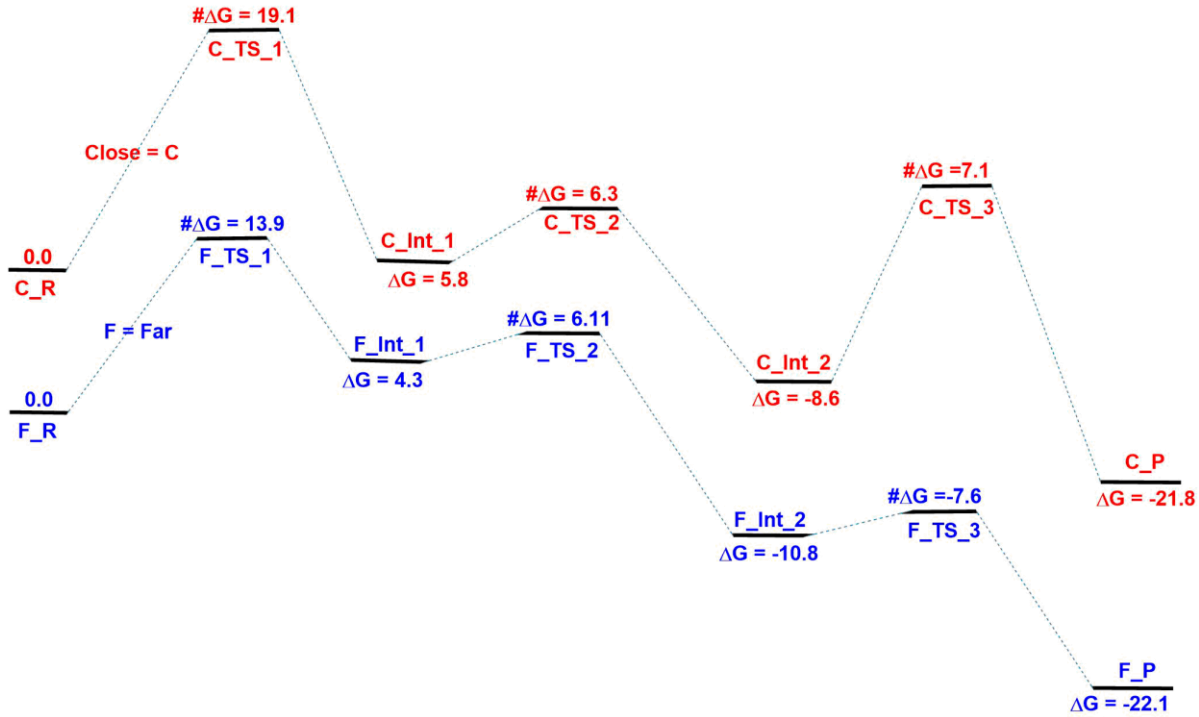

Figure 6.12 A comparison of the free energy profiles for the close (red) and far-cleave (blue) cases, for the real molecular machine system.

As shown in the **Figure 6.12,** for the real molecular machine system, there is a difference of 5.2 kcal/mol between the first transition states, with the far-cleave case being more favorable. On the other hand, for the second and third transition states, there is a difference of 0.1 kcal/mol and 14.7 kcal/mol respectively. This result underscores the point that was also made in the earlier sections, that the location of the ring along the track has a significant effect on the rate of the cleavage reaction.

This result has significant implications for the molecular machine system. Consider the situation when the ring is midway along the track between the two glue sites, with both the bulk moieties attached to the track, as shown in **Figure 6.13** below. In this situation, we have the possibility of a "far-cleave", i.e., of the NEt_3 attacking one of the two bulk species with the ring distant from both. As is now clear, the rate of dissociation of the bulk, $k_{far\text{-}cleave}$, will be faster than if the ring were close ($k_{close\text{-}cleave}$). Therefore, with free NEt_3 available in the well mixed homogeneous system, the bulk can be removed from the track, leading to the species **A** (with one bulk remaining and the other cleaved), and then to **B** (with both the bulk moieties cleaved), as shown in **Figure 6.13**. However, this possibility, now seen to be feasible, would be completely undesirable, because the absence of bulk would eliminate all asymmetry, and therefore all directionality, which is the principal reason for including the bulk in the design of

the molecular machine.[1] It can be argued that the rate of reattachment of the bulk to the track would also be low in this scenario, with the ring being distant from both the bulk species. However, given the well mixed nature of the homogeneous system, there is no certainty that the bulk would reattach to the track before the ring has reached either of the two glue sites, and even if the bulk were to reattach, the ring would also be executing random, non-directional motion along the track all the time prior to its reattachment. In other words, this probable scenario would either eliminate directionality in the motion of the ring altogether, or, in the best case, significantly reduce it. Thus, $k_{far\text{-}cleave}$ being actually greater than $k_{close\text{-}cleave}$ should have had serious, detrimental implications for the directionality of the motion of the ring along the track.

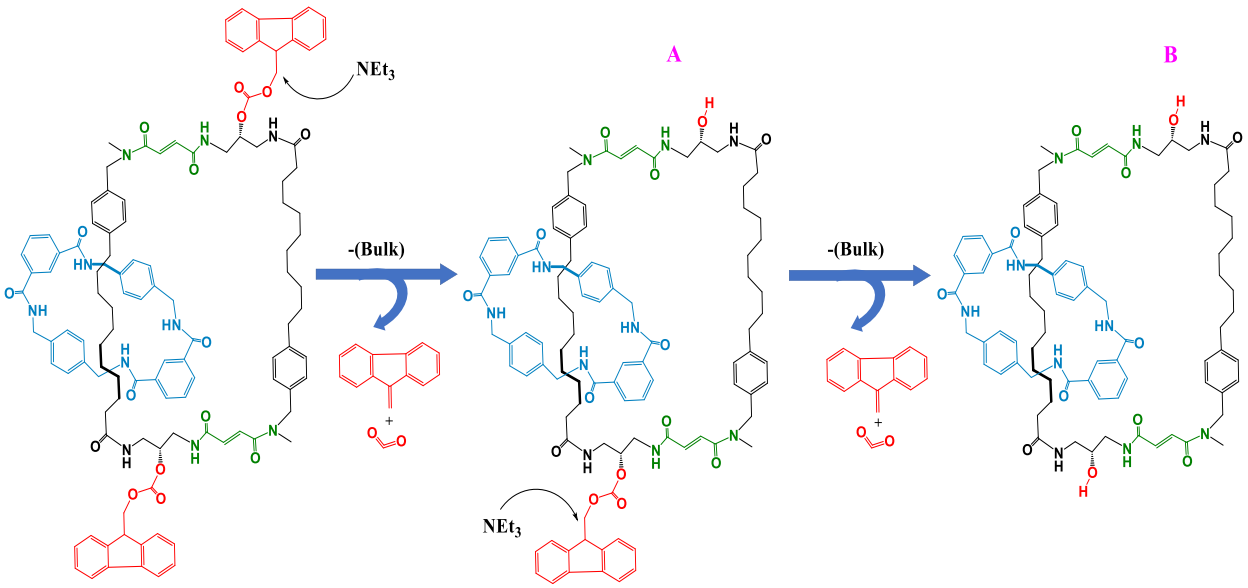

Figure 6.13 The ring at the centre of the track between the two glue sites, with both the bulk species attached. After nucleophilic attack of one NEt_3 molecule, **A** would be formed. In the next step, further attack by NEt_3 on **A** would lead to the removal of other bulk as well, producing **B**.

What is interesting, of course, is that such consequences of $k_{far\text{-}cleave}$ being greater than $k_{close\text{-}cleave}$ do not actually manifest in the molecular machine system designed by Leigh and co-workers[1]. The NMR data that they have reported clearly indicates that the ring executes net directional motion along the track. How is this possible, given the conclusions drawn here? This is the question that is addressed in the next section.

6.3.4. Synchronicity in Interactions between the ring, NEt_3 and the bulk gives rise to directional motion in the molecular machine.

The answer to the question posed at the end of the previous section is that there is an alternative to the mechanism proposed by Leigh and co-workers[1], some process is taking place that ensures that the ring maintains its net directional movement around the track. Such a process is proposed here, and shown through computational studies to be feasible.

The mechanism proposed is based on an important interaction that can serve to hamper the attack of NEt_3 on the proton of the flurenyl methane group of the bulk (which leads to the eventual cleavage of the bulk from the track): hydrogen bonding between the nitrogen of NEt_3 molecules and the N-H groups of the ring. The ring, a benzylic amide macrocycle, possesses four N-H groups, two in each hemisphere of the ring, all well separated from each other, thereby allowing for the ease of approach of multiple NEt_3 molecules. Since the N-H---N hydrogen bonding interaction is well documented to be a strong hydrogen bonding interaction,[23] it stands to reason that up to four NEt_3 groups can bind to the ring without any steric encumbrance. Now, since the ratio of the catenane to NEt_3 present in the system is about 1:1, and that the possibility of interaction between the catenane and NEt_3 is 4:1, a significant amount of NEt_3 can be trapped by the ring as it moves along the track. This is illustrated in **Figure 6.14** below. What the figure also shows is the favourability of this interaction: the binding of one, two, three and four NEt_3 groups is calculated to be favourable by 23.2 kcal/mol, 32.9 kcal/mol, 42.7 kcal/mol and 57.0 kcal/mol respectively. In other words, the possibility of NEt_3 interacting with the bulk (shown in red in **Figure 6.12**) is vastly reduced when the ring (in blue) traps multiple NEt_3 as it moves along the track. It is also possible that the N-H sites on the track at the glue sites can also trap NEt_3 molecules. It is, of course, also possible that the attack of NEt_3 on the bulk could still happen for a random case where the NEt_3 has not been trapped by the ring, but it is much more probable that, on average, as long as the ring is in transit along the track, and yet to reach the glue sites (shown in brown near the red bulk moieties), the probability of the attack of NEt_3 on the bulk would be significantly reduced.

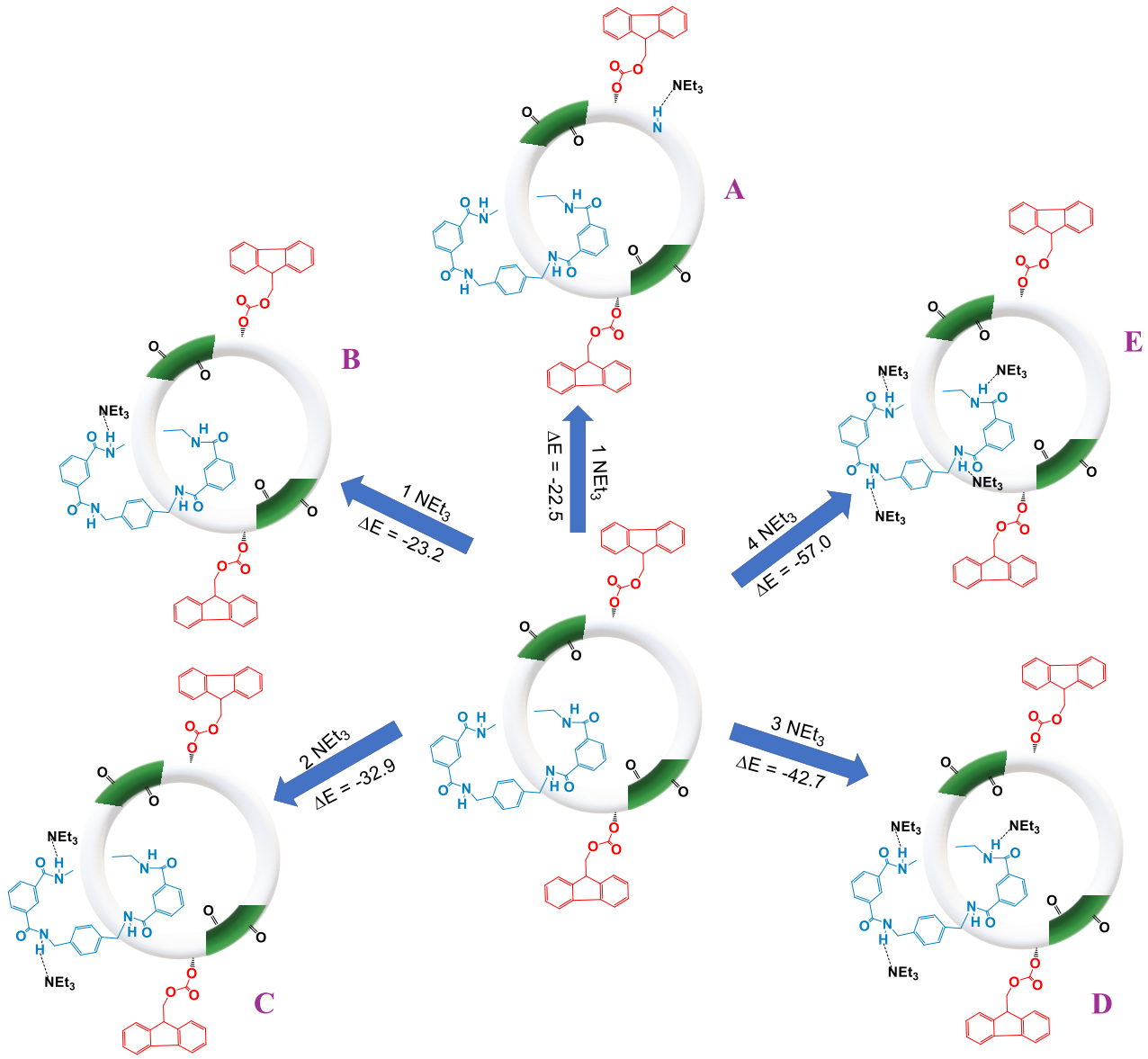

Figure 6.14 The binding of NEt_3 with the N-H groups on the ring (shown in blue) through hydrogen bonding with the nitrogen of NEt_3. The ΔE of binding is reported in kcal/mol.

This situation would change once the NEt_3 is at a glue site. Now, there would be competition between the nitrogen of the NEt_3 and the oxygen atoms of the fumaramide residues, for the same N-H groups on the benzylic amide ring. Our calculations indicate that the hydrogen bonding between the N-H and the oxygen is stronger than the N-H---N interaction, as shown in the **Figures 6.15.A** and **6.15B**: when we tried to break the strong N-H---O interaction to get N-H---N interactions with an NEt_3 molecule, we found that the NEt_3 always got expelled from the N-H site, with the N-H---O interaction being restored. This is due to the fact that each oxygen atom is able to bind to two N-H groups at the same time, leading to a stable structure. The powerful stabilization gained from these dual N-H---O interactions has also been exploited in

various systems employed in asymmetric organocatalysis.[24] Hence, once the ring, laden with up to four NEt_3 molecules, reaches the glue site, it would be likely to relinquish its "cargo" of NEt_3 and bind through N-H---O interactions to the glue. This would release all the NEt_3 molecules that the ring had been carrying, and they would also now be conveniently placed in close proximity to the bulk. Any one of the released NEt_3 molecules can then perform the nucleophilic attack on the bulk, thereby leading to its cleavage. Once the obstacle of the bulk has been removed, the ring can then proceed along the track, and again attract its cargo of NEt_3 molecules, which it can then ferry to the next glue site, to attack the next bulk moiety on its path, while the cleaved bulk behind is returned to the track through the reattachment mechanism (mentioned in the Introduction). And thus, the system can continue to function in an elegant autonomous fashion, with each of the desired reactions happening in an exact sequence, allowing the ring to move with net directionality along the track. The crucial, hidden contribution of the ring is therefore now revealed: it is seen to do actual work as it moves along the track, performing as a "cargo-train" and transporting its "goods" (NEt_3) from one bulk site to the other. In doing so, it ensures that the probability of NEt_3 attacking the bulk is maximized when required and minimized the rest of the time. The entire cycle is illustrated in **Figure 6.16** below.

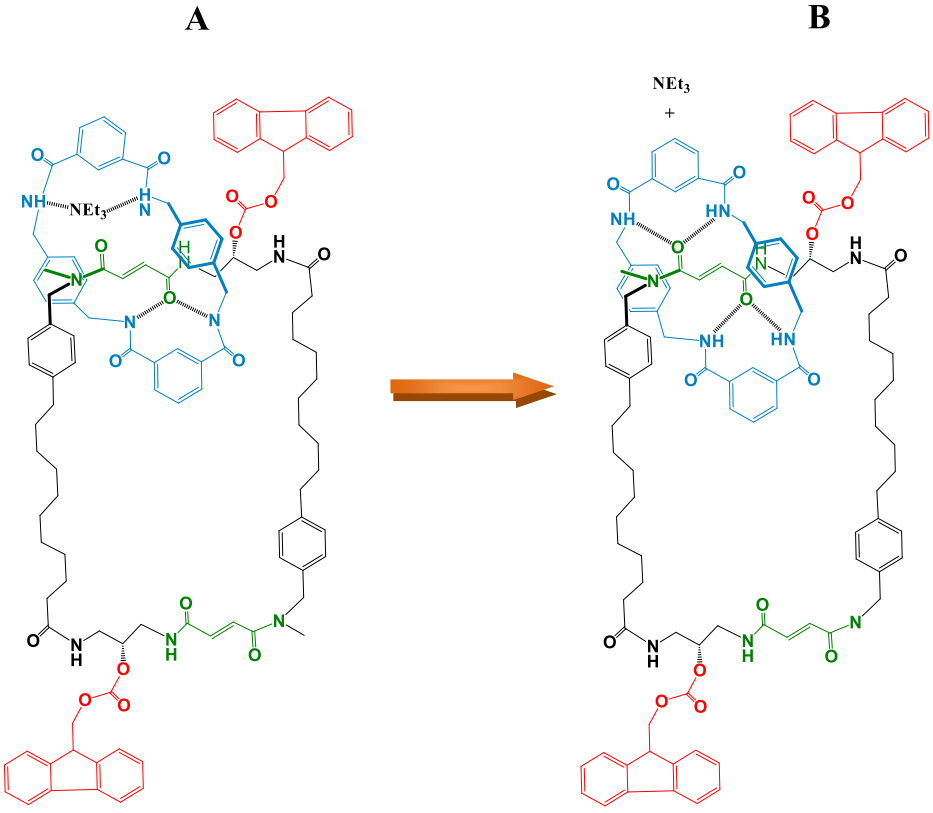

Figure 6.15. A. Starting point of a geometry optimization favoring N-H---N interaction. **B**. N-H---O interaction restored at the end of the geometry optimization.

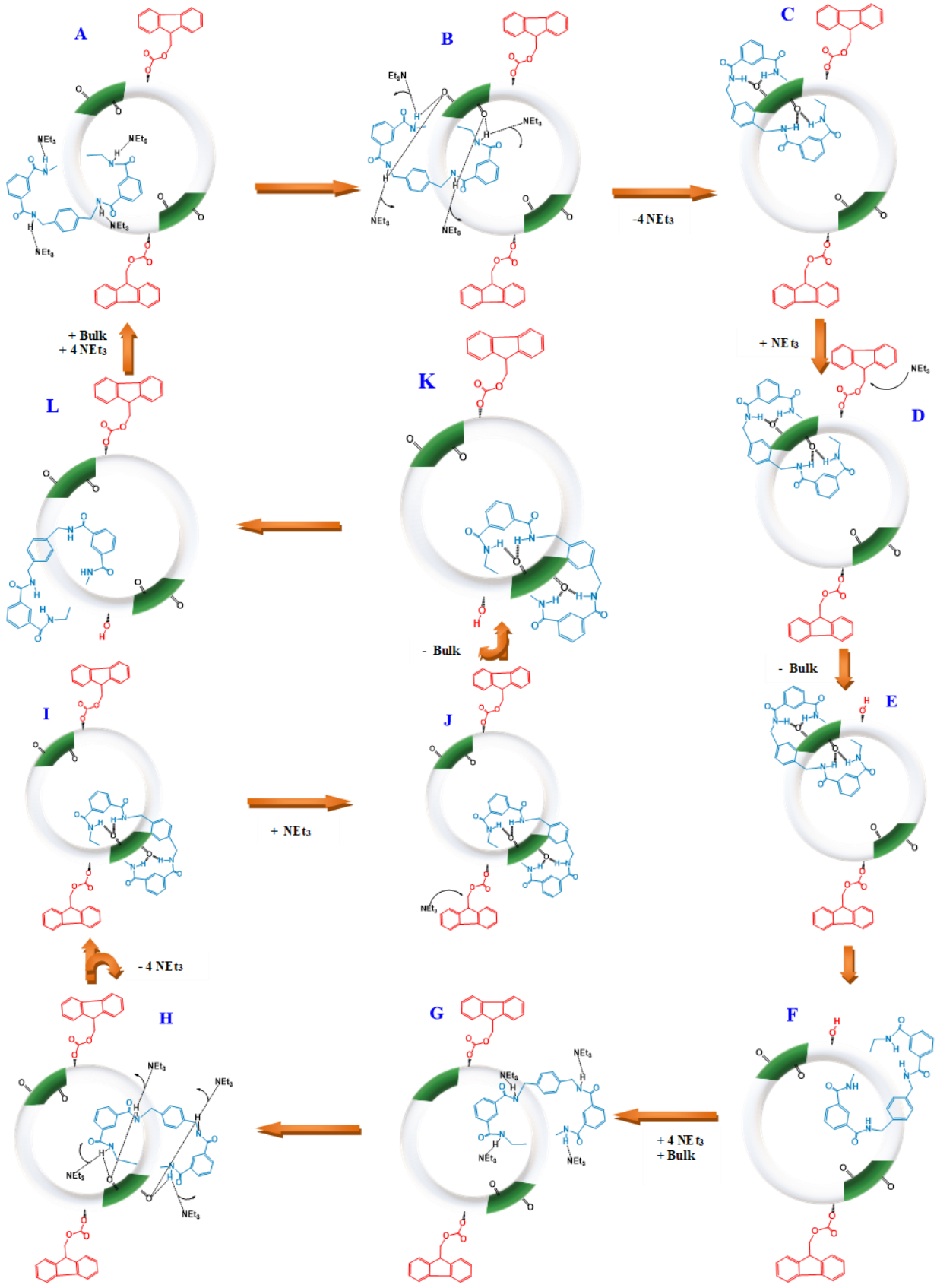

Figure 6.16. Proposed mechanism for the directional motion of the ring along the track.

6.4 Conclusions

The current work reports a computational study that delves into the mechanism by which net directionality has been achieved in an efficient catenane molecular machine reported by Leigh and coworkers.[1] Our studies reveal very calibrated interactions between the different components of the machine: the benzylic amide macrocycle (the "ring") travelling along a larger cyclic ring ("the track"), fumaramide residues (the "glue"), and NEt_3. According to our hypothesis, their interaction has the elegance of a choreographed dance, with up to four NEt_3 molecules interacting with the ring through N-H---N hydrogen bonding interactions as the ring travels around the track between two glue sites. Upon reaching a glue site, new hydrogen bonding interactions between the glue and the ring supplant the NEt_3-ring interactions, thereby liberating the NEt_3 molecules to act as nucleophilic proton extractors from 9-fluorenylmethoxycarbonyl groups (the "bulk") near the bulk site. Such groups are reattached to the track after the crossing of the ring in its onward journey along the track, and the whole process involving the NEt_3, ring, glue and bulk are repeated at the next site, as the ring thereby executes net directional motion along the track.

The accidental perfection in performance achieved by this system reveals design principles that can be exploited in the future to create new molecular machines. Its success is shown to be crucially dependent on the synergism and cooperation between four different components of the molecular machine: NEt_3, the ring, the glue and the bulk. Such a design feature - that of four components of the molecular machine alternating between interacting and not interacting as required - has never been deliberately employed in the past to design molecular machines. This can provide a fillip to create new, elegant designs for molecular machines, assembling them with different component parts that would synchronize their competing non-covalent interactions in order to achieve useful work, while displaying efficiency and directionality. The most significant aspect in the design would be the focus on exploiting relatively weak non-covalent interactions, in stark contrast to the traditional design principle (also exploited in the molecular machine discussed here) of exploiting Brownian ratchet mechanisms, which depend on employing steric factors to create asymmetry in barriers when a sequence of events is repeatedly performed. The current work therefore holds significance for the design of elegant molecular machines in the future.

6.5 References

1. M. R. Wilson, J. Sola, A. Carlone, S. M. Goldup, N. Lebrasseur, D. A. Leigh, *Nature* **2016**, *534*, 235.

2. M. Schliwa, G. Woehlke, *Nature* **2003**, *422*, 759.

3. S. Erbas-Cakmak, D. A. Leigh, C. T. McTernan, A. L. Nussbaumer, *Chem. Rev.* **2015**, *115*, 10081.

4. (a)M. C. Jimenez, C. D. Buchecker, J.-P. Sauvage, *Angew. Chem. Int. Ed.* **2000**, *39*, 3284. (b) C. J. Bruns, J. F. Stoddart, *Acc. Chem. Res.*, **2014**, *47*, 2186.

5. (a) P. Thordarson, E. J. A. Bijsterveld, A. E. Rowan, R. J. M. Nolte, *Nature*, **2003**, *424*, 915. (b) B. Lewandowski, G. D. Bo, J. W. Ward, M. Papmeyer, S. Kuschel, M. J. Aldegunde, P. M E Gramlich, D. Heckmann, S. M. Goldup, D. M D'Souza, A. E Fernandes, D. A. Leigh, *Science*, **2013**, 339, 189.

6. (a) V. Serreli, C.-F. Lee, E. R. Kay, D. A. Leigh, *Nature*, **2007**,445, 523. (b) G. Ragazzon, M. Baroncini, S. Silvi, M. Venturi, A. Credi, *Nature Nanotech.*, **2015,** 10, 70. (c) C. Chuyang, P. R. McGonigal, S. T. Schneebeli, H. Li, N. A. Vermeulen, C. Ke, J. F. Stoddart, *Nature Nanotech*. **2015**,*10*, 547.

7. M. v. Delius, E. M. Geertsema, D. A. Leigh, *Nature Chem.*, **2010**, *2*, 96.

8. S. Kassem, A. T. L. Lee, D. A. Leigh, A. Markevicius, J. Sola, *Nature Chem.* **2016,** *8*, 138.

9. (a) N. Koumura, R. W. J. Zijlstra, R. A. van Delden, N. Harada, & B. L. Feringa, *Nature*, **1999**, *401*, 152. (b) R. Eelkema, M. M Pollard, J. Vicario, N. Katsonis, B. S. Ramon, C. W M Bastiaansen, D. J Broer, B. L Feringa, *Nature*, **2006**, *440*, 163. (c) L. Greb, J.-M Lehn, *J. Am. Chem. Soc*. **2014**, *136*, 13114. (d) Q. Li, G. Fuks, E. Moulin, M. Maaloum, M. Rawiso, I. Kulic, J. T. Foy, N. Giuseppone, Nature Nanotech, **2015**, 10, 161. (e) L. Greb, A. Eichhöfer, J.-M. Lehn, *Angew. Chem. Int. Ed.* **2015**, *54*, 14345.

10. (a) H. L. Tierney, C. J. Murphy, A. D. Jewell, A. E. Baber, E. V. Iski, H. Y. Khodaverdian, A. F. McGuire, N. Klebanov, E. C. H. Sykes, *Nature Nanotech.*, **2011**, *6*, 625. (b) U. G. E. Perera, F. Ample, H. Kersell, Y. Zhang, G. Vives, J. Echeverria, M. Grisolia, G. Rapenne, C. Joachim, S.-W. Hla, *Nature Nanotech.*, **2013**, 8, 46.

11. R. Ahlrichs, M. Bar, M. Haser, H. Horn, C. Kolmel, *Chem. Phy. Lett.* **1989**, *162*, 165.

12. J. P. Perdew, K. Burke, M. Ernzerhof, *Phys. Rev. Lett*. **1997**, *78*, 1396.

13. S. Ansgar, H. Christian, A. Reinhart, *J. Chem. Phys.* **1994**, *100*, 5829.

14. K. Eichkorn, O. Treutler, O. H. M. Haser, R. Ahlrichs, *Chem. Phys. Lett*. **1995**, *240*, 283.

15. M. Sierka, A. Hogekamp, R. Ahlrichs, *J. Chem. Phys*. **2003**, *118*, 9136.

16. A. Klamt, G. Schuurmann, *Chem. Soc, Perkin Trans.***1993**, *2*, 799.

17. K. Fukui, *Acc. Chem. Res*. **1981**, *14*, 363.

18. a) J. Hepburn, G. Scoles, R. Penco, *Chem. Phys. Lett.* **1975**, *36*, 451; b) R. Ahlrichs, R. Penco, G. Scoles, *Chem. Phys*. **1977**, *19*, 119; c) S. *J.* Grimme, *Comput. Chem*. **2004**, *25*, 1463; d) S. *J.* Grimme, *Comput. Chem.* **2006**, *27*, 1787; e) S. Grimme, J. Antony, S. Ehrlich, H. *J.* Krieg, *Chem. Phys*. **2010**, *132*, 154104.

19. Petachem. http://www.petachem.com.

20. P. C. Hariharan, J. A. Pople, *Theoret. Chim. Acta*, **1973**, *28*, 213.

21. E. R. Johnson, S. Keinan, P. Mori-Sanchez, J. Contreras- Garcia, A. J. Cohen, W. Yang, *J. Am. Chem. Soc.* **2010**, *132*, 6498-6506.

22. J. Contreras-Garcia, E. R. Johnson, S. Keinan, R. Chaudret, J.-P. Piquemal, D. N. Beratan, W. Yang, *J. Chem. Theory Comput.* **2011**, ***7***, 625-632.

23. R. Adhikary, J. Zimmermann, J. Liu, R. P. Forrest, T. D. Janicki, P. E. Dawson, S. A. Corcelli, F. E. Romesberg *J. Am. Chem. Soc.*,**2014**, *136*,13474.

24. S. Sarkhel, G. R. Desiraju, *Proteins*, **2004**, *54*,247.

Chapter 7

Summary and Future Outlook

Chapter 7

Summary and Future Outlook

7.1 Focus of this Thesis

In order to understand nucleophilic attack chemistry in the area of the main group catalyzed hydroboration reaction, external catalyst-free hydroboration, the cyanosilylation reaction, and lastly, for a chemical fuel-driven molecular motor, mechanistic studies have been systematically carried out with the aid of density functional theory (DFT). Main group chemistry holds a lot of promise, as it can help researchers and industries alike to transition from the costly, toxic and scarce transition metals to safer and greener alternatives. Two reactions that are important from the purview of synthetic chemistry are hydroboration and cyanosilylation as they form valuable products and intermediates that are useful for industry. As there is a paucity of computational reports investigating the role of nucleophiles in the working of these reactions in main group chemistry, we have chosen to study these with DFT. We have made attempts to explore some unsolved questions in three very important fields: (1) the main group catalyst hydroboration reaction, (2) solvent-free and catalyst-free hydroboration and cyanosilylation, and (3) a chemical fuel-driven molecular motor. We have provided insights into the role of the ligand of main group compounds acting as a catalytic center in hydroboration, explored the solvent-free and catalyst-free chemistry for hydroboration and cyanosilylation, and, lastly, unraveled the hidden role of various components of a molecular motor that has been designed by Leigh and coworkers in their bid to achieve net directionality in a catenane system. Furthermore, quantum chemical calculations with DFT, NCI plots, and ab initio molecular dynamics (AIMD) calculations have been carried out to quantify the role of nucleophilic attack chemistry in main group chemistry. This can be summarized as follows:

(1) DFT calculations have been performed to shed light on the explicit role of nucleophilic attack chemistry in main group compounds. The catalytic property of an experimentally pre-synthesized calcium compound having a β-diketiminato ligand with a methyl-pyridine sidearm has been studied in this chapter[1]. Through DFT calculations, we have done a mechanistic study of the calcium compound acting as a catalyst for the hydroboration of aldehydes with

pinacolborane (HBpin) under ambient reaction conditions. The calculations reveal that the role of calcium in the chemistry is to bind two ligands, each of which is then capable of acting as a catalytic site for hydroboration. Therefore, the calcium center enables the formation of a dual-site catalyst, which can be more efficient than just employing a pyridine moiety as a single-site catalyst in the reaction.

(2) Next, we have explored the nucleophilic attack of HBpin in the hydroboration reaction in solvent-free and catalyst-free conditions[2]. We have demonstrated that during this process, HBpin not only acts as a reactant and solvent but also as an internal catalyst. In this chapter, we have done mechanistic investigations with DFT for a range of substrates: benzaldehyde, acetophenone, benzoic acid, and p-methoxyphenylacetylene. Experimental kinetic studies have been conducted for the hydroboration of p-methoxyphenylacetylene with HBpin. which has further corroborated these computational findings. These insights have been further tested through experiments conducted by our collaborators, where they confirmed our hypothesis that the product forms without the use of external catalyst and solvent for the case of p-methoxyphenylacetylene. They also found a high yield when they used excess HBpin in the presence of the solvent without any external catalyst.

(3) The insights gained from Chapter 4 propelled us to further investigate one more industry-important nucleophilic addition reaction: cyanosilylation. We demonstrated that TMSCN, when used as the cyanating reagent, serves not only as a substrate for the cyanosilylation reactions but also as the catalyst[2]. In this chapter, we have done mechanistic investigations with DFT taking benzaldehyde as one of the substrates. These insights have been further tested by experiments by our collaborators, and for the first time, it has been shown that using an excess amount of TMSCN in solution allowed the cyanosilylation reaction to take place with good yields without the need of a catalyst, which further validates the computational findings.

(4) Next, after looking into the two nucleophilic addition reactions, we have explored the role of nucleophilic attack chemistry in the functioning of molecular motors. In this chapter, we have computationally investigated the mechanism by which net directionality has been achieved in an efficient catenane molecular machine reported by Leigh and coworkers.[3] We have further shown very calibrated interactions between the different components of the machine: the benzylic amide macrocycle (the “ring”) traveling along a larger cyclic ring (“the track”), fumaramide residues (the “glue”), and NEt_3. We have come up with and then tested a

hypothesis, according to which up to four NEt3 molecules interact with the ring through N-H---N hydrogen bonding interactions, as the ring travels around the track between two glue sites. When the ring reaches a glue site, it favors stronger N-H---O interactions with the track than N-H---N interactions with the NEt_3. Now, NEt_3 is free to act as a nucleophilic, proton extractor and attacks the bulk molecule, which clears the path for the ring to move in the forward direction. Now, as the ring moves and crosses the bulk position, the bulk reattaches to the track and up to four NEt_3 molecules also bind back with the ring. The entire process involving the NEt_3, ring, glue and the bulk are then repeated at the next site, which leads to the net directional motion of the ring along the track.

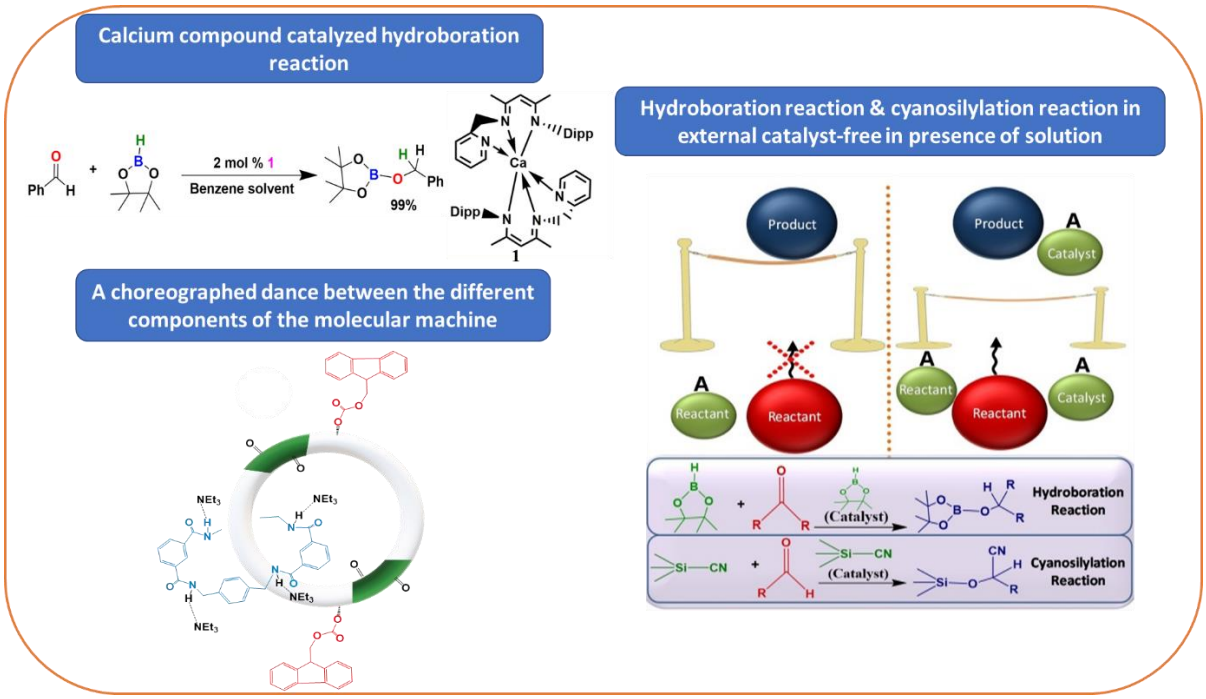

Figure 7.1 Representation of the research work done in this thesis

7.2 Computational Methods

The calculations with DFT have been performed using the Turbomole 7.1 suites of programs.[4] The geometry optimizations have been done with the Perdew, Burke, and Erzenhof density functional (PBE)[5] and a triple-ζ basis set augmented by a polarization function (Turbomole basis set TZVP) have been employed to describe the electronic configuration of the atoms.[6] The resolution of identity (ri),[7] along with the multipole accelerated resolution of identity (marij)[8] approximations were used for an accurate and efficient treatment of the electronic Coulomb term in the density functional calculations. Solvent effects using the COSMO model[9] and dispersion corrections (DFT-D3)[10] have been incorporated. Internal

energy and entropy contributions were obtained from frequency calculations done on the DFT structures at 298.15 K; thus, the energies reported are the ΔG values in this thesis work.

Furthermore, the NCI plot analysis[11] has been performed to quantify the noncovalent interactions. AIMD simulations have been carried out with the TeraChem 1.9 quantum chemistry package,[12] using the B3-LYP functional and the 6-31g* basis set.

7.3 Future Outlook

Insights gained from the work presented in this thesis shed light on critical areas of research and are also likely to help experimentalists to design systems in which the influence of nucleophilic attack chemistry can be kept in mind to improve the efficiency of the main group systems considerably. In this thesis work, a mechanistic study has been done for a system where a calcium compound acts as a catalyst for the hydroboration reaction. In the mechanism, it has been shown that, unlike traditional catalysts where the metal center acts as the catalyst, it is the the ligand that acts as the catalytic center and the role of the metal is to bring two ligands close and provide a dual-site for the catalysis. This insight has not been explored much by the experimentalists and in the future new catalysts with main group compounds can be synthesized, where the onus of being catalytic center can be shifted from the metal to the ligands.

As “the best catalyst is no catalyst”, the next two chapters have explored this very possibility for two important reactions: hydroboration and cyanosilylation. Through computational investigations, we have shown why experimentalists are able to achieve a high yield in solvent-free and catalyst-free conditions for hydroboration as well as for cyanosilylation. The reason is simply that one of the reactants, HBpin for hydroboration and TMSCN for the cyanosilylation case, acts not only as substrate and solvent but also as the catalyst. Furthermore, in order to mimic the same conditions in the presence of solvent and achieve high yield, we have proposed that if the concentration of HBpin and TMSCN in the respective reactions is increased to the right extent, then high yield can be achieved in the presence of a solvent. This idea has been tested by our experimental collaborators, and they have found that at a 1:5 ratio of substrate to HBpin and a 1:10 ratio of the substrate to TMSCN, the yield for both the respective reactions was comparable to the one they got in solvent-free and catalyst-free conditions. Hence, since there are many substrates that require a solvent to dissolve and since the reactions for such cases cannot take place without the solvent, our

proposed hypothesis of increasing the concentration of the internal catalyst can be used to obtain high yields without employing an external catalyst.

Lastly, one of the more interesting insights from this thesis work is from the last working chapter, where we have done a computational mechanistic study on a fuel-driven molecular motor system. We have found that each component used by Leigh and coworkers[3] have specific tasks, and their elegant interactions is what makes the motor move in a net directional fashion. The insights gained from this work can, in the future, be utilized to design more efficient molecular motors with better directionality in the system.

7.4 References

1. S. Yadav, R. Dixit, M. K. Bisai, K. Vanka, S. S. Sen, *Organometallics* **2018,** *37*, 4576.

2. R. Dixit, M. K. Bisai, S. Yadav, V. Yadav, S. S. Sen, K. Vanka, *Organometallics*, **2021,** *40*, 1104.

3. M. R. Wilson, J. Sola, A. Carlone, S. M. Goldup, N. Lebrasseur, D. A. Leigh, *Nature*, **2016**, *534*, 235.

4. TURBOMOLE V 7.0 2015, a development of University of Karlsruhe and Forschungszentrum Karlsruhe GmbH, 1989-2007 TURBOMOLE GmbH, since 2007; available from http://www.turbomole.com. & TURBOMOLE V 7.1 2016, a development of University of Karlsruhe and Forschungszentrum Karlsruhe GmbH, 1989-2007 TURBOMOLE GmbH, since 2007; available from http://www.turbomole.com

5. J. P. Perdew, K. Burke, M. Ernzerhof, *Phys. Rev. Lett*. **1997**, *78*, 1396.

6. F. Weigend and R. Ahlrichs, *Phys. Chem. Chem. Phys*. **2005**, 7, 3297.

7. K. Eichkorn, O. Treutler, O. H. M. Haser, R. Ahlrichs, *Chem. Phys. Lett*. **1995**, *240*, 283.

8. M. Sierka, A. Hogekamp, R. Ahlrichs, *J. Chem. Phys*. **2003**, *118*, 9136.

9. A. Klamt and G. Schuurmann, ***J. Chem. Soc.*** *Perkin Trans.* **1993**, *2*, 799.

10. (a) J. Hepburn, G. Scoles and R. Penco, *Chem. Phys*. *Lett.* **1975**, *36*, 451; (b) S. Grimme, *J. Comput. Chem.* **2004**, *25*, 1463; (c) S. Grimme, *J. Comput. Chem.*,2006, **27**, 1787; (d) S. Grimme, J. Antony, S. Ehrlich, and H. Krieg, *J. Chem. Phys*. **2010**, *132*, 154104.

11. a) E. R. Johnson, S. Keinan, P. M. Sanchez, J. C. Garcia, A. J. Cohen, W. Yang, *J. Am. Chem. Soc*. **2010**, *132*, 6498. b) J. C. Garcia, E. R. Johnson, S. Keinan, R. Chaudret, J. P. Piquemal, D. N. Beratan, W. Yang. *J. Chem. Theory Comput*. **2011**, *7*, 625.

12. Petachem. http://www.petachem.com

ABSTRACT

Name of the Student: Ruchi Dixit **Registration No.: 10CC16A26013**

Faculty of Study: Chemical Science **Year of Submission: 2022**

CSIR Lab: NCL, Pune **Name of the Supervisor: Dr. Kumar Vanka**

Title of the thesis: Understanding Nucleophilic Attack Chemistry in Main Group Compounds with Density Functional Theory

---

Nucleophilic attack chemistry has been an effective means of initiating chemical reactions in order to realise many important industrial products. The knowledge of the role of the nucleophile and its effect on the rate of the reaction can be of great value to chemists. However, there is still a need to study its influence in the hydroboration reaction, in cyanosilylation and for emerging and important areas of research such as that of molecular motors. Density functional theory (DFT) could be employed to provide insight into the role that the nucleophile plays, whether during its addition reactions or when it acts as a base.

The aim of this thesis is to study nucleophilic attack chemistry in main group compounds. Main group reactions provide a less toxic, more abundant and cheaper alternative to transition metals. Thus, due to aforementioned reasons, coupled with a scarcity of computational investigations on these environmentally benign compounds, we have chosen main group compounds for our investigations. We have studied a calcium compound, which has been employed as a catalyst for the hydroboration reaction and found out that the ligands in this compound act as dual site catalytic centres, instead of the metal centre acting as the catalyst. In our further investigations, we have explored the reasons for the high yield observed in solvent-free and catalyst-free conditions for the hydroboration reaction and for cyanosilylation and ascertained that HBpin and TMSCN act as “internal catalysts”. The explicit role of the substrate acting as an internal catalyst has been investigated thoroughly, and we hypothesized that using these internal catalysts in excess in the presence of solvent would lead to high yields, which was then experimentally corroborated. Lastly, the role of nucleophilic attack chemistry in the functioning of a [2]catenane molecular motor to provide it with net directionality in its motion has been scrutinized, where we have determined that the nucleophile acts like a ‘cargo’ and travels with the ring and acts as a nucleophile by extracting a proton from the ‘bulk’ when needed.

Furthermore, TOF calculations, volume correction in the entropy, and NCI plot analyses have been employed in our investigations into the role of nucleophilic attack chemistry.

Details of the publications emanating from the thesis work

1) List of publication(s) in SCI Journal(s) (published & accepted) emanating from the thesis work

(1) Sandeep Yadav, **Ruchi Dixit**, Milan Kumar Bisai, Kumar Vanka, and Sakya S. Sen, Alkaline Earth Metal Compounds of Methylpyridinato β-Diketiminate Ligands and Their Catalytic Application in Hydroboration of Aldehydes and Ketones, *Organometallics* **2018** *37,* (24), 4576-4584, DOI: 10.1021/acs.organomet.8b00568.

(2) **Ruchi Dixit**, Milan Kumar Bisai, Sandeep Yadav, Vinita Yadav, Sakya S. Sen, and Kumar Vanka, Substrate, Catalyst, and Solvent: The Triune Nature of Multitasking Reagents in Hydroboration and Cyanosilylation, *Organometallics*, **2021,** 40 (8), 1104-1112 DOI: 10.1021/acs.organomet.1c00070.

2) List of Papers with abstract presented (oral/poster) at national/international conferences/seminars with complete details.

i) Presented a poster entitled "Substrate, Solvent and Catalyst: The Triune Nature of Multitasking Reagents in Hydroboration and Cyanosilylation" at Science day, CSIR NCL Pune, 24-25 Feb 2021.

Abstract

A truly green chemical process would avoid the use of an external catalyst, while still achieving high efficiency. This has been realized in the very recent past for hydroboration, cyanosilylation, acetalization and the aza-Michael addition, among other reactions. The current, combined computational and experimental study, unlocks the secret to how this highly desirable outcome is accomplished: one of the reactants in the process also acts as the catalyst. Specifically, this is shown (i) for the important hydroboration reaction, with pinacolborane (HBpin) as the hydroborating reagent and benzaldehyde, acetophenone, benzoic acid and *p*-methoxyphenylacetylene as the hydroborated substrates, and (ii) for cyanosilylation, with trimethylcyanosilane (TMSCN) as the cyanosilylating agent and benzaldehyde as the substrate. The mechanistic understanding thus gained has then been further exploited experimentally to bring hydroboration and cyanosilylation closer to experimental conditions in catalysis. These insights can potentially be expanded to the rapidly growing area of solvent-free and internal catalyst chemistry.

ii) Presented a poster entitled "Alkaline Earth Metal Compounds of Methylpyridinato *β*-Diketiminate Ligands and Their Catalytic Application in Hydroboration of Aldehydes and Ketones" at the sixteenth Theoretical Chemistry Symposium, BITS Pilani, -2019 Pune, 13-16, Feb 2019.

Abstract

Ever increasing demand for green and sustainable chemical processes has set up a drive to replace transition metals with earth-abundant, nontoxic, and environmentally benign alternatives. In this regard, the alkaline earth metal complexes have attracted significant attention[1]. Herein, we have used a β-diketiminato ligand with methyl-pyridine side arm to synthesize calcium compound. Further to obtain mechanistic insight, full quantum chemical calculations were done with density functional theory (DFT) at the dispersion and solvent corrected PBE/TZVP level of theory. It was found that the role of the calcium compound in the chemistry is to bind two ligands, each of which is then capable of acting as a catalytic site for the hydroboration. Therefore, the calcium enables the formation of a dual site catalyst, which would be more efficient than just employing a pyridine moiety as a single site catalyst in the reaction. Furthermore, calculations with the energetic span model (ESM), developed by Shaik and co-workers,[2] provide insight into the relative efficiency values for the reactions with and without the calcium catalyst [2.83×10^{-9} s^{-1} (with catalyst) vs 5.48×10^{-12} s^{-1} (without catalyst)]. It was found that the efficiency of the reaction is increased by a factor of about 500, which shows the distinct effect of the calcium catalyst complex on the efficiency of the hydroboration.

ORGANOMETALLICS

Article

Cite This: *Organometallics* 2018, 37, 4576–4584

pubs.acs.org/Organometallics

Alkaline Earth Metal Compounds of Methylpyridinato β-Diketiminate Ligands and Their Catalytic Application in Hydroboration of Aldehydes and Ketones

Sandeep Yadav,[†,§,∥] Ruchi Dixit,[‡,§,∥] Milan Kumar Bisai,[†,§] Kumar Vanka,*[,‡,§] and Sakya S. Sen*[,†,§]

[†]Inorganic Chemistry and Catalysis Division, CSIR-National Chemical Laboratory, Dr. Homi Bhabha Road, Pashan, Pune 411008, India

[‡]Physical and Material Chemistry Division, CSIR-National Chemical Laboratory, Dr. Homi Bhabha Road, Pashan, Pune 411008, India

[§]Academy of Scientific and Innovative Research (AcSIR), New Delhi 110020, India

Supporting Information

ABSTRACT: Ever increasing demand for green and sustainable chemical processes has set up a drive to replace transition metals with earth-abundant, nontoxic, and environmentally benign alternatives. In this regard, the alkaline earth metal complexes have attracted significant attention. Herein, we have used a β-diketiminato ligand with methyl-pyridine side arm to synthesize magnesium (**1**) and calcium (**2**) compounds. The constitutions of **1** and **2** have been confirmed by single crystal X-ray studies, which show that the magnesium and calcium atom in **1** and **2** possesses octahedral geometry. Subsequently, we have used them as catalysts (1 mol %) for hydroboration of a wide range of aldehydes using pinacolborane (HBpin) at room temperature. The strategy has further been extended to ketones with 2 mol % catalyst loading. DFT calculations have been performed to understand the mechanism.

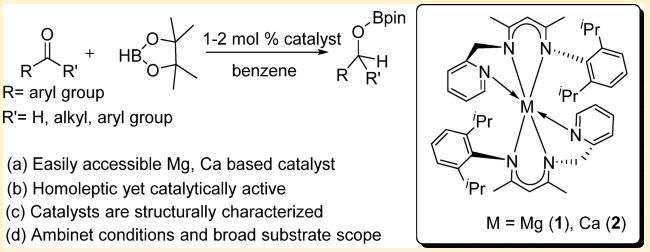

INTRODUCTION

In alkaline earth (Ae) metal chemistry, steric saturation of the coordination sphere of the alkaline earth metals usually dominates over the electronic effect. Therefore, the exploration for the new ligands, which can satisfy the coordination requirements of the alkaline earth metals, continues to be of significant current interest. Insofar, the alkaline earth metal chemistry has been driven by the use of monoanionic bidentate ligand systems such as amidinate $[RC\{NR\}_2]^-$,[1] guanidinate $[RNC(NR_2)NR]^-$,[1] trizenide $[(R_2N_3)]^-$,[2] β-diketiminate $[(R)NC(Me)C(H)C(Me)N(R)]^-$,[3] diboxmethanide $[(4,6\text{-}R\text{-}NCOC_6H_2)_2CH]^-$,[4,5] silylated aminopyridinato $[(2\text{-}R_3SiNH\text{-}6\text{-}MeC_5H_3N)]^-$,[6] etc. The strong binding affinity to the metal center and easily tunable steric and electronic properties of these ligands have been exploited for the stabilization of a plethora of hydrocarbon soluble alkaline earth metal complexes, including a compound with a Mg(I)−Mg(I) bond.[7] Recently, Roesky's group synthesized a [LCaI(μ-ICaI-μ)ICaL] chain stabilized by two chelating β-diketiminate ligands (L = $CH\{Et_2NCH_2CH_2N(CMe)\}_2$).[8] The result shows that an additional N→Ae donation can be beneficial to stabilize highly electrophilic alkaline earth metal complexes. This hypothesis is further boosted when Kay and co-workers reported a series of alkaline earth metal complexes of bidentate silylated aminopyridinato ligands as an alternative of amidinate or guanidinate ligands.[6]

The introduction of a methyl-pyridine side arm in the β-diketiminato framework leads to a ligand that is tridentate in its nacnac imino-pyridine state (2,6-iPr_2-$C_6H_3NC(Me)CHC(Me)NH(CH_2py)$). The pendant pyridine group on one of the nitrogen centers provides steric support as well as additional electronic stabilization to the metal center. The group of Wolczanski recently employed such tridentate chelating ligand for preparing a variety of iron and chromium complexes.[9] Chen and co-workers reported β-diketiminato rare-earth metal complexes of composition Ln-$(CH_2SiMe_3)_3(THF)_2$ (Ln = Sc and Y) using the same ligand.[10] Harder and co-workers have demonstrated the utility of *para*-phenyl and pyridine-bridged bis(β-diketiminate) ligand for the stabilization of multinuclear magnesium hydride complexes.[11] During the preparation of this manuscript, work by Westerhausen and co-workers demonstrating the coordination chemistry of *N*-(2-pyridylethyl)-substituted bulky amidinates and triazenides of magnesium has been published.[12] Despite their ongoing popularity and versatility, there are no examples of group 2 complexes supported by nancnac methylpyridinato ligands in the literature. Herein, we report the synthesis and isolation of homoleptic magnesium and calcium complexes stabilized by nancnac methylpyridinato

Received: August 8, 2018
Published: December 3, 2018

DOI: 10.1021/acs.organomet.8b00568
Organometallics 2018, 37, 4576–4584

Scheme 1. Synthetic Approaches for Accessing Magnesium (1) and Calcium (2) Compounds of Methylpyridinato β-Diketiminate Ligands

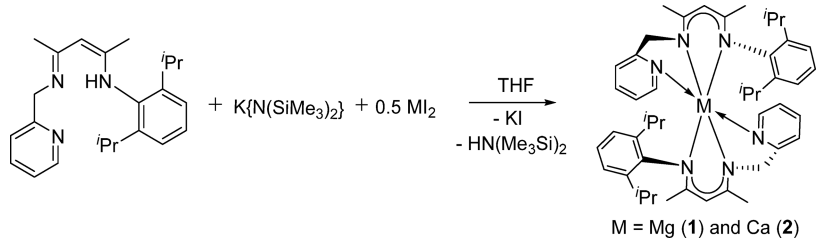

ligand. Although homoleptic alkaline earth metal complexes are usually considered catalytically incompetent, these magnesium and calcium complexes were found to catalyze hydroboration of aldehydes and ketones with HBpin under mild conditions with high yields.

RESULTS AND DISCUSSION

Synthesis and X-ray Studies. The ligand synthesis was accomplished following the procedures given by Chen and co-workers.[10] Deprotonation of the ligand with $KN(SiMe_3)_2$ in THF at room temperature led to the formation of the potassium salt of the ligand. The latter was subsequently reacted with MgI_2 and CaI_2 to lead to the homoleptic complexes of composition L_2M (M = Mg (**1**) and Ca (**2**)) (Scheme 1). Single crystals were grown from the concentrated solution of *n*-hexane at −4 °C. The direct addition of $[M\{N(SiMe_3)_2\}_2]$ (M = Mg and Ca) to the ligand has also afforded homoleptic L_2M complexes with concomitant release of $HN(SiMe_3)_2$.

1 and **2** were characterized by multinuclear NMR spectroscopy. The disappearance of an N−H resonance in the ^1H NMR spectrum indicates complete deprotonation of the ligand. Both **1** and **2** display two sets of doublets for the isopropyl groups, one septet, and two singlets for the methyl groups in their respective ^1H NMR spectrum. The molecular structures of **1** and **2** were confirmed by single crystal X-ray analysis.[13] It is of note that in **1** and **2**, no solvent molecule is coordinated to metal center. To check the coordination of solvent molecule in the solvent phase, we have performed DOSY NMR of complex **2**, and we have observed that the complex does not interact with THF strongly because the two THF signals show higher diffusion coefficients, indicating THF molecules are moving much faster than the solute (see the Supporting Information, Figure S7). **1** crystallizes in the triclinic space group $P\bar{1}$ (Figure 1). The geometry around the Mg atom is distorted octahedral, with two nacnac methylpyridinato ligands completing the environment. The $Mg-N_{nacnac}$ bond lengths are 2.1226(19), 2.1237(19), 2.224(2), 2.2303(19) Å, which are longer than the average Mg−N bond length (2.111(2) Å) in homoleptic β-diketiminato magnesium complex, [((DIPP-nacnac)$_2$Mg), DIPP-nacnac = (2,6-*i*Pr$_2$C$_6$H$_3$)NC(Me)C-(H)C(Me)N(2,6-*i*Pr$_2$C$_6$H$_3$)] complex, reported by Harder and co-workers.[14] The pyridyl group coordinates to the magnesium center with $Mg-N_{pyridyl}$ bond lengths of 2.270(2) and 2.290(2) Å, which are longer than the $Mg-N_{nacnac}$ bonds. The longer $Mg-N_{pyridyl}$ bond with respect to the $Mg-N_{nacnac}$ bond indicates that the pendant pyridyl groups act as neutral donors, while the backbone is an anionic ligand.

Compound **2** crystallizes in the monomeric space group *C*2/*c* and exhibits crystallographic C2-symmetry (Figure 2).

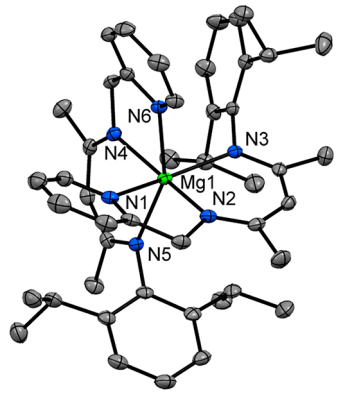

Figure 1. Molecular structure of **1** in the solid state with anisotropic displacement parameters depicted at the 50% probability level. Hydrogen atoms are omitted for clarity. Selected bond lengths [Å] or angles [deg]: Mg1−N2 2.1226(19), Mg1−N4 2.1237(19), Mg1−N3 2.224(2), Mg1−N5 2.2303(19), Mg1−N1 2.270(2), Mg1−N6 2.290(2); N2−Mg1−N4 168.02(8), N2−Mg1−N3 87.75(7), N4−Mg1−N3 99.10(7), N2−Mg1−N5 98.54(7), N4−Mg−N5 88.29(7), N3−Mg1−N5 110.63(7), N2−Mg1−N1 76.31(7), N4−Mg1−N1 94.30(7), N3−Mg1−N1 157.79(7), N5−Mg1−N1 87.28(7), N2−Mg−N6 94.40(7), N4−Mg1−N6 75.88(7), N3−Mg1−N6 90.16(7), N5−Mg1−N6 155.80(7), N1−Mg1−N6 75.99(7) .

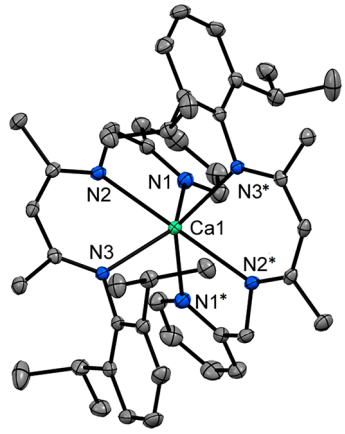

Figure 2. Molecular structure of **2** in the solid state with anisotropic displacement parameters depicted at the 50% probability level. Hydrogen atoms are omitted for clarity. Selected bond lengths [Å] or angles [deg]: Ca1−N2 2.4486(9), Ca1−N2 2.4487(9), Ca1− N3 2.4722(9), Ca1−N3 2.4722(9), Ca1−N1 2.5305(10), Ca1−N1 2.5305(10); N2−Ca1−N2 178.11(5), N2−Ca1−N3 104.22(3), N2−Ca1−N3 76.69(3), N2−Ca1−N3 76.69(3), N2−Ca1−N3 104.22(3), N3−Ca1−N3 124.38(4), N2−Ca1−N1 109.88(3), N2−Ca1−N1 68.52(3), N3−Ca1−N1 135.35(3), N3−Ca1−N1 91.48(3), N2−Ca1−N1 68.52(3), N2−Ca1−N1 109.88(3), N3−Ca1−N1 91.48(3), N3−Ca1−N1 135.35(3), N1−Ca1−N1 75.62(5).

DOI: 10.1021/acs.organomet.8b00568
Organometallics 2018, 37, 4576−4584

Table 1. Hydroboration of Aldehydes Using Compound 1 and 2[a]

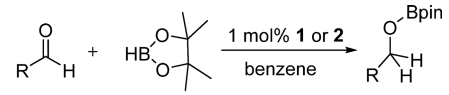

R= aryl group

Entry	Substrate	Time (h)	Catalyst	Yield (%)
3a	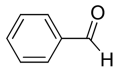	2	**1**	99
			2	99
3b	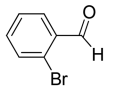	2	**1**	91
			2	90
3c	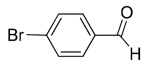	2	**1**	99
			2	96
3d	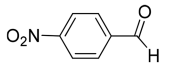	2	**1**	99
			2	99
3e	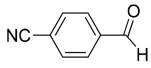	2	**1**	99
			2	99
3f	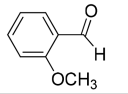	2	**1**	98
			2	98
3g	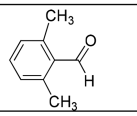	2	**1**	98
			2	95
3h	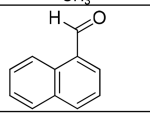	2	**1**	99
			2	97
3i	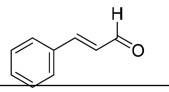	2	**1**	78
			2	75
3j	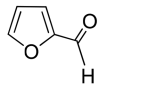	2	**1**	96
			2	94

[a]Reaction condition: Aldehyde, 0.25 mmol. Catalyst, 1 mol %. Room temperature in benzene. Reaction time, 2 h. Yields are calculated based on the integration area of product and starting material signals in the ^{1}H spectrum using mesitylene as an internal standard.

The molecular structure of **2** is identical to that of **1**. Similar to the magnesium atom, the calcium atom is coordinated by six nitrogen atoms and is in distorted octahedral geometry. The Ca−N bond lengths range from 2.4486(9) to 2.4722(9) Å, which are longer than the mean Ca−N bond in ((DIPP-nacnac)$_2$Ca) complex (2.379(1) Å).[14] The slight increase in the bond lengths is likely due to the more steric crowding in **2**. The bond distances of pyridine nitrogen to Ca metal center are 2.5305(10) and 2.5305(10) Å, which are longer than the β-diketaminate backbone N−Ca bond lengths. The N−Ae bond distances of Ca are longer as compared to the Mg due to the increase in the metal size.

Catalytic Application. The use of transition metal free catalysts for hydroboration of aldehydes and ketones has been recently explored in-depth. Catalysts derived from both s-[15−26] and p-block[27−35] elements have been reported with good success. A majority of catalysts derived from alkaline earth metals are heteroleptic in nature. Recently, homoleptic complexes of alkaline earth metals have been shown as potent catalysts. For example, Harder and co-workers demonstrated the catalytic activity of bora-amidinate (bam) complexes ^{DIPP}NBN-Mg·(THF)$_3$ and ^{DIPP}NBN-Ca·(THF)$_4$ in the intramolecular alkene hydroamination, in which the bora-amidinate ligand functions as a noninnocent ligand and partakes in substrate deprotonation and product protonation.[36] The metal−ligand cooperative catalysis has been further shown for tetranuclear Sr and Ba complexes by the same group for intramolecular alkene hydroamination, alkene hydrophosphination, pyridine hydroboration, pyridine hydrosilylation, and alkene hydrosilylation.[37] In contrast to these above-mentioned

DOI: 10.1021/acs.organomet.8b00568
Organometallics 2018, 37, 4576−4584

Table 2. Hydroboration of Ketones Using Compound 1 and 2[a]

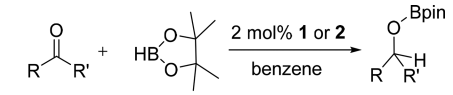

Entry	Substrate	Time	Catalyst	Yield (%)
4a	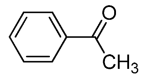	3h	**1**	95
			2	96
4b	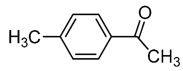	3h	**1**	99
			2	96
4c	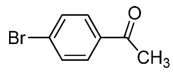	3h	**1**	99
			2	99
4d	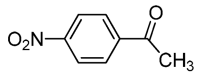	3h	**1**	99
			2	99
4e	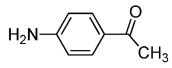	3h	**1**	99
			2	98
4f	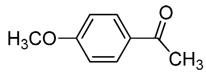	3h	**1**	97
			2	95
4g	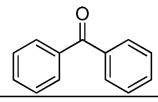	3h	**1**	99
			2	99
4h	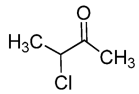	3h	**1**	85
			2	82

[a]Reaction condition: Ketone, 0.25 mmol. Catalyst, 2 mol %. Room temperature in benzene. Reaction time, 3 h. Yields are calculated based on the integration area of product and starting material signals in the ^{1}H spectrum using mesitylene as an internal standard.

noninnocent ligands, amidinates or β-diketiminates are usually traditional spectator ligands, which bind to the metal and provide a pocket for the substrate binding in homogeneous catalysis without participating in the catalytic cycle. Usually homoleptic alkaline earth metal complexes having spectator ligands are considered as catalytically incompetent. Nevertheless, the group of Roesky has recently reported benzamidinate stabilized homoleptic alkaline earth metal complexes for catalyzing hydrophosphination of styrene.[38] A further encouragement comes from the works of Harder and Speilmann, who described β-diketiminate calcium hydride catalyzed hydroboration of 1,1-diphenylethylene, although the subsequent mechanistic studies revealed that the calcium hydride complex was not a bonafide catalyst.[39] Preliminary NMR scale experiments have revealed the activity of **1** and **2** toward hydroboration reaction at ambient conditions, as evidenced by the clean conversion of benzaldehyde and pinacolborane (HBpin) in benzene to the corresponding alkoxypinacolboronate ester. The conversion is 99% with 1 mol % catalyst loading of **1** and **2**.

Encouraged by these results, we have assessed the utility of **1** and **2** in the hydroboration of a variety of aldehydes and ketones by HBpin at ambient conditions to afford the corresponding alkoxypinacolboronate esters (Tables 1 and 2). No repressing issue was noticed for the *ortho* substituents (entry **3b**, **3g**). Benzaldehydes with substitution at *ortho*, *meta*, and *para*-position do not have significant impact on the reactivity. Electron withdrawing substituents (Br (entry **3b**, **3c**), NO_2 (entry **3d**), CN (entry **3e**)) as well as electron donating substituents (CH_3 (entry **3g**), OCH_3 (entry **3f**)) are well-tolerated. The reaction of furfural with HBpin led to exclusive hydroboration of the carbonyl functionality instead of dearomatization of the furfural ring (entry **3j**). Exclusive 1,2-addition of HBpin to cinnamaldehyde was observed as a result of the highly electrophilic character of the carbonyl moiety (entry **3i**), although with a drop in the yield. Hydroboration of sterically hindered 2,6-dimethylbenzaldehyde (entry **3g**) also gave good yield at the same reaction conditions. To demonstrate the applicability of the reported protocol, 4-cyanobenzaldehyde and 4-bromoacetophenone were acid hydrolyzed after completion of reaction and their corresponding alcohols were isolated in quantitative yield.

Aromatic ketones were identified as equally suitable substrates for hydroboration, demonstrated by the clean conversion of acetophenone (entry **4a**), although higher catalyst loadings (2 mol %) and slightly extended reaction times (3 h) were necessary to attain productive conversion. Reduction of a wide variety of aromatic ketones bearing both electron withdrawing (*p*-Br (entry **4c**), *p*-NO_2 (entry **4d**)) as well as electron donating (*p*-NH_2 (entry **4e**), *p*-OMe (entry

DOI: 10.1021/acs.organomet.8b00568
Organometallics 2018, 37, 4576−4584

Scheme 2. Reaction Profile for the Hydroboration Reaction with the Calcium Catalyst 2[a]

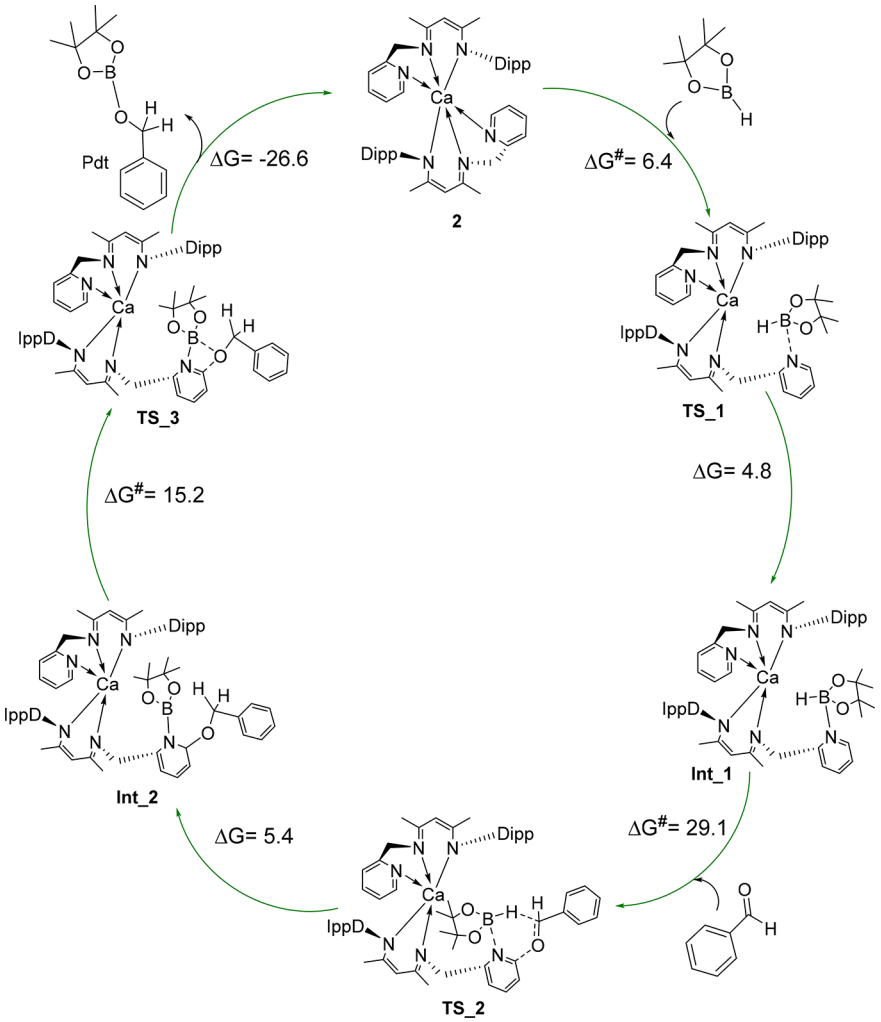

[a]The values (in kcal/mol) have been calculated at the PBE/TZVP level of theory.

4f)) functional groups to the respective boronate esters was successful under the reaction conditions. Sterically hindered benzophenone was cleanly converted in 3 h at room temperature with 2 mol % catalyst loading to the corresponding borate ester (entry **4g**). Even aliphatic ketone was also smoothly converted (entry **4h**), revealing the versatility of our synthetic methodology. However, substrates such as esters, amides, and pyridine were not reduced, even at a higher catalyst loading and under forcing conditions.

We have compared the activity of **1** and **2** with the known alkaline earth metal catalysts for benzophenone. Hill's magnesium catalyst,[20] Okuda's $[Mg(thf)_6][HBPh_3]_2$,[21] and Stasch's phosphinoamido-magnesium-hydride[22] were recorded with large TOFs of 500 h^{-1}, 1000 h^{-1} (in absence of DMSO), and 1760 h^{-1}, respectively. Our previously reported Ca-based catalyst, $[PhC(NiPr)_2CaI]$,[24] showed a TOF of 8.6 h^{-1}. In comparison, both **1** and **2** are found to give a TOF of 33 h^{-1} for reduction of benzophenone, which is definitely lower than magnesium based heteroleptic catalysts but higher than the calcium one. The decrease in TOF can be attributed to the saturation of coordination sites of **1** and **2**. It should be noted here that analogous β-diketiminato compounds of composition $(DIPP\text{-}nacnac)_2M$ (M = Mg and Ca)[14] are not reported for the hydroboration of aldehydes and ketones. This indicates the importance of the incorporation of the pyridinato moiety in the ligand framework, which binds to the metal center in a hemilabile manner and assists in improving the catalytic activity.

To obtain additional mechanistic insight, full quantum chemical calculations were done with density functional theory (DFT) at the dispersion and solvent corrected PBE/TZVP level of theory. In the first step of the reaction, HBpin approaches catalyst **2** and forms **Int_1** (see Scheme 2 and Figure S8 in the Supporting Information) in which N of one of the pyridine ligand breaks its interaction with the calcium atom and forms a new N−B bond (likely the Lewis acid base adduct, in which N and B contain positive and negative charges respectively) with the B center of HBpin. The thermodynamics (ΔG) for this step is unfavorable by 4.8 kcal/mol. This occurs via a "two atoms involved transition state" (**TS_1**) where no bond breaking but only N···B bond formation occurs with a very low free energy ($\Delta G^{\#}$) barrier of only 6.4 kcal/mol. In the next step, benzaldehyde approaches the B−H bond of **Int_1**. This is the prelude to the nucleophilic attack by the carbonyl oxygen of benzaldehyde to the adjacent sp^2 carbon of pyridine N of **Int_1**, further leading to the neutralization of the charge of N and to the hydride being transferred from the negatively charged center B to the carbonyl carbon of benzaldehyde,

DOI: 10.1021/acs.organomet.8b00568
Organometallics 2018, 37, 4576−4584

which leads to the formation of **Int_2**. This step is favorable by 5.4 kcal/mol. This occurs through a very flexible six membered (C···N···B···H···C···O) transition state (**TS_2**) with a barrier of 29.1 kcal/mol. This is the slowest step of the hydroboration reaction. The ΔG values corresponding to the barriers have been calculated at room temperature. The values are on the higher side, even after volume corrections for the translational entropy term (for further details, please see the computational details section in the Supporting Information). This is because the entropy loss during the reaction is overestimated in the calculations, leading to the high values for the barriers. The real values for the barrier heights are, therefore, likely to be much lower.

In the transition state corresponding to this step, there is a significant amount of B−H bond activation (1.47 Å distance in the transition state), which allows the hydride transfer from the boron to the carbonyl carbon center, along with the simultaneous occurring of C═O bond cleavage and the formation of another C−O bond. In the last step of the reaction, intramolecular bond forming and bond breaking takes place. The O center of carbonyl group attacks the B center, along with the formation of the B−O bond and the simultaneous breaking of the N−B and C−O bonds. The last step is very favorable, by 26.6 kcal/mol. This occurs after the surmounting of a four membered transition state (**TS_3**) with a barrier of 15.2 kcal/mol, and also leads to the regeneration of catalyst **2**. The fact that the final product is thermodynamically stable, and that the barrier for the slowest step is lower than without the mediation of the catalyst, indicates that the addition of the calcium compound **2** has a salutary effect on the hydroboration reaction. This reaction profile is also shown as a plot of the energy with regard to the reaction coordinate (along with the corresponding figures) in Figure S8 of the Supporting Information. Furthermore, calculations with the energetic span model (ESM), developed by Shaik and co-workers,[40] provide insight into the relative efficiency values for the reactions with and without the calcium catalyst [2.83×10^{09} s^{-1} (using catalyst **2**) vs 5.48×10^{12} s^{-1} (without catalyst)]. The TOF values are seen to be quite low, but this is due to the overestimation of the entropy loss in the calculations, leading to the higher values for the barriers, as explained earlier. However, since this overestimation affects the barriers for both the catalyst and noncatalyst cases, what is important to note is that the efficiency of the system is increased by a factor of about 500, which shows the distinct effect of the calcium catalyst complex on the efficiency of the hydroboration.

We have also investigated the possibility of the calcium center participating in the catalysis process. Several different mechanisms have been studied in this regard, and are discussed in the SI (see Figures S9, S10, S11, and S12). However, these mechanisms have not been seen to be as favorable as the mechanism that is discussed above. We have also investigated the possibility of decoordinating the side arm, i.e., the methylene bridged pyridyl moiety, so as to leave one coordination site free for the aldehyde reactant to approach the calcium center. However, this was found to be significantly unfavorable—by 8.6 kcal/mol (ΔE value). Hence, the calculations suggest that it is the pyridyl moiety without the methylene bridge that is thermodynamically more likely to open its coordination site and provide space for the incoming reagents, in comparison to the methylene bridged pyridyl moiety. The role of the calcium in the chemistry is therefore to bind two ligands, each of which is then capable of acting as a catalytic site for the hydroboration. Therefore, the calcium enables the formation of a dual site catalyst, which would be more efficient than just employing a pyridine moiety as a single site catalyst in the reaction.

■ CONCLUSIONS

The search for new chelating ligands with good donor properties is ongoing in alkaline earth metal chemistry. Here, we have synthesized well-defined homoleptic compounds of Mg (**1**) and Ca (**2**) using a tridentate monoanionic β-diketiminate ligand with a pendant pyridyl moiety. Single crystal X-ray studies show both **1** and **2** are six-coordinated and exhibit distorted octahedral geometry. Despite being homoleptic, both **1** and **2** are active toward the hydroboration of a variety of aldehydes and ketones under mild conditions, and their activities are better than some heteroleptic alkaline earth metal compounds. The introduction of pyridyl moiety in the nacnac system led to increase the catalytic activity presumably due to its hemilabile bonding with the metal center. Such catalysts may thus provide a cheap and effective alternative for expensive late transition metal species in addition to a remarkably broad substrate scope.

■ EXPERIMENTAL SECTION

All experiments were carried out under an inert atmosphere of argon applying standard Schlenk techniques or in a glovebox. The solvents used were purified by an MBRAUN solvent purification system MB SPS-800. All chemicals purchased from Sigma-Aldrich were used without further purification. ^{1}H and ^{13}C NMR spectra were recorded in C_6D_6 and DMSO-d_6 using a Bruker Avance DPX 200 or a Bruker Avance DRX 500 spectrometer and were referenced to external $SiMe_4$. LC−mass spectra were obtained using an Agilent Technologies 6120. Elemental analyses were performed at the CSIR-National Chemical Laboratory, Pune. Melting points were measured in a sealed glass tube on a Stuart SMP-30 melting point apparatus and were uncorrected. The ligand, LH (2,6-^{i}Pr-C_6H_3NC(Me)CHC(Me)-NH(CH_2py)), was prepared according to the literature.[10]

Synthesis of 1. THF (30 mL) was added to a mixture of ligand (1.05 g, 3 mmol) and KN($SiMe_3$)$_2$ (0.60 g, 3 mmol). The reaction mixture was stirred for 1 h, after that it was transferred to another flask containing MgI_2 (0.42 g, 1.5 mmol) in 10 mL of THF, and the resulting mixture was stirred overnight. The volatile was removed under a vacuum, and highly soluble homoleptic complexes were extracted with hexane. Crystallization was done in concentrated solution of hexane at −4 °C to give reddish yellow crystals of **1** (79%). ^{1}H NMR (200 MHz, $CDCl_3$, 25 °C) δ = 8.69 (d, $^3J_{HH}$ = 5.1 Hz, 2H, Py-*H*), 7.83 (td, $^3J_{HH}$ = 7.8 Hz and $^4J_{HH}$ = 1.6 Hz, 2H, Py-*H*), 7.35−7.51 (m, 6H, Py-*H*), 7.19−7.31 (m, 6H, Ar-*H*), 4.96 (s, 2H, MeC(N)C*H*), 4.77 (s, 4H, NC*H*2), 3.07 (sep, *J* = 6.86 Hz, 4H, ArC*H*Me2), 2.17 (s, 6H, *Me*C), 1.87 (s, 6H, *Me*C), 1.38 (d, $^3J_{HH}$ = 7.1 Hz, 12H, ArCH*Me*2), 1.26 (d, $^3J_{HH}$ = 7.0 Hz, 12H, ArCH*Me*2); ^{13}C NMR (100.6 MHz, $CDCl_3$, 25 °C) δ = 165.4, 160.0, 155.2 (imine-C and Py-*C*), 149.2, 146.4, 137.9, 136.8, 128.3, 122.7, 121.9, 120.4 (Ar-*C* and Py-*C*), 94.4 (MeC(N)CH), 48.7 (NCH2), 28.0 (ArCHMe$_2$), 23.7 (ArCH*Me*$_2$), 22.9 (ArCH*Me*2), 21.7 (*Me*C), 19.2 (*Me*C). Anal. Calcd for $C_{46}H_{66}N_6Mg$ (727.36): C, 75.96; H, 9.15. Found: C, 74.97; H, 8.52. ESI-HRMS calcd. for $C_{46}H_{67}N_6Mg$ [M + H]$^+$ = 727.5272, found 727.4588.

Synthesis of 2. *Method A.* THF (30 mL) was added to a mixture of ligand (1.05 g, 3 mmol) and KN($SiMe_3$)$_2$ (0.60 g, 3 mmol). The reaction mixture was stirred for 1 h, after that it was transferred to another flask containing CaI_2 (0.44 g, 1.5 mmol) in 10 mL of THF, and the resulting mixture was stirred overnight. The volatile was removed under a vacuum, and highly soluble homoleptic complexes were extracted with hexane. Crystallization was done in concentrated solution of hexane at −4 °C to give yellow crystals of **2** (65%).

DOI: 10.1021/acs.organomet.8b00568
Organometallics 2018, 37, 4576−4584

Method B. THF (30 mL) was added to a mixture of ligand (1.05 g, 3 mmol) and $Ca[N(SiMe_3)_2]_2$ (0.54 g, 1.5 mmol). The resulting brown color solution was stirred overnight. It was filtered through Celite, and the volatile was removed under a vacuum. Single crystals suitable for XRD were grown from the concentrated solution of hexane at −4 °C, which afforded yellow crystals of **2** (74%). ^{1}H NMR (200 MHz, $CDCl_3$, 25 °C) δ = 8.52 (d, $^3J_{HH}$ = 4.7 Hz, 2H, Py-*H*), 7.64 (td, $^3J_{HH}$ = 7.7 Hz and $^4J_{HH}$ = 2.1 Hz, 2H, Py-*H*), 7.27−7.32 (m, 6H, Py-*H*), 7.02−7.09 (m, 6H, Ar-*H*), 4.78 (s, 2H, MeC(N)C*H*), 4.59 (s, 4H, NCH_2), 2.92 (sep, J = 6.74 Hz, 4H, $ArCHMe_2$), 1.99 (s, 6H, *Me*C), 1.68 (s, 6H, *Me*C), 1.20 (d, $^3J_{HH}$ = 7.1 Hz, 12H, $ArCHMe_2$), 1.07(d, $^3J_{HH}$ = 7.0 Hz, 12H, $ArCHMe_2$). Anal. Calcd for $C_{46}H_{66}N_6Ca$ (743.13): C, 74.35; H, 8.95. Found: C, 74.48; H, 8.87. ESI-HRMS calcd. for $C_{46}H_{67}N_6Ca$ $[M + H]^+$ = 743.5048, found 743.4993.

Crystal Structure Determination. X-ray intensity data measurements of compound **1** and **2** were carried out on a Bruker SMART APEX II CCD diffractometer with graphite-monochromatized (Mo Kα = 0.71073 Å) radiation. The X-ray generator was operated at 50 kV and 30 mA. A preliminary set of cell constants and an orientation matrix were calculated from three sets of 36 frames. Data were collected with ωscan width of 0.5° at different settings of φ and 2θ keeping the sample-to-detector distance fixed at 5.00 cm. The X-ray data collection was monitored by APEX2 program (Bruker, 2006).[41] All the data were corrected for Lorentzian, polarization, and absorption effects using SAINT and SADABS programs (Bruker, 2006). SHELX-97 was used for structure solution and full matrix least-squares refinement on F^2.[42] All the hydrogen atoms were placed in geometrically idealized position and constrained to ride on their parent atoms. An ORTEP III[43] view of both compounds were drawn with 50% probability displacement ellipsoids and H atoms omitted for clarity.

Crystal Data of **1**. CCDC 1836442. $C_{46}H_{60}MgN_6$, 1.5(C_6H_{14}), M = 850.56, pale pink plate, 0.31 × 0.22 × 0.06 mm^3, triclinic, space group $P\bar{1}$, a = 15.3738(7) Å, 15.4978(7) Å, c = 22.9087(11)Å, α = 76.035(2)°, β = 75.845(2)°, δ = 71.315(2)°, V = 4934.0(4)Å^3, Z = 4, T = 100(2) K, $2\theta_{max}$ = 50.00°, D_{calc} (g cm^{-3}) = 1.145, F(000) = 1860, μ (mm^{-1}) = 0.078, 99063 reflections collected, 17328 unique reflections (R_{int} = 0.0397), 15532 observed ($I > 2\sigma(I)$) reflections, multiscan absorption correction, T_{min} = 0.976, T_{max} = 0.995, 1091 refined parameters, S = 1.024, $R1$ = 0.0652, $wR2$ = 0.1768 (all data R = 0.0699, $wR2$ = 0.1801), maximum and minimum residual electron densities; $\Delta\rho_{max}$ = 1.124, $\Delta\rho_{min}$ = −0.581 (eÅ^{-3}).

Crystal Data of **2**. CCDC 1836447. M = 808.21, colorless block, 0.22 × 0.16 × 0.06 mm^3, monoclinic, space group $C2/c$, a = 13.8404(5) Å, b = 24.8889(7) Å, c = 13.2292(4) Å, β = 98.6200(10), V = 4505.6(2) Å^3, Z = 4, T = 100(2) K, $2\theta_{max}$ = 50.00°, D_{calc} (g cm^{-3}) = 1.191, F(000) = 1756, μ (mm^{-1}) = 0.181, 38181 reflections collected, 4398 unique reflections (R_{int} = 0.0220), 4311 observed ($I > 2\sigma(I)$) reflections, multiscan absorption correction, T_{min} = 0.961, T_{max} = 0.989, 247 refined parameters, 153 restraints, S = 1.095, $R1$ = 0.0337, $wR2$ = 0.0860 (all data R = 0.0341, $wR2$ = 0.0863), maximum and minimum residual electron densities; $\Delta\rho_{max}$ = 0.254, $\Delta\rho_{min}$ = −0.189 (eÅ^{-3}).

■ ASSOCIATED CONTENT

Supporting Information

The Supporting Information is available free of charge on the ACS Publications website at DOI: 10.1021/acs.organomet.8b00568.

Complete computational details and catalytic procedure (PDF)

Additional data (XYZ)

Accession Codes

CCDC 1836442 and 1836447 contain the supplementary crystallographic data for this paper. These data can be obtained free of charge via www.ccdc.cam.ac.uk/data_request/cif, or by emailing data_request@ccdc.cam.ac.uk, or by contacting The Cambridge Crystallographic Data Centre, 12 Union Road, Cambridge CB2 1EZ, UK; fax: +44 1223 336033.

■ AUTHOR INFORMATION

Corresponding Authors

*E-mail: k.vanka@ncl.res.in.

*E-mail: ss.sen@ncl.res.in.

ORCID

Sandeep Yadav: 0000-0003-2780-3770

Kumar Vanka: 0000-0001-7301-7573

Sakya S. Sen: 0000-0002-4955-5408

Author Contributions

‖Sandeep Yadav and Ruchi Dixit contributed equally.

Notes

The authors declare no competing financial interest.

■ ACKNOWLEDGMENTS

This work was supported by Science and Engineering Research Board, India (SB/S1/IC-10/2014) and Ramanujan Research Grant (SB/S2/RJN-073/2014). S.Y., M.K.B., and R.D. thank CSIR, India for the research fellowships. K.V. and R.D. acknowledge "'MSM'" (CSC0129) and DST (EMR/2014/000013) for funding. We thank Dr. Rajesh G. Gonnade for helping in single crystal X-ray studies and Dr. Sapna Ravindranathan for the DOSY NMR experiment. We thank the reviewers for their critical input to improve the quality of the manuscript.

■ REFERENCES

(1) (a) Moxey, G. J.; Ortu, F.; Sidley, L. G.; Strandberg, H. N.; Blake, A. J.; Lewis, W.; Kays, D. L. Synthesis and characterisation of magnesium complexes containing sterically demanding N,N′-bis-(aryl)amidinate ligands. *Dalton Trans.* **2014**, *43*, 4838−4846. (b) Schwamm, R. J.; Day, B. M.; Mansfield, N. E.; Knowelden, W.; Hitchcock, P. B.; Coles, M. P. Catalytic bond forming reactions promoted by amidinate, guanidinate and phosphaguanidinate compounds of magnesium. *Dalton Trans.* **2014**, *43*, 14302−14314. (c) Day, B. M.; Knowelden, W.; Coles, M. P. Synthetic and catalytic intermediates in a magnesium promoted Tishchenko reaction. *Dalton Trans.* **2012**, *41*, 10930−10933. (d) Schwamm, J.; Coles, M. P. Catalytic C−C Bond Formation Promoted by Organo- and Amidomagnesium(II) Compounds. *Organometallics* **2013**, *32*, 5277−5280. (e) Yadav, S.; Swamy, V. S. V. S. N.; Gonnade, R. G.; Sen, S. S. Benz−amidinato Stabilized a Monomeric Calcium Iodide and a Lithium Calciate(II) Cluster featuring Group 1 and Group 2 Elements. *ChemistrySelect* **2016**, *1*, 1066−1071. (f) Day, B. M.; Mansfield, N. E.; Coles, M. P.; Hitchcock, P. B. Bicyclic guanidinate compounds of magnesium and their activity as pre-catalysts in the Tishchenko reaction. *Chem. Commun.* **2011**, *47*, 4995−4997. (g) Jones, C. Bulky guanidinates for the stabilization of low oxidation state metallacycles. *Coord. Chem. Rev.* **2010**, *254*, 1273−1289. (h) Glock, C.; Loh, C.; Goerls, H.; Krieck, S.; Westerhausen, M. Sterically Encumbered Amidinates and Guanidinates of Calcium and Strontium. *Eur. J. Inorg. Chem.* **2013**, *2013*, 3261−3269. (i) Barman, M. K.; Baishya, A.; Nembenna, S. Bulky guanidinate stabilized homoleptic magnesium, calcium and zinc complexes and their catalytic activity in the Tishchenko reaction. *J. Organomet. Chem.* **2015**, *785*, 52−60.

(2) (a) Hauber, S.-O.; Lissner, F.; Deacon, G. B.; Niemeyer, M. Stabilization of Aryl−Calcium, −Strontium, and −Barium Compounds by Designed Steric and π-Bonding Encapsulation. *Angew. Chem., Int. Ed.* **2005**, *44*, 5871−5875. (b) Barrett, A. G. M.; Crimmin, M. R.; Hill, M. S.; Hitchcock, P. B.; Kociok-Köhn, G.; Procopiou, P. A. Triazenide Complexes of the Heavier Alkaline Earths: Synthesis,

DOI: 10.1021/acs.organomet.8b00568
Organometallics 2018, 37, 4576−4584

Characterization, And Suitability for Hydroamination Catalysis. *Inorg. Chem.* **2008**, *47*, 7366−7376.
(3) (a) Nembenna, S.; Roesky, H. W.; Nagendran, S.; Hofmeister, A.; Magull, J.; Wilbrandt, P.-J.; Hahn, M. A. A well-defined hydrocarbon-soluble calcium monofluoride, $[\{LCaF(thf)\}_2]$: the application of soluble calcium derivatives for surface coating. *Angew. Chem., Int. Ed.* **2007**, *46*, 2512−2514. (b) Barrett, A. G. M.; Crimmin, M. R.; Hill, M. S.; Hitchcock, P. B.; Procopiou, P. A. Trifluoromethyl coordination and C-F bond activation at calcium. *Angew. Chem., Int. Ed.* **2007**, *46*, 6339−6342. (c) Ruspic, C.; Harder, S. Big Ligands for Stabilization of Small Functionalities in Calcium Chemistry. *Inorg. Chem.* **2007**, *46*, 10426−10433. (d) Westerhausen, M.; Digeser, M. H.; Gückel, C.; Nöth, H.; Knizek, J.; Ponikwar, W. 3,4-Dimethyl-2,5-bis(trimethylsilyl)phospha- and 3,4-Dimethyl-2,5-bis(trimethylsilyl)-arsacyclopentadienides of Calcium. *Organometallics* **1999**, *18*, 2491−2496. (e) Sarish, S. P.; Jana, A.; Roesky, H. W.; Schulz, T.; John, M.; Stalke, D. Heavier Alkaline Earth Metal Borohydride Complexes Stabilized by β−Diketiminate Ligand. *Inorg. Chem.* **2010**, *49*, 3816−3820. (f) Sarish, S. P.; Nembenna, S.; Nagendran, S.; Roesky, H. W. Chemistry of Soluble β-Diketiminatoalkaline-Earth Metal Complexes with M-X Bonds (M = Mg, Ca, Sr; X = OH, Halides, H). *Acc. Chem. Res.* **2011**, *44*, 157−170.
(4) Koehne, I.; Herbst-Irmer, R.; Stalke, D. Bis(4-methylbenzoxazol-2-yl)methanide in s-Block Metal Coordination. *Eur. J. Inorg. Chem.* **2017**, *2017*, 3322−3326. (b) Koehne, I.; Bachmann, S.; Niklas, T.; Herbst-Irmer, R.; Stalke, D. A Novel Bulky Heteroaromatic Substituted Methanide Mimicking NacNac: Bis(4,6-*tert*-butylbenzoxazol-2-yl)methanide in s-Block Metal Coordination. *Chem. - Eur. J.* **2017**, *23*, 13141−13149.
(5) Koehne, I.; Graw, N.; Teuteberg, T.; Herbst-Irmer, R.; Stalke, D. Introducing NacNac-Like Bis(4,6-isopropylbenzoxazol-2-yl)-methanide in s-Block Metal Coordination. *Inorg. Chem.* **2017**, *56*, 14968−14978.
(6) Ortu, F.; Moxey, G. J.; Blake, A. J.; Lewis, W.; Kays, D. L. Alkaline Earth Complexes of Silylated Aminopyridinato Ligands: Homoleptic Compounds and Heterobimetallic Coordination Polymers. *Inorg. Chem.* **2013**, *52*, 12429−12439.
(7) Green, S. P.; Jones, C.; Stasch, A. Stable magnesium(I) compounds with Mg-Mg bonds. *Science* **2007**, *318*, 1754−1757.
(8) Sarish, S. P.; Jana, A.; Roesky, H. W.; Schulz, T.; Stalke, D. A. $[I\text{-}Ca\text{-}I\text{-}Ca\text{-}I\text{-}Ca\text{-}I]^{2+}$ Chain Stabilized by Two Chelating β-Diketiminate Ligands. *Organometallics* **2010**, *29*, 2901−2903.
(9) Morris, W. D.; Wolczanski, P. T.; Sutter, J.; Meyer, K.; Cundari, T. R.; Lobkovsky, E. B. Iron and Chromium Complexes Containing Tridentate Chelates Based on Nacnac and Imino- and Methyl-Pyridine Components: Triggering C—X Bond Formation. *Inorg. Chem.* **2014**, *53*, 7467−7484.
(10) Xu, X.; Chen, Y.; Zou, G.; Sun, J. Single, double and triple deprotonation of a β-diketimine bearing pendant pyridyl group and the corresponding rare-earth metal complexes. *Dalton Trans.* **2010**, *39*, 3952−3958.
(11) (a) Harder, S.; Spielmann, J.; Intemann, J.; Bandmann, H. Hydrogen Storage in Magnesium Hydride: The Molecular Approach. *Angew. Chem., Int. Ed.* **2011**, *50*, 4156−4160. (b) Harder, S.; Spielmann, J.; Intemanna, J. Synthesis and thermal decomposition of a pyridylene-bridged bis-β-diketiminate magnesium hydride cluster. *Dalton Trans.* **2014**, *43*, 14284−14290.
(12) Kalden, D.; Krieck, S.; Görls, H.; Westerhausen, M. Coordination Chemistry of *N*-(2-Pyridylethyl)-Substituted Bulky Amidinates and Triazenides of Magnesium. *Eur. J. Inorg. Chem.* **2018**, 4361−4369.
(13) (a) Kottke, T.; Stalke, D. *J. Appl. Crystallogr.* **1993**, *26*, 615−619. (b) Stalke, D. *Chem. Soc. Rev.* **1998**, *27*, 171−178. The CCDC numbers of **1** and **2** are 1836442 and 1836447. These data can be available free of charge from https://www.ccdc.cam.ac.uk/.
(14) Harder, S. Homoleptic β-Diketiminato Complexes of the Alkaline-Earth Metals: Trends in the Series Mg, Ca, Sr, and Ba. *Organometallics* **2002**, *21*, 3782−3787.
(15) Mukherjee, D.; Osseili, H.; Spaniol, T. P.; Okuda, J. Alkali Metal Hydridotriphenylborates $[(L)M][HBPh_3]$ (M = Li, Na, K): Chemoselective Catalysts for Carbonyl and CO_2 Hydroboration. *J. Am. Chem. Soc.* **2016**, *138*, 10790−10793.
(16) McLellan, R.; Kennedy, A. R.; Mulvey, R. E.; Orr, S. A.; Robertson, S. D. 1-Alkali-metal-2-alkyl-1,2-dihydropyridines: Soluble Hydride Surrogates for Catalytic Dehydrogenative Coupling and Hydroboration Applications. *Chem. - Eur. J.* **2017**, *23*, 16853−16861.
(17) Osseili, H.; Mukherjee, D.; Spaniol, T. P.; Okuda, J. Ligand Influence on Carbonyl Hydroboration Catalysis by Alkali Metal Hydridotriphenylborates $[(L)M][HBPh_3]$ (M = Li, Na, K). *Chem. - Eur. J.* **2017**, *23*, 14292−14298.
(18) Osseili, H.; Mukherjee, D.; Beckerle, K.; Spaniol, T. P.; Okuda, J. Me_6TREN-Supported Alkali Metal Hydridotriphenylborates $[(L)M][HBPh_3]$ (M = Li, Na, K): Synthesis, Structure, and Reactivity. *Organometallics* **2017**, *36*, 3029−3034.
(19) Bisai, M. K.; Das, T.; Vanka, K.; Sen, S. S. Easily Accessible Lithium Compound Catalyzed Mild and Facile Hydroboration and Cyanosilylation of Aldehydes and Ketones. *Chem. Commun.* **2018**, *54*, 6843−6846.
(20) Arrowsmith, M.; Hadlington, T. J.; Hill, M. S.; Kociok-Köhn, G. Magnesium-Catalysed Hydroboration of Aldehydes and Ketones. *Chem. Commun.* **2012**, *48*, 4567−4569.
(21) Mukherjee, D.; Shirase, S.; Spaniol, T. P.; Mashima, K.; Okuda, J. Magnesium Hydridotriphenylborate $[Mg(thf)_6][HBPh_3]_2$: A Versatile Hydroboration Catalyst. *Chem. Commun.* **2016**, *52*, 13155−13158.
(22) Fohlmeister, L.; Stasch, A. Ring-Shaped Phosphinoamido-Magnesium-Hydride Complexes: Syntheses, Structures, Reactivity, and Catalysis. *Chem. - Eur. J.* **2016**, *22*, 10235−10246.
(23) Harinath, A.; Bhattacharjee, J.; Nayek, H. P.; Panda, T. K. Alkali metal complexes as efficient catalysts for hydroboration and cyanosilylation of carbonyl compounds. *Dalton Trans.* **2018**, *47*, 12613−12622.
(24) Yadav, S.; Pahar, S.; Sen, S. S. Benz-amidinato calcium iodide catalyzed aldehyde and ketone hydroboration with unprecedented functional group tolerance. *Chem. Commun.* **2017**, *53*, 4562−4564.
(25) Pollard, V. A.; Orr, S. A.; McLellan, R.; Kennedy, A. R.; Hevia, E.; Mulvey, R. E. Lithium diamidodihydridoaluminates: bimetallic cooperativity in catalytic hydroboration and metallation applications. *Chem. Commun.* **2018**, *54*, 1233−1236.
(26) Harder, S. From Limestone to Catalysis: Application of Calcium Compounds as Homogeneous Catalysts. *Chem. Rev.* **2010**, *110*, 3852−3876.
(27) Lawson, J. R.; Wilkins, L. C.; Melen, R. L. Tris(2,4,6-trifluorophenyl)borane: An Efficient Hydroboration Catalyst. *Chem. - Eur. J.* **2017**, *23*, 10997−11000.
(28) Yang, Z.; Zhong, M.; Ma, X.; De, S.; Anusha, C.; Parameswaran, P.; Roesky, H. W. An Aluminum Hydride That Functions like a Transition-Metal Catalyst. *Angew. Chem., Int. Ed.* **2015**, *54*, 10225−10229.
(29) Jakhar, V. K.; Barman, M. K.; Nembenna, S. Aluminum Monohydride Catalyzed Selective Hydroboration of Carbonyl Compounds. *Org. Lett.* **2016**, *18*, 4710−4713.
(30) Pollard, V. A.; Fuentes, M. A.; Kennedy, A. R.; McLellan, R.; Mulvey, R. E. Comparing Neutral (Monometallic) and Anionic (Bimetallic) Aluminum Complexes in Hydroboration Catalysis: Influences of Lithium Cooperation and Ligand Set. *Angew. Chem., Int. Ed.* **2018**, *57*, 10651−10655.
(31) Bisai, M. K.; Pahar, S.; Das, T.; Vanka, K.; Sen, S. S. Transition Metal Free Catalytic Hydroboration of Aldehydes and Aldimines by Amidinato Silane. *Dalton Trans.* **2017**, *46*, 2420−2424.
(32) Hadlington, T. J.; Hermann, M.; Frenking, G.; Jones, C. Low Coordinate Germanium(II) and Tin(II) Hydride Complexes: Efficient Catalysts for the Hydroboration of Carbonyl Compounds. *J. Am. Chem. Soc.* **2014**, *136*, 3028−3031.
(33) Schneider, J.; Sindlinger, C. P.; Freitag, S. M.; Schubert, H.; Wesemann, L. Diverse Activation Modes in the Hydroboration of

DOI: 10.1021/acs.organomet.8b00568
Organometallics 2018, 37, 4576−4584

Aldehydes and Ketones with Germanium, Tin, and Lead Lewis Pairs. *Angew. Chem., Int. Ed.* **2017**, *56*, 333−337.
(34) Wu, Y.; Shan, C.; Sun, Y.; Chen, P.; Ying, J.; Zhu, J.; Liu, L.; Zhao, Y. Main group metal−ligand cooperation of N-heterocyclic germylene: an efficient catalyst for hydroboration of carbonyl compounds. *Chem. Commun.* **2016**, *52*, 13799−13802.
(35) Chong, C. C.; Hirao, H.; Kinjo, R. Metal-Free σ-Bond Metathesis in 1,3,2-Diazaphospholene-Catalyzed Hydroboration of Carbonyl Compounds. *Angew. Chem., Int. Ed.* **2015**, *54*, 190−194.
(36) Freitag, B.; Fischer, C. A.; Penafiel, J.; Ballmann, G.; Elsen, H.; Färber, C.; Piesik, D. F.; Harder, S. Bora-amidinate as a cooperative ligand in group 2 metal catalysis. *Dalton Trans.* **2017**, *46*, 11192−11200.
(37) Freitag, B.; Stegner, P.; Thum, K.; Fischer, C. A.; Harder, S. Tetranuclear Strontium and Barium Siloxide/Amide Clusters in Metal-Ligand Cooperative Catalysis. *Eur. J. Inorg. Chem.* **2018**, *2018*, 1938−1944.
(38) He, M.; Gamer, M. T.; Roesky, P. W. Homoleptic Chiral Benzamidinate Complexes of the Heavier Alkaline Earth Metals and the Divalent Lanthanides. *Organometallics* **2016**, *35*, 2638−2644.
(39) Harder, S.; Spielmann, J. Calcium-mediated hydroboration of alkenes: "Trojan horse" or "true" catalysis? *J. Organomet. Chem.* **2012**, *698*, 7−14.
(40) Kozuch, S.; Shaik, S. How to Conceptualize Catalytic Cycles? The Energetic Span Model. *Acc. Chem. Res.* **2011**, *44*, 101−110.
(41) *APEX2, SAINT, and SADABS*; Bruker AXS, Inc.: Madison, WI, 2006.
(42) Sheldrick, G. M. A short history of *SHELX*. *Acta Crystallogr., Sect. A: Found. Crystallogr.* **2008**, *64*, 112−122.
(43) Farrugia, L. J. *ORTEP*-3 for Windows - a version of *ORTEP*-III with a Graphical User Interface (GUI). *J. Appl. Crystallogr.* **1997**, *30*, 565−565.

DOI: 10.1021/acs.organomet.8b00568
Organometallics 2018, 37, 4576−4584

ORGANOMETALLICS

pubs.acs.org/Organometallics Article

Substrate, Catalyst, and Solvent: The Triune Nature of Multitasking Reagents in Hydroboration and Cyanosilylation

Ruchi Dixit, Milan Kumar Bisai, Sandeep Yadav, Vinita Yadav, Sakya S. Sen,* and Kumar Vanka*

Cite This: *Organometallics* 2021, 40, 1104–1112 Read Online

ACCESS | Metrics & More | Article Recommendations | Supporting Information

ABSTRACT: A truly green chemical process would avoid the use of an external catalyst, while still achieving high efficiency. This has been realized in the very recent past for hydroboration, cyanosilylation, acetalization, and the aza-Michael addition, among other reactions. The current combined computational and experimental study unlocks the secret to how this highly desirable outcome is accomplished: one of the reactants in the process also acts as the catalyst. Specifically, this is shown (i) for the important hydroboration reaction, with pinacolborane (HBpin) as the hydroborating reagent and benzaldehyde, acetophenone, benzoic acid and *p*-methoxyphenylacetylene as the hydroborated substrates, and (ii) for cyanosilylation, with trimethylcyanosilane (TMSCN) as the cyanosilylating agent and benzaldehyde as the substrate. The mechanistic understanding thus gained has then been further exploited experimentally to bring hydroboration and cyanosilylation closer to experimental conditions in catalysis. These insights can potentially be expanded to the rapidly growing area of solvent-free and internal catalyst chemistry.

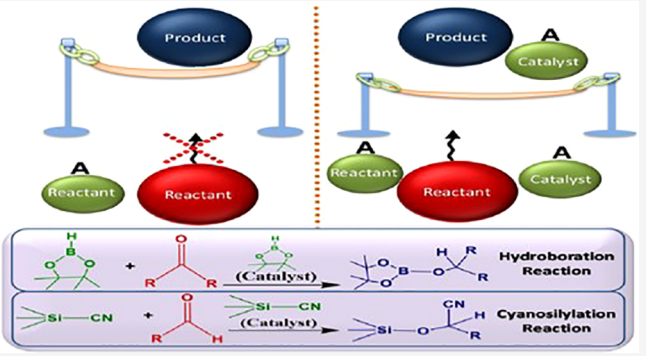

INTRODUCTION

"The best catalyst is no catalyst"[1] sums up the need for green processes in the current age, and it is gratifying to see the increasing application of this dictum to a wider and wider variety of chemical reactions, including hydroboration,[2−5] cyanosilylation,[6,7] acetalization,[8] and the aza-Michael addition.[9] However, in order for this to become even more of an important area of development, it is necessary to understand and establish the principles on which this chemistry is founded. The current combined computational and experimental work represents a comprehensive attempt in this direction. To this end, we have focused on two different, important chemical processes: hydroboration and cyanosilylation.

Hydroboration is one of the most significant chemical reactions employed in academia and industry today, owing to the wide synthetic applicability of functionalized boronates. The hydroborating agent of choice today is pinacolborane, HBpin, shown in Figure 1 below. The presence of two B−O bonds allow it to stabilize the positive charge on the boron upon loss of the hydride, thus making hydride transfer with HBpin facile and efficient. It has therefore been employed for a variety of hydroboration reactions,[10] with substrates as varied as alkenes, alkynes, carboxylic acids, aldehydes, ketones, imines, amides, carbodiimides, pyridines, esters, and allylic alcohols. What has made HBpin even more attractive is the recent report by Hreczycho and co-workers,[2] where aldehyde hydroboration was demonstrated to occur in neat HBpin, without the need for an external catalyst. This result has led to increased interest in HBpin chemistry, with several reports emerging in the space of a year.[3,4,11,12]

What these recent results show is that HBpin is able to efficiently hydroborate different substrates without the need for a solvent or an external catalyst, while the same efficiency is not obtained in solution in external-catalyst-free conditions.[2] It is this unusual and interesting behavior that has served as the starting point of our investigations. Specifically, we have proposed and validated a hypothesis that explains the behavior of HBpin with the aid of density functional theory (DFT) as well as with experimental kinetic studies. What we have found is that neat HBpin, in addition to acting as the "solvent" for the reaction as well as one of the reactants (as the hydroborating agent), also does duty as a catalyst in facilitating the hydroboration chemistry. Therefore, HBpin can be termed as also acting as an "internal catalyst" during the hydroboration process. We have then employed the insights gained to design and execute experiments that show how one can do hydroboration chemistry in solution with HBpin without loss of yield, thereby bringing this new, external-catalyst-free

Received: February 5, 2021
Published: April 6, 2021

https://doi.org/10.1021/acs.organomet.1c00070
Organometallics 2021, 40, 1104−1112

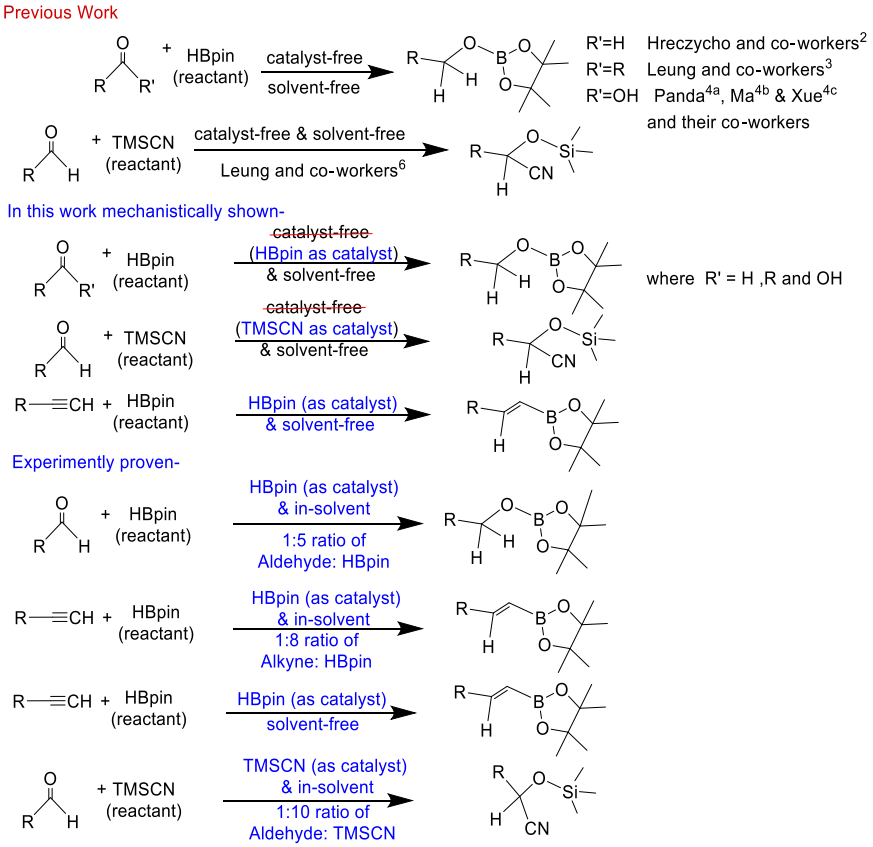

Figure 1. Previously reported hydroboration cases under solvent-free and catalyst-free conditions, as well as new systems designed in the current work with the aid of mechanistic insights through DFT, experimentally proving heterofunctionalization in solution, not through mediation by an external catalyst but by one of the reactants acting as the catalyst (an "internal catalyst").

hydroboration chemistry closer to the realm of experimental conditions in catalysis.

We were then able to extend the insights gained to the important cyanosilylation reaction, by showing how transformations occurring in neat trimethylsilyl cyanide (TMSCN) followed the same principles as were discovered for hydroboration chemistry. The current work thus furthers different fields of important chemical transformations, by demonstrating how the same reaction can take place efficiently in solution without the need for external catalysts, through this newly discovered "internal catalyst" driven chemical process.

COMPUTATIONAL DETAILS

All of the calculations in this study have been performed with density functional theory (DFT), with the aid of the Turbomole 7.1 suite of programs,[13] using the PBE functional.[14] The TZVP[15] basis set has been employed. The resolution of identity (RI)[16] and the multipole accelerated resolution of identity (marij)[17] approximations have been employed for an accurate and efficient treatment of the electronic Coulomb term in the DFT calculations. Solvent corrections were incorporated with optimization calculations using the COSMO model,[18] with benzene (ε = 2.27), HBpin (ε = 2.48), hexane (ε = 1.88), and toluene (ε = 2.38) as the solvents. The dielectric constant of HBpin was determined to be 2.48, using the linear relationship between the Onsager electric field and the vibrational frequencies.[19] The harmonic frequency calculations were performed for all stationary points to confirm them as local minima or transition-state structures. In addition, intrinsic reaction coordinate (IRC)[20] calculations were done with all of the transition-state structures in order to further confirm that they represented the correct transition states, yielding the correct reactant and product structures for each case. The values reported are ΔG values, with zero-point energy corrections and internal energy and entropic contributions included through frequency calculations on the optimized minima, with the temperature taken to be 25.0 °C for aldehyde and carboxylic acid hydroboration and 80.0 °C for ketone hydroboration and the cyanosilylation of aldehyde. These different temperatures were considered, keeping in mind the experimental conditions employed in the reporting literature. Finally, the temperature of 100.0 °C was taken for the hydroboration of alkyne. Further single-point calculations have been done for case I (the aldehyde case) with the B3-LYP hybrid functional and the TZVP basis set. In order to calculate the ΔG values, the enthalpy and entropy contributions have been taken from calculations done at the PBE/TZVP level of theory.

All of the components of the Gibbs free energy values obtained are shown in Table S10a–o in the Supporting Information. This includes volume corrections, in order to account for the unreasonable enhancement in translational entropy that is generally observed when computational softwares are employed. The total entropy calculated is the sum of translational, rotational, and vibrational components, but while the rotational and vibrational components are acceptable, the calculation of the translational entropy involves the determination of the volume, which is inaccurately calculated in computational software from the ideal gas equation, an approach that is not applicable for solid solutes dissolved in a solvent. Therefore, the translational entropy term in the calculated structures has been corrected through a free volume correction introduced by Mammen et al.,[21] in which the translational entropy of molecules in solution (ΔS_{Trans}(sol)) has been described by a "free volume" model. This approach provides corrections based on the Sackur–Tetrode equation for translational entropy. In the free volume model, it is assumed that the volume used by the molecule in solution is lower than the total volume, and hence, this "free volume" is determined from the equation

https://doi.org/10.1021/acs.organomet.1c00070
Organometallics 2021, 40, 1104–1112

$$V_{free} = C_{free}\left(\sqrt[3]{\frac{10^{27}}{[X]N_0}} - \sqrt[3]{V_{molec}}\right)^3$$

Here, V_{molec} is the molecular volume, [X] is the concentration of molecules (mol/L) in solution, and N_0 is Avogadro's number. Hence, by insertion of this value of V_{free} in the Sackur–Tetrode equation, the translational entropy is calculated. The total entropy is then calculated by adding the entropic contributions from the rotational and vibrational components to this corrected translational entropy value.

RESULTS AND DISCUSSION

HBpin Chemistry. As was mentioned in the Introduction, HBpin facilitates the hydroboration of a range of different substrates under solvent-free and external-catalyst-free conditions, but the same chemistry does not occur in solution in the absence of an external catalyst. So, what explains this unusual behavior of HBpin? What we propose is that the strength of HBpin—the stabilizing effect of its B–O bonds, as mentioned in the Introduction—is also its weakness. This is because there exists the possibility that the substrate, instead of abstracting the hydride from the boron, can attack one of the two B–O bonds, thereby leading to an unwanted side product. This is shown in Figure 2, for the case of the aldehyde

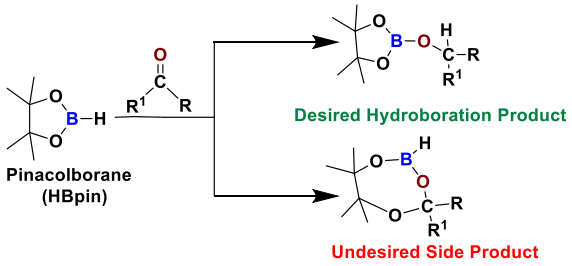

Figure 2. Competition between the desired hydroboration reaction and an undesired side reaction when pinacolborane (HBpin) is employed as the hydroborating agent in solution.

substrate studied by Hreczycho and co-workers.[2] If this side reaction is kinetically competitive with the desired hydroboration reaction, then the yield of the desired main product would be reduced.

Now, why is the yield restored in the absence of *both* solvent and external catalyst in neat HBpin? We propose that this is due to the ready availability of HBpin molecules in close proximity to each other in neat HBpin. This allows an additional HBpin molecule to act as a hydride-relaying catalyst in the hydroboration process, thereby converting the constrained four-membered transition state for the hydroboration reaction to a more favorable six-membered transition state (see Figure 3). It is, of course, true that a similar conversion from a four- to a six-membered transition state could occur for the undesired side reaction as well, but now the extra HBpin would act as a reactant rather than as a catalyst, and the reaction would result in a strained, unfavorable six-membered heterocycle.

As will be shown below, we have proved the validity of this hypothesis with the aid of DFT calculations, taking benzaldehyde, acetophenone, benzoic acid, and *p*-methoxyphenylacetylene as substrates, as well as with experimental kinetic studies with *p*-methoxyphenylacetylene as the substrate.

Case I: Hydroboration with Aldehyde. The free energy surfaces obtained for the two reactions—the desired hydroboration reaction (in blue) and the undesired side reaction (in red)—are shown together in Figure 4. The hydroboration reaction is seen to be thermodynamically favorable by 26.8 kcal/mol and has a barrier of 32.8 kcal/mol.

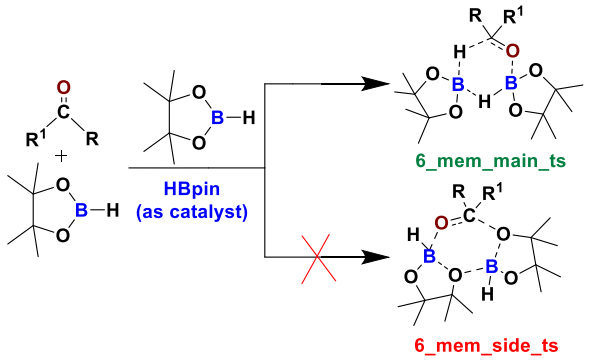

Figure 3. An additional HBpin molecule acts as a catalyst and nullifies the competition, increasing the yield of the desired hydroborated product, in liquid HBpin.

While this suggests that the desired reaction itself has a high barrier, another issue is that the first part of the side reaction, indicated with an "A", is kinetically competitive, consisting of two steps having barriers of 32.1 and 32.3 kcal/mol, respectively. The heterocyclic intermediate formed from the side reaction, Int_2, lies 16.8 kcal/mol above the separated reactants HBpin and benzaldehyde. From this point, there could potentially be a second part to this process, shown as "B" in Figure 4. This would happen if Int_2 were to be approached by another benzaldehyde molecule: it could proceed to give the hydroborated product. However, "B" would be unlikely to take place. As Figure 4 reveals, the barrier for the next step, 48.8 kcal/mol, would be too high. The free energy surface for the side reaction therefore indicates that the system can be trapped in "A", moving back and forth between Int_2 and the starting reactants. While the starting reactants, thus re-formed, would then be able to also pass through the pathway shown in blue to give the desired product, the kinetic competition provided by "A" would act to reduce the yield of the overall reaction.

The same is seen to be true if the reactions were to be considered in neat HBpin. Since the dielectric constants of benzene and HBpin are quite similar (2.27 and 2.48, respectively), the values of the two free energy profiles are also similar (see Figure S1 in the Supporting Information). Therefore, regardless of whether the "solvent" was benzene or liquid HBpin, the yield of the final hydroborated product would be reduced by the competing side reaction occurring between the benzaldehyde and HBpin reactants.

However, in liquid HBpin, there exists a second possibility. As was mentioned above, an extra HBpin molecule can now act as a hydride-relaying catalyst. The result would be the conversion of the four-membered transition state to a six-membered transition state (see Figure 5) and a reduction in barrier from 33.1 to 25.7 kcal/mol. A similar benefit is not received for the side reaction: it is true that the presence of an additional HBpin would create a six-membered heterocycle, as had been shown in Figure 3, but calculations show that such a product would be unfavorable by 21.8 kcal/mol in comparison to the starting reactants. Since this value is itself higher than the barrier for the desired hydroborating reaction, it is clear that the barrier for the formation of this six-membered

https://doi.org/10.1021/acs.organomet.1c00070
Organometallics 2021, 40, 1104–1112

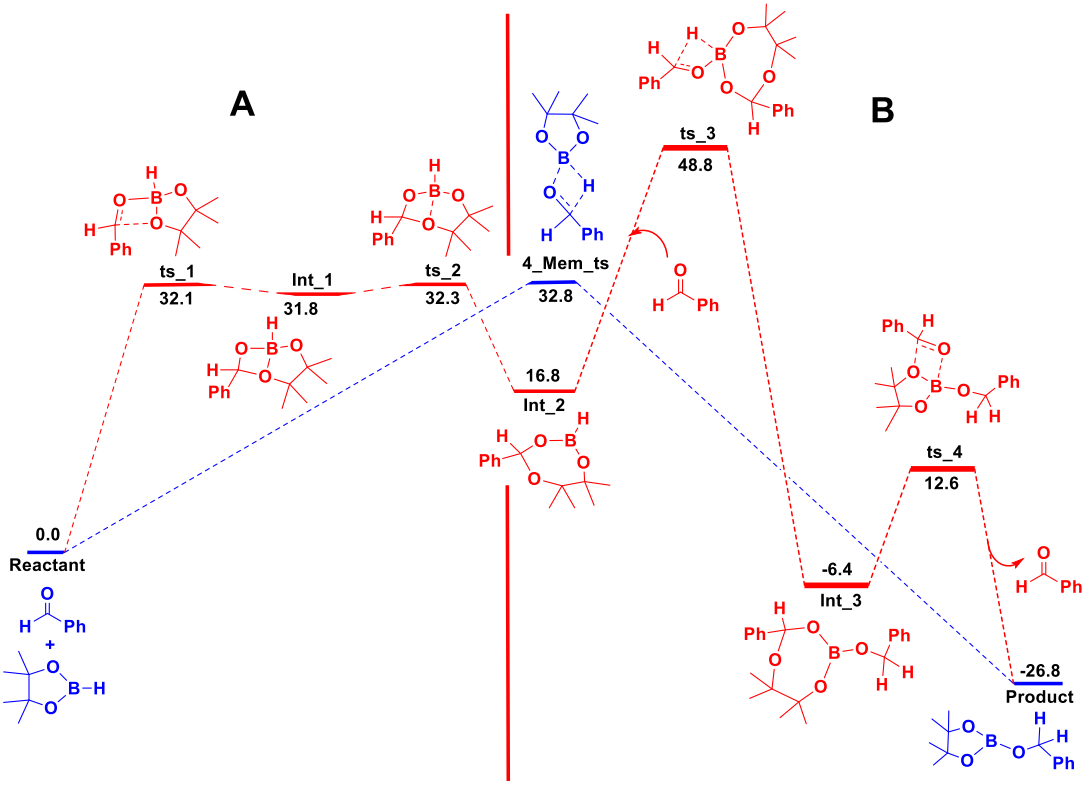

Figure 4. Free energy profile of the desired hydroboration reaction and the undesired side reaction for benzaldehyde with HBpin, in benzene solvent. The Gibbs free energy values (in kcal/mol) have been calculated at the PBE/TZVP level of theory.

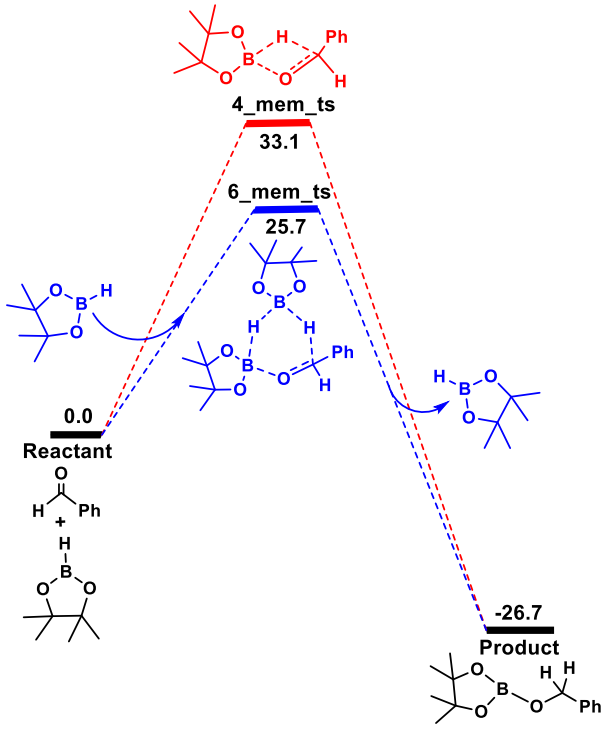

Figure 5. Free energy profile for the alternative pathway for benzaldehyde hydroboration in HBpin solvent. The Gibbs free energy values (in kcal/mol) have been calculated at the PBE/TZVP level of theory.

heterocycle side product would be much higher. Thus, the presence of an extra HBpin acting as a catalyst eliminates the competition between the two competing processes and leads to the preferred formation of the desired hydroborated complex.

In order to get a clearer picture, we have further done single point calculations using the hybrid B3-LYP functional and the TZVP basis set, and observed the same trend as before. For further details, please see the ESI.

A final point in this section pertains to the fact that our work shows that the B−O bond in HBpin is susceptible to attack (leading to side reactions, as discussed above). This gives rise to the question: could HBpin molecules attack the B−O bonds in each other, thus leading to the formation of extended heterocyclic systems? We have explored this possibility through DFT as well as with *ab initio* molecular dynamics (AIMD) simulations and found that, indeed, such equilibria are also possible, especially in liquid HBpin, where the close proximity of HBpin molecules would facilitate such chemistry. Specifically, we have found that three HBpin monomers can form a trimeric heterocyclic species. The spontaneous collision of three molecules would be an unlikely event in general but is more likely in this case, as the HBpin molecules, being present in close proximity in the liquid form, would experience trimolecular collisions. The section Possibility of trimer formation in HBpin: ab initio molecular dynamics (AIMD) simulations in the Supporting Information discusses these findings in more detail. Such a trimer would protect its B−O bonds from attack and thereby suppress side reactions, while allowing the desired reaction to take place (see Figure S21 in the Supporting Information). However, the energetics of the transformation also suggest that the monomer:trimer equilibrium would lie toward the side of the monomers. Hence, the HBpin trimer represents a minor species in liquid HBpin, thereby suggesting that that such species represent interesting but minor players in hydroboration chemistry.

https://doi.org/10.1021/acs.organomet.1c00070
Organometallics 2021, 40, 1104−1112

Experimental Studies of Hydroboration of Benzaldehyde with HBpin in Solution. What we considered next were the same reactions in solution, in benzene solvent. The results for this are shown in Figure S3 in the Supporting Information. As with the liquid HBpin case, the barriers in benzene solvent become favorable once an additional HBpin molecule is considered, with the barrier found to be 26.5 kcal/mol. The significant drop in barrier height from 32.8 kcal/mol for the four-membered transition state to 26.5 kcal/mol for the six-membered transition state would be feasible if an extra HBpin molecule could act as a catalyst: i.e., if excess HBpin were to be employed. Under these circumstances, one would then not have to employ an external catalyst. In order to put these insights to the test, we decided to conduct experiments in benzene solvent, evaluating the possibility of the hydroboration of benzaldehyde with excess HBpin. Several reactions were performed by varying the stoichiometry of benzaldehyde and HBpin in benzene in the absence of an external catalyst. Even after 12.0 h of reaction time, only a 20.0% product yield was observed when benzaldehyde and HBpin were treated in a 1:1 ratio. However, gratifyingly, the reaction yield increased from 20.0% to >99.0% when the concentration of HBpin was increased from 1.0 to 5.0 equiv (see Table S7 in the Supporting Information for further details).

Furthermore, we note that increasing the concentration of HBpin even further, say from 1.0 to 8.0 or 10.0 equiv, i.e. to a significant excess of HBpin, would lead the system from a trimolecular reaction toward a pseudobimolecular reaction. In such a situation, when the ΔG values for the six-membered transition state case are calculated, one can consider one molecule of benzaldehyde as one reactant and have two HBpin molecules, in close proximity to one another, as the other reactant species: i.e., the entropic cost of having an additional HBpin molecule in the reaction would be further reduced. Such a situation has been considered in the current work, and the results (see Figure S4 in the Supporting Information) show that the barrier is reduced to 22.8 kcal/mol. Moreover, the efficiency for the hydroboration reaction in solution, calculated using the energetic span model (ESM)[22−24] (for more details on the ESM method, please see the Supporting Information) and shown in Table S1 in the Supporting Information, indicates that the reaction mechanism involving the six-membered transition state in benzene solvent is 4.1×10^4 times more efficient than the corresponding mechanism involving a four-membered transition state (shown in Figure S3 in the Supporting Information). Now, the mechanism proposed in Figure S4, with a significant excess of HBpin, is *2.5 × 10^7 times more efficient*, which shows the value of moving the system toward a pseudobimolecular reaction.

What is also important to note here is that the reactions were seen to take place in benzene with >99.0% yield at room temperature. Now, recovering and recycling unused HBpin after the completion of the reaction could be a potential stumbling block to this approach. However, the recovery and recycling of HBpin can be done by fractional distillation, as it has a very low boiling point. In other words, this proposed new approach can be both practical and effective in execution.

Furthermore, we have shown that the hydroboration, with HBpin, of carboxylic acid and acetophenone is facilitated by the presence of an additional Hbpin molecule, following the same principles discussed here. These have been discussed in more detail in the Supporting Information.

Case II: Hydroboration of the Alkyne *p*-Methoxyphenylacetylene with HBpin in Solution. Having validated with experiments the conclusions reached from DFT calculations, we also decided to check whether the insights gained held good for substrates other than aldehyde. To this end, we proceeded to conduct experimental studies for the external-catalyst-free hydroboration of the alkyne *p*-methoxyphenylacetylene by HBpin in solution. External-catalyst-aided hydroboration of alkynes has been reported in the literature,[26] but this would represent the first example of the same reaction in solution without the aid of an external catalyst.

We proceeded with experiments testing the DFT conclusions. A brief screening of the molar ratio of the substrate was carried out for the hydroboration of *p*-methoxyphenylacetylene with HBpin in order to achieve the best conversion (see Table S8 in the Supporting Information). When the reaction of *p*-methoxyphenylacetylene and HBpin in the ratio of 1:1 under solvent-free and external-catalyst-free conditions was conducted, a good yield (64.0%) was achieved. On the other hand, in benzene solvent, a good yield (68.0%) was achieved when *p*-methoxyphenylacetylene and HBpin in significant excess were used in a ratio of 1:8. For further details, please see the Supporting Information.

DFT calculations show that under solvent-free and external-catalyst-free conditions the presence of an additional HBpin molecule would act as a hydride-relaying catalyst and that would reduce the barrier for the desired hydroboration reaction, as shown in Figures S5 and S6 in the Supporting Information (Figure S5, for a trimolecular reaction and Figure S6 for the corresponding pseudobimolecular case, as discussed above). On the other hand, the hydroboration of *p*-methoxyphenylacetylene in the aromatic solvent benzene was achieved when the ratio of *p*-methoxyphenylacetylene and HBpin in significant excess was 1:8. This suggests that a significant excess of HBpin, i.e. a pseudobimolecular reaction, is the preferred route of hydroboration of *p*-methoxyphenylacetylene in benzene solvent. We have therefore considered one molecule as one reactant and have optimized two HBpin molecules in close proximity as the other reactant species. This leads to a reduced barrier of 34.0 kcal/mol (see Figure 6). The TOF calculated using the energetic span model (ESM) (see Table S2 in the Supporting Information) shows that the mechanism following this pseudobimolecular path is 2.17×10^3 times favored over the mechanism shown in red that does not involve an extra HBpin molecule. Moreover, even if the reaction goes through the trimolecular path, as shown in Figure 7, the mechanism involving an extra molecule of HBpin would still be favored. This pathways is found to be 2.24 times more efficient (see Table S2).

We have also performed kinetic experiments to further understand the effect of HBpin on the hydroboration reaction. The rate order with respect to the [HBpin] was determined for the hydroborylation of *p*-methoxyphenylacetylene. The order was determined using the initial rate method (see Figure S15 and also Table S6 in the Supporting Information). The order of the reaction with respect to HBpin was determined to be 1.58. This indicates that, for a reaction to proceed, more than one molecule of HBpin is required. This is consistent with our hypothesis (and the attending calculations) that an extra HBpin molecule is participating in the hydroboration reaction.

Cyanosilylation Chemistry: Cyanosilylation of Aldehydes with TMSCN in Solution. Leung and co-workers[6] reported the successful cyanosilylation of aldehyde with

https://doi.org/10.1021/acs.organomet.1c00070
Organometallics 2021, 40, 1104−1112

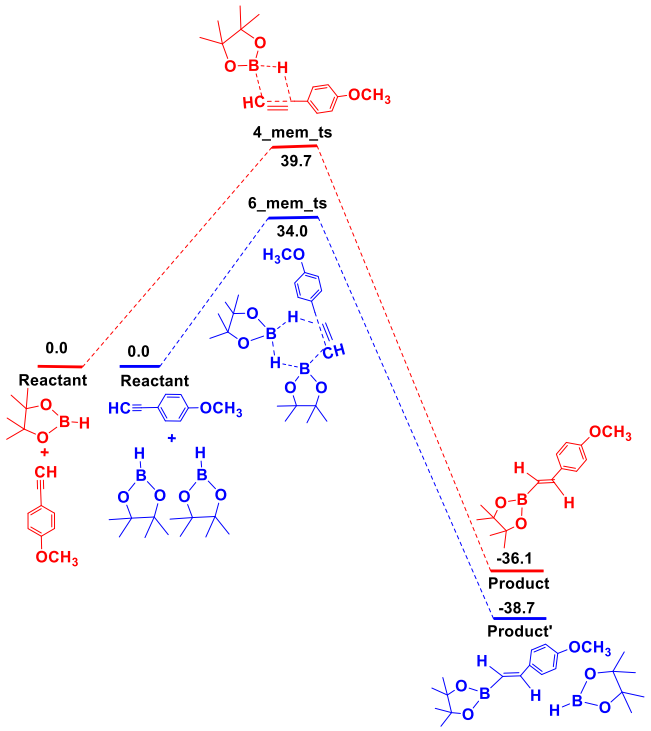

Figure 6. Free energy profiles of the desired hydroboration reaction with and without the assistance of an additional HBpin molecule for the *p*-methoxyphenylacetylene substrate in a significant excess of HBpin in benzene solvent. The Gibbs free energy values (in kcal/mol) have been calculated at the PBE/TZVP level of theory.

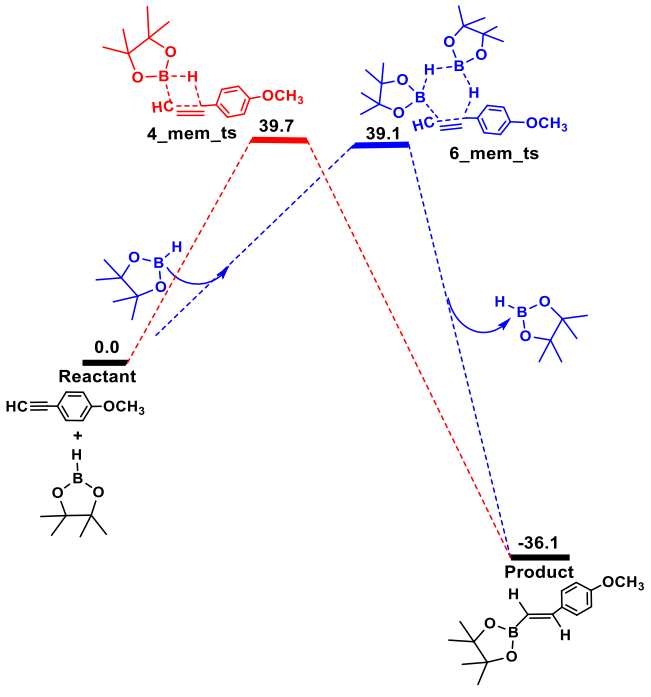

Figure 7. Free energy profiles of the desired hydroboration reaction with and without the assistance of an additional HBpin molecule for the *p*-methoxyphenylacetylene substrate in benzene solvent. The Gibbs free energy values (in kcal/mol) have been calculated at the PBE/TZVP level of theory.

TMSCN in the absence of solvent and catalyst, with benzaldehyde as the substrate. As for the case of hydroboration, we have considered the possibility that the presence of an additional TMSCN molecule can affect the kinetics of the reaction favorably.

Hence, this was investigated experimentally. When TMSCN was used in significant excess in benzene solvent, a high yield of 75.0% was achieved in the absence of an external catalyst (a benzaldehyde:TMSCN ratio of 1:10 at 80.0 °C and for 18.0 h; see Table S9 in the Supporting Information).

As was explained in previous cases, here the significant excess concentration of TMSCN in solvent was used (1) to make TMSCN act as a catalyst, (2) to mimic the solvent-free conditions, and (3) to overcome the resulting entropy, as the reaction was done in the solvent phase. Due to this significantly high concentration of TMSCN in the reaction, it becomes clear that the pseudobimolecular pathway would be preferred over the mechanism proposed in Figure S13. We have therefore, in the DFT calculations, optimized two TMSCN molecules in close proximity and have considered the same as the starting species (see Figure 8). Corey and coworkers had shown that cyanosilylation can proceed through the formation of an isocyanide intermediate.[27,28] Likewise, in our proposed mechanism, the reaction progresses through the formation of TMS-NC (Int_1) when an additional TMSCN molecule is involved (see Figure 8). We observed that the barrier for the slowest step (40.0 kcal/mol) of this proposed pathway is 2.5 kcal/mol lower than the pathway involving a 1:1 ratio of TMSCN and benzaldehyde (see Figure S12 in the Supporting Information). A barrier of 40.0 kcal/mol is achievable at the elevated temperature of 80 °C.[25,29] As Figure 8 illustrates, the other TMSCN molecule does not participate in the mechanism but still functions to stabilize the transition state by favorable interactions with the NC triple bond: NCI plots that we have determined reveal the noncovalent interactions between the Si of the other TMSCN and the CN (or NC) group (the green isosurfaces shown in Figure S14 in the Supporting Information). More details about the NCI plots have been provided in the Supporting Information. In addition, from ESM calculations (shown in Table S5), the pathway involving an additional TMSCN molecule was 35.3 times more efficient than the pathway for the 1:1 case. The reason for the increased efficiency is that the difference in the energies of the intermediates and the transition states is not significant along the reaction pathway when an additional TMSCN molecule is employed. This, as is known from the Sabatier principle,[30] is a favorable situation.

As expected from the DFT studies, a higher ratio of TMSCN to benzaldehyde was required in this case, as well as a higher temperature, but here too the experiments have validated the insights gained from the computational studies and provided proof that the cyanosilylation of different substrates with TMSCN could proceed without the aid of external catalysts in solution, through "internal catalyst" chemistry.

Therefore, the calculations and experiments with HBpin and TMSCN show that internal catalysis chemistry can indeed act as a substitute for external catalysis, provided higher concentrations and slightly elevated temperatures are employed. One question that could be asked is whether a system with higher temperatures and concentrations would be preferable to another with lower temperatures and concentrations but with an external catalyst. We note here that in the latter case the following points are true:

https://doi.org/10.1021/acs.organomet.1c00070
Organometallics 2021, 40, 1104−1112

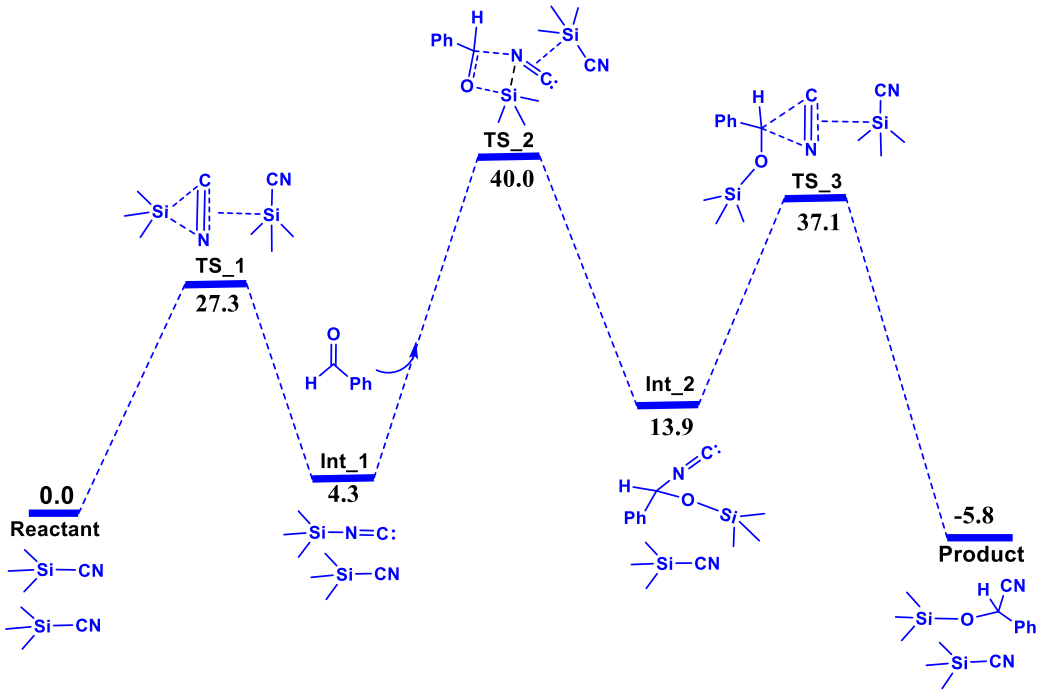

Figure 8. Free energy profiles for the benzaldehyde cyanosilylation reaction with TMSCN, in a significant excess of TMSCN in benzene solvent, with additional TMSCN considered to be a catalyst. The Gibbs free energy values (in kcal/mol) have been calculated at the PBE/TZVP level of theory.

(1) There is a need to synthesize the external catalyst. Sometimes, the synthesis can be tedious and multistep.
(2) While the catalyst is prepared, if one uses noble transition metals, then the entire process becomes expensive. On the other hand, if main-group catalysts or first-row transition-metal-based catalysts are employed, they usually turn out to be air and moisture sensitive. As a result, an appropriate ligand has to be prepared.
(3) Catalyst recycling is a major issue.
(4) The efficiency of the catalyst is lost over multiple uses.

Moreover, while the cyanosilylation of aldehyde usually occurs at room temperature, the hydroboration of alkynes takes place at elevated temperatures, even in the presence of an external catalyst. For example, we have shown recently that the hydroboration of alkynes using easily accessible lithium compounds ((2,6-di-*tert*-butylphenolate)lithium (**1a**) and 1,1′-dilithioferrocene (**1b**))[10b] has been achieved at 373 K and 12 h in toluene.

If one employs an internal catalyst, most of the issues raised above are resolved. It is true that all the internal catalyst cases that we have considered do require elevated temperatures and concentrations, but there are additional benefits:

(1) Obtaining the product becomes much easier and there is no need to remove traces of catalyst after the reaction, something that can cause impurities or degrade the product.
(2) Using internal catalysts could be very effective in large-scale processes, something that is very important from an industrial application point of view.

CONCLUSIONS

There is an important, environmentally beneficial area of research that has seen impressive growth in recent years. This pertains to the field of solvent-free and external-catalyst-free chemistry.[2−9] The current work, employing both computational and experimental approaches, aims to provide a mechanistic understanding of this chemistry. Specifically, we have explored two important functionalization reactions: hydroboration and cyanosilylation. Investigations with DFT for a range of substrates, (i) benzaldehyde, acetophenone, benzoic acid, and *p*-methoxyphenylacetylene for the case of hydroboration in neat HBpin and (ii) benzaldehyde for the case of cyanosilylation in neat TMSCN, reveal the favorable intervention of an additional HBpin or TMSCN molecule during the reaction, which makes the chemistry more efficient in the respective cases. In other words, HBpin and TMSCN act not only as reactants and solvents during the reaction but also as internal catalysts. Experimental kinetic studies conducted for the hydroboration of *p*-methoxyphenylacetylene with HBpin corroborate these computational findings. These insights have been further tested by experiments, which have validated the computational findings by showing, for the first time, that the use of excess HBpin and TMSCN in solution allowed the hydroboration and cyanosilylation reactions to take place with good yields without the need for an external catalyst. This has significance because it opens up possibilities of allowing such internal-catalyst-aided reactions to occur for substrates that dissolve poorly in neat HBpin or TMSCN.

There is also an expanded significance to the obtained results, pertaining to the growing family of reactions taking place under solvent-free and external-catalyst-free conditions. These include acetalization,[8] the aza-Michael addition,[9] and many more. For instance, in the case of the acetalization of imines, a proton shuttle mechanism has been hypothesized,[8] thereby implying the possibility of the imine in question acting as both reactant and catalyst. One can therefore envisage doing the same chemistry by exploiting the potential of the imine to act as an internal catalyst, by making use of the strategy

https://doi.org/10.1021/acs.organomet.1c00070
Organometallics 2021, 40, 1104−1112

discussed in the current work. A similar approach could potentially be employed for the aza-Michael addition reaction of cyclohexylamine to diethyl maleate[9] or the conversion of an aziridine to an oxazolidinone[31] or the synthesis of tetrazoles by choline azide.[32] Furthermore, microkinetic modeling can also be considered in the future in order to get a clearer picture of the internal catalysis process. Hence, the current work is of considerable general significance for internal-catalyst-aided chemical transformations.

■ ASSOCIATED CONTENT

Supporting Information

The Supporting Information is available free of charge at https://pubs.acs.org/doi/10.1021/acs.organomet.1c00070.

Complete computational details and catalytic procedure (PDF)

Cartesian coordinates for the calculated structures (XYZ)

Movements of the monomeric and trimeric HBpin (MP4)

■ AUTHOR INFORMATION

Corresponding Authors

Sakya S. Sen − *Inorganic Chemistry and Catalysis Division, CSIR-National Chemical Laboratory, Pune 411008, India; Academy of Scientific and Innovative Research (AcSIR), Ghaziabad 201002, India;* orcid.org/0000-0002-4955-5408; Email: ss.sen@ncl.res.in

Kumar Vanka − *Physical and Material Chemistry Division, CSIR-National Chemical Laboratory, Pune 411008, India; Academy of Scientific and Innovative Research (AcSIR), Ghaziabad 201002, India;* orcid.org/0000-0001-7301-7573; Email: k.vanka@ncl.res.in

Authors

Ruchi Dixit − *Physical and Material Chemistry Division, CSIR-National Chemical Laboratory, Pune 411008, India; Academy of Scientific and Innovative Research (AcSIR), Ghaziabad 201002, India*

Milan Kumar Bisai − *Inorganic Chemistry and Catalysis Division, CSIR-National Chemical Laboratory, Pune 411008, India; Academy of Scientific and Innovative Research (AcSIR), Ghaziabad 201002, India*

Sandeep Yadav − *Inorganic Chemistry and Catalysis Division, CSIR-National Chemical Laboratory, Pune 411008, India; Academy of Scientific and Innovative Research (AcSIR), Ghaziabad 201002, India;* orcid.org/0000-0003-2780-3770

Vinita Yadav − *Organic Chemistry Division, CSIR-National Chemical Laboratory, Pune 411008, India; Academy of Scientific and Innovative Research (AcSIR), Ghaziabad 201002, India*

Complete contact information is available at: https://pubs.acs.org/10.1021/acs.organomet.1c00070

Author Contributions

K.V. conceived the idea. The computational studies were done by R.D. M.K.B. and S.Y. performed the catalysis, and V.Y. did the kinetic studies. K.V., S.S.S., and R.D. wrote the manuscript together.

Notes

The authors declare no competing financial interest.

■ ACKNOWLEDGMENTS

K.V. is grateful to the Department of Science and Technology (DST) (EMR/2014/000013) for providing financial assistance. R.D., M.K.B., and S.Y. thank the Council of Scientific and Industrial Research (CSIR) for providing Research Fellowships. S.S.S. is grateful for a CSIR-Young Scientist Contingency Grant (YSA000726). We thank Dr. Sayan Bagchi and Sushil Sakpal for assistance in finding the dielectric constant of HBpin. The support and the resources provided by "PARAM Brahma Facility" under the National Supercomputing Mission, Government of India, at the Indian Institute of Science Education and Research (IISER) Pune are gratefully acknowledged. We thank the reviewers of the manuscript, whose suggestions have helped improve the quality of the work presented.

■ REFERENCES

(1) Sheldon, R. A. E Factors, Green Chemistry and Catalysis: an Odyssey. *Chem. Commun.* **2008**, 3352−3365.

(2) Stachowiak, H.; Kazmierczak, J.; Kucinski, K.; Hreczycho, G. Catalyst-free and solvent-free hydroboration of aldehydes. *Green Chem.* **2018**, *20*, 1738−1742.

(3) Wang, W.; Luo, M.; Yao, W.; Ma, M.; Pullarkat, S. A.; Xu, L.; Leung, P. H. Catalyst-free and solvent-free hydroboration of ketones. *New J. Chem.* **2019**, *43*, 10744−10749.

(4) (a) Harinath, A.; Bhattacharjee, J.; Panda, T. K. Facile Reduction of Carboxylic Acids to Primary Alcohols under Catalyst-Free and Solvent-Free Conditions. *Chem. Commun.* **2019**, *55*, 1386−1389. (b) Wang, W.; Luo, M.; Zhu, D.; Yao, W.; Xu, L.; Ma, M. Green Hydroboration of Carboxylic Acids and Mechanism Investigation. *Org. Biomol. Chem.* **2019**, *17*, 3604−3608. (c) Xu, X.; Yan, D.; Zhu, Z.; Kang, Z.; Yao, Y.; Shen, Q.; Xue, M. Catalyst-Free Approach for Hydroboration of Carboxylic Acids under Mild Conditions. *ACS Omega* **2019**, *4*, 6775−6783.

(5) Pandey, V. K.; Donthireddy, S. N. R.; Rit, A. Catalyst-Free and Solvent-Free Facile Hydroboration of Imines. *Chem. - Asian J.* **2019**, *14*, 3255−3258.

(6) (a) Wang, W.; Luo, M.; Yao, W.; Ma, M.; Pullarkat, S. A.; Xu, L.; Leung, P. H. Catalyst-free and Solvent-free Cyanosilylation and Knoevenagel Condensation of Aldehydes. *ACS Sustainable Chem. Eng.* **2019**, *7*, 1718−1722. (b) Pahar, S.; Kundu, G.; Sen, S. S. Cyanosilylation by Compounds with Main-Group Elements: An Odyssey. *ACS Omega* **2020**, *5*, 25477−25484.

(7) Iida, H.; Hamana, H.; Matsumoto, K. Highly Efficient Cyanosilylation of Aldehydes and Ketones under Microwave, Solvent-Free, and Lewis Acid-Free Conditions. *Synth. Commun.* **2007**, *37*, 1801−1805.

(8) Lillo, V. J.; Mansilla, J.; Saa, J. M. The role of proton shuttling mechanisms in solvent-free and catalyst-free acetalization reactions of imines. *Org. Biomol. Chem.* **2018**, *16*, 4527−4536.

(9) Blaha, M.; Trhlikova, O.; Podesva, J.; Abbrent, S.; Steinhart, M.; Dybal, J.; Duskova-Smrckova, M. Solvent-free, catalyst-free aza-Michael addition of cyclohexylamine todiethyl maleate: Reaction mechanism and kinetics. *Tetrahedron* **2018**, *74*, 58−67.

(10) (a) Shegavi, M. L.; Bose, S. K. Recent advances in the catalytic hydroboration of carbonyl compounds. *Catal. Sci. Technol.* **2019**, *9*, 3307−3336. (b) Bisai, M. K.; Yadav, S.; Das, T.; Vanka, K.; Sen, S. S. Lithium compounds as single site catalysts for hydroboration of alkenes and alkynes. *Chem. Commun.* **2019**, *55*, 11711−11714. For more references on hydroboration please see References in the Supporting Information.

(11) Harinath, A.; Bhattacharjee, J.; Panda, T. K. Catalytic Hydroboration of Organic Nitriles Promoted by Aluminum Complex. *Adv. Synth. Catal.* **2019**, *361*, 850−857.

(12) Liu, W.; Ding, Y.; Jin, D.; Shen, Q.; Yan, B.; Ma, X.; Yang, Z. Organic Aluminum Hydrides Catalyze Nitrile Hydroboration. *Green Chem.* **2019**, *21*, 3812−3815.

(13) TURBOMOLE V7.1 2016, a development of University of Karlsruhe and ForschungszentrumKarlsruhe GmbH, 1989−2007, TURBOMOLE GmbH, since 2007; available from http://www.turbomole.com.
(14) Perdew, J. P.; Burke, K.; Ernzerhof, M. Generalized Gradient Approximation Made Simple. *Phys. Rev. Lett.* **1996**, *77*, 3865−3868.
(15) Schafer, A.; Huber, C.; Ahlrichs, R. Fully optimized contracted Gaussian basis sets of triple zeta valence quality for atoms Li to Kr. *J. Chem. Phys.* **1994**, *100*, 5829−5835.
(16) Eichkorn, k.; Treutler, O.; Ohm, H.; Haser, M.; Ahlrichs, R. Auxiliary basis sets to approximate Coulomb potentials. *Chem. Phys. Lett.* **1995**, *240*, 283−290.
(17) Sierka, M.; Hogekamp, A.; Ahlrichs, R. Fast evaluation of the Coulomb potential for electron densities using multipole accelerated resolution of identity approximation. *J. Chem. Phys.* **2003**, *118*, 9136−9148.
(18) Klamt, A.; Schuurmann, G. Cosmo: a new approach to dielectric screening in solvents with explicit expressions for the screening energy and its gradient. *J. Chem. Soc., Perkin Trans. 2* **1993**, *2*, 799−805.
(19) Bagchi, S.; Fried, S. D.; Boxer, S. G. A Solvatochromic Model Calibrates Nitriles' Vibrational Frequencies to Electrostatic Fields. *J. Am. Chem. Soc.* **2012**, *134*, 10373−10376.
(20) Fukui, K. The path of chemical reactions - the IRC approach. *Acc. Chem. Res.* **1981**, *14*, 363−368.
(21) Mammen, M.; Shakhnovich, E. I.; Deutch, J. M.; Whitesides, G. M. Estimating the Entropic Cost of Self-Assembly of Multiparticle Hydrogen-Bonded Aggregates Based on the Cyanuric Acid Melamine Lattice. *J. Org. Chem.* **1998**, *63*, 3821−3830.
(22) Kozuch, S.; Martin, J. M. L. What Makes for a Bad Catalytic Cycle? A Theoretical Study on the Suzuki-Miyaura Reaction within the Energetic Span Model. *ACS Catal.* **2011**, *1*, 246−253.
(23) Uhe, A.; Kozuch, S.; Shaik, S. Software News and Update Automatic Analysis of Computed Catalytic Cycles. *J. Comput. Chem.* **2011**, *32*, 978−985.
(24) Kozuch, S.; Shaik, S. How to Conceptualize Catalytic Cycles? The Energetic Span Model. *Acc. Chem. Res.* **2011**, *44*, 101−110.
(25) Yamakawa, M.; Ito, H.; Noyori, R. The Metal-Ligand Bifunctional Catalysis: A Theoretical Study on the Ruthenium(II)-Catalyzed Hydrogen Transfer between Alcohols and Carbonyl Compounds. *J. Am. Chem. Soc.* **2000**, *122*, 1466−1478.
(26) Bismuto, A.; Cowley, M. J.; Thomas, S. P. Aluminum-Catalyzed Hydroboration of Alkenes. *ACS Catal.* **2018**, *8*, 2001−2005.
(27) Ryu, H. D.; Corey, J. E. Enantioselective Cyanosilylation of Ketones Catalyzed by a Chiral Oxazaborolidinium Ion. *J. Am. Chem. Soc.* **2005**, *127*, 5384−5387.
(28) Ryu, D. H.; Corey, E. J. Highly Enantioselective Cyanosilylation of Aldehydes Catalyzed by a Chiral Oxazaborolidinium. *Ion. J. Am. Chem. Soc.* **2004**, *126*, 8106−8107.
(29) Wang, L. P.; Titov, A.; McGibbon, R.; Liu, F.; Pande, V. S.; Martinez, T. J. Discovering chemistry with an ab initio nanoreactor. *Nat. Chem.* **2014**, *6*, 1044−1048.
(30) Laursen, A. B.; Varela, A. S.; Dionigi, F.; Fanchiu, H.; Miller, C.; Trinhammer, O. L.; Rossmeisl, J.; Dahl, S. Electrochemical Hydrogen Evolution: Sabatier's Principle and the Volcano Plot. *J. Chem. Educ.* **2012**, *89*, 1595−1599.
(31) Phung, C.; Ulrich, R. M.; Ibrahim, M.; Tighe, N.T. G.; Lieberman, D. L.; Pinhas, A. R. The solvent-free and catalyst-free conversion of an aziridine to an oxazolidinone using only carbon dioxide. *Green Chem.* **2011**, *13*, 3224−3229.
(32) Mehraban, J. A.; Azizi, K.; Jalali, M. S.; Heydari, A. Choline Azide: New Reagent and Ionic Liquid in Catalyst-Free and Solvent-Free Synthesis of 5-Substituted-1H-Tetrazoles: A Triple Function Reagent. *Chemistry Select* **2018**, *3*, 12175−12180.

https://doi.org/10.1021/acs.organomet.1c00070
Organometallics 2021, 40, 1104−1112